Depositional Environments and Provenance of the Wajid Sandstone, Abha-Khamis Mishayt Area, Southwestern Saudi Arabia

by

Lameed Olabode Babalola

A Thesis Presented to the

FACULTY OF THE COLLEGE OF GRADUATE STUDIES

KING FAHD UNIVERSITY OF PETROLEUM & MINERALS

DHAHRAN, SAUDI ARABIA

In Partial Fulfillment of the
Requirements for the Degree of

MASTER OF SCIENCE

In

GEOLOGY

December, 1999

DEPOSITIONAL ENVIRONMENTS AND PROVENANCE OF THE WAJID SANDSTONE, ABHA-KHAMIS MUSHAYT AREA, SOUTHWESTERN SAUDI ARABIA

BY

LAMEED OLABODE BABALOLA

A Thesis Presented to the

DEANSHIP OF GRADUATE STUDIES

KING FAHD UNIVERSITY OF PETROLEUM & MINERALS

DHAHRAN, SAUDI ARABIA

In Partial Fulfillment of the
Requirements for the Degree of

MASTER OF SCIENCE

In

GEOLOGY

DECEMBER 1999

UMI Number: 1402601

Bell & Howell Information and Learning Company
300 North Zeeb Road
P.O. Box 1346
Ann Arbor, MI 48106-1346

KING FAHD UNIVERSITY OF PETROLEUM AND MINERALS
DHAHRAN 31261, SAUDI ARABIA

DEANSHIP OF GRADUATE STUDIES

This thesis written by *LAMEED OLABODE BABALOLA* under the supervision of his Thesis Committee has been presented and accepted by the Dean of the College of Graduate Studies in partial fulfillment of the requirements for the degree of MASTER OF SCIENCE in Geology.

Thesis Committee

Dr. Mahbub Hussain (Chairman)

Dr. Badrul M. Imam (Member)

Dr. Mustafa M. Hariri (Member)

Dr. Mustafa M. Hariri
Department Chairman

Dr. Abdallah M. Al-Shehri
Dean, College of Graduate Studies

10/5/2000

Date

DEANSHIP OF GRADUATE STUDIES

Dedicated to

my parents (Chief and Mrs. Alimi Ojo Babalola);

wife (Saadat)

and

sons (Ridwanallah and Habibllah)

ACKNOWLEDGEMENT

My sincere appreciations are due to my thesis advisor Dr. Mahbub Hussain for his invaluable contributions to the success of this research. The guidance and assistance received from him during the field work, laboratory and final production of this thesis are indeed appreciated. The contributions from other members of my thesis committeee, Dr. Mustafa M. Hariri and Badrul M. Imam are also thankfully acknowledged. In addition to to being a member of this thesis advisory commiittee, Dr Mustafa M. Hariri (as the departmental chairman), also facilitated all the administrative needs in the course of my studentship. The professional advice benefitted from Dr. Badrul Imam, especially in the areas of stratigraphy, petrography and diagenesis is duly acknowledged.

Drs. Nazrul Islam Khandaker and Abdul Aziz A. Al-Laboun, former members of my thesis committee are also remembered for their individual contributions to the success of this research. Dr. Al-Laboun is thanked for reading and making valuable comments on the first draft of this thesis. All my course instructors, other faculty members and all staff (including Fadhel, Mushabab and Sami) of the department are thanked for their individual and collective assistance. The Late Mr. Ameerudeen Salahudeen is also remembered. May Allah be pleased with his soul and grant him eternal rest (amin).

I wish to express my deep appreciation to Dr. Assad Ahmed Thukair (Chairman of Chemistry) for providing me with chemicals and laboratory glassware. My unreserved gratitude also goes to Dr. John Shirokoff and Abdul Rasheed Muhammed of the Research Institute for assisting me with the XRD and SEM analyses, respectively. Mr Azeez Ullah Khan is thanked for lending me a hand in the field and in the preparation of the thin section slides. Mr. Ahmed Moosa of Petroleum Engineering Department is thankfully acknowledged for assisting me with porosity determination

It is also my pleasure to say thank you to the following brothers and their families, AbdulKareem Bala. Adinoyi, Yahaya Garba Oloriegbe, AbdulSemiu Gbadebo, Taofeek Ayinde, Abdullah Umar, Wale Adejumo, Qamar'deen Abidogun, AbdulRahaman Jarad and Mohammed Khalifah for their individual and collective assistance in cash and kind during this study.

My family members including my younger sister (Hassana Babalola), aunt (Mrs. Bola Ojo), uncles (Usthman and Abdul Malik Babalola) and others are thanked for their moral support and endurance during the period of this study.

I duly appreciate and thank the university authorities (KFUPM) for granting me the university's graduate studentship. The financial assistance enjoyed from the King Abdul Aziz City for Science and Technology (KACST) and American Association of Petroleum Geologists (through a Limited Grant project and AAPG Grant-in-Aid awards for 1998, respectively) is gratefully acknowledged.

Above all, my greatest gratitude is due to Allah for granting me the patience and knowledge to successfully pass through this stage of my academic career. Al-hamdulillah!al-hamdulillah!! Al-hamdulillah rob'l-alamin!!!.

TABLE OF CONTENT

TITLE PAGE....................i

CERTIFICATION....................ii

DEDICATION....................iii

ACKNOWLEDGEMENT....................iv

TABLE OF CONTENT....................v

LIST OF FIGURES....................viii

LIST OF TABLES....................xii

LIST OF PLATES....................xiii

ABSTRACT....................xiv

CHAPTER ONE....................1
INTRODUCTION....................1
1.1. Introductory Statement....................1
1.2. Objectives....................3
1.3. Location of the study area....................3
1.4 General Geology....................6
1.5. Previous Studies on Wajid Sandstone....................9

CHAPTER TWO....................14
METHODS OF STUDY....................14
2.1. Introduction....................14
2.2. Field Investigation....................14
2.3. Laboratory Analyses....................16
2.3.1. Thin Section Petrography....................16
2.3.2. Heavy Mineral Separation....................17
2.3.3. Scanning Electron Microscopy (SEM)....................18
2.3.4. Geochemical Sample Preparation....................18
2.3.5. Clay Mineralogy and X-Ray Diffraction....................18

CHAPTER THREE....................20
STRATIGRAPHY....................20
3.1. Basement Complex....................20
3.2. Lithofacies of the Wajid Sandstone....................21
3.2.1. Basal Conglomerates....................21
3.2.2. The Red Unit....................22
3.2.3. The Upper Unit....................26

3.3. Paleocurrent Analysis............................29
3.4. Correlation of the lithofacies with type sections in Wadi Ad Dawasir............31

CHAPTER FOUR............................34
PETROGRAPHY............................34
4.1. Introduction............................34
4.2. Thin Section Petrography............................35
4.2.1. Quantitative Mineralogy............................35
4.2.2. Matrix............................41
4.2.3. Porosity............................44
4.3. Diagenesis............................44
4.3.1. Compaction and Pressure Solution............................44
4.3.2. Cementation............................47
4.3.3. Dissolution............................54
4.4. Scanning Electron Microscopy (SEM)............................55
4.5. X-Ray Diffractometry (XRD)............................55
4.6. Clay Mineralogy............................59
4.6.1. Introduction............................59
4.6.2. Descriptive Mineralogy............................60
4.6.3. Quantitative Mineralogy............................60
4.7. Heavy Mineral Analysis............................63
4.7.1. Introduction............................63
4.7.2. Heavy Mineral Distribution............................64
4.7.3. Descriptive Mineralogy............................71
4.7.4. Multivariate Analyses............................81
4.7.4.1. Introduction............................81
4.7.4.2. R-Mode Analysis............................82
4.7.4.3. Q-Mode Analysis............................90

CHAPTER FIVE............................96
GEOCHEMISTRY............................96
5.1. Introduction............................96
5.2. Distribution of Elements............................98
5.2.1. Basement Complex Samples............................113
5.2.2. Wajid Sandstone............................114
5.3. Geochemical distinction between Red and Grey Units............................117
5.4. Multivariate Analyses of the Geochemical Data............................120
5.4.1. R-Mode Analysis............................120
5.4.3. Q-Mode Analyses of the Geochemical Data............................133

CHAPTER SIX............................141
DISUSSION AND CONCLUSION............................141
6.1. Provenance............................141
6.1.1. Introduction............................141
6.1.2. Petrofacies and Provenance............................142
6.1.3. Heavy Mineral Evidence............................143

6.1.4. Geochemical Evidence....147
6.2. Tectonic Setting And Sedimentation....153
6.3. Depositional Environments....156
6.4. Origin of the Ferruginous Horizons....160
6.5. Origin of the Kaolinitic Claystone....162
6.6. Conclusions....163

REFERENCES....165

LIST OF FIGURES

Figure 1.1. Geological map of Saudi Arabia showing Wajid Sandstone at the study area...2

Figure 1.2. Map showing the location of the studied localities. The inset map of Saudi Arabia also shows the general study area represented by Abha City.........................4

Figure 1.3. Geological map of Abha Quadrangle...8

Figure 1.4. General stratigraphic succession of the wajid Sandstone (after Kellog *et al*, 1986)...12

Figure 2.1. Flow chart showing the outline of the approaches and objectives of this study..15

Figure 3.1. Photograph and generalized stratigraphic collumn showing the Wajid Sandstone overlying the Precambrian basement complex rocks nonconformably.........22

Figure 3.2. Photographs showing the unconformities separating (a) the basement and Wajid Sandstone and the Red and the Grey Unit..23

Figure 3.3. Photographs showing (a) thick ferruginous beds and (b) ferruginous material occurring as fracture infills...25

Figure 3.4. Photographs showing kaolinitic claystoneand intraformational clasts in Wajid Sandstone: (a) Kaolinitic claystone lenses and (b) The intraformational clasts (dominantly claystone) derived from kaolinite-rich claystone horizons are common in Wajid Sandstone...27

Figure 3.5. Photographs showing typical cross stratifications in Wajid Sandstone: (a) unidirectional cross beds in the Red Unit and (b) bi-directional cross beds in the Grey Unit..28

Figure 3.6. Rose diagrams showing the general trends of paleocurrent directions. Note the predominantly northerly trend...30

Figure 3.7. Tentative correlation of the informal units of this study with the type section...32

Figure 4.1. Photomicrographs showing: (a) Typical composition of Wajid Sandstone. and generally poor to well sorted. (b) Packing inhomogeneity is an evidence of the dissolution of the calcite cement...36

Figure 4.2. Ternary diagrams showing QFL distribution for different tectonic settings (adapted from Dickinson *et al*, 1983). Q = quartz, F = feldspar and L = lithic grains.....42

Figure 4.3. QFL ternary diagrams showing the compsition of Wajid Sandstone: (a) Red Unit and (b) Grey Unit. The plots suggest derivation of the Wajid Sandstone from a cratonic source (Q = quartz, F = feldspar and L = rock fragments)........................43

Figure 4.4. Typical x-ray diffractogram showing general mineralogical phases of the Wajid Sandstone..56

Figure 4.5. X-ray diffractogram of a representative sample from the Red Unit. Note the characteristic hematite peak..57

Figure 4.6. X-ray diffractograms showing typical spectra of kaolinite: (a) unglycolated and (b) glycolated sample...61

Figure 4.7. Bivariate relation between opaque minerals and ZTR index in the total grain counts: (a) Red Unit and (b) Grey Unit...68

Figure 4.8. Relative distribution of opaque minerals and ZTR in the Wajid Sandstone: (a) Opaque minerals and (b) ZTR index..69

Figure 4.9. Relative distribution of heavy minerals in the Wajid Sandstone: (a) Localities and (b) Units... 70

Figure 4.10. Ternary diagrams showing factor laodings for heavy minerals: (a) Ahad Rufaïdah and (b) Al Habalah I..84

Figure 4.11. Ternary diagrams showing factor loadings for heavy minerals: (a) Al Habalah II and Al Soudah...85

Figure 4.12. Dendrograms showing clustering of heavy minerals: (a) Ahad Rufaidah and Al Habalah I..87

Figure 4.13. Dendrograms showing clustering of heavy minerals: (a) Al Habalah II and Al soudah...88

Figure 4.14. Ternary diagram and dendrogram of the Q-mode factor and cluster analyses of heavy mineral samples: (a) Ternary diagram and (b) Dendrogram........................93

Figure 4.15. Heavy mineral distribution in the different factors as delineated by Q-mode factor analysis : (a) factor 1 and (b) factor 2..94

Figure 4.16. Heavy mineral distribution in factor 3 as delineated by Q-mode factor analysis: (a) Red Unit and Grey Unit..95

Figure 5.1. Relative distribution of the different elements in the basement samples: (a) Major elements and (b) Trace elements....102

Figure 5.2. Relative distribution of the different elements in the Wajid Sandstone: (a) Major elements and (b) Trace elements....103

Figure 5.3. Bivariate plots of 100*(Al_2O_3/SiO_2) and 100*(Fe_2O_3/SiO_2) in the Wajid Sandstone: (a) Red Unit and (b) Grey Unit....104

Figure 5.4. Bivariate plots of Al_2O_3/(Al_2O_3-SiO_2) and Fe_2O_3/(Fe_2O_3/SiO_2) in the Wajid Sandstone: (a) Red Unit and (b) Grey Unit....105

Figure 5.5. Bivariate plots of Al_2O_3/(Al_2O_3+Fe_2O_3) and Fe_2O_3/TiO_2 in the Wajid Sandstone: (a) Red Unit and Grey Unit....106

Figure 5.6. Discriminant diagram proposed by Roser and Kosch (1986) for identifying different sandstones and argillites. ARC = Oceanic island arc, ACM = Active continental margin and PCM = Passive Continental Margin....107

Figure 5.7. Discriminant plots of Roser and Kosch (1986) for Wajid Sandstone: (a) Red Unit and (b) Grey Unit. ARC = Oceanic Island Arc, ACM = Active Continental Margin and PCM = Passive Continental Margin....108

Figure 5.8. Ternary diagrams of (a) Al_2O_3-SiO_2-LOI and (b) Al_2O_3-SiO_2-TiO_2 for kaolinite-rich samples from the Red Unit. These plots are within the composition field of kaolin deposits derived from granitic source terrain (da Costa and Moraes, 1998)....109

Figure 5.9. Ternary diagrams of (a) Al_2O_3-SiO_2-Fe_2O_3 and (b) Al_2O_3-SiO_2-K_2O for kaolinite-rich samples from the Red Unit. These plots are within the composition field of kaolin deposits derived from granitic source terrain (da Costa and Moraes, 1998)....110

Figure 5.10. Ternary diagrams of (a) Al_2O_3-SiO_2-LOI and (b) Al_2O_3-SiO_2-TiO_2 for kaolinite-rich samples from the Grey Unit. These plots are within the composition field of kaolin deposits derived from granitic source terrain (da Costa and Moraes, 1998)....111

Figure 5.11. Ternary diagrams of (a) Al_2O_3-SiO_2-Fe_2O_3 and (b) Al_2O_3-SiO_2-K_2O for kaolinite-rich samples from the Red Unit. These plots are within the composition field of kaolin deposits derived from granitic source terrain (see da Costa and Moraes, 1998)....112

Figure 5.12. Distribution of elements in thje Red and Grey Units: (a) Major elements and (b) Trace elements....118

Figure 5.13. Distribution of oxides in the Red and Grey Units..........................119

Figure 5.14. Ternary diagrams showing the distribution of different factors in samples from Ahad Rufaidah Locality: (a) Elements and Oxides..................................123

Figure 5.15. Ternary diagrams showing the distribution of different factors in samples from Al Habalah I Locality: (a) Elements and Oxides......................................124

Figure 5.16. Ternary diagrams showing the distribution of different factors in samples from Al Habalah II Locality: (a) Elements and Oxides....................................125

Figure 5.17. Ternary diagrams showing the distribution of different factors in samples from Al Soudah Locality: (a) Elements and Oxides...126

Figure 5.18. Dendrogram showing clustering among different elements and oxides in Ahad Rufaidah samples: (a) Elements and (b) Oxides.......................................127

Figure 5.19. Dendrogram showing clustering among different elements and oxides in Al Habalah I samples: (a) Elements and (b) Oxides...128

Figure 5.20. Dendrogram showing clustering among different elements and oxides in Al Habalah II samples: (a) Elements and (b) Oxides...129

Figure 5.21. Dendrogram showing clustering among different elements and oxides in Al Soudah samples: (a) Elements and (b) Oxides..130

Figure 5.22. Ternary diagrams of factor loadings for Q-mode sample anlaysis: (a) Elements and ((b) Oxides data. 136

Figure 5.23. Relative distribution of elements in the samples characterized by fator loadings in the Q-mode fcator analysis: (a) Major elements and (b) Trace elements....137

Figure 5.24. Relative distribution of oxides in the samples characterized by high factor loadings in the Q-mode analysis...138

Figure 5.25. Grouping of the samples based on their relative distribution in Q-mode cluster analysis: (a) Elemental and (b) Oxides data...139

LIST OF TABLES

TABLE 1.1. Table showing locations of the studied outcrops 5

TABLE 4.1. Table showing the modal composition of Wajid sandstone. 39

TABLE. 4.2. Table showing cementation phases in the Wjid Sandstone....................52

TABLE 4.3. Modal composition determination from X-Ray diffraction analysis.........58

TABLE 4.4. X-ray diffraction of the separated clay fraction from the Red and Grey Units..62

TABLE 4.5. Distribution of heavy minerals in the Wajid Sandstone.......................65

TABLE 4.6. Summary of the factor loadings for the heavy mineral assemblages in the Wajid Sandstone: (a) Ahad Rufaidah, (b) Al Habalah I, (c) Al Habalah II and (d) Al Al Soudah..83

TABLE 4.7. Summary of the cluster groups for the heavy mineral assemblages in the Wajid Sandstone: (a) Ahad Rufaidah, (b) Al Habalah I, (c) Al Habalah II and (d) Al Al Soudah..89

TABLE 4.8. Factor and cluster Q-Mode Analyses listing associations of samples for different factors and groups: Heavy mineral data...92

TABLE 5.1. Distribution of some selected trace elements in the basement samples......99

TABLE 5.2. Distribution of some selected trace elements in the Wajid Sandstone.....100

TABLE 5.3. Summary of the factor loadings for elements: (a) Ahad Rufaidah, (b) Al Habalah I, (c) Al Habalah II and (c) Al Soudah...121

TABLE 5.4. Summary of the factor loadings for the oxides: (a) Ahad Rufaidah, (b) Al Habalah I, (c) Al Habalah II and (c) Al Soudah 122

TABLE 5.5. Linkage among different elements and oxides as determined by cluster data: (a) Ahad Rufaidah, (b) Al Habalah I, (c) Al Habalah II and (c) Al Soudah.........131

TABLE 5.6. Summary of the distribution of factors derived from the Q-mode factor Analysis of the Wajid Sandstone samples: (a) Elemental and (b) Oxide data............135

TABLE 5.7. Linkage of the cluster groups in Q-mode analysis of the Wajid Sandstone samples: Elemental and Oxides data...140

LIST OF PLATES

PLATE 1..38

PLATE 2..46

PLATE 3..49

PLATE 4..51

PLATE 5..73

PLATE 6..75

PLATE 7..77

PLATE 8..80

APPENDICES

Appendix I..180

Appendix II...209

Appendix III..214

Appendix IV..235

ABSTRACT

NAME: Lameed Olabode Babalola

TITLE OF THESIS: Depositional Environments and Provenance of the Wajid Sandstone, Abha-Khamis Mushayt Area, Southwestern Saudi Arabia

MAJOR FIELD: Geology

DATE OF DEGREE: December 1999

A multidisciplinary approach (including thin section petrography, heavy mineral analysis, trace element chemistry, scanning electron microscopy and X-ray diffractometry) was utilized to investigate the depositional environments and provenance of the sediments of the Lower Paleozoic Wajid Sandstone exposed in the Abha-Khamis Mushayt area of southwestern Saudi Arabia. The origin of the associated ferruginous horizons and kaolinitic claystone was also investigated. The Wajid Sandstone in the study area is represented by an approximately 300m thick sequence of medium to coarse grained, poor to well-sorted, mineralogically mature, pebbly sandstone and conglomerate. On the basis of color and abundance of ferruginous horizons, the sequence was divided into two units ; a lower Red Unit and an upper Grey Unit.

The dominance of zircon, tourmaline and rutile in the heavy mineral suites of the Wajid Sandstone supports the mineralogical maturity of the sediments. The overall optical attributes (color, crystal types, inclusions e.t.c) of these heavy minerals indicate an acidic to intermediate source terrain. The presence of epidote and kyanite indicates contributions from metamorphic terrain. The association of high SiO_2, Al_2O_3-TiO_2 with low concentrations of P_2O_5, CaO, MgO, TiO_2, Cr, Co, Ni and V indicates a dominantly intermediate to felsic source terrain. The values of the Cr/Ni, V/Cr and V/Ni ratios are also in agreement with the inferred felsic to intermediate source terrain. The factor and cluster associations of the trace elements Cr, Co, Ni, Sr and V also support this interpretation.

The mineralogical maturity of the sediments (over 95% quartz), indicates a stable cratonic setting of the source terrains. A tectonically stable continental margin was inferred from the plots of the normalized Al_2O_3 and Fe_2O_3 and $Al_2O_3/(Al_2O_3+Fe_2O_3)$ versus Fe_2O_3/TiO_2. The bivariate plots of K_2O/Na_2O and SiO_2 also favor a passive margin tectonic environment with minor oceanic island arc influence. Paleocurrent distribution (mainly northern orientation), heavy mineral and trace element chemistry as well as the regional tectonic framework suggest highlands in Yemen as the major source of the sediments. Minor variability of the paleocurrent distribution in the northeast direction suggests the Arabian Shield as an additional source of the sediments.

The overall textural attributes, sedimentary structure (mainly large scale, low angle cross-bedding and cross-lamination), paleocurrent orientation and facies geometry (vertically stacked blocky sand bodies, channel fills and bars) indicate a braided river depositional environment. SEM and XRD studies showed that authigenic hematite and goethite are the dominant iron minerals of the Red Unit. The observed textural morphologies from SEM study showed that the associated claystone is mainly composed of authigenic kaolinite.

MASTER OF SCIENCE DEGREE
KING FAHD UNIVERSITY OF PETROLEUM AND MINERALS
Dhahran, Saudi Arabia
December 1999

الخلاصة

الاسم: لاميد أولا بود بابالولا

العنوان: الأصل والبيئات الترسيبية لحجر وجيد الرملي، منطقة أبها- خميس مشيط، جنوب غرب المملكة العربية السعودية.

التخصص الرئيسي: الجيولوجيا.

تاريخ نيل الدرجة: ديسمبر ١٩٩٩م.

تم استخدام منهج متعدد الطرائق (يشتمل على دراسة الشرائح الصخرية، تحليل المعادن الثقيلة، كيمياء العناصر الأثر، طريقة المجهر الإلكتروني الماسح وطريقة تشتت الأشعة السينية) لتقصي البيئات الترسيبية واصل رسوبيات حجر وجيد الرملي من العمر الباليوزوي الأسفل المتكشف في منطقة أبها خميس مشيط بجنوب غرب المملكة العربية السعودية.كما تم التحري عن اصل طبقات الحجر الطيني الكاوليني والحديدي المصاحبة. يمثل حجر وجيد الرملي بمنطقة الدراسة تتابعاً رسوبياً بسمك ٣٠٠ متر تقريباً من المدملكات والحجر الرملي الحصوي الناضج معدنياً والجيد إلى فقير التصنيف و الخشن إلى متوسط الحبيبات. تم تقسيم التتابع الرسوبي على أساس اللون وشيوع الطبقات الحديدية إلى وحدتين: الوحدة الحمراء السفلي والوحدة الرمادية العليا.

إن شيوع الزركون، التورمالين والروتايل فى طاقم المعادن الثقيلة بحجر وجيد الرملي يؤكد النضج المعدني لهذه الرسوبيات. دلت كل الصفات الضوئية (اللون، الأنواع البلورية، المتدخلات البلورية.. الخ) لهذه المعادن الثقيلة على أن المصدر أحزمة قارية متوسطة إلى حمضية كما أن الابيدوت يشير إلى أحزمة متحولة كصخور مصدريه أيضاً. إن تضامن نسبة عالية من SiO_2 و Al_2O_3/TiO_2 وتركيزات منخفضة من P_2O_5, CaO, MgO, Ti, Cr, Co, Ni, V يدل على غلبة الأحزمة المتوسطة إلى الفلسية كمصدر للرسوبيات، كما وتؤكد ذلك قيم نسب V/Ni, V/Cr, Cr/Ni. عضدت أيضا قيم المعامل والعنقود البيانيين لعناصر الأثر مثل Cr, V, Sr Ni, Co, هذا التفسير.

دل النضج المعدني للرسوبيات (اكثر من ٩٥%) على بيئة رواسخ مستقرة للأحزمة المصدر. وكما تم التعرف على وجود حافة قارية مستقرة تكتونياً من خلال التمثيل البياني لقيم $Al_2O_3/(Al_2O_3+Fe_2O_3)$ و Fe_2O_3 و Al_2O_3 المطبعة مقابل قيم Fe_2O_3/TiO_2. إن التمثيل البيئي ثنائي التغاير ل SiO_2 و K_2O/Na_2O يشير إلى بيئة حافة قارية مستقرة تكتونياً مع تأثير بعض الذر القوسية المحيطية. إن اتجاه التيار القديم للترسيب (غالباً فى اتجاه الشمال) المعادن الثقيلة وكيمياء العناصر الأثر والإطار التكتوني الإقليمي كلها ترجح مرتفعات اليمن كمصدر رئيسي لهذه الرسوبيات. كمايعنى التغيير المحلى الطفيف للتيار القديم فى اتجاه الشمال الشرقي إن الدرع العربي يمثل مصدراً إضافيا للرسوبيات.

إن الصفات النسيجية الكلية للصخور والتراكيب الرسوبية (هى فى الغالب تطبق و تصفح متقاطع بزوايا منخفضة ومقاييس كبيرة) واتجاه التيار القديم وهندسة السحنات الصخرية (أجسام رملية كتلية مدمجة رأسياً) كلها دلائل على بيئة ترسيب لانهار متعرجة. أوضحت دراسات تشتت الأشعة السينية و المجهر الإلكتروني الماسح أن الهيماتايت والجيوثايت محليي المنشأ هما المعدنان الحديديان الغالبان فى الوحدة الحمراء. كما وتدل المورفولوجيا النسيجية التي تمت ملاحظتها بواسطة المجهر الإلكتروني إلى أن الحجر الطيني المصاحب يتكون فى الأساس من كاولين محلى المنشأ.

درجة ماجستير العلوم

جامعة الملك فهد للبترول والمعادن

الظهران- المملكة العربية السعودية

ديسمبر ١٩٩٩

CHAPTER ONE

INTRODUCTION

1.1. Introductory Statement

The type section of the Wajid Sandstone located at the Jabal al-Wajid lies between longitudes 44° 25'E and 44° 35'E and latitude 19° 51'N in the southern part of the Arabian Peninsula. It also outcrops continuously in the south at the Wadi ad Dawasir on latitude 20° 30'N and extends to Najran on latitude 17° 35'N and longitude 44° 45'E at the western end. The Wajid Sandstone is also exposed as small isolated bodies along the southwest where it caps the hillocks of Precambrian shield and extends to Yemen (Figure 1.1). The Wajid Sandstone serves as one of the main aquifers in the Kingdom of Saudi Arabia. The large surface area this Sandstone provides favorable hydrologic conditions for natural recharge from rainfall and infiltration from runoff (I. A.G. Research Series, 1978).

Despite the economic importance of this Lower Paleozoic Sandstone as an acquifer, very limited studies have so far been undertaken on its sedimentology and stratigraphy. Data concerning the geologic age, depositional environments and the provenance of this Sandstone have also been very sketchy and inconclusive.

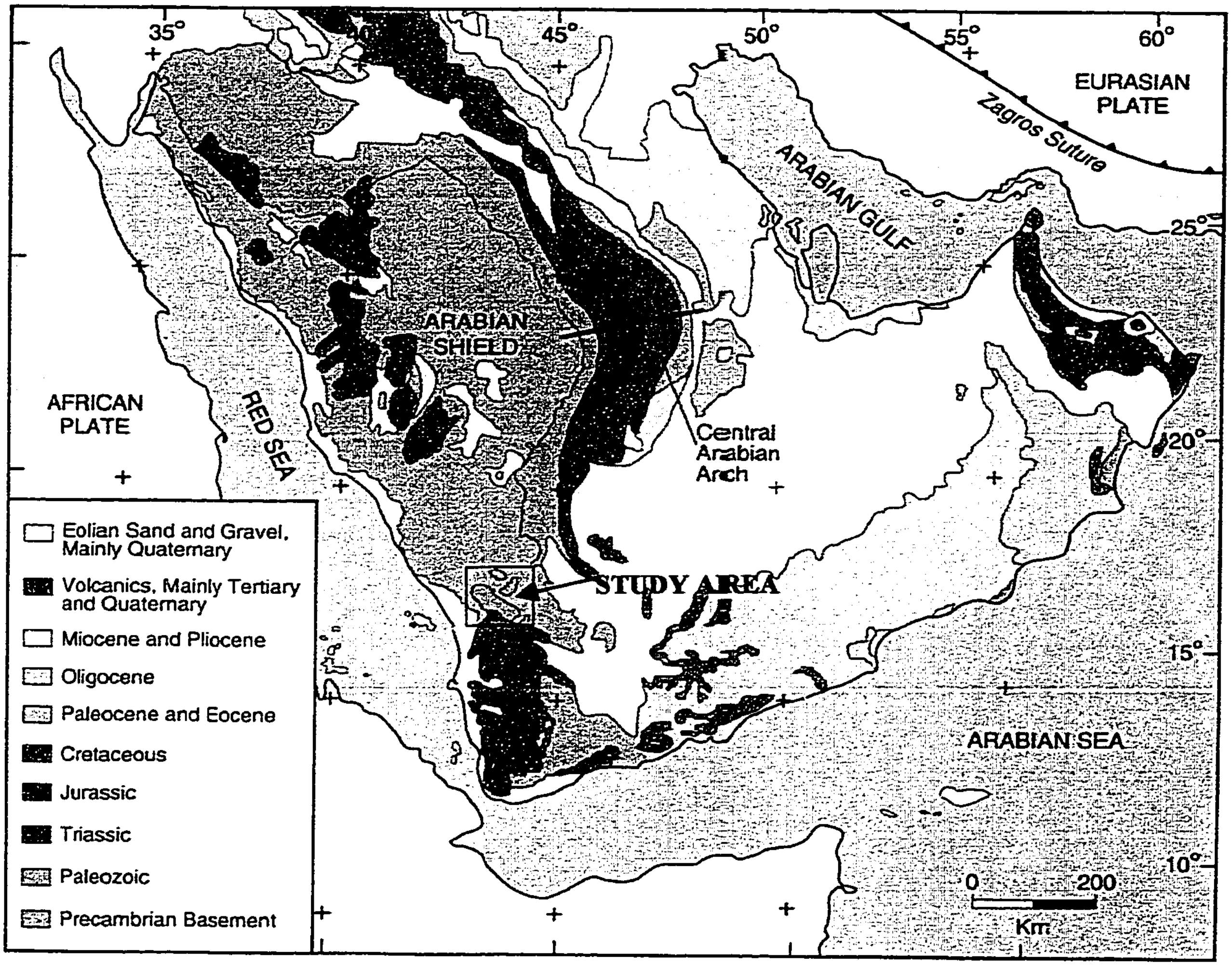

Figure 1.1. Geological map of Saudi Arabia showing the Paleozoic Wajid Sandstone at the Study Area (adapted from USGS, 1965).

The current study which involves detailed field investigations, thin section petrography, heavy mineral analysis and microanalyses including geochemistry, scanning electron microscopy and X-ray diffractometry is likely to add to our knowledge of this important geologic formation.

1.2. Objectives

The overall objectives of this research is to investigate the provenance and depositional envionments of the Wajid Sandstone that outcrops at the Abha - Khamis Mushayt area in the southwestern part of Saudi Arabia.This research attempts to achieve the following objectives:

- Investigate the provenance of the sediments based on petrography, heavy mineral types and associations, geochemical evidence and paleocurrent data.
- Determine the origin of the white kaolinitic claystone and iron-rich horizons that abound within the essentially sandstone sequence in the studied area.
- Characterize the facies and determine their depositional environments.

1.3. Location of the study area

The area of study, Abha-Khamis Mushayt area of the Asir Region, Saudi Arabia is located between longitudes 42° and 43° and latitudes 17° and 18° (Figure 1.2). The Wajid

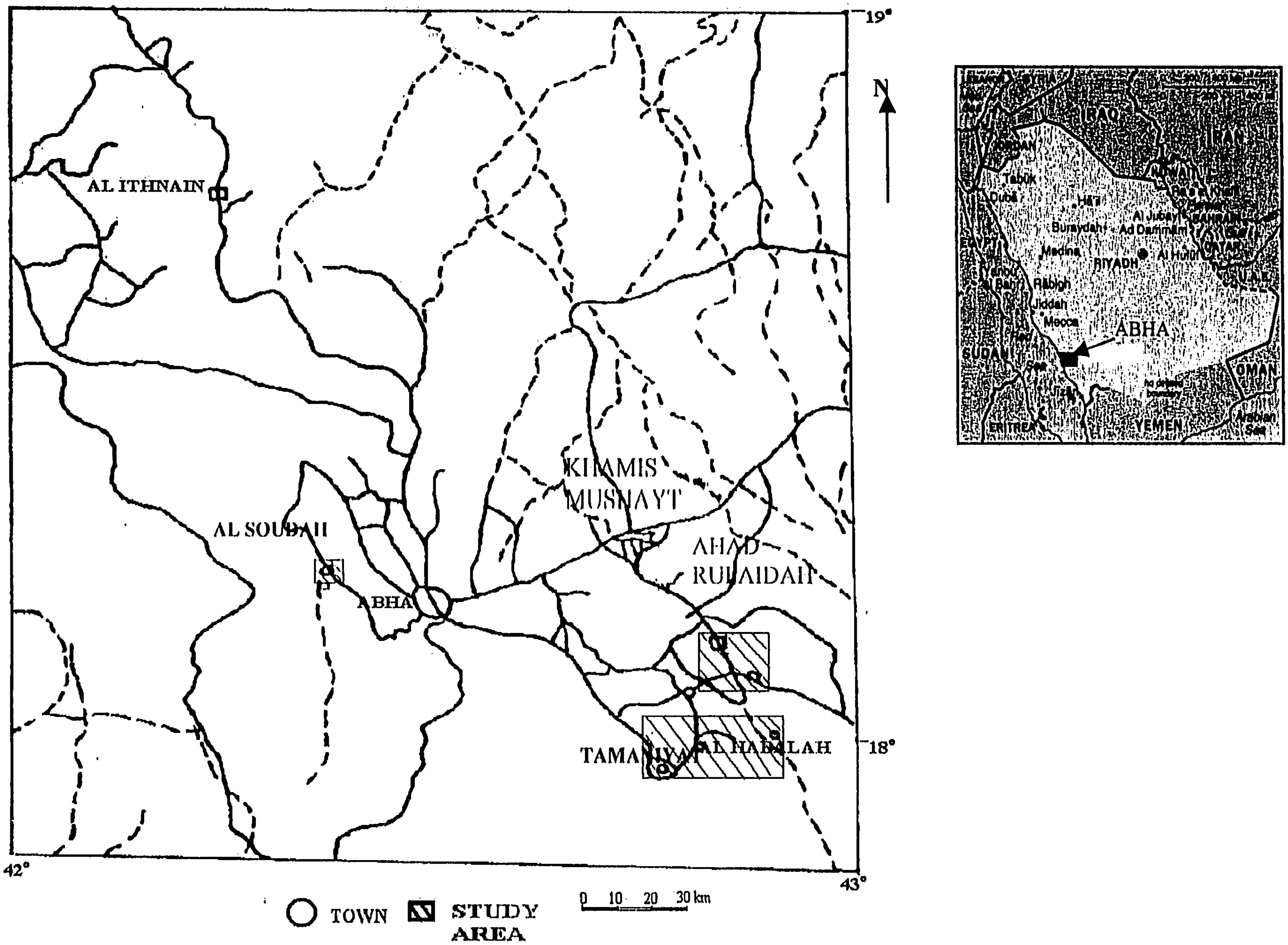

Figure 1.2. Map showing the locations of the studied localities. The inset map of Saudi Arabia also shows the general study area represented by Abha City.

TABLE 1.1. Table showing locations of the studied outcrops

Locality	Outcrop	Longitude	Latitude	Samples
Ahad Rufaidah	1	042° 50' 25"E	18° 09' 32"N	AR1 - AR3 & AR7 - AR9
	2	042° 50' 22"E	18° 09' 47"N	AR4 - AR6 & AR10 - AR17
	3	042° 44' 25"E	18° 02' 18"N	AR18-AR32 & ARL3SCS
	4	042° 50' 10"E	18° 06' 30"N	AR33-AR52, ARLC4K1 & ARLC4K2
Al Habalah	1	042° 46' 07"E	18° 00' 55"N	HA1-HA34
	2	042° 46' 17"E	18° 00' 37"N	HA23 - HA35 & OUT2I
	3	42° 44' 42"E	17° 59' 15"N	HA36 - HA43
	4	042° 46' 52"E	17° 58' 35"	HA53 - HA64
	5	042° 48' 07"E	18° 00' 38"N	HA44-HA52, OUT5I 1 & 2, OUT5K & OUT5QTZ
	6	042° 49' 43"E	18° 02' 47"N	HAP24-HAP64,OUT6QTZ, OUT6K & OUT6C
	7	042° 52' 26"E	18° 00' 19"N	HAP1 - HAP23
Al Soudah	1	042° 22' 17"E	18° 17' 42"N	S1 - S8, S13 - S22 & S28 - S31
	2	042° 21' 53"E	18° 17' 15"N	S32 - S35
	3	042° 21' 46"E	18° 17' 33"N	S9 - S12, S23 - S26

Sandstone present in this area occurs as isolated hills or outliers in an essentially basement terrain. The table below shows the locations of the fourteen outcrops investigated in this research. Sample locations are also indicated in this table. The samples are labeled starting with the lowest numeral from the base to the top of each of the outcrops.

1.4. General Geology

The geology of the Abha quadrangle (within which the studied localities lie) and its adjacent areas was mapped by various earlier workers including Brown and Jackson (1959), Coleman (1973a, b), Ratte and Andreasen (1974), Prinz, (1975), Simonson (1980), Stoesser (1984) and Greenwood *et al* (1982).

The Abha quadrangle is underlain by some of the Proterozoic rocks of the Arabian Shield (Greenwood, 1985). These basement rocks consist of an older (800 to 1000 Ma) ensimatic volcanic-arc complex and a younger (700 to 800 Ma) continental-margin (Andean-type) volcanic-arc complex (Greenwood *et al*, 1982). The Baish, Bahah, and Jiddah groups represent the older ensimatic complex while the Ablah and Halaban Groups constitute the continental-margin complex (Brown *et al*, 1989). Rocks of these complexes have been metamorphosed on regional scale to greenschists and amphibolite facies.

The Baish Group is composed mainly of metavolcanic rocks and beds of basalt while the Jiddah Group is made up of metavolcanics, thin to thick bodies of basalt, andesite and dacite. Rocks of the Bahah Group include biotite-quartz schist, carbonaceous phyllite, marble beds, carbonaceous slate, chert, greywacke, bedded andesite and dacite tuffs. The Ablah Group, confined to the western part of the quadrangle, marks the earliest phase of the formation of the continental margin complex. This group is composed of metamorphosed epiclastic sedimentary rocks. The interbedded basaltic, andesitic, dacitic, metavolcanic and epiclastic sedimentary rocks of the Halaban Group represent the later part of volcanic - arc addition to the quadrangle. Gabbroic, granodioritic, dioritic and granitic intrusives represent the Late Proterozoic intrusions that cut across all the older rock suites of this area.

The Wajid Sandstone overlies the metamorphosed volcanic and sedimentary rocks of the Baish, Bahah, Jeddah and Halaban Groups as well as the upper Proterozoic plutonic rocks ranging from gabbro to granite. The cessation of the igneous activity and subsequent peneplanation of the area was followed by widespread deposition of the Wajid Sandstone. Tertiary laterite, columnar basalt, sparse Quaternary basalt and surfacial materials complete the successions in the Ablah quadrangle (Figure 1.3).

The volcanic-arc complex and Proterozoic intrusive rocks in the southern part of the Arabian Shield are superimposed by many north-trending faults or fault zones which divide the shield into several north trending belts, referred to as tectonic belts (Greenwood *et al*, 1982). These belt bounding fault zones separate the rocks into units that are different in age, metamorphic grade, deformation style or lithofacies. These belts as represented in the Abha area, are the Bidah, the Ablah, the Tayyah, the Khadra and the Tathlith belts (Figure 1.3).

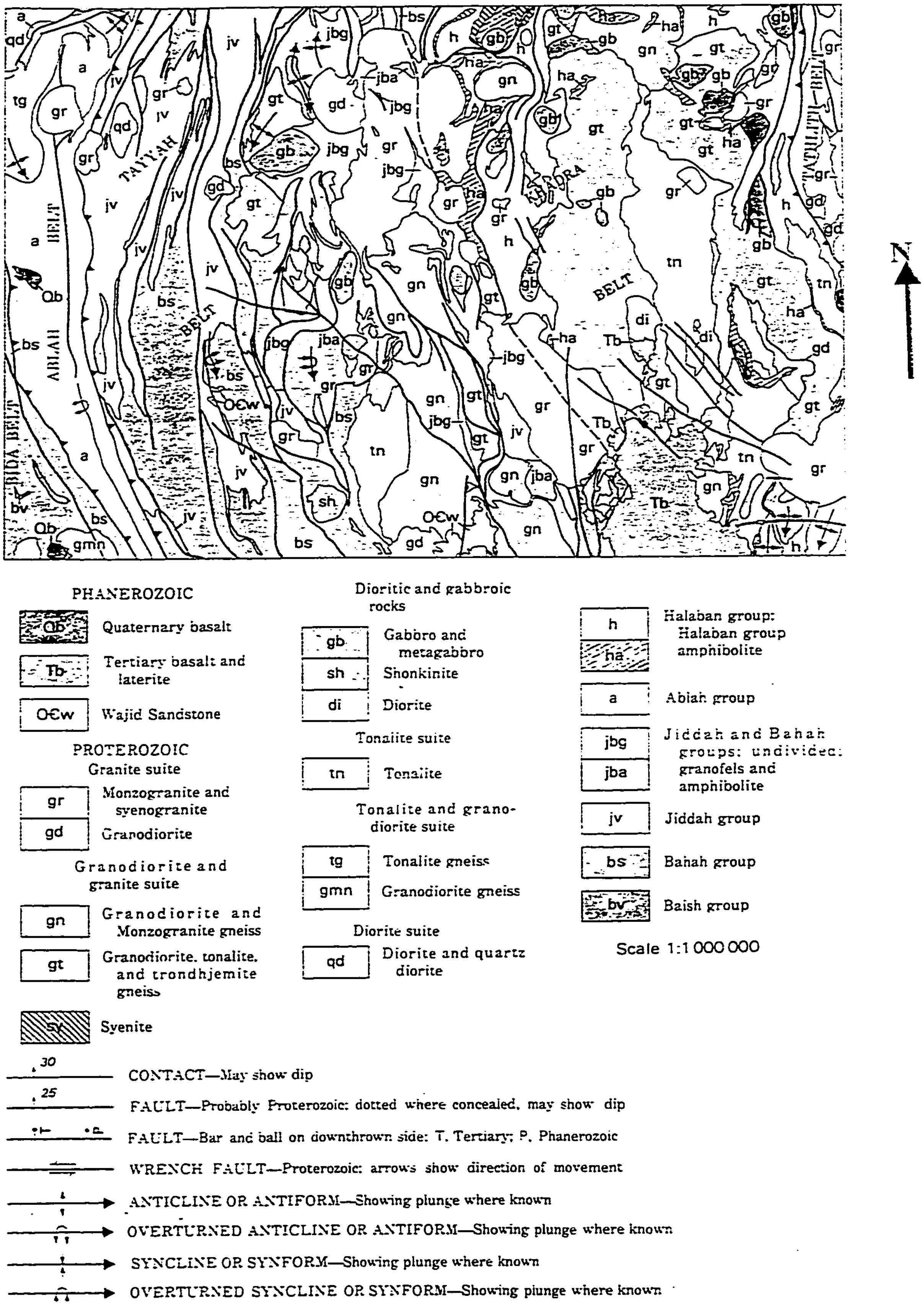

Figure 1.3. Geological map of Abha Quadrangle. This map shows the general geological and structural settings of the study area.

1.5. Previous Studies on Wajid Sandstone

The Wajid Sandstone was first recognized and named by Gierhart and Owen (1948, cited in Power *et al,* 1966) at the Jabal al-Wajid (type section) in the southwestern part of Saudi Arabia. It is equivalent to the Wajid Sandstone of Gierhart and Ramirez (1949), Steineke *et al,* (1958), Brown and Jackson (1959), Jackson *et al,* (1963); Wajid Formation of Intaconsult (1969), Pallister (1982) and Kellogg *et al* (1986) and the Ayn; Wajid and Bani Khurb Formations of Minatone (1984).

Powers *et al* (1966) formally described and documented the stratigraphy of the Wajid Formation at the type locality in Wadi Ad Dawasir and several other regions where it outcrops. The Wajid Sandstone nonconformably overlies the Precambrian basement complex and disconformably underlies the Late Permian, marine Khuff Formation (Powers *et al,* 1966; Intaconsult, 1969 and Pallister, 1982). It attains a maximum thickness of 950m at its type locality (Powers *et al,* 1966). However, a lesser thickness ranging between 500m and 600m was reported from borehole data (Ablabouvette and Villemur, 1973 and Brown *et al* 1989).

At the type locality, the Wajid Sandstone commences with a basal conglomerate unit overlying the basement complex. This unit, generally composed of cross-bedded sandstone and poorly consolidated quartz gravel conglomerate grades upward into well sorted, friable sandstone with limonite and hematite concretions as well as minor dolomite fragments (Gierhart and Ramirez, 1949 cited in Powers *et al,* 1966). The middle unit is composed of poorly sorted subangular, friable sands and sandstone intercalated with bands of hematite and quartzite beds. The upper section is constituted by greyish green to red silty shale with minor interbedded tan to purple fine grained sandstone (Henry and Brankamp, 1950; cited in Powers *et al*, 1966).

The absence of any body fossils in the Wajid Sandstone made its precise age assignment difficult. However, based on its stratigraphic position, lying between the Precambrian basement complex and Late Permian Khuff Formation, it was assigned Permian and older by Powers *et al* (1966). Based on the presence of trace fossils, algae and lithological similarity of the Wajid Sandstone to the Saq Formation, Hemer (1968) and Dabbagh and Rogers (1983) suggested a Cambro-Ordovician age for the Formation. The recovery of Silurian chitinozoan species *Conchitina latiformis, Cmicraceanthan robusta and Ancryrochitina nodosa* (Hemer, 1968), trace fossils *Scolithus (Tigillites) and Cruziana spp.* and conical structures in the thin shaly beds of the basal unit of the Wajid Sandstone suggest a Lower Ordovician or younger age (Alabouvette and Villemur, 1973). Tigillites are common in the Lower Ordovician to Lower Devonian Tabuk Formation in northern Arabia (Powers *et al*, 1966). Further evidence in support of an Ordovician age is the recovery of Ordovician hydrozoan *Disophyllum cf pellatum* that is typical of the glaciogene sediments of the Tigray in northern Ethiopia, equivalents of the Wajid Sandstone sediments (Dow *et al*, 1971 and Beyth, 1973). Helal (1964) suggested Permo-Carboniferous age for this Sandstone. McClure (1980) supported this age assignment based on palynological evidence.

Hadley and Schmidt (1975) indicated a fluvialtile depositional setting for the conglomerate beds in the upper unit of the Wajid Sandstone at the Bani Khatmah area.

McClure (1980) and Beydoun (1982) supported the glacial origin earlier suggested by Helal (1964).

Sable (1982) described the Wajid Sandstone outcrops in the northwestern corner of the Jabal Shaqan quadrangle and its extension further to the north as being mineralogically mature, poorly cemented by iron oxides and hydroxides with the iron occurring as concretions and massive layers at the basal parts. Pallister (1982) subdivided the Wajid Sandstone to Ilman and Shum Formations.

Dabbagh and Rogers (1983) ascribed the depositional setting of the sediments of this Sandstone to fluvial braided stream system in the southern and shallow marine in the northern areas, respectively. Based on trace fossil assemblages, these authors also conclusively correlated the Wajid Sandstone with those of the Cambro-Ordovician Saq Formation in the Central Arabian basin. Minatome (1984) studied the geology of the Wajid area in the southwestern Arabia and subdivided its successions into three formations; the Ayn, Wajid and Bani Khurb Formations with the term Wajid Formation applied only to the middle succession.

Kellog *et al* (1986) studied and mapped the Cambro-Ordovician Wajid Formation in Wadi Tathlith quadrangle. They differentiated the Formation into four members, each, beginning with a conglomeratic layer. These members consisting of Dibsiyah, Sanamah, Khusayyayn and Juwayl members are separated by distinctive discontinuities (Figure 1.4). Based mainly on grain size parameters, Moshrif (1988) attributed the sediments of the southern part of the Wajid Sandstone to a fluvial environment.

Greenwood (1985) documented a 235m thick sequence of the Wajid Sandstone in the Abha quadrangle. The sediments of the sequence encountered here were described as

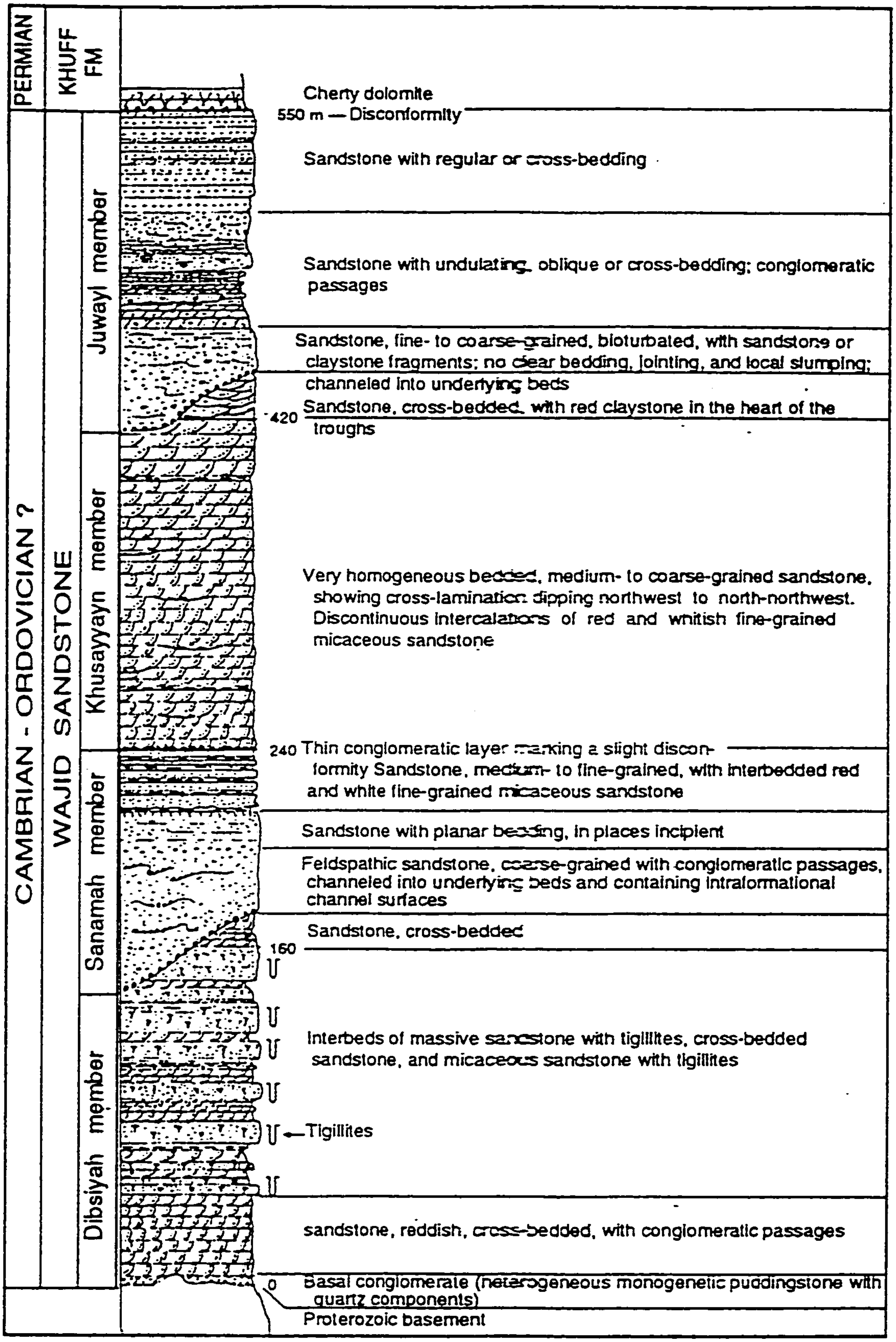

Figure 1.4. General stratigraphic succession of the Wajid Sandstone (After Kellog *et al*, 1986).

being essentially tabular to wedge shaped cross-bedded light brown to reddish quartz sandstone.

Vaslet (1989; 1990) correlated the Wajid Sandstone of Minatome (1984) to Qasim and Zarqa Formations in the central and northwest Arabia. This author also assigned the Sanamah, Khusayyayn and Juwayl Members of Kellogg *et al* (1986) to Ordovician and correlated them with the Sarah and Zarqa Formations and the Dibsiyah to the Saq Formation of the central Arabia.

Al-Laboun (1993), reviewed the nomenclature of the Paleozoic and Lower Mesozoic lithostratigraphic units of Saudi Arabia including the Wajid Sandstone. Stump and van der Eem (1994) studied the stratigraphy, depositional environments and periods of deformation of the Wajid Sandstone exposed in the southwestern Saudi Arabia. They attributed the four members of this sandstone, the Dibsiyah, Sanamah, Khussayyayn and Juwayl Members of Kellogg *et al* (1986) to depositional settings ranging from middle shelf, shallow marine, lagoonal, braided river system, fluviatile deltaic and eolian environments. Stump and van der Eem (1995) also elevated Wajid to group status and subdivided it to five formations (Dibsiyah, Sanamah, Qusaibah Shale, Khussayyayn and Juwayl) based on palynomorph taxa and recognition of several periods of uplift, which produced intraregional hiatuses between these units.

Hussain *et al* (1997) differentiated the Wajid in the Abha - Khamis Mushayt area of the Asir Region informally into lower and upper units based on texture, mineralogy and whole rock geochemistry. Based on on paleocurrent data, sand body geometry, mineralogy and textural attributes, these authors suggested a braided river sequence and a local provenance from a generally southerly direction.

CHAPTER TWO

METHODS OF STUDY

2.1. Introduction

This study involved detailed field investigation to measure and map the outcrops followed by laboratory analyses of samples and data interpretations. A summary of the approaches and the objectives of this study is outlined as flow chart (Figure 2.1)

2.2. Field Investigation

Fourteen (14) outcrops of the Wajid Sandstone in three different localities: Ahad Rufaidah (AR), Al Soudah (S) and Al Habalah (HA and HAP) areas in the Asir Region were mapped and logged during a six-week long field trip. The investigated outcrops in Ahad Rufaidah, Al Soudah and Al Habalah I (with samples labelled HA) localities represent the Red Unit while outcrops in Al Habalah area II (with samples labelled HAP) include the upper part of the Red and the entire Grey Unit recognized in this study. Field data including lithologic description, paleocurrent and fracture trends were noted during

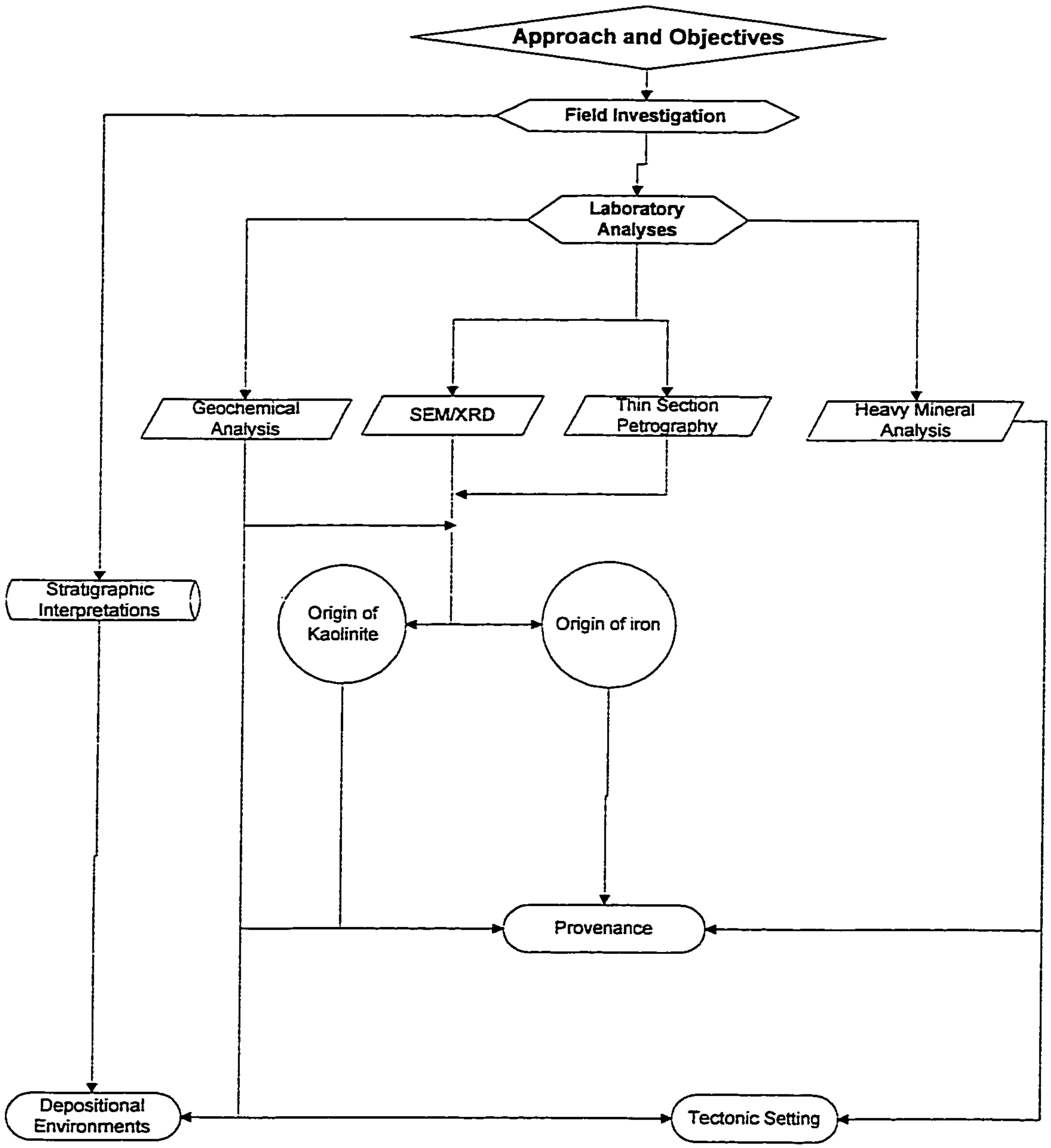

Figure 2.1. Flow chart showing the outline of the approaches and objectives of this study.

this fieldwork. A total of three hundred (300) samples representing different lithologic units were also collected for laboratory investigation.

2.3. Laboratory Analyses

Of the three hundred samples collected during the field investigation, eighty-three (83) were processed for petrographic analysis. A total of eighty-seven (87) samples including ten (10) basement rock samples were processed for elemental (ICP) and bulk composition (XRF) geochemistry while forty-two (42) others were analyzed using scanning electron microscopy (SEM) and x-ray diffractometer (XRD). A total of forty-four (44) samples were also processed for heavy mineral analysis.

2.3.1. Thin Section Petrography

Virtually all the samples except the highly compacted ferruginous and quartzite samples were impregnated with epoxy under vacuum pump. The impregnation was allowed to cure overnight. The slabs were smoothly polished with calcium carbide on plane glass and mounted on glass slide. The glass-mounted slabs were subsequently polished for thin section microscopy after curing.

2.3.2. Heavy Mineral Separation

The samples for heavy mineral analysis were soaked overnight in detergent solution in order to disaggregate them. They were subsequently wet sieved with a 63μ-sieve mesh. The residues were dried in an oven and sieved into different size fractions. A 2-3ϕ (250-125μ) class-fraction (Carver, 1971 and Uddin and Lunderbeg, 1998) was chosen for analysis.

The heavy minerals were separated from the samples with the use of tribromomethane (bromoform) with a 2.89 specific gravity. The separation setup includes a separating flask mounted on retort stand. At the lower end of which was placed a glass beaker containing separating funnel and filter paper. The heavy liquid was poured into the separating flask with the flask's valves being tightly closed. Sample of known weight was poured into the flask contained heavy liquid, stirred frequently and left to stand for sometime to allow all the heavies to settle at the lower end of the flask. The recovered heavy mineral fraction was drained into the filter paper containing separating funnel and was rinsed off the heavy liquid severally by washing with acetone. These residues were subsequently dried and weighed.

The heavy mineral grains were mounted by sprinkling them evenly on epoxy contained glass slides. Heavy mineral petrography was carried out with aid of Zeiss Auxio-phot optical binocular microscope and reference to relevant literature (Krumbein and Pettijohn, 1966 and Scholle, 1979). Total grain counts range generally from 200 to 500 grains per sample with only few samples below or above this range. The wellpreserved grains were photographed. Ten (10) samples, rich in opaque minerals, were analyzed with XRD and SEM for better identification of the opaque minerals.

2.3.3. Scanning Electron Microscopy (SEM)

For the purposes of observing the microstructures, grain boundary and better characterization of the sediments as well as elemental determination SEM analysis was carried out. The samples for SEM study were placed in holders (platinum disc) held with carbon paint, dried and gold coated in a vacuum with sputter coater. The coated samples were subsequently scanned with SEM (models JSM-5800LV and JSM-840) under electron beam not greater than 20KeV.

2.3.4. Geochemical Sample Preparation

The elemental and bulk chemistry of the samples were determined by using inductive coupled plasma (ICP) and X-ray fluorescence (XRF) respectively. The samples were powdered using agate mortar and pestle, rock crushing machine and dry sieved with 106μ sieve. The analyses of the powdered residues were subsequently carried out in a commercial laboratory (Chemex Labs, Canada) following standard industrial protocols.

2.3.5. Clay Mineralogy and X-Ray Diffraction

The clay fractions of sixteen (16) samples were separated using the standard technique outlined by Folk (1968). The technique enables complete separation of the clay content ($\leq 4\phi$ or 63μ) out of the clay-rich silt to fine sand sediments. The separated fraction was centrifuged, oven dried, later made into paste with acetone and spread evenly on glass slide. The clay fraction from all the sixteen (16) samples and a batch of other twenty-four (24) powdered samples were analyzed for their mineralogical phases using a XRD device (JEOL Model JDX-3530).

X-ray diffraction experimental procedure involves subjecting the powdered materials to Cu fine focus tube at 40kV and 30mA using a divergent slit of 1 degree, scatter slit of 1 degree and 0.2mm nickel filter. The scanning speed and interval for data collection was 0.01 degree at 2θ per second with scanning angle of 4° to 80° for the general mineralogical detection and 2° to 30° for the clay mineralogy. In order to identify the expandable clay (e.g. montimorilonite), the clay samples were subsequently glycolated by exposing them the ethylene glycol vapor overnight at about 100°C in oven.

CHAPTER THREE

STRATIGRAPHY

3.1. Basement Complex

The basement complex is exposed in all the three studied localities. In Al Soudah area, the Wajid Sandstone overlies the basement complex comprising of mica schists, quartzite veins and talc nonconformably. Mica schists, granites and pegmatites are the dominant basement rocks in contact with the Wajid Sandstone in the Ahad Rufiadah locality. In Al Habalah locality, granite constitutes the main basement rock. Some of the granites (e.g. those underlying Wajid Sandstone at outcrop 1) in Al Habalah area are bedded. In places, schists, xenoliths of different metamorphic rocks as well as veins of some igneous rocks including, diorites were encountered close to the contacts. Elsewhere in the area, chlorite greenschists, mica schists, amphibolites, gabbro and granites outcrops were observed.

3.2. Lithofacies of the Wajid Sandstone

The Wajid Sandstone at the study area is represented by a 300m thick sequence composed dominantly of coarse to medium grained cross bedded sandstone and kaolinite-rich silty claystone overlying the basement complex nonconformably (Figure 3.1). The thickness of the Sandstone increases towards the east with thickness of about 55m at Al Soudah, 110m at Ahad Rufaidah to about 300m at Al Habalah National Park respectively.

Based mainly on the color and distribution of iron-rich horizons, the Wajid Sandstone in the study area has been informally divided into two major lithofacies in this study: the Red Unit and Grey Unit. (Figures 3.1). These units are separated by an approximately 50cm to 1m thick conglomerate bed. A generalized stratigraphic succession of the study area is presented in Figure 3.1. The stratigraphic succession of the individual outcrops is included in Appendix I. These units and the basal conglomerate deposit marking the surface of unconformity are briefly described below.

3.2.1. Basal Conglomerates

The base of the Wajid Sandstone commences with a lag deposit that marks the regional surface of unconformity. The thickness of this conglomerate bed varies from a thin 20cm to a thick 2m in places. Quartz pebbles and cobbles, and rock fragments, mostly intraformational claystone constitute the sediments of this regional surface of unconformity (Figure 3.2a). The pebbles vary in size, ranging in length from few mm to

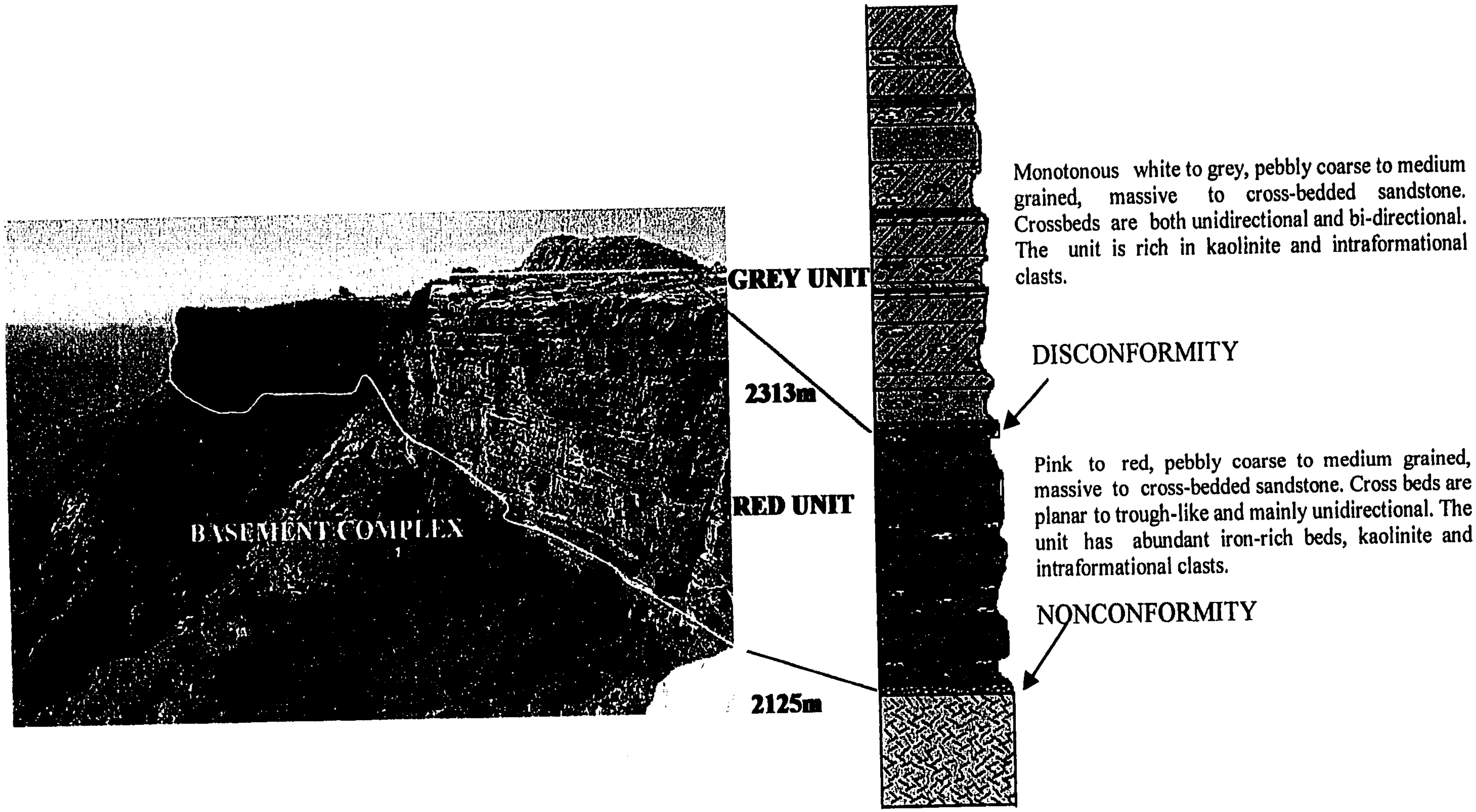

Figure 3.1. Photograph and generalized stratigraphic column showing the Wajid Sandstone overlying the Precambrian basement complex rocks nonconformably.

Figure 3.2. Photographs showing unconformities that separate (a) the basement and Wajid Sandstone and (b) the Red and the Grey Unit. The conglomerates are both monomitic and polymitic. Their long axes could be up to 10cm or more.

10cm and in width, from 4 to 5cm. These pebbles vary in shape from angular to well - rounded.

3.2.2. Red Unit

Overlying the conglomerate horizons are alternating successions of dominantly red-pink, occasionally brick red, grey to white, massive to cross-bedded sandstones of the Red Unit. These sediments vary from predominantly pebbly coarse, medium to occasionally fine-grained, moderate to fairly well sorted and largely friable to indurated aggregate. Quartzite horizons measuring up to ~14m thick at base of outcrop 2 in Al Soudah locality, 10m thick at base of outcrop 1 and 3m thick at the tops of outcrops 5 and in the Al Habalah locality occur within this unit.

Ferruginous horizons are widely distributed in this Red Unit. These occur as parts of cross bed foresets, thin beds (few centimeters to about 2 meters) and fracture infills (Figures 3.3a and 3.3b). The iron-rich sediments also occur as concretions and nodules reflecting differential cementation and matrix strength. Claystone (kaolinite lenses) and patches of caliche are in close association with the ferruginous horizons of this unit. The claystone occurs as thinly laminated to cross-laminated lenses (Figure 3.4a). The surfaces of these claystone lenses are occasionally pebbly.

Intraformational clasts, consisting dominantly of claystone clasts and rarely other rock fragments, are also characteristic of this unit (Figure 3.4b). These clasts are also common within the claystone lenses. The length of the clasts ranges from few millimeters to about 10cm and could be up to 4cm in width. The imbrications trend of these clasts is to NW orientation. This trend is generally in agreement with cross bed readings.

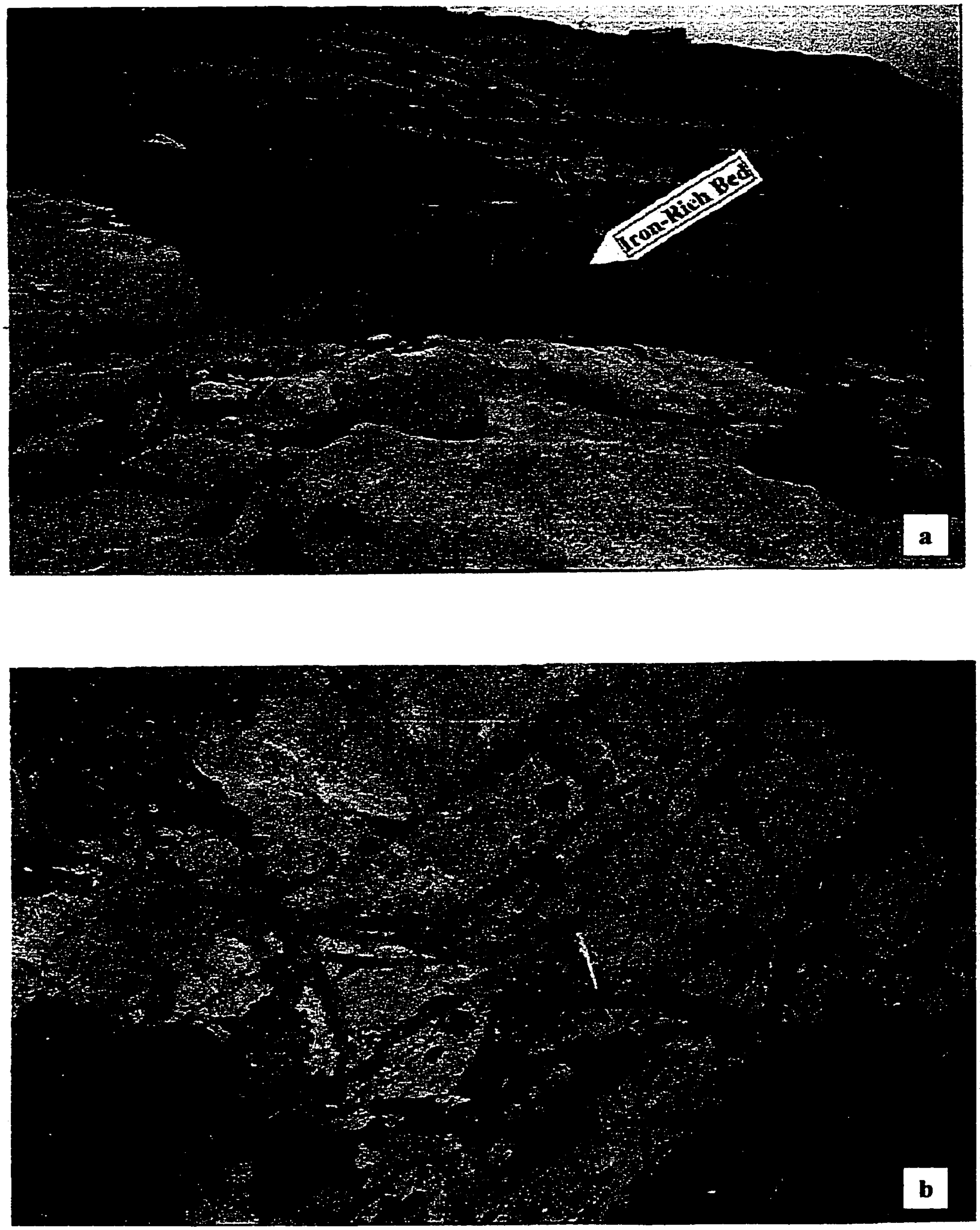

Figure 3.3. Photographs showing (a) Thick ferruginous beds and (b) Ferruginous material occurring as fracture infills.

Cross stratifications are dominantly low angle (mostly below 20°), planar to trough-like and unidirectional (Figure 3.5a) with minor variability. The thickness of the cosets and foresets range from 1 to 3m and 2cm to 10cm respectively. The cross-beds azimuths trend mostly to the north.

The grain size distribution in the Red Unit appears blocky. However, a fining upward sequence is also apparent especially in the kaolinite-rich intervals.

Fractures represented by sets, which are up to 35cm long and trending dominantly in north-south and east-west are common in this unit. The fractures are healed in places by ferruginous materials (Figure 3.3b).

3.2.3. The Upper Unit

A conglomerate bed with a thickness ranging from 50cm to ~ 1m was observed at an elevation of 2387m in outcrop 6 and 2313m in outcrop 7, respectively in the Al Habalah locality II. This bed marks the transition from the Red Unit to the Grey Unit. The conglomerates are composed of both quartz pebbles and intraformational clasts represented by granite fragments and claystone clasts (Figure 3.2b). The Grey Unit is about 76m and 123m thick in outcrops 6 and 7 respectively. A basal light grey, coarse grained, friable, thickly bedded to massive, fining upward sandstone sequence follows the conglomerate beds in both outcrops. The sediments of this unit are generally composed of a monotonous sequence of white-greyish, pebbly, coarse to medium, occasionally fine-grained, massive to cross-bedded sandstone. Fining upward trend that commences the kolainitic claystone in the Red Unit is also present within this unit. The kaolinitic claystone in this unit appears brighter and more friable than that in the underlying Unit.

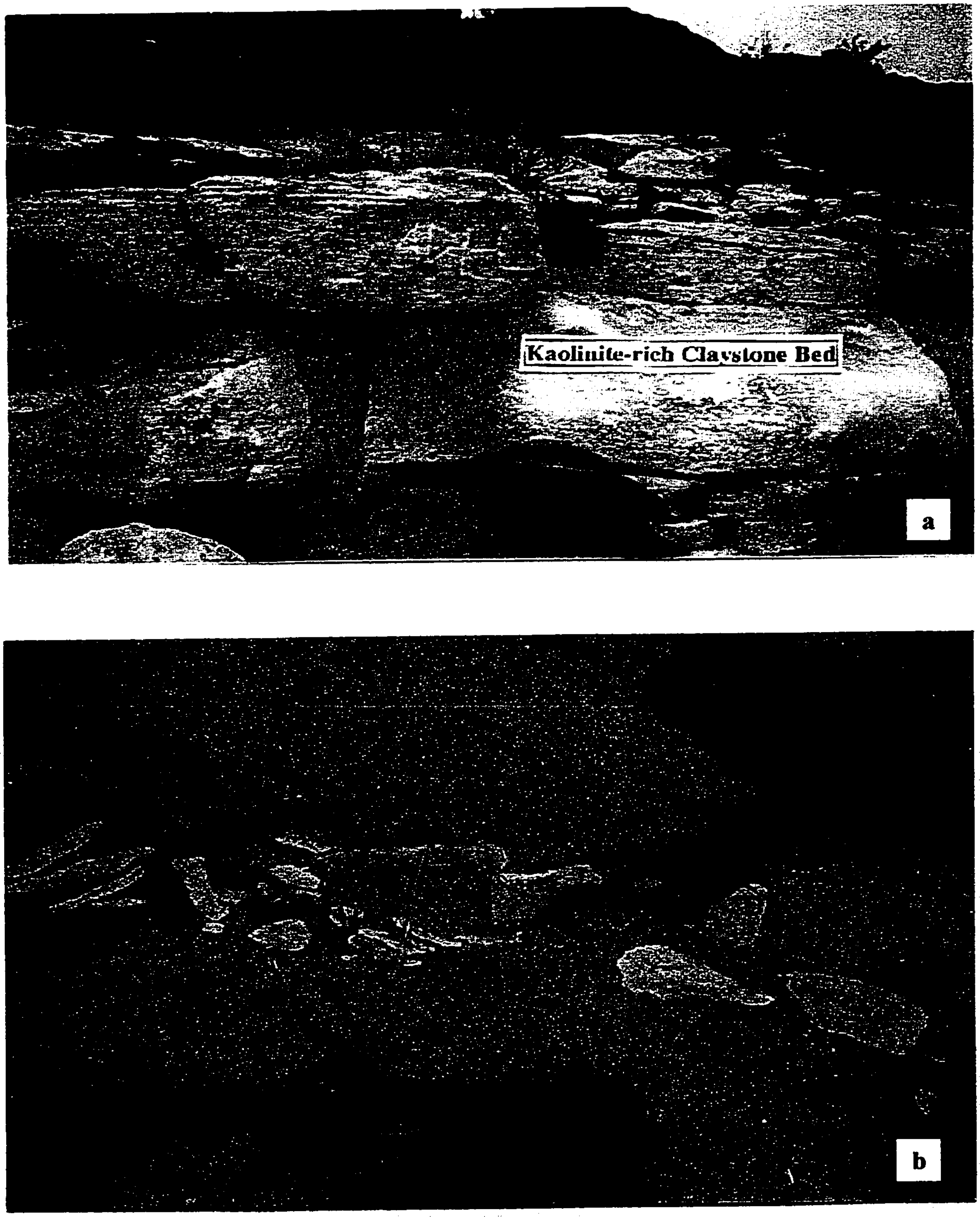

Figure 3.4. Photographs showing kaolinitic claystone lenses and intraformational clasts in Wajid sandstone: (a) Kaolinitic claystone lenses are abundant in both the Red and Grey Units. (b)The intraformational clasts (dominantly claystone) derived from kaolinite-rich claystone horizons, are common in Wajid Sandstone. The individual clasts are up to 40cm long in dimension.

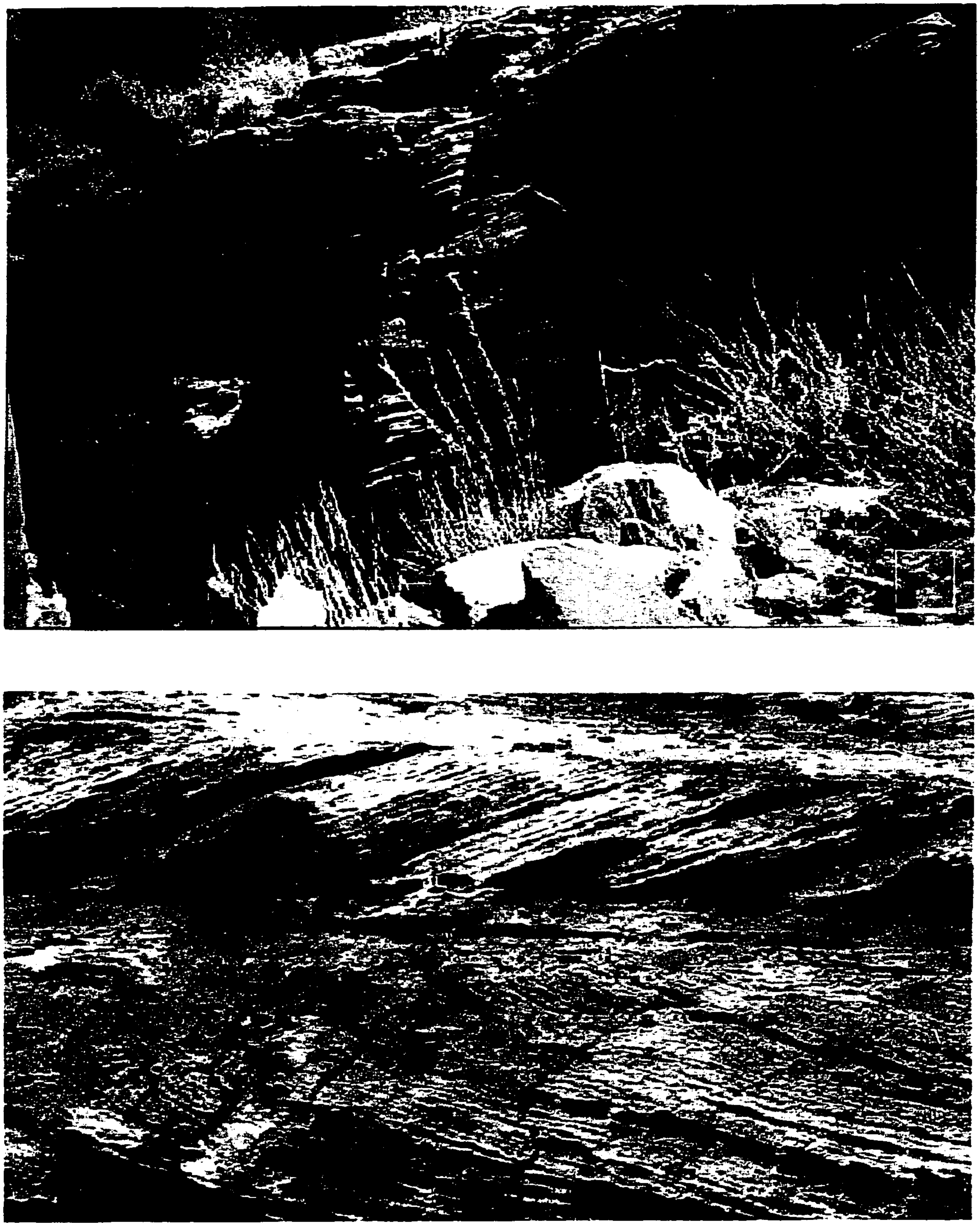

Figure 3.5. Photographs showing typical cross stratifications in Wajid Sandstone (a) uni-directional cross beds in the Red Unit and (b) bi-directional cross beds in the Grey Unit.

This might be attributed to the lower concentration of ferruginous materials in this unit. Both kolainite lenses and intraformational claystone clasts observed in the Red Unit are also present in this unit. However, small patches of caliche that commonly associate with the iron-rich beds and kaolinite lenses in the Red Unit are absent in the intervals of this unit

The highly indurated quartzite beds observed in the Red Unit are also present within this unit. The quartzite beds are up to 3m thick and cap the top of outcrop 6 in the Al Habalah locality II. The quartz grains of the quartzite beds are highly compacted. The grain boundaries are however, still apparent. Pebbles and cobble size fragments are common in this quartzite interval.

Cross stratifications of this unit are essentially low angle (<20°), planar, both unidirectional and bi-directional (Figure 3.5). The thickness of the foresets varies from 2cm to 10cm and trend predominantly to the north. However a minor variability in the easterly direction is apparent.

3.3. Paleocurrent Analysis

The three hundred (300) paleocurrent readings acquired during the field study, are presented as rose diagrams (Figure 3.6 and Appendix I) using Oriana (R) for windows. The observed trends indicate a dominantly northerly current flow direction suggesting a predominantly southernly source of the sediments.

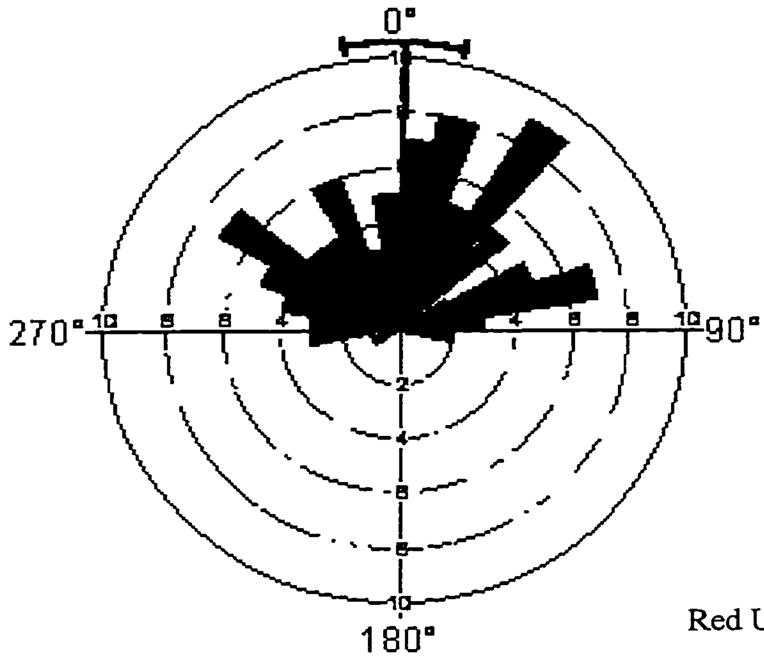

Red Unit

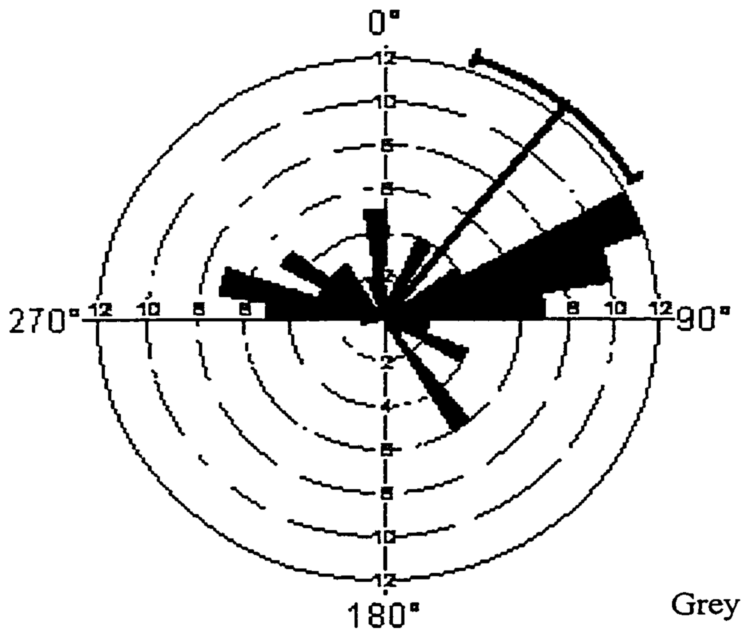

Grey Unit

Figure 3.6. Rose diagrams showing the general trends of paleocurrent distribution in Wajid Sandstone. Note the predominantly northerly trend.

3.4. Correlation with type sections in Wadi Ad Dawasir

The Wajid Sandstone succession at the type locality, Wadi Ad Dawasir is divided into four members: Dibisyah Member followed in ascending order by Sanamah, Khussayyayn and Juwayl members (Kellog *et al*, 1986). Stump et al (1995) upgraded the Wajid Formation to group status. In addition to recognizing the above members as formations, they named the Silurain Red Mudstone overlying the Sanamah as Qusaiba Shale based on the assumption that this unit is correlatable with the Qusaiba Shale of Central Arabia. The most recent subdivision of the Wajid succession is that of Laboun (1999; personal communication). This author subdivided the Wajid Sandstone into Dibisyah, Sanamah, Madarah Shale (equivalent of the Qusaiba Shale of Stump *et al*, 1995), Khussayyayn, Juwayl and Ruhayah Formations. This subdivision was based on pronounced unconformities separating the formations.

Correlation of the Wajid Sandstone exposed in the study area with other localities, most importantly the type sections at Wadi Ad Dawasir appears difficult because of limited data and lack of definitive correlation tool especially fossils and marker beds. With the recognition of these shortcomings, a tentative correlation is attempted in this study. Based on a reconnaissance field investigation at the type locality (Wadi Ad Dawasir), the lower unit (Red Unit) is probably correlative with the lower Dibisiyah Formation while the upper unit (Grey Unit) is equivalent to the Khussayyayn Formation (Figure 3.7). The overall lithology of the outcrops at latittude 20° 06' 76"N; longititude 44° 06' 77"E and 20° 15' 16"N and longitude 44° 17' 28"E in Wadi Ad Dawasir appear similar to those of the Red Unit in the Abha-Khamis Mushayt area. These outcrops which

KELLOG *ET AL* (1986)			LABOUN (1999, Personal Comm.)		THIS STUDY
AGE	MEMBER		AGE	FORMATION	INFORMAL UNIT
			TRIASSIC AND YOUNGER		
PERMIAN	KHUFF FORMATION		PERMIAN	RUHAIYAH	
CAMBRIAN- ORDOVICIAN	WAJID SANDSTONE	JUWAYL MEMBER	CARBO-PERMIAN	JUWAIL	
		KHUSAYYAN	DEVONIAN	KHUSAYYAN	GREY UNIT
		SANAMAH	SILURIAN	MADARAH	PROBABLY ERODED
			ORDOVICIAN	SANAMAH	
		UPPER DIBISIYAH	CAMBRIAN	UPPER DIBISIYAH	
		LOWER DIBISIYAH		LOWER DIBISIYAH	RED UNIT

Figure 3.7. Tentative correlation of the informal units with the type sections at Wadi ad Dawasir.

unconformably overly the basement rocks (diorite and pegmatites) commence with pebbles and conglomerate and tallus of ferruginous materials at the base. The overlying sediments are essentially red to brown, pebbly coarse grained and well cross-bedded sandstone. The lower unit is overlain in places by grey, bidirectionally cross-bedded, *tigillites* bearing upper unit (upper Dibisiyah). These *tigillites* bearing upper Dibissiyah at the type locality is absent in Abha-Khamis Mushayt area. It has been probably eroded.

The absence of *tigillites* and the occurrence of kaolinite lenses, in the Grey Unit of this study, diffrentiate it from the upper Dibisiyah. The overall lithology of the Grey Unit appears similar to that of the Devonian Khussayyayn Formation of the type locality. Like the Grey Unit, the Khussayyayn Formation also lacks *tigillites* and is rich in claystone. The absence of sedimentary sequence containing tillites, moraines, paleovalleys and striations (Vaslet, 1989, 1990) indicate the absence of the Sanamah Formation in the investigated area.

Based on the similarity in lithology and structures (cross stratifications), Laboun (1999; personal communication) correlated the Grey Unit with the Khussayyayn at the type locality. However, fish remains that were earlier reported from the Khussayyayn to the south (Najran) of the study area are absent in the Grey Unit.

CHAPTER FOUR

PETROGRAPHY

4.1. Introduction

The compositions of sandstones indicate the provenance (Blatt. 1967a, Dickinson and Suczek, 1979) and tectonic settings at provenance (Dickinson, 1985 and Dickinson *et al*, 1983). In addition, compositions of sandstones also provide clue on climate (Basu, 1985 and Girty, 1991) and physiography (Lewis and McChonchie, 1994). The extent of weathering and the selective destruction of minerals on their way from source to the depocenter may be a function of time. Roedder (1990) and Rooney and Basu (1994) used clay mineral content of sandy sediments to interpret the primary source rocks, their sedimentation history and Eh and pH of the diagenetic fluid. Moral-Cardona *et al* (1996) combined quartz grain surface features, petrologic and heavy mineral evidence to determine provenance.

4.2. Thin Section Petrography

Thin section petrography shows that the Wajid Sandstone is dominantly a pebbly, coarse to medium, occasionally silty to fine grained quartz rich sandstone. The grains are largely angular to subrounded, occasionally rounded to well-rounded and generally moderate to well-sorted Figure 4.1a. Packing is essentially tight to loose with floating grain texture (Plate 1, Figure a,) prominent in the thickly cemented ferruginous samples. Packing inhomogeneity was also observed (Figure 4.1b).

4.2.1. Quantitative Mineralogy

Quartz dominates the modal composition of the studied samples with its absolute values averaging between 65 and 69% in the investigated localities (Table 4.1). Quartz grains are represented by both monocrystalline and polycrystalline varieties with the monocrystalline type being the dominant variety (Plate 1, Figure c). Both varieties of quartz exhibit straight to undulose extinction and appear unstrained. The polycrystalline grains are equant to subequant in shape and are dominantly characterized by more than three subgrains with suture contact. Zircon, tourmaline, rutile, feldpar, hornblende, biotite and muscovite as well as fluid were observed as inclusions in the quartz grains.

Feldspar occurs as minor (up to 4%) constituent in the samples. Only a few grains of microcline and plagioclase were recorded. These grains, are, however, mostly degraded (Plate 1, Figures e-f).

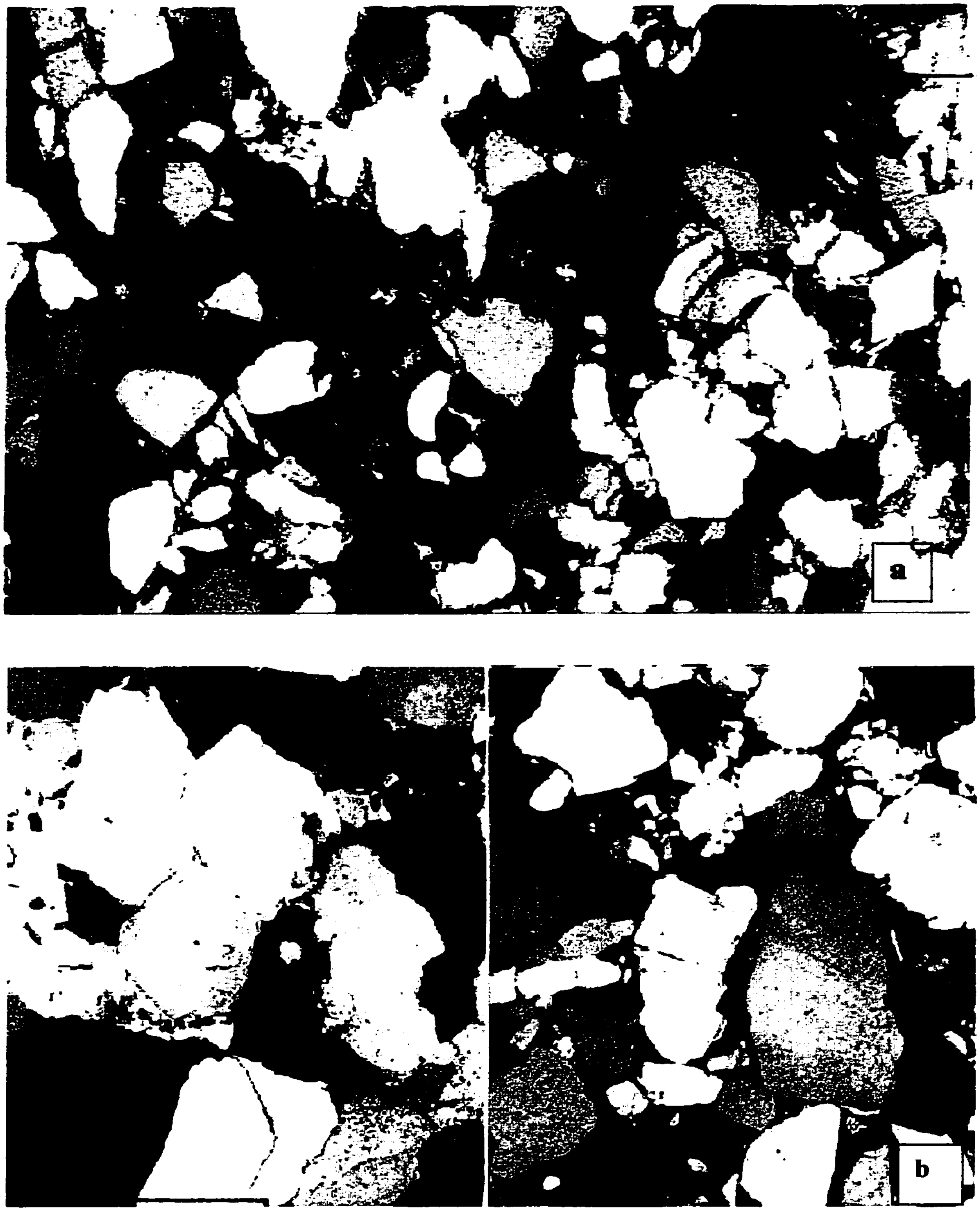

Figure 4.1. Photographs showing: (a) Typical composition of Wajid Sandstone. This Sandstone is typically coarse to medium grained, occasionally fine, dominantly angular to subrounded and generally poor to well sorted. (b) Packing inhomogeneity shown in (b) is an evidence of the dissolution of calcite cement.

PLATE 1

Figure a.	Photomicrograph showing distributions of floating grains in thickly cemented ferruginous sample. Note the poor sorting and angular to fairly rounded nature of the grains (mag. x50).
Figure b.	This photomicrograph shows characteristic mica deformation that indicates moderate to high degree of compaction in sediments. The mica is in contact with coarse-grained quartz (mag. x125).
Figures c & d.	Photomicrographs depicting the nature of grain contacts. Figure c also shows a polycrystalline quartz grain. This grain makes point (PC) long (LC), concavoconvex (CC), and suture (SC) contacts with the other surrounding grains (mag. X 40 and x125, respectively).
Fgures e & f.	Photomicrographs showing corroded microcline (feldspar) grains. Corroded grains like these indicate dissolution of the labile minerals in the Wajid Sandstone (mag. x125 and x40, respectively).


a
Quartz
Deformed Mica
b
LC
PC
c
SC
CC
d
Corroded Microcline
Quartz
e
f

PLATE 1

TABLE 4.1. Table showing the modal composition of Wajid Sandstone. As listed in the table, quartz is the most abundant component of the framework grains.

Ahad Rufaidah											
Sample	**Qtz.**	**Feldspars**	**Mica**	**L.G.**	**H.M.**	**Matrix**	**Cement**	**Porosity**	**Q**	**F**	**L**
AR51	70	0	0	0	0	2	20	8	100	0	0
AR49	74	1	0	2	<1	2	15	6	96.1	1.3	2.597
AR47	70	0	1	0	<1	3	12	10	100	0	0
AR39A	75	0	0	3	0	2	12	8	95.15	0	3.85
AR35	71	0	0	0	0	6	8	13	100	0	0
AR32	76	<1	0	0	0	2	15	6	98.7	1.3	0
AR31	72	0	0	0	0	2	18	8	100	0	0
AR28	74	0	1	2	2	10	6	5	97.47	0	2.532
AR26	64	0	4	0	2	2	25	3	100	0	0
AR24	79	0	0	0	<1	2	12	6	100	0	0
AR21	71	0	2	0	0	6	5	15	100	0	0
AR20	64	1	2	0	1	5	15	12	98.46	1.54	0
AR19	72	0	0	0	0	3	20	5	100	0	0
AR18	70	0	1	0	<1	2	25	6	100	0	0
AR15	75	1	1	<1	2	2	20	5	98.57	1.43	0
AR14	76	0	1	0	0	2	15	6	100	0	0
AR12	77	1	0	0	0	2	8	12	98.72	1.28	0
AR9A	65	2	2	0	<1	2	25	3	97.01	2.99	0
AR8	68	4	3	0	<1	2	8	14	94.44	5.56	0
AR6	72	2	2	0	<1	10	7	6	97.3	2.7	0
AR4B	70	1	1	0	<1	2	20	5	98.46	1.34	0
AR1	62	4	3	0	<1	2	20	3	89.86	5.8	4.348
Average	**66**	**2**	**1.5**	**0**	**0**	**2**	**20**	**5.5**	94.93	2.9	2.174
Al Habalah I											
Sample	**Qtz.**	**Feldspars**	**Mica**	**L.G.**	**H.M.**	**Matrix**	**Cement**	**Porosity**	**Q**	**F**	**L**
OUT2I	61	0	2	3	<1	3	25	5	95.45	0	4.55
OUT5I1	73	1	0	1	0	2	18	5	97.33	1.33	1.33
OUT5QTZ	92	0	0	1	0	0	5	3	98.92	0	1.07
HA62	70	0	1	0		3	18	8	100	0	0
HA58	72	0	0	0	0	3	10	15	100	0	0
HA55	69	1	1	0	<1	3	5	20	98.57	1.43	0
HA53	70	2	0	0	<1	2	20	5	98.6	1.4	0
HA49	67	1	2	2	<1	2	7	18	95.71	1.43	2.86
HA45	65	0	2	1	0	2	10	20	98.48	0	1.51
HA43	70	0	1	2	0	2	20	5	97.22	0	2.77
HA41B	72	1	1	0	0	2	6	18	98.63	1.37	0
HA40	63	1	5	3	<1	2	8	18	94.02	1.5	4.48
HA39	69	1	1	3	0	5	6	15	94.52	1.37	4.1
HA38	66	2	1	0	<1	2	22	6	96.96	3.04	0
HA36	70	1	0	2	<1	2	6	18	95.89	1.37	2.74
HA32	80	1	2	2	0	3	12	10	96.25	1.25	2.5
HA31B	65	1	2	2	<1	2	12	10	95.59	1.47	2.94
HA31	70	1	1	2	0	2	14	10	95.89	1.37	2.74
HA29	61	0	2	3	<1	6	20	7	95.31	0	4.69
HA27	70	0	2	0	1	2	25	5	100	0	0

HA25	70	0	1	0	<1	3	25	5	100	0	0
HA24	71	0	0	0	<1	2	20	6	100	0	0
HA22	71	3	2	0	<1	3	15	5	95.95	4.05	0
HA20	68	0	0	0	<1	5	15	10	100	0	0
HA18	62	2	1	2	<1	7	20	5	93.94	3.03	3.03
HA16	74	1	0	1	<1	2	18	6	97.18	1.41	1.408
HA15	71	1	0	2	0	4	7	15	95.95	1.37	2.7
HA12	62	1	2	1	<1	2	30	6	96.49	1.75	1.75
Unlabelled	69	0	2	0	<1	10	8	12	100	0	0
*HA28	5	0	0	0	0	90		3			
Average	**69.41**	**0.758**	**1.172**	**1.1379**	**0.09**	**3.03**	**14.72**	**1.03**	**97.34**	**1.03**	**1.6126**
					Al Habalah II						
Sample	**Qtz.**	**Feldspars**	**Mica**	**L.G.**	**H.M.**	**Matrix**	**Cement**	**Porosity**	**Q**	**F**	**L**
OUT6QTZ	63	0	0	0	0	2	30	5	100	0	0
HAP52	64	1	1	0	<1	3	10	20	98.43	1.56	0
HAP40	71	0	0	2	<1	3	8	15	97.26	0	2.74
HAP33	68	1	2	2	1	3	13	10	95.77	1.41	2.817
HAP29	68	1	2	2	<1	3	8	15	95.77	1.41	2.817
HAP28	60	0	1	0	<1	4	20	7	100	0	0
HAP25	61	0	2	0	0	6	25	6	100	0	0
HAP24	62	0	2	0	<1	10	10	15	100	0	0
HAP16	67	0	2	3	1	2	5	20	95.71	0	4.286
HAP10	66	0	1	2	<1	2	8	20	97.05	0	2.94
HAP9	68	0	1	4	1	2	6	18	93.15	1.37	5.48
HAP8	67	0	3	3	<1	3	5	18	95.71	0	4.286
HAP7	69	1	1	2	<1	2	4	20	98.83	1.39	2.77
HAP6	68	0	2	2	0	3	5	20	97.14	0	2.857
HAP5	66	0	2	3	0	3	7	19	95.65	0	4.35
HAP1	69	1	0	2	<1	2	20	5	95.83	1.39	2.77
*OUT6C	5	0	0	0	0	92	3				
Average	**66**	**1**	**0.5**	**1**	**<1**	**2.5**	**15**	**12.5**	**97.13**	**1.48**	**1.385**
					AL Soudah						
Sample	**Qtz.**	**Feldspars**	**Mica**	**L.G.**	**H.M.**	**Matrix**	**Cement**	**Porosity**	**Q**	**F**	**L**
S23	71	0	1	0	0	3	5	20	100	0	0
S21	73	0	1	0	<1	6	4	15	100	0	0
S20	67	0	1	1	<1	2	25	3	97.1	1.45	1.45
S19A	67	1	1	3	0	2	8	18	94.44	1.39	4.167
S17	68	0	1	1	<1	4	7	18	98.59	0	1.408
S14	71	0	1	0	1	2	6	20	100	0	0
S13	67	0	1	0	<1	5	18	8	100	0	0
S12	75	1	1	0	<1	2	8	12	98.68	0	1.315
S10	67	0	0	0	<1	2	25	5	100	0	0
S8	71	0	1	1	0	5	4	18	98.63	0	1.37
S7	67	0	0	6		2	5	20	91.78	0	8.22
S4	73	0	0	0	0	10	12	5	100	0	0
S2	72	0	1	0	1	2	4	20	100	0	0
S1	66	0	1	0	<1	2	25	5	100	0	0
Average	**68.5**	**0**	**1**	**0**	**0**	**2.5**	**15**	**12.5**	**100**	**0**	**0**

Muscovite is the dominant mica species identified in the studied samples. Only a few grains of biotite were recorded. The distribution of mica ranges from 0 to 5%. Most of the mica grains identified are between the framework showing deformation because of compaction (Plate 1, Figure b).

There is virtually little or no rock fragments in the investigated sediments. Only a few grains of chert and intermediate rock fragments (sample OUT2I) were identified. The lithic grains content generally varies from 0 to 6% in the absolute modal composition.

Accessory component includes of zircon, tourmaline, rutile, epidote, and hornblende. The quantity of the accessory component is generally low, amounting to as low as <1 to 1% of the total modal composition.

On the basis of the recalculated QFL, the sediments of the Wajid Sandstone are classified as quartz arenites. The QFL values of the analyzed samples largely range from 95 to 100% for quartz, feldspar (0 to 3%) and rock fragments (1.4 to 2.3); Figures 4.2 and 4.3.

4.2.2. Matrix

The amount of matrix in the Wajid Sandstone is poor ranging from 2 to 6% of the absolute modal composition, and averages between 2 and 3%. However, values as high as 10% were recorded in some of the clay-rich samples. This low matrix and exceptionally high quartz contents evidence the mineralogical maturity of the Wajid Sandstone.

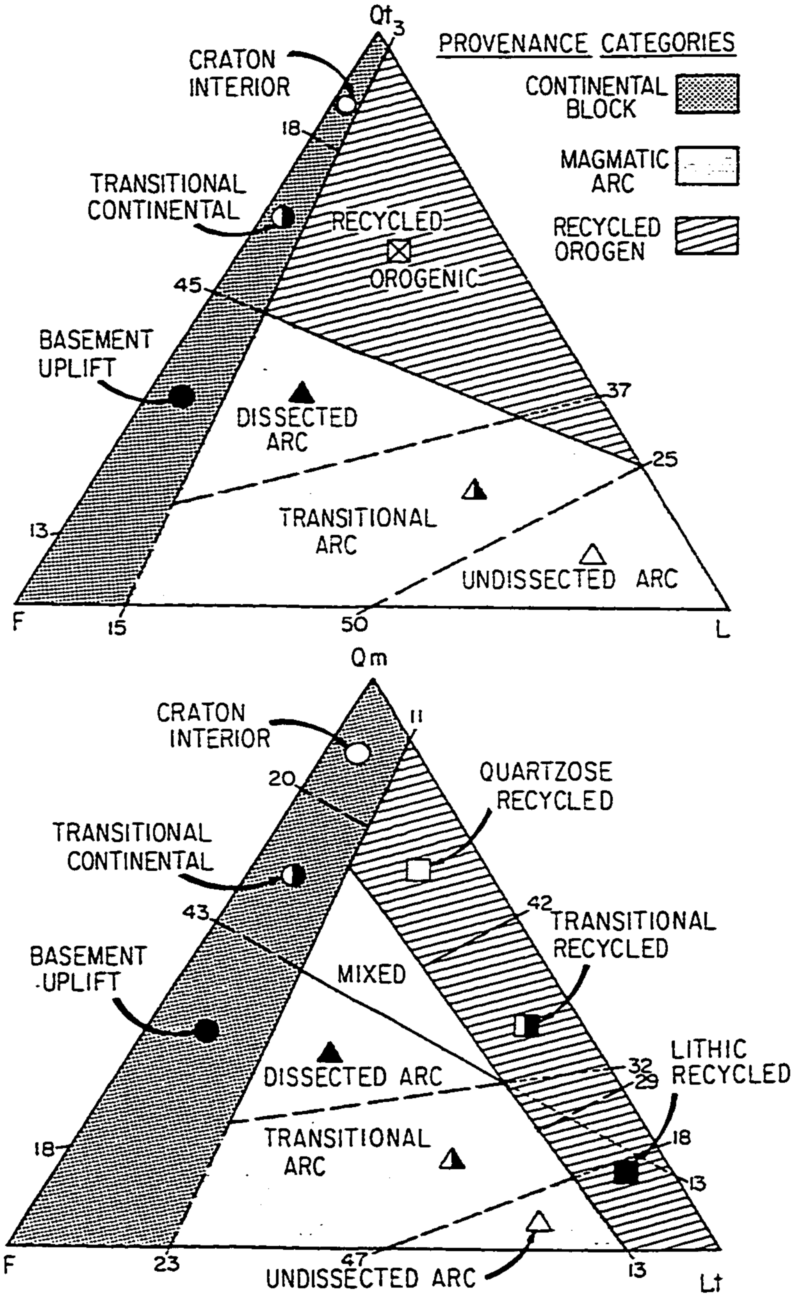

Figure 4.2. Ternary diagrams showing QFL distribution for different tectonic settings (adapted from Dickinson *et al,* 1983). Q = quartz, F = feldspar and L = lithic grains.

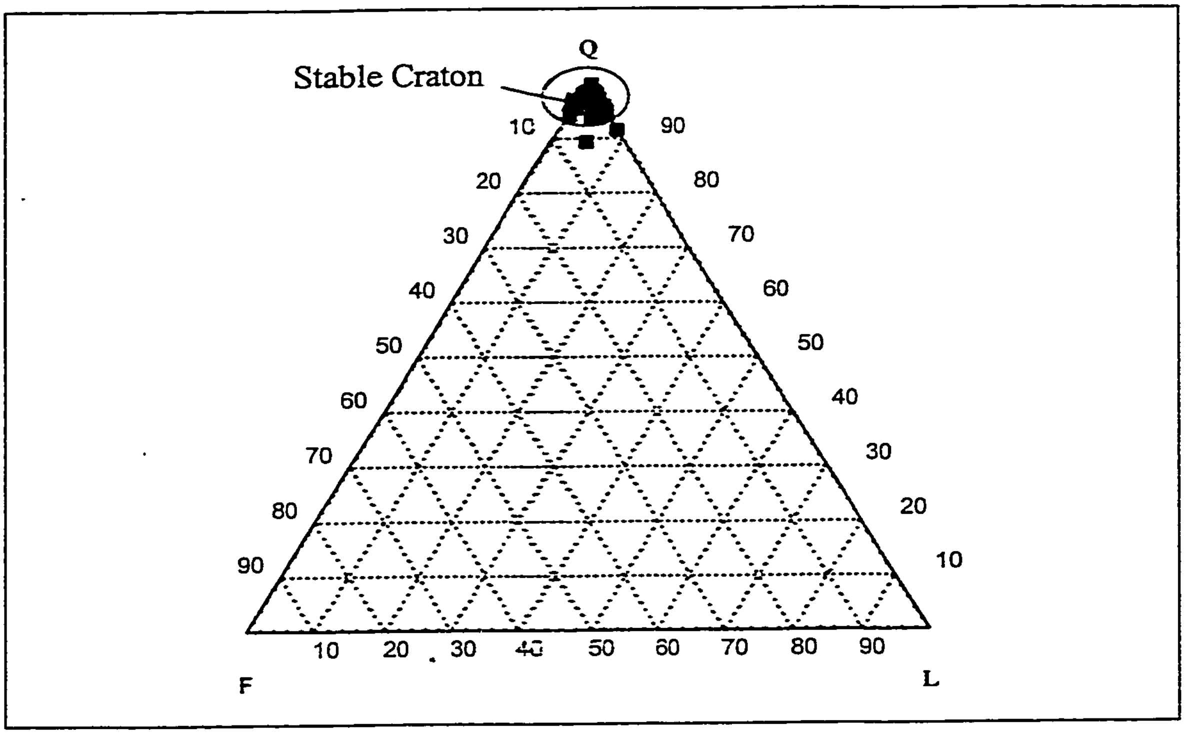

(a)

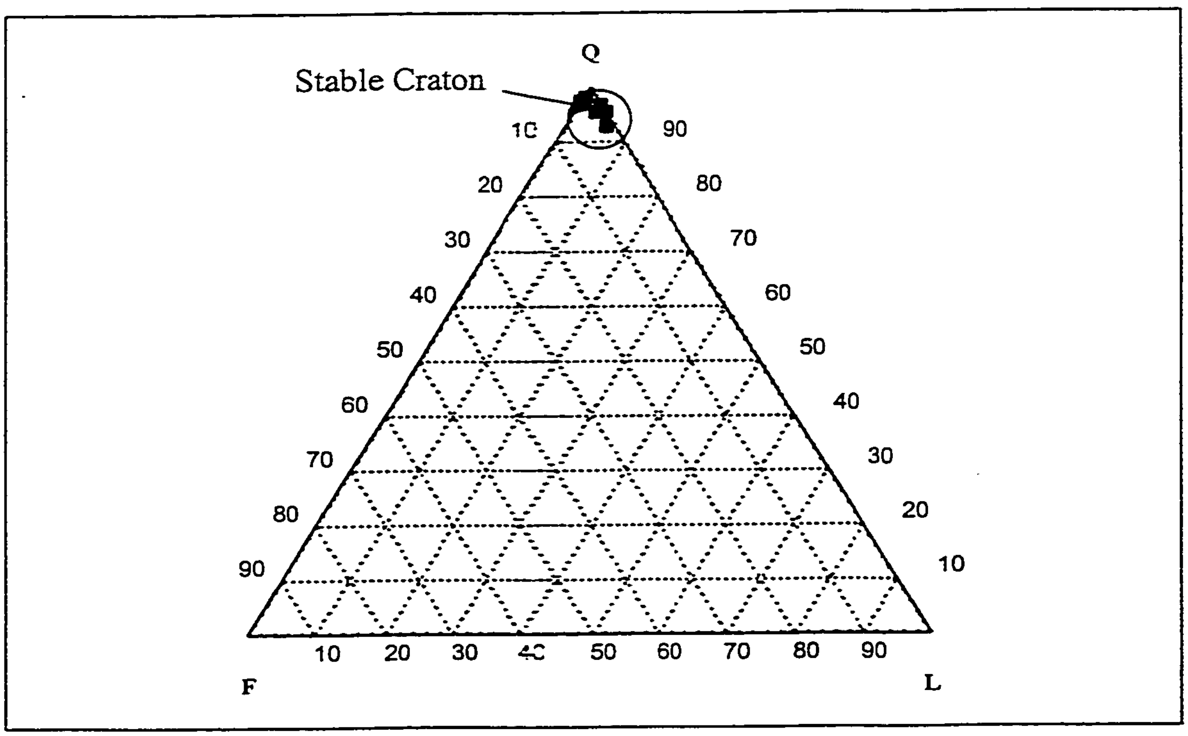

(b)

Figure 4.3. QFL ternary diagrams showing the composition of Wajid Sandstone: (a) Red Unit and (b) Grey Unit (Al Habalah II Locality). The plots suggest derivation of the Wajid Sandstone from a stable cratonic source (Q = quartz, F = feldspar and L = rock fragments).

4.2.3. Porosity

The porosity of the sediments investigated ranges from a low 3 to a high 20%. The densely cemented and tightly packed samples are extremely low in porosity. On the other hand, the loosely packed but poorly cemented samples are highly porous. Both primary intergranular and secondary intragranular porosities are present. As indicated in section 4.3.3 the intragranular porosity was most likely developed by the dissolution of calcite cement.

4.3. Diagenesis

4.3.1. Compaction and Pressure Solution

All the four major types of contacts targential (point), long, concavoconvex and suture contacts (Plate 1, Figures c - d) were observed in the samples from Wajid Sandstone. The presence of suture contact and deformed mica in between other framework minerals (Plate 1, Figure b), suggest high degree of compaction and pressure solution of the sediments. The presence of floating grain texture (Plate 2, Figure a) and the dominance of point to concaconvex contacts especially in the highly ferruginized samples, might be due to dissolution of early calcite cement and/or some of the detrital grain's rather than implying poor to moderate degree of compaction.

PLATE 2

Figure a.	Photomicrograph of typical ferruginous sandstone in the Red Unit. Note the distribution of floating grains in a densely cemented ferruginous sample. The grains are typically angular and exhibit targential contact.
Figures b & c.	Photomicrographs showing typical book-stack textural morphology of kaolinite. The preservation of these morphologies indicates the authigenic origin of the kaolinite in Wajid Sandstone
Figure d.	Granular to blocky textural morphology of kaolinite is shown in this photomicrograph. This morphology also indicates the authigenic nature of the clay mineral in the Wajid Sandstone.
Figure e.	Photomicrograph showing ball-shaped forms of hematite in Wajid Sandstone. The delicate nature of this textural morphology suggests the authigenic origin of hematite in the analyzed samples.
Figure f.	Typical fan-shaped morphology of hematite is shown by this SEM photomicrograph. This form corroborates the inferred authigenic origin of hematite in this study.

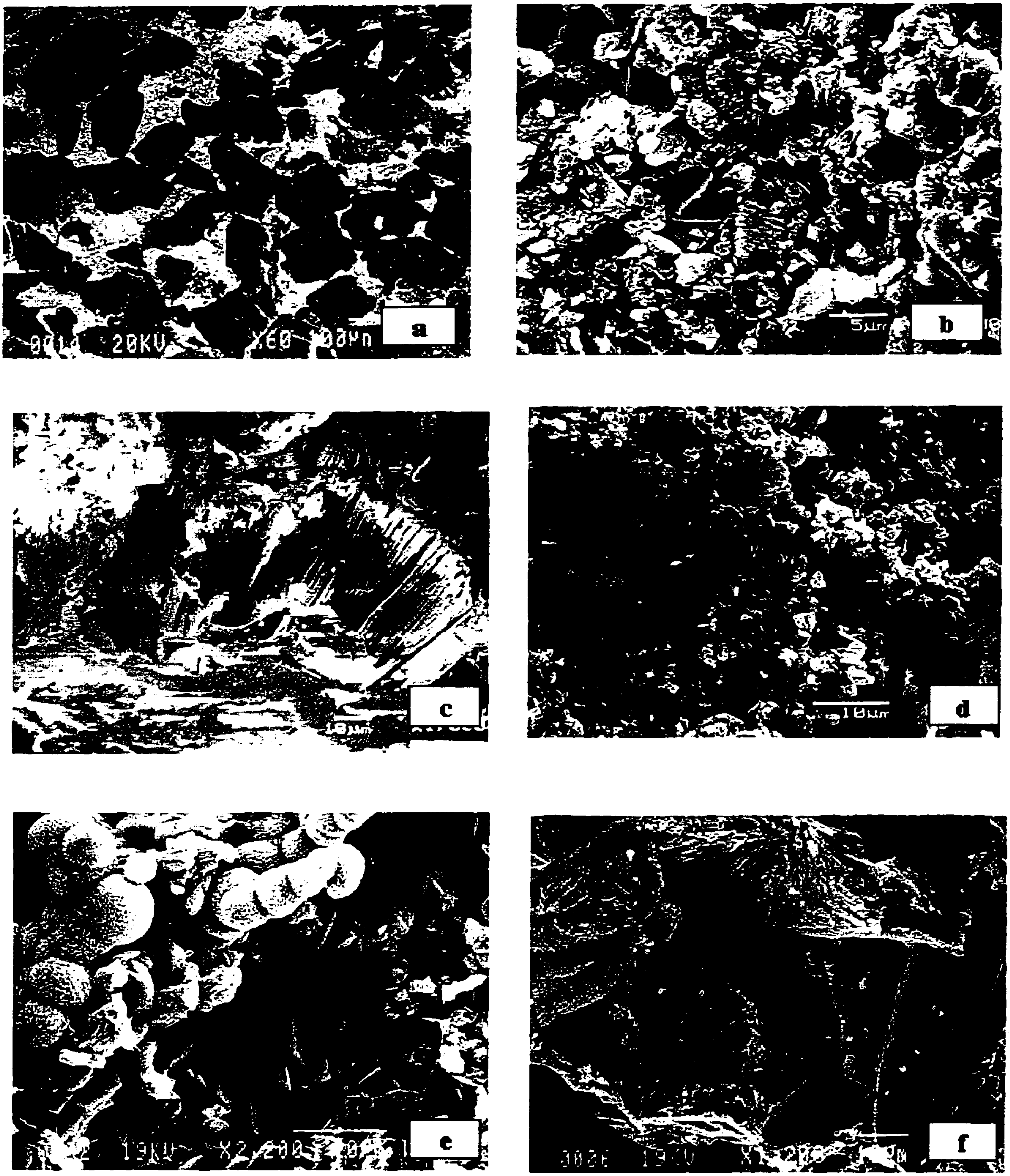

PLATE 2

4.3.2. Cementation

The amount of cement in the samples studied ranges between 5 and 30%. The cementing materials are predominantly ferruginous (hematite and goethite) and calcareous (calcite). Quartz overgrowth and microcrystallites occurring as silica cement as well as kaolinite also formed substantial parts of the cementing materials.

Ferruginous cement is the predominant cementing material in the Red Unit. The other types of cement include calcite, silica, and kaolinite. On the other hand, calcite cement constitutes the main cementing material in the Grey Unit. Subordinate amount of ferruginous material, silica, and kaolinite was also observed in the unit. Silica cement is well developed in the highly compacted quartzite samples.

More than one stage of cementation is apparent in the investigated sediments. The earliest cementation episode was by calcite (Table 4.2). Due to replacement by other cementing materials, calcite cement occurred mostly as patches and thin rims around the detrital grains. Where not replaced, calcite cement occurs as thick, poiklitic calcite (Plate 3, Figure f, Plate 4, Figure b) occupying most of the available pores. The grains appear to float where the cement is very dense. The calcite cement in sandstone is often precipitated as a result of leaching of calcium from detrital minerals and other primary carbonate components of the sediments by acidic meteoric or groundwater.

The occurrence ferruginous (mainly hematite) cement set the stage for the next cementation episode in the investigated Sandstone. In most samples, especially in the Red Unit, hematite and goethite occur as an important cementing material. This cementing material, confers on most of the samples floating grain texture (Plate 1, Figure a, Plate 3,

PLATE 3

Figures a and b.	Photomicrographs showing quartz overgrowth in Wajid Sandstone. The presence of well-developed euhedra hexagonal microcrystallites suggests advanced stage of quartz overgrowth in the sediments. Note the presence ferruginous cement within the quartz microcrystallites in Figure b. The penetrating nature of this ferruginous material indicates that it probably replaced the silica cement (mg. x160 and x125, respectively).
Figure c.	A photomicrograph showing the presence of both calcite and ferruginous cements in the same sample. These cements are restricted to different parts of the sample (sample HA25), mag. x40.
Figure d.	Photomicrograph showing the typical replacement relationship between calcite and ferruginous cement in the Red Unit. This photomicrograph shows the replacement of calcite by ferruginous cement (mag. x125).
Figure e.	A Coarse quartz grain with muscovite inclusion. Note kaolinite as the cementing material in the sample. (mag. x125).
Figure f.	Poikilotic calcite cement is most common in non-ferruginous sediments in the Wajid Sandstone (mag. x40).

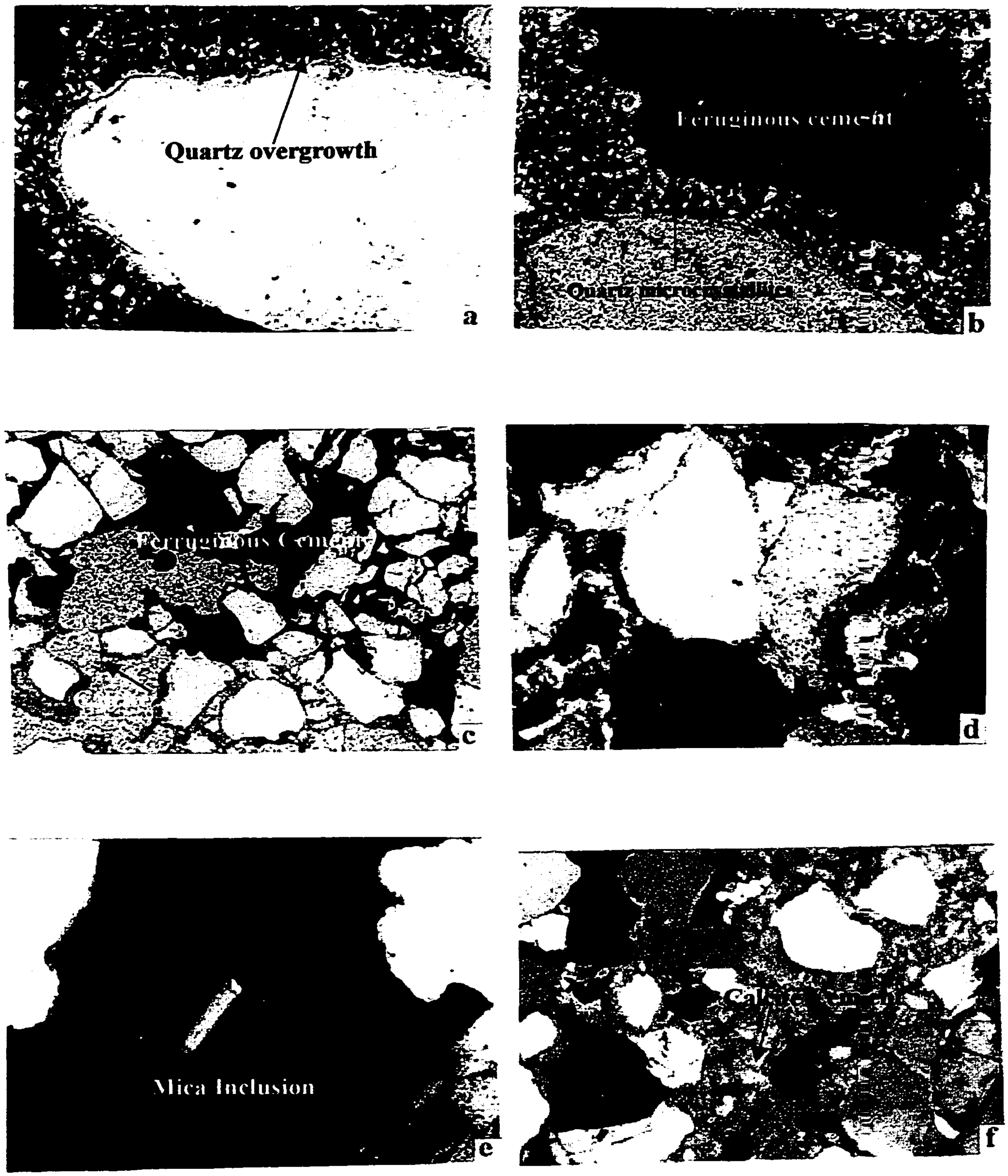

PLATE 3

PLATE 4

Figure a. Photomicrograph showing a broken and slightly decomposed hornblende grain embedded in calcite cement. The small grain at the right hand of the photomicrograph is a zircon (mg. x40).

Figures b and c. Corroded hornblende grains are shown in these photomicrographs. Note the thick poikilotic calcite cement and coarse quartz grains in b. Quartz grains in Figure c are equally coarse and show mainly long contact (mag. x125).

Figure d: This photomicrograph shows a fresh grain of microcline and sort of gradation in grain size. Note the poorly sorted nature of the sample (mag. x40).

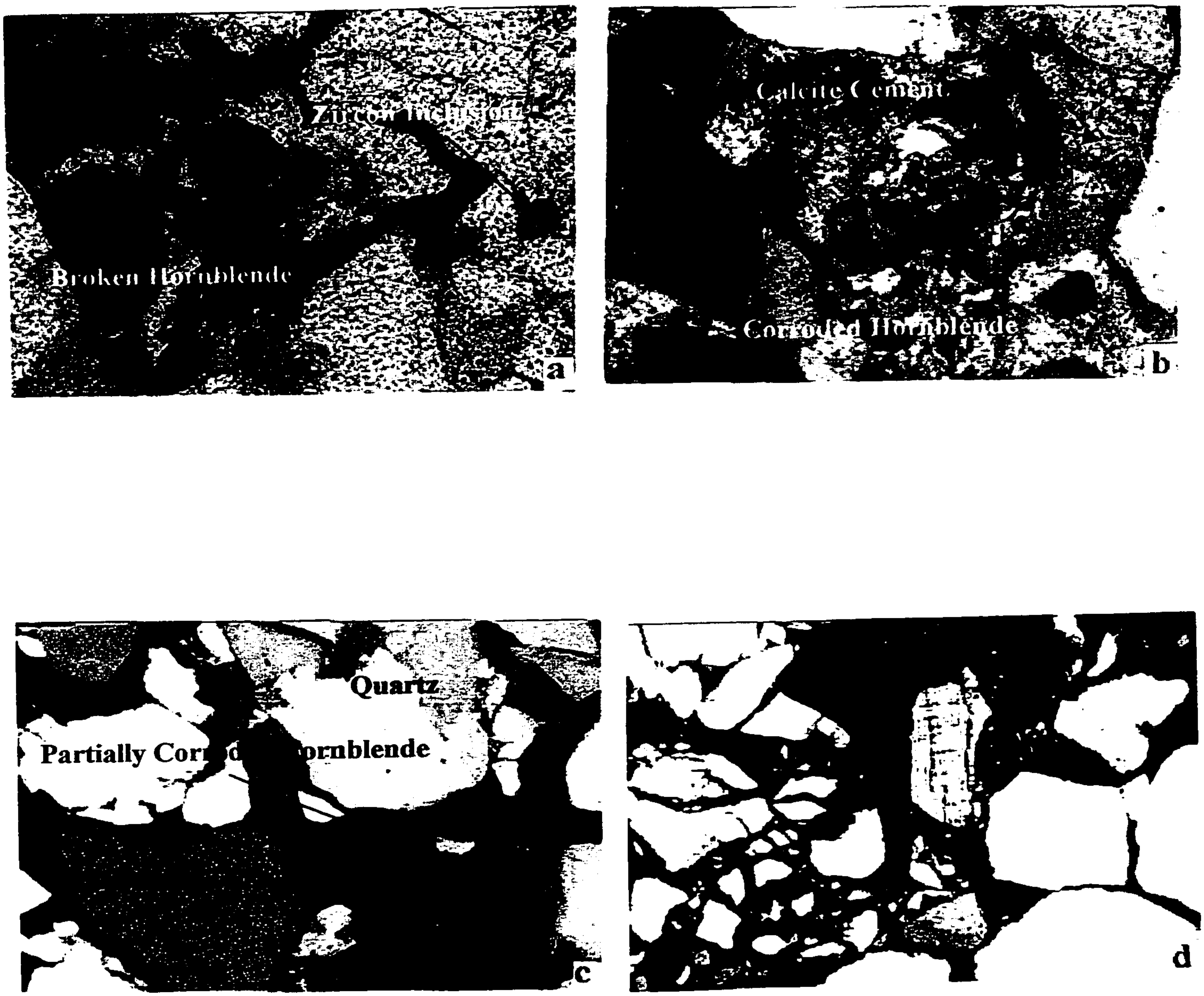
Broken Hornblende
a
Calcite Cement
Corroded Hornblende
b
Quartz
c
d

PLATE 4

TABLE 4.2. Table showing cementation phases in the Wajid Sandstone.

Cement/process	Early	Late
Calcite		
Quartz overgrowth		
Ferruginous cement		
Feldspar dissolution/ kaolinization		

Figure c). The relationship of the ferruginous cement with the primary calcite cement is replacement (Plate 3, Figures c -d). Where both types of cements are present, the ferruginous cement virtually occupies the core of the pore spaces leaving the calcite cement as mere rims and patches around the detrital grains. Calcite replacement by hematite and/or goethite is also evident by the negative correlation of Ca and Fe plots. Textural morphologies of the hematite cement observed in scanning electron micrographs indicate its authigenic nature (Plate 2, Figures e - f).

Quartz overgrowth starts as incipient overgrowth around the rims of the grains, which gradually, grows inward towards the cores of the pore spaces and totally fills up pores. The inward growth of the quartz cement gives the sediments a tightly packed interlocking appearance. The hexagonal bipyramidal microcrystallites of quartz occupying the central part of the pore spaces (Plate 3, Figures a -b) indicate that the quartz cement in the sediment postdates the primary calcite cement. Relicts of calcite cement were observed in samples that are dominantly cemented by silica. The silica cement was also probably precipitated before the ferruginous cement (Plate 3, Figure b). The well-formed euhedral crystal of this silica cement suggests that it is in an advanced stage of quartz cement development.

Possible sources of silica cement include dissolution of tests of silica precipitating organisms (e.g. radiolaria, sponge and diatoms), alteration of unstable volcanic glass and rock fragments and weathering and diagenetic dissolution of detrital silicates especially feldspar by meteoric waters. Pressure solution effects on quartz, clay diagenesis (e.g. illitization of smectite in adjacent shale) and rising of hot fluid related to rifting and magmatism are other most probable sources of silica cement (see de Ros, 1998, Houseknect, 1988, Pittman, 1979, Imam, 1986). Waugh (1970) attributed the source of silica cement in the Penrith sandstone to siliceous dusts from eolian abrasion of quartz grains. The main source of silica cement in Wajid Sandstone is probably the dissolution of feldspar and koalinization. The abundance of koalinite in the succession and the recovery of degraded feldspar grains (Plate 1, Figures e & f) suggest this mode of origin. Silica is one of the important products of alteration of feldspar to kaolinite. The following equation shows a typical transformation of feldspar to produce kaolinite and release silica.

$$\underset{\text{K-Feldspar}}{4KAlSiO_2} + 4H^{+1} + \underset{\text{Water}}{2H_2O} \longrightarrow 4K^{-1} + \underset{\text{Kaolinite}}{Al_4Si_4O_{10}(OH)_8} + \underset{\text{Silica}}{8SiO_2}$$

Pressure solution is also another probable source of quartz cement in Wajid Sandstone. This is indicated by the presence of suture contact in the studied samples.

4.3.3. Dissolution

Dissolution effect is indicated by the corroded nature of the feldspar and hornblende grains (Plate 1, Figures e & f, Plate 4, Figure a - c). Floating grain texture in the irons-rich samples) and packing inhomogeneity (Figures 4.1a) also suggest the role of dissolution process in porosity modification. These features, floating grains and packing inhomogeneity are probably caused by leaching and dissolution of the early calcite cement by acidic groundwater or meteoric water before the precipitation of the late ferruginous cement. The effects of corrosion on grains are also evidenced by penetration of the cements into the grains.

4.4. Scanning Electron Microscopy (SEM)

The energy dispersive x-ray (EDX) of bulk samples show that virtually all the samples are extremely rich in silica and by implication rich in quartz. High amounts of Fe were recorded in the samples from the Red Unit. Significant amounts of Al were also recorded. The high content of Al in the samples may be due to the presence of kaolinite - rich claystone in some of the samples.

SEM study shows quartz grain surface morphology, grain contacts and grains relationship with the cementing material (Plate2, Figure a). This study, also show that the ferruginous materials, heamatite and goethite occur as pore filling cement with delicate honeycomb, ball shaped bodies occupying shallow holes, and fan-shaped coating in between and around quartz grains (Plate2, Figures e-f). Delicate book-stack and granular morphologies of kaolinite are also revealed by SEM photomicrographs (Plate 2, Figure b - d).

4.5. X-Ray Diffractometry (XRD)

The XRD data reveal mineralogical phases dominated by quartz with subordinate amounts of calcite and hematite, goethite and kaolinite (Table 4.3 and Figures 4.4 and 4.5). The hematite and goethite are largely restricted to the samples from the lower Red Unit.

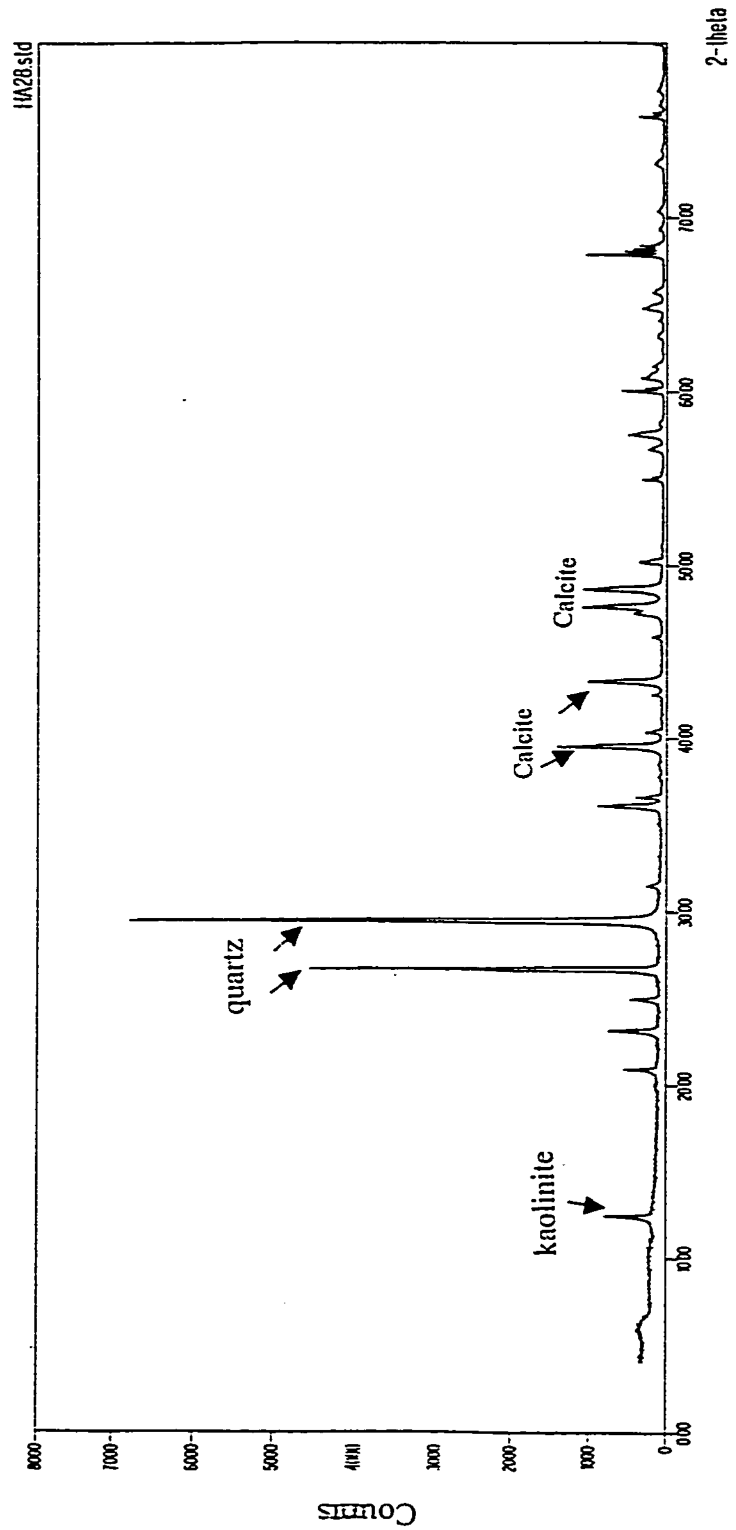

Figure 4.4. Typical x-ray diffractogram showing general mineralogical phases of the Wajid Sandstone. Note the characteristic peaks of quartz, calcite and kaolinite.

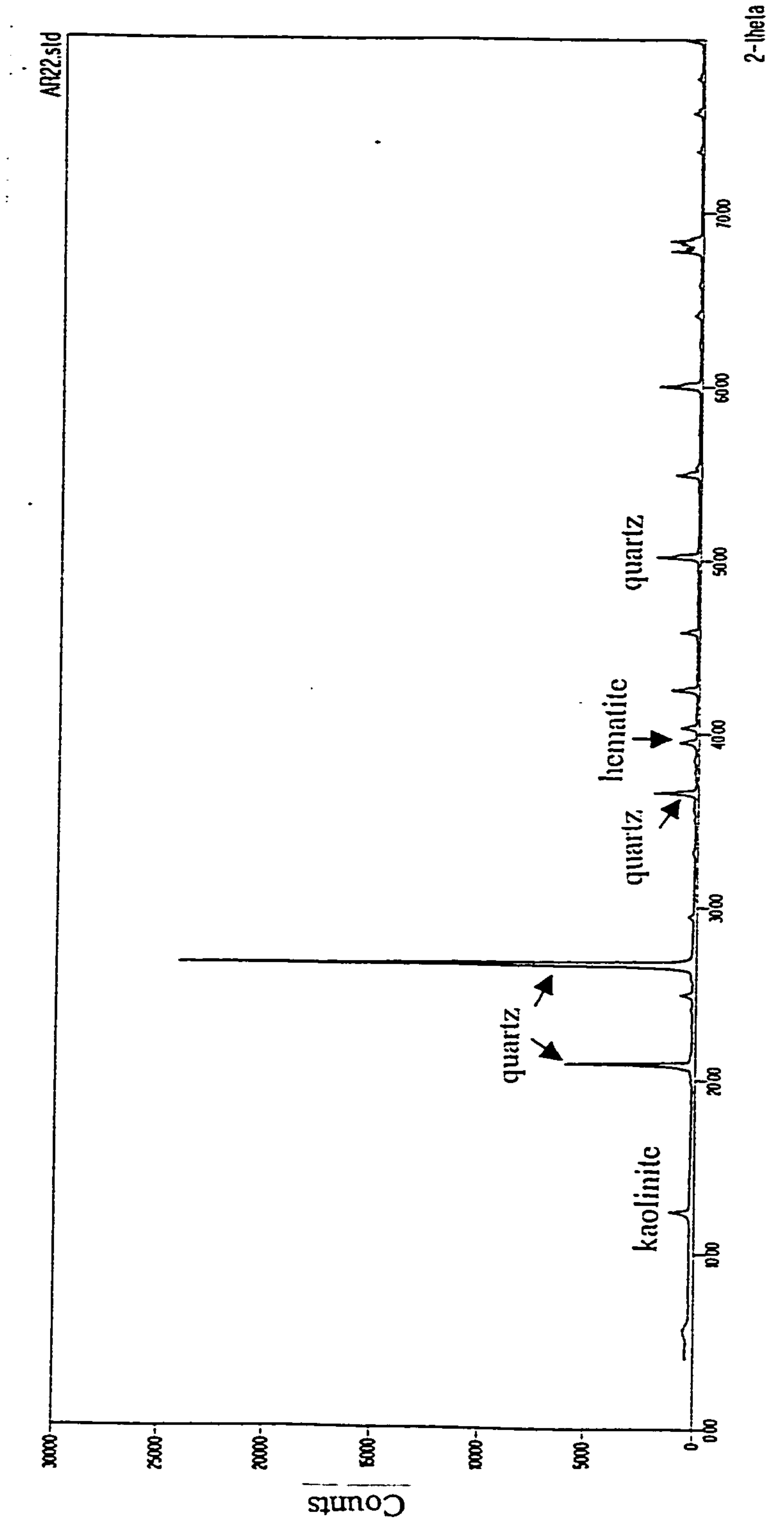

Figure 4.5. X-ray diffractogram of a representative sample from the Red Unit. Note the characteristic hematite peak.

TABLE 4.3: Modal composition determination from X-ray diffraction analysis. Note the dominance of quartz in the analyzed samples.

Sample	Quartz	Goethite	Hematite	Kaolinite	Calcite	Chamosite
AR15	97	3				
AR19	93		2			2
AR21	89		2	2	5	
AR22	96		1	2	1	
ARLC4K3	85			3	10	
HA24	95	2	1	2		
HA27	96	2				2
HA28	38			4	58	
HA30	35				64	
HA31	25				25	
HA28	98			2		
HAP9	96			2	2	
HAP10	94			3	3	
HAP11	95			3		
HAP16	97			3		
HAP28	97			3		
HAP37	98			2		
OUT5I2	94	3	3			
OUT6C	5			15	80	
OUT6I	80	9	1	10		
S2	96			2		
S20	95	5				
S28	98		2			
S39	95	5				

4.6. Clay Mineralogy

4.6.1. Introduction

Clay mineral analysis was carried out for the purposes of determining the origin of the silty to fine sandy claystone lenses observed in the outcrop sections in the field. In addition, the clay mineral data was used to complement other lines of evidence utilized for the provenance and paleoenvironmental interpretations of the Wajid Sandstone.

On the basis of textural morphologies, Keller (1978) related the constituent of kaolin minerals (including kaolinite and halloysite) to different modes of origin and parent rock sources. Karlsson *et al* (1979) noted the systematic change in clay mineral composition with depth and used such changes to interpret the source rocks, paleoclimate, rate of deposition, and postdepositional changes. Louail *et al* (1979) identified the association of kaolinite, semectite and mica assemblage as being primarily characteristic of nearshore facies while marine facies contains smectite and glauconite. Murray and Heckroodt (1979) inferred that the primary kaolins of South Africa were derived from weathering of granite, other feldspathic igneous rocks and sedimentary rocks. da Costa and Moraes (1998) applied mineralogical and geochemical analyses to determine the genesis of kaolin deposits in the Amazon region. These authors concluded that the kaolins which, comprised dominantly kaolinite, are mainly derived from sedimentary, metamorphic and volcanic felsic rocks in the region.

4.6.2 Descriptive Mineralogy

Claystone in the studied succession occurs, as white colored friable, silty to very fine sandy clay lenses in both the Red and the Grey Units. The close assocaition of the claystone lenses with the ferruginous horizons often makes the claystone stained pinkish and mottled in the Red Unit.

In thin sections, the clay mineral, mainly kaolinite, occurs as cryptocrystalline crystals forming part of the pore filling cements (Plate 3, Figure e). The SEM studies indicate that kaolinite is the dominant clay mineral in the Wajid Sandstone. Kaolinite shows the typical book stack morphology with the kaolinite plates (Plate 2, Figures b -c). Granular-vermicular and blocky morphological textures are also common (Plate 2, Figure d). The fact that none of the glycolated samples showed any shift of peak confirms the monomineralic nature of the clay and suggests the absence of smectite, montimorillonite and any other expandable clay minerals.

4.6.3. Quantitative Mineralogy

XRD study confirmed that the dominant mineral phase is kaolinite. With the exception of two samples, the amount of kaolinite in the samples studied range from 60 to 90% (Table 4.4, Figure 4.6).

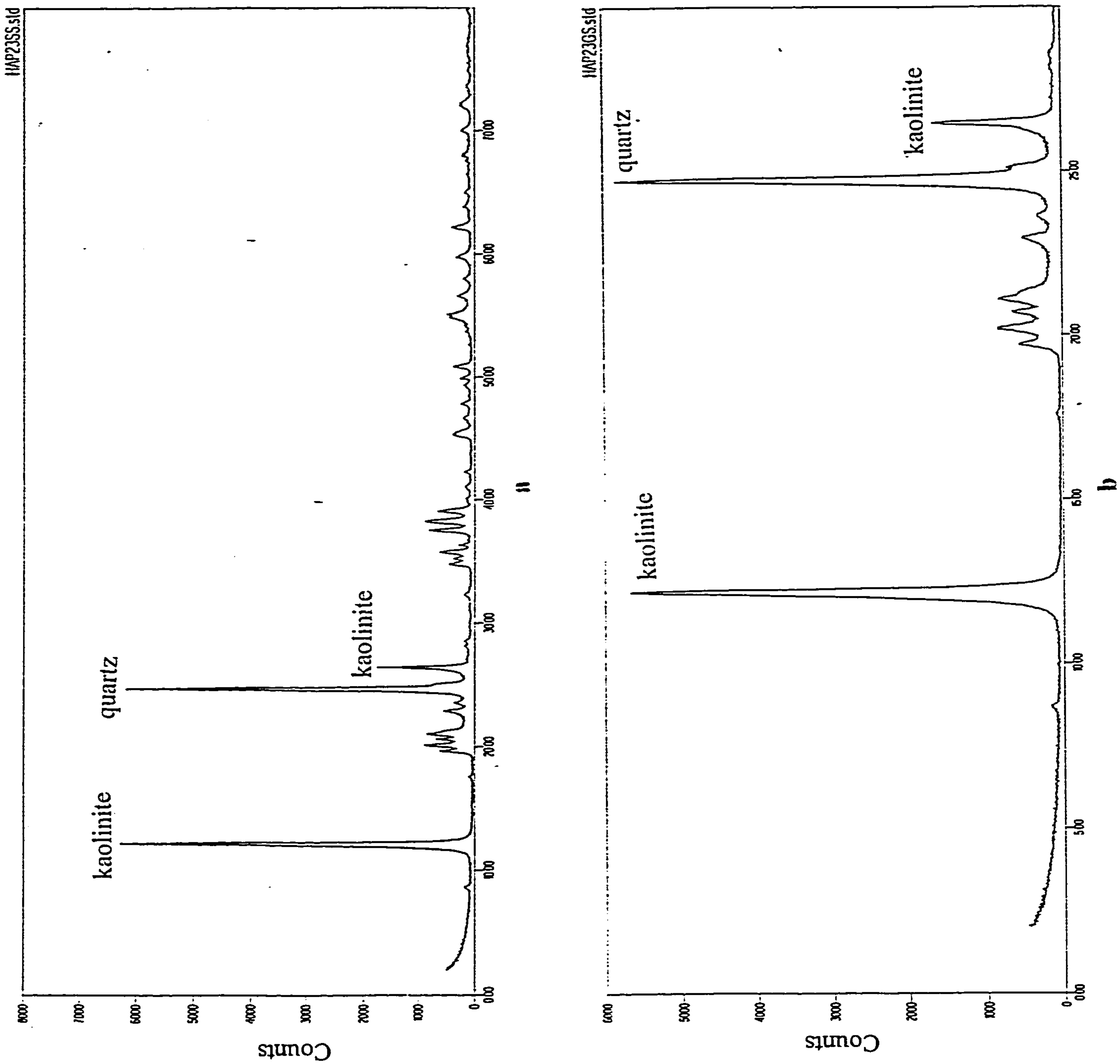

Figure 4.6. X-ray diffractograms showing typical spectra of kaolinite: (a) unglycolated and (b) glycolated sample. Note the characteristic kaolinite peaks at 12.1°-12.3° (high) and 24.6° (weak). Also there is no shift of the peak position of the glycolated sample.

TABLE 4.4. X-ray diffraction data of the separated clay fraction from the Red and Grey Units. This table shows that kaolinite is the main clay mineral in the analyzed samples.

Sample	Quartz	Hematite	Kaolinite
AR20	30	10	60
AR23	15		85
AR52	20		80
ARLC4K1	15		85
ARLC4K2	30		70
HA9	10		90
HA18	30	5	65
HA20	35		65
HA23	40	5	55
HA49	20		80
HAP2	15		85
HAP11	25	10	65
HAP17	10		90
HAP19	50		50
HAP23	15		85

4.7. Heavy Mineral Analysis

4.7.1. Introduction

Heavy mineral analysis has proven to be very useful in provenance determinations, paleogeograhic reconsrtuction and unroofing orogenic history (Krynine, 1942; van Andel, 1959; Hubert 1971; Johnson *et al* 1985; Goldstein, 1992; Schaffer and Dorr, 1997; and Uddin and Lundberg, 1998). However, heavy mineral petrogenetic records in sediments are often partially or totally obliterated by weathering at source and outcrops, mechanical abrasion, hydraulic equivalence and diagenetic alteration (Morton, 1985; Mange and Maurer, 1992; Morton and Johnson, 1993; Morton and Hallsworth, 1994, 1999).

Hubert (1962) proposed the ZTR index as a measure of mineralogical maturity of sandstones. This author inferred that the modification of heavy mineral suites by intrastratal solution (Pettijohn, 1941) is volumetrically unimportant. Schaffer and Dorr (1997) ascribed high content of apatite and predominance of non-reddish zircon to erosion of felsic rocks, and well rounded detrital zircon to recycled sediments. High content of glossy zircon, rutile and garnet contents indicate metamorphic rocks source in the hinterland.

Based on heavy mineral suites dominated by ultrastable zircon, tourmaline and rutile, Uddin and Lundberg (1998) recognized a felsic to intermediate source rocks in a cratonic setting in the Eocene-Oligocene sequence of the Himalayas. Rostovtseva and

Shaprio (1998) utilized heavy mineral suites to determine the provenance of the Paleocene-Eocene clastic rocks of the Khamndorsky Islands.

Morton (1985), Mange and Maurer (1992) and Morton and Hallsworth (1994; 1999) suggested the use of a combination of conventional heavy mineral analysis with varietal studies as a means of limiting the influence of intrastatal solution and other ateration processes on heavy minerals in provenance interpretations.

In this study, heavy mineral study was conducted to achieve a number of objectives including determination of provenance and reconstruction of paleogeographic and tectonic settings of the study area.

4.7.2. Heavy Mineral Distribution

The Heavy mineral concentration in all the forty-four (44) samples analyzed is generally low. The concentration of heavy mineral minerals ranges from 0.009 to 4.01wt% in Ahad Rufaidah, 0.2 to 4.3wt% in Al Habalah locality I, 0.19 to 0.68wt% in Al Habalah locality II and 0.29 to 2.72wt% in Al Saudah locality (Table 4.5).

Opaque minerals dominate the heavy mineral assemblages in Ahad Rufaidah and Al Habalah area I, ranging between 24.68 and 91% and ~26 and 99% respectively. In Al Habalah Area II and Al Soudah, the distribution of the opaque minerals are lower than in the other two areas (Table 4.5). Only few samples in Habalah Area II and Al Soudah recorded values in excess of 45% of opaque minerals in the total counts.

TABLE 4.5. Distribution of heavy minerals in the Wajid Sandstone

Sample	Sample Weight (gm.)	Heavy Mineral (gm.)	Heavy Mineral (%)	Total Grains	Opaques (%)	ZTR in total grains(%)	ZTR in nonopaques(%)	Tourmaline(%)	Zircon(%)	Rutile (%)	Epidote (%)	Hornblende (%)	Kyanite (%)	?Sphene (%)	Unknown (%)
Ahad Rufaidah Locality															
AR39	13.4	0.03	0.22	157	73.2	25.48	95.24	88.09	7.14	0	2.38	2.38			
AR32	5	0.03	0.6	457	42	56.24	96.98	50.57	38.1	8.3	0.75	2.26			
AR17	8.72	0.35	4.01	319	90.9	8.78	94.55	56.62	31	6.89		3.45			
AR14	8.02	0.3	3.74	336	83.3	16.67	100	64.28	27.8	8.93					
AR13	11.2	0.26	2.32	220	68.2	30.45	95.71	40	52.9	2.86	2.86		1.4		
AR11A	14.6	0.09	0.62	339	37.2	46.61	74.18	49.29	19.7	5.16	18.8	3.75			3.29
AR10	17.5	0.4	2.28	182	72	23.63	84.31	33.33	49	1.96	15.7				
AR8	16.5	0.12	0.72	316	24.7	61.39	82.51	43.27	27.7	10.5	16.8	0.84	0.8		
AR6	33.1	0.03	0.09	165	73.9	27.27	92.83	65.22	33.9	8.69		2.17			
AR2	17.6	0.08	0.46	250	53.2	38.4	95.56	66.67	12.8	2.56	17.1				0.85
ARLC3SC	30	0.1	0.33	244	43.4	48.36	85.5	76.81	4.35	4.35	3.62	1.45	0.7		8.69
Habalah I Locality															
HA58	6.82	0.06	0.88	384	88.5	11.46	100	36.36	61.4	2.27					
HA57	11.5	0.025	0.22	572	45.5	50.87	93.27	79.8	8.65	4.81	3.63	2.56		1	
HA52	23.2	0.09	0.39	376	37	54.52	86.5	60.76	21.5	4.22	12.7				0.84
HA50	9.61	0.02	0.2	130	92	6.92	90	10	80	0					10
HA45	5.78	0.04	0.69	390	71.8	24.61	87.27	61.82	22.7	2.73	6.36	6.36			
HA44	9.22	0.11	1.19	257	76.3	21.4	90.16	63.93	26.2		1.63	6.56			1.63
HA41	15.9	0.03	0.19	578	26	66.08	89.25	56.54	26.9	5.84	7.01	3.74			
HA40	9	0.02	0.22	174	37.4	48.85	77.98	68.81	5.5	3.67	18.3	2.75		1	
HA39	7.44	0.03	0.4	391	41.7	55.75	95.61	71.93	21.5	2.19	1.32	2.63	0.4		
HA36	16.1	0.69	4.3	323	99.1	0.93	100	0	66.3	33.3					
HA26	12.1	0.02	0.16	493	32.5	65.52	96.99	63.06	33	3.9	2.4	0.6			
HA21	21.9	0.4	1.82	211	64	31.75	88.16	56.58	26.3	5.26	9.2				2.63
HA15	10.8	0.09	0.83	311	50.1	37.62	80.13	30.13	47.3	2.74	10.3			1	1.37
HA14	8.39	0.07	0.83	275	65.5	33.09	95.79	61.05	33.7	1.05	2.1	1.05			
HA7	7.87	0.18	2.29	238	94.5	5.04	92.31	61.54	23.1	7.69		7.69			
HA5	6.63	0.06	0.9	279	84.3	15.41	97.73	65.9	31.8						2.27

Habalah II Locality															
Sample	**Sample Weight (gm.)**	**Heavy Mineral (gm.)**	**Heavy Mineral (%)**	**Total Grains**	**Opaques (%)**	**ZTR in total grains (%)**	**ZTR in nonopaques (%)**	**Tourmaline(%)**	**Zircon(%)**	**Rutile (%)**	**Epidote (%)**	**Hornblende (%)**	**Kyanite (%)**	**?Sphene (%)**	**Unknown (%)**
HAP32	10.4	0.03	0.29	297	40.4	59.26	99.43	69.49	23.7	6.21		0.56			
HAP25	10.6	0.02	0.19	546	44	53.29	95.09	63.36	24.8	4.9	4.25	0.65			
HAP24	23	0.06	0.26	488	20.5	70.02	98.19	49.48	41.2	7.47	1.29	0.51			
HAP22	5.84	0.04	0.68	315	76.2	23.49	98.67	38.67	40	20		1.33			
HAP20	18.9	0.03	0.16	301	29.9	65.11	92.89	36.49	38.9	17.5	5.69	1.42			
HAP16	14.6	0.03	0.2	260	32.7	62.69	93.14	58.28	30.3	4.57	5.71	1.14			
HAP13	7.52	0.01	0.13	215	53	38.6	82.17	35.64	27.7	18.8	7.92			5	4.95
HAP3	26.7	0.07	0.26	484	31	64.05	92.81	44.91	44.9	2.99	4.49	1.5	0.6		0.6
Al Soudah Locality															
S21	31.4	0.13	0.41	474	20	66.67	83.37	29.81	38.5	14.8	11.9	4.75		0	
S17	16.6	0.07	0.42	307	32.6	59.93	88.89	45.89	35.8	7.25	8.21				
S13	32.1	0,11	0.34	547	26.9	62.16	85	25	39	21	11.3	1.75		1	1.25
S12	19.8	0.54	2.72	306	98	1.63	83.33	66.67	0	16.7	16.7				
S8	10.2	0.03	0.29	523	13.2	77.44	89.2	48.46	35.2	5.5	8.81	1.1		1	0.22
S2	30	0.93	3.1	439	43.3	51.94	91.57	56.22	24.5	10.8	8.03	0.4			

The ultrastable heavy minerals represented largely by zircon, tourmaline and rutile dominate the translucent part of the recovered assemblages. In Ahad Rufaidah, ZTR index accounts for 74.18 to 100%, Al Habalah area I 77.98 to 100%, Al Habalah area II 78.08 to 99.4% and in Al Soudah 83.33 to 91.57% respectively (Table 4.5). The ZTR index in the total grain counts correlates with the opaques proportion with correlation coefficient (r^2) values ranging from 0.93 to 0.99 (Figure 4.7). Average distribution of the opaques, ZTR and all the major nonopaque minerals in the localities and established units are shown represented in Figures 4.8 and 4.9.

In addition to zircon, tourmaline and rutile, other common heavy minerals including mica (not counted present study), epidote, hornblende, kyanite and sphene were also observed. The opaque minerals represented by authigenic hematite and goethite, which often occur, as coating on the quartz grains and unidentified heavy minerals. SEM and XRD data indicate the presence of chromite and ilmenite in opaque fraction of the sediments.

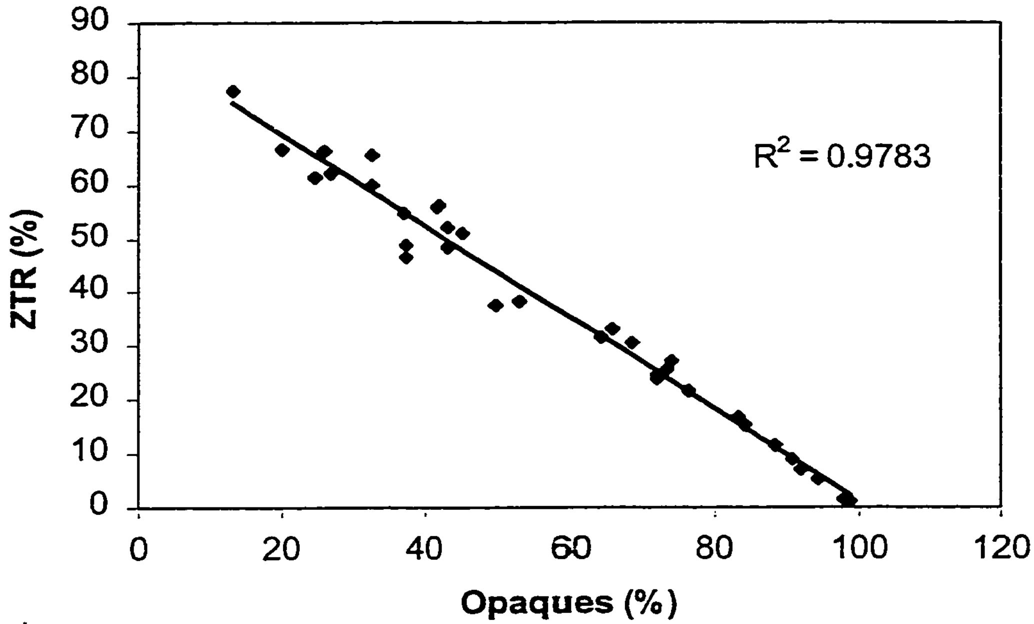

(a)

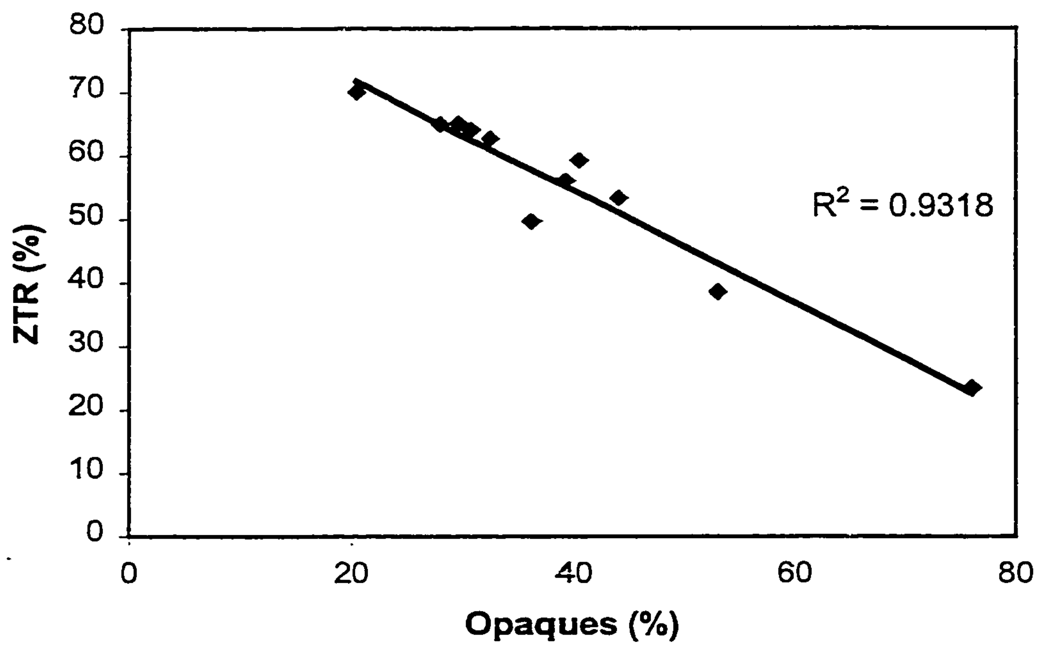

(b)

Figure 4.7. Bivariate relation between opaque minerals and ZTR index in the total grain counts: (a) Red Unit and (b) Grey Unit. Note a strong negative correlation between the opaque minerals and the ZTR index in these plots.

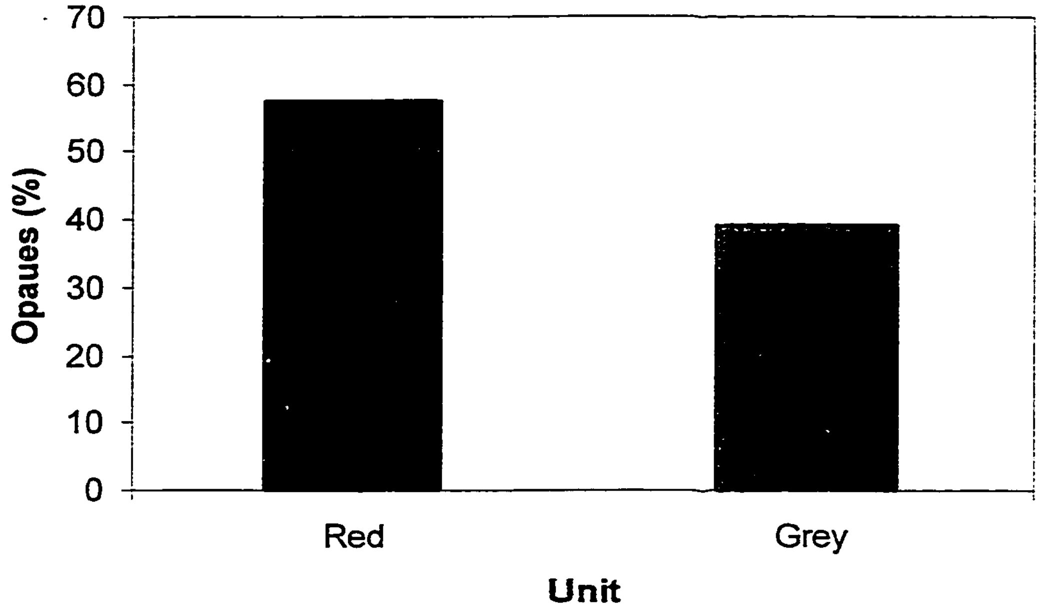

(a)

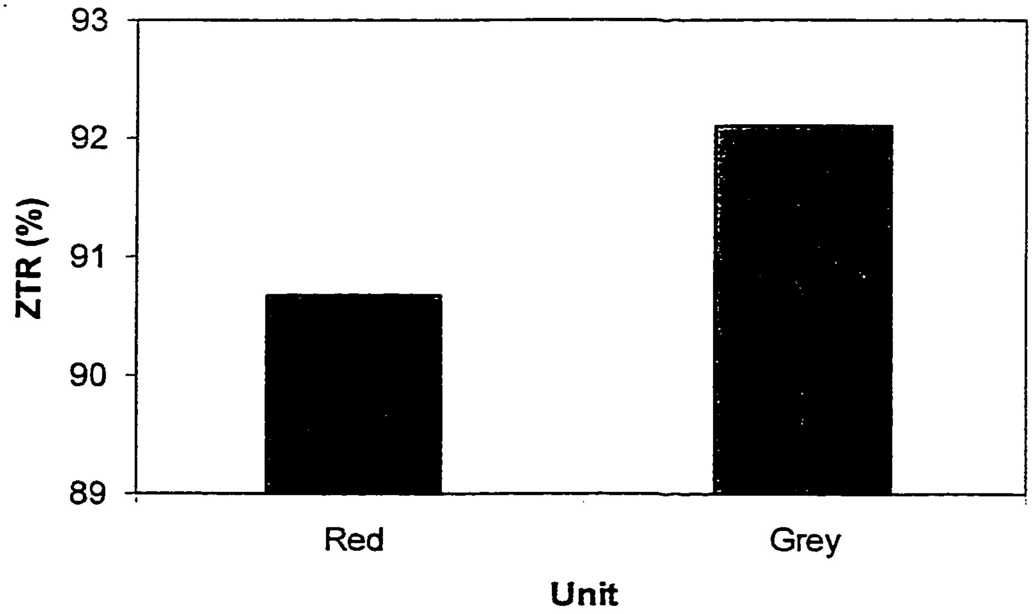

(b)

Figure 4.8. Relative distribution of opaque minerals and ZTR in the Wajid Sandstone: (a) Opaque minerals and (b) ZTR index. Note that the opaque minerals are higher in the Red Unit than in the Grey Unit. On the other hand, the ZTR index is slightly higher in the Grey Unit than in the Red Unit.

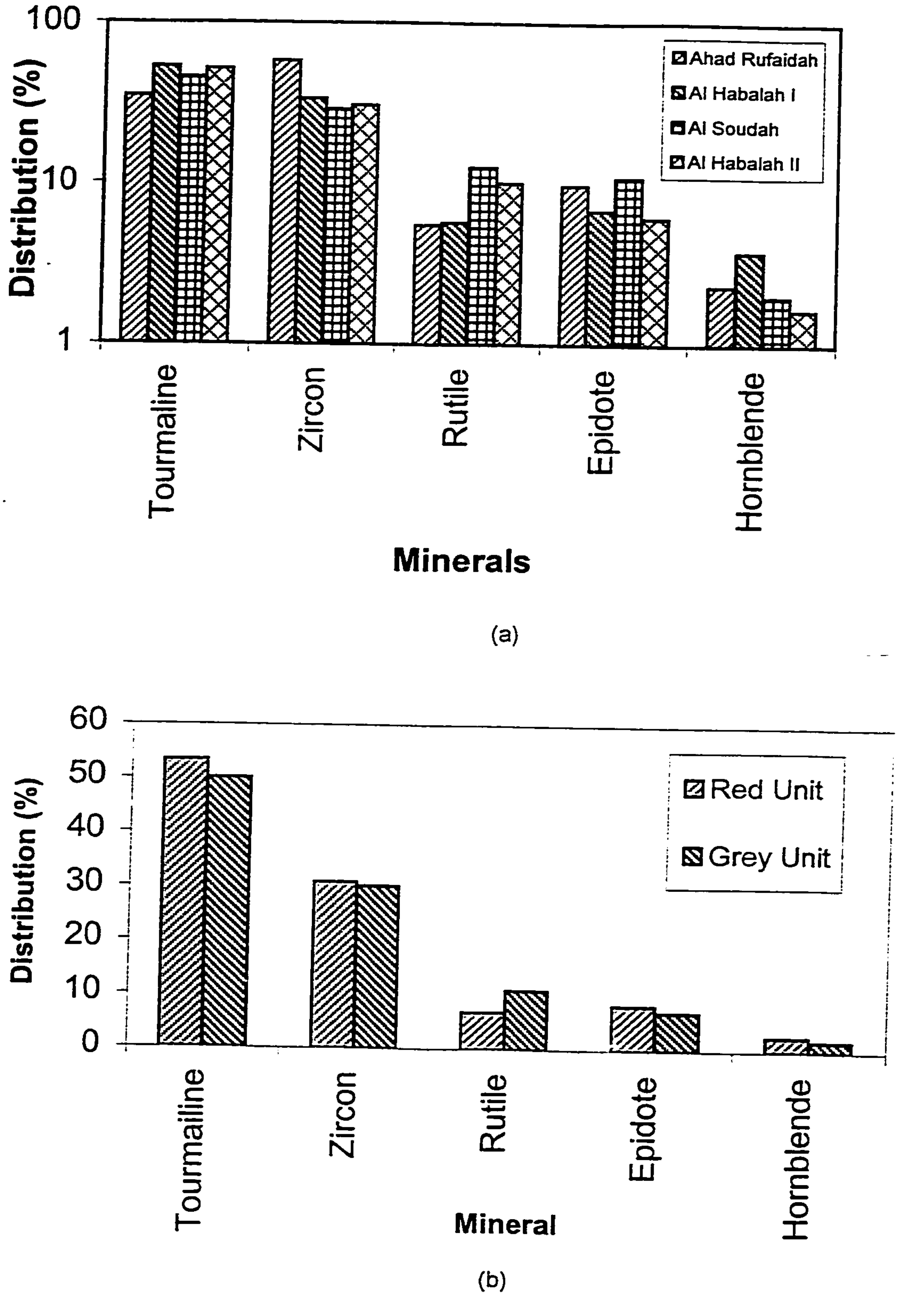

Figure 4.9. Relative distribution of heavy minerals in the Wajid Sandstone (a) Localities and (b) Units.

4.7.3. Descriptive Mineralogy

Tourmaline dominates the ZTR index and the total non-opaque suites. The distribution of tourmaline accounts for about 40 to 88% in Ahad Rufaidah, 10 to 80% in Al Habalah Area I, 36 to 69.5% in Al Habalah Area II and 83.3 to 91.57 in Al Soudah Area. The tourmaline grains observed are generally idiomorphic, fragmented, lath shaped with pyramidal to rounded terminations (Plate 5, Figures c-i). A Few of the grains, are partially rounded to well rounded and show overgrowth (Plate 5, Figures a, b, f). The gains are mainly red brown to pinkish, with some pale yellow to bluish green. They exhibit high birefringence, parallel extinction and strong pleochroism. External striations and inclusions including some rod-like, needle to lath-shaped crystals and fluid bubbles are observed in some of the grains (Plate 5, Figures g -h).

Zircon forms the second most abundant mineral species in the samples constituting about 4.35 to 53% in Ahad Rufaidah, 5.5 to 80% in Al Habalah Area I, 12.24 to ~ 45% in Al Habalah Area II and 0 to 39% in Al Soudah Areas respectively. The zircon grains are colorless to pale yellow with characteristic admantine luster, high birefringence, relief and show parallel extinction. The grains are generally of rounded to euhedral crystals with rounded to pyramidal ends. These grains contain a lot of inclusions comprising of fluids and also needle to lath-shaped crystals (Plates 6 and 7). Stress strains are observed in some of the grains.

Rutile occurs in the analyzed samples as prismatic rounded to euhedral crystals (Plate 7, Figures g - i). The grains are yellow to deep red brown in color and show characteristic oblique crossing striation patterns (Plate 7, Figure i). The distribution of

PLATE 5

Figures a, b and f:	Rounded tourmaline grains. The presence of such grains indicates derivation from reworked sediments. The grain labeled 'a' appears to be well abraded and has overgrowth (mag. x160).
Figure c:	An hypiodiomorphic grain of tourmaline (mag. x160).
Figure d, f:	Idiomorphic grains of tourmaline. Most of the grains are yellow in color (mag. x160).
Figures g, h and i:	Fragments of tourmaline. These specimens represent the dominant pink to brown red tourmaline variety in the Wajid Sandstone. Note the presence of inclusions in these grains.

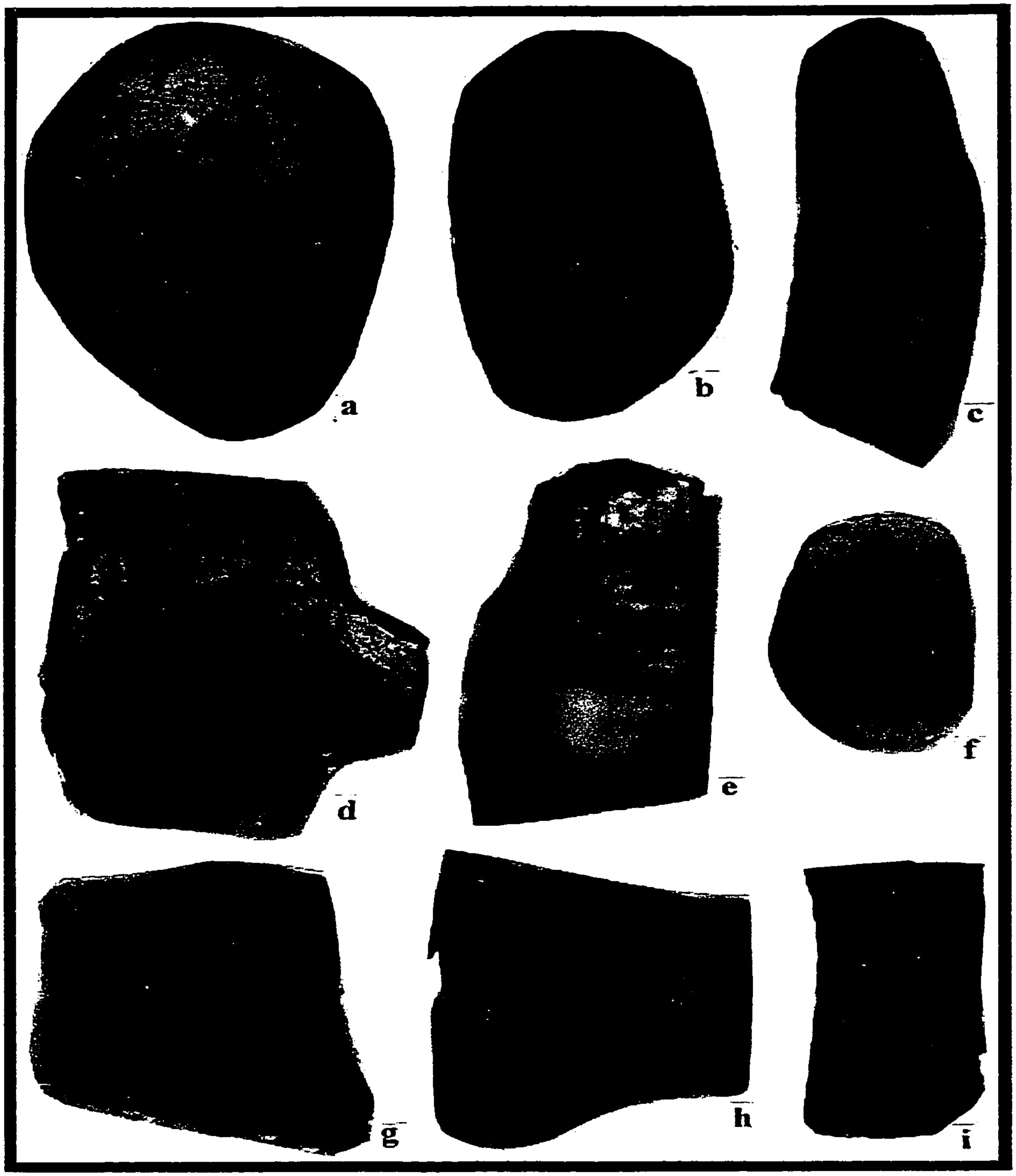

PLATE 5

PLATE 6

Figure a.	An euhedral zircon grain with prismatic terminal ends. Note the abundance of inclusions (mag. x250).
Figure b.	Photomicrograph of a well-rounded zircon showing prismatic crystal boundary (mag. x250).
Figures: c & d.	Angular to subrounded zircon grains. These grains contain abundant fluid and mineral inclusions (mag. x250 and 160 respectively)
Figure e:	A zircon grain showing prismatic crystal boundary. Note the abundance of inclusions in the grain (mag. x160).
Figure f:	A well-rounded zircon grain showing both fluid inclusion and inclusion of long rod-like, unknown minerals (mag. x160).

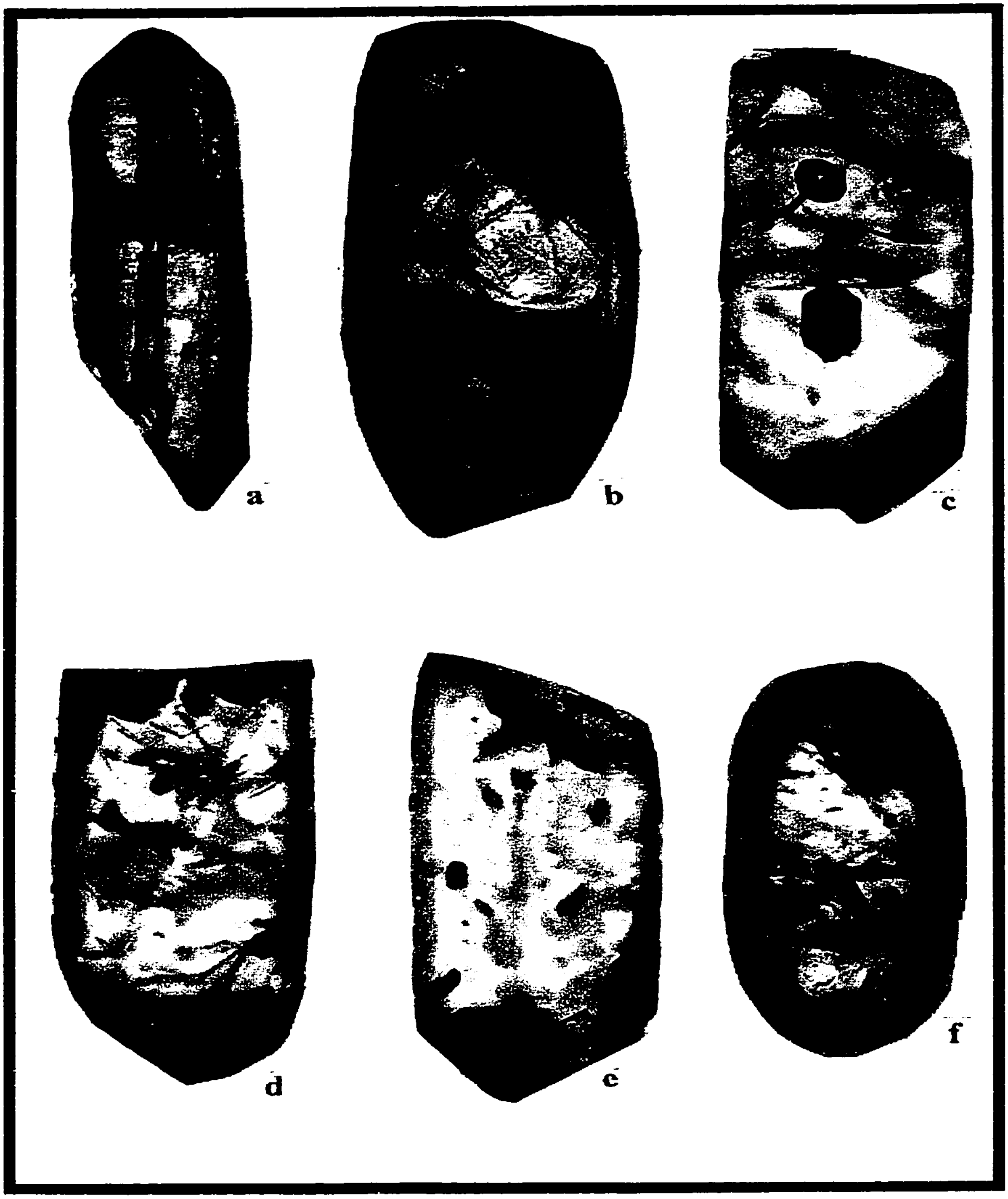

PLATE 6

PATE 7

Figure a.	An euhedral zircon grain with fairly rounded terminal ends. The grain shows typical adamantine luster and inclusions (mag. x250).
Figure b.	A partly rounded euhedral zircon. Note the abundance of inclusions in the grain (mag. x160).
Figure c & f.	Rounded zircon grains (mag. x125 and x160, respectively)
Figure d.	A well-rounded zircon grain (mag. x125).
Figure e.	An euhedral zircon grain with prismatic edge (mag. x160).
Figure g & h.	Euhedral rutile grains showing prismatic crystal boundary. Note the abundance of inclusions (mag. x125).
Figure i.	A rutile grain fragment. This specimen shows the characteristic rutile striations (mag. x125).

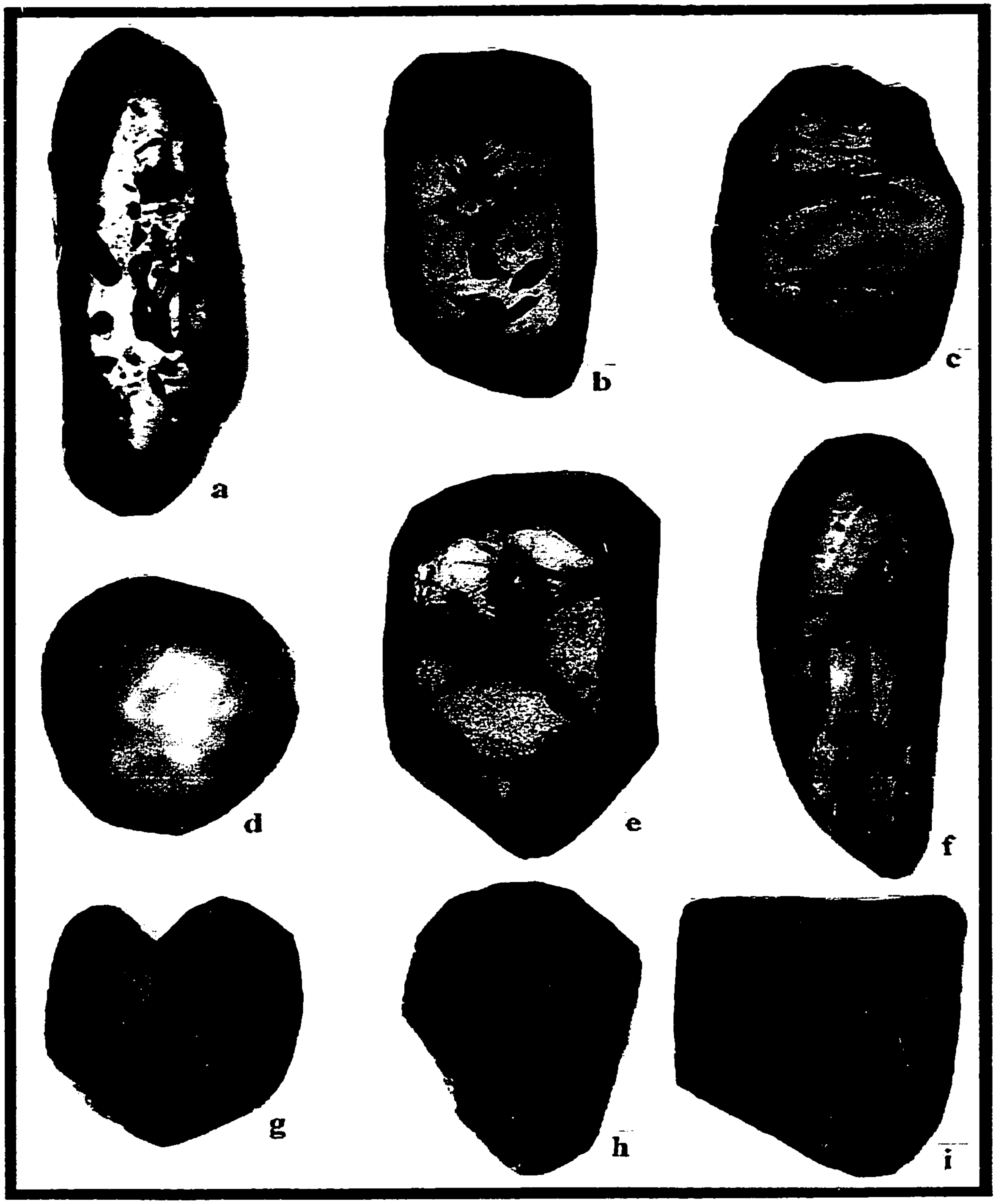

PLATE 7

rutile in the heavy mineral fraction range from zero to 18.77%, 1.05 to 33.33%, 2.99 to 18.81%, 5.5 to 21 % in Ahad Rufaidah, Al Habalah I and II and Al Soudah localities respectively.

Epidotes are common in most of the analyzed samples. The distribution of epidotes range from Zero to 18.77% in Ahad Rufaidah, 2.16 to 18.34 in Al Habalah I, 1.29 to12.75% in Al Habalah II and 8.03 to 16.67% in Al Soudah lo-calities repectively. The grains are angular to subangular, pale yellow to pale green (Plate 8, Figures e and f), show one set of cleavages and parallel extinction. The characteristic weak pleochroism distinguishes epidotes from tourmaline grains in the samples.

Hornblende also occurs frequent though, less abundant than epidote. The grains are platy with hacksaw edges. The hornblende grains show characteristics oblique extinction, strong pleochroism, yellowish to greenish coloration and two sets of cleavages (Plate 8, Figures a - d). The distribution of hornblende ranges from 0.84 to 3.75% in Ahad Rufaidah, 0.6 to 7.69% in Al Habalah I, 0.56 to 6.12% in Al Habalah II and 0.4 to 4.75% Al Soudah localities respectively.

Kyanite is rare in the studied samples. Only a few grains were identified from the samples in Ahad Rufaidah and Al Habalah Areas I and II. The kyanite grains are as colorless to light grey and platy to bladed in shape (Plate 8, Figure h). They show low birefringence and relief.

PLATE 8

Figure a-d.	Photomicrograph of hornblende grains showing hacksaw edges. Two-cleavage traces characteristic of hornblende are apparent in these grains. There are inclusions in the grains as well (mag. x160).
Figure e-f.	These photomicrographs represent typical epidote grains observed in the Wajid Sandstone. The epidotes are distinguished from tourmaline on the basis of their low pleochroism (mag. x125).
Figure g	Photomicrograph of a fragment of tourmaline. This variety is not as common as the pink to red brown variety in the Wajid Sandstone (mag. x125).
Figure h	A platy kyanite. This kyanite shows low relief, birefringence and traces of characteristic cleavage (mag. x125).
Figure i	An opaque mineral in Wajid Sandstone. The opaque minerals are by far the most abundant of the heavy mineral assemblages in the Wajid Sandstone (x125).

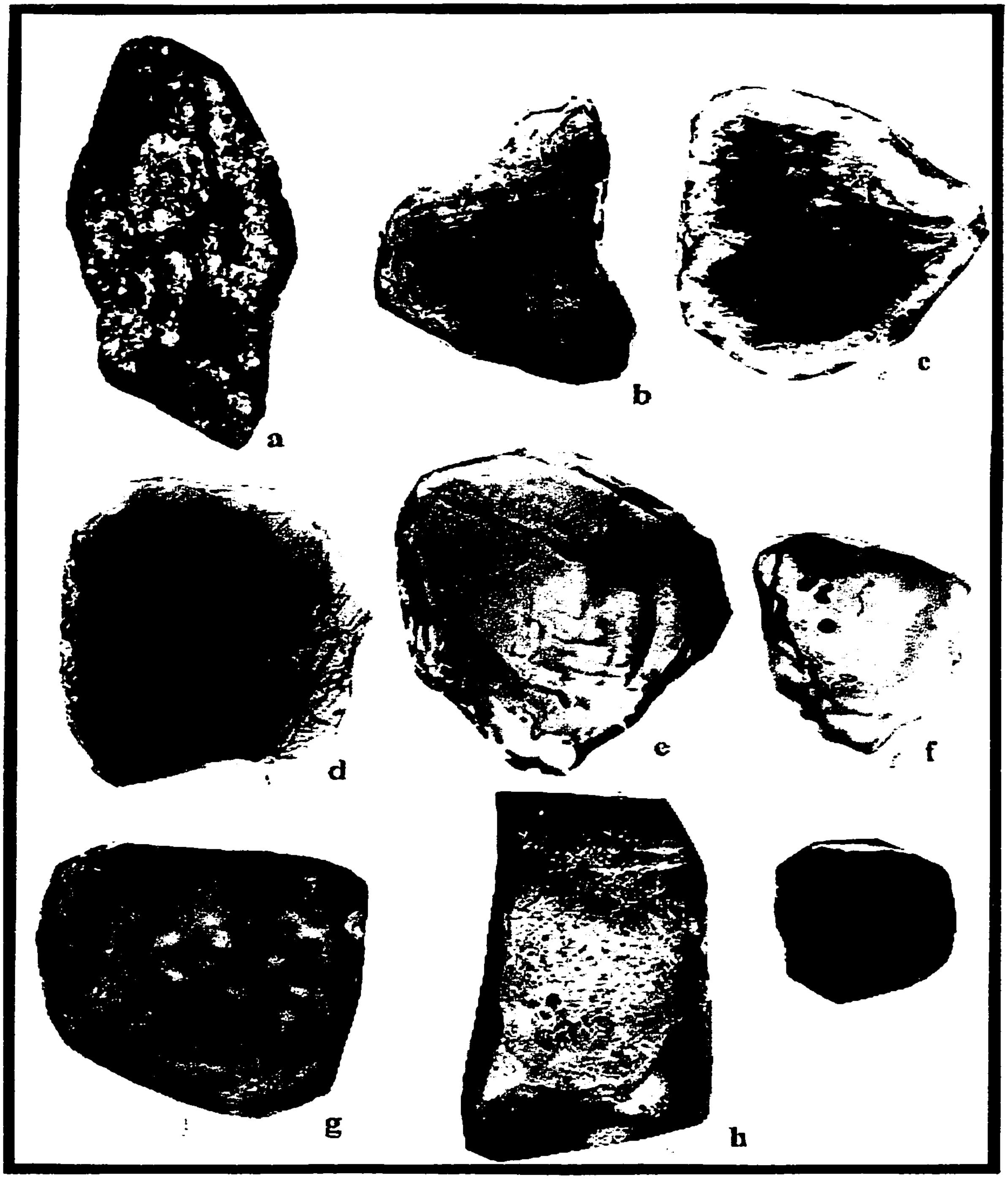

PLATE 8

4.7.4. Multivariate Statistical Analyses

4.7.4.1. Introduction

Multivariate statistical techniques including cluster, factor and discriminant analyses have been extensively utilized in geological studies such as interpreting depositional environments (Klovan, 1966), provenance study and mineral exploration (Miller *et al*, 1977; Ewa *et al*, 1992; Morsy, 1993; Chork and Salminen, 1993 and Borovec, 1996).

Factor analysis attempts to determine the minimum number of independent dimensions needed to account for most of the information in the table of similarity coefficients (Klovan, 1966). For geological applications, it is specifically aimed at recognizing geological factors and reducing data for the purposes of representation (Morsy, 1993).

The classical work of Imbrie and van Andel (1964) is one of the first applications of factor analysis to heavy mineral studies. Using vector analysis as a tool, these authors defined end members and applied these practically to heavy mineral data from the Gulf of California and Orinoco-Guayana shelf. They concluded that provenance interpretations were additionally enhanced compared with the traditional heavy mineral assemblage analytical technique. Briggs (1965) also applied correlation matrix, cluster and factor analyses to interpret provenance from heavy mineral suites. Statteger (1987) analyzed heavy mineral data with the version of the extended Q - mode factor to establish a model of lithological end members for provenance interpretation in terms of plate tectonics.

According to Mezzadri and Saccani (1988), the application of Q-mode factor analysis to heavy mineral assemblages facilitated a more detailed delineation of source terranes.

Cluster analysis organizes data into meaningful structures. That is, it attempts to group components of a given data set depicting similar trends of events or characters to interpretable and manageable associations. In this study, the single linkage method, which

joins objects into successively larger clusters using some measures of similarity, was used to carry out the cluster analysis.

In the present study, both factor and cluster analyses were attempted to additionally enhance the provenance interpretations from the heavy mineral assemblages. In essence, these analyses were carried out with an aim of extracting provenance diagnostic factor end members and cluster associations to supplement provenance interpretation from the heavy mineral data.

4.7.4.2. R-Mode Analysis

4.7.4.2.1. Factor Analysis

A total of three factors were extracted from the heavy mineral assemblages of each of the four locaties. The R-mode factor analysis involving varimax rotation principal components was employed in the analysis of the heavy mineral data (Appendix II). The factors extracted are summarized in Table 4.6 and plotted as ternary diagrams in Figures 4.10 and 4.11. The significance of these factors is discussed in the interpretation section and presented in details as Appendix II.

TABLE 4.6. Summary of the factor loadings for the heavy mineral assemblages in the Wajid Sandstone: (a) Ahad Rufaidah (b) Al Habalah I, (c) Al Habalah II and (d) Al Soudah.

(a)

Factor	Strong Positive (>0.6)	Moderate Positive (<0.6 - 0.45)	Weak Positive (<0.45 -0.2)	Strong/Mod. Negative	Eigen-value	Var. (%)
Factor 1	Tourmaline and hornblende		Rutlile	Zircon and Kyanite	3.189	39.87
Factor 2	Epidote	Unknown	Kyanite	Opaques	2.39	28.87
Factor 3	Tourmaline and Unknown		Rutile & Zircon		1.26	15.8

(b)

Factor	Strong Positive (>0.6)	Moderate Positive (<0.6 - 0.45)	Weak Positive (<0.45 -0.2)	Strong/Mod. Negative	Eigene-value	Var. (%)
Factor 1	Zircon & Unknown		Rutile & Opaques	Tourmaline & Hornblende	3.51	31.09
Factor 2	Opaques	Zircon	Horblende & Unknown	Epidote & Sphene	1.7	18.91
Factor 3	Rutile		Unknown		1.286	14.28

(c)

Factor	Strong Positive (>0.6)	Moderate Positive (<0.6 - 0.45)	Weak Positive (<0.45 -0.2)	Strong/Mod. Negative	Eigene-value	Var. (%)
Factor 1	Epidote, Hornblende			Zircon	2.68	38.33
Factor 2	Rutile & Zircon	Zircon	Unknown		2.1	30.2
Factor 3	Opaques	Rutile	Unknown		1.18	16.9

(d)

Factor	Strong Positive (>0.6)	Moderate Positive (<0.6 - 0.45)	Weak Positive (<0.45 -0.2)	Strong/Mod. Negative	Eigen-value	Var. (%)
Factor 1	Opaques, Rutile and Epidote			Zircon	4.19	52.39
Factor 2		Tourmaline	Opaques	Sphene, Rutile, Zircon & Unknown	2.11	30.2
Factor 3	Hornblende & Zircon	Sphene		Opaques and Tourmaline	2.14	7.53

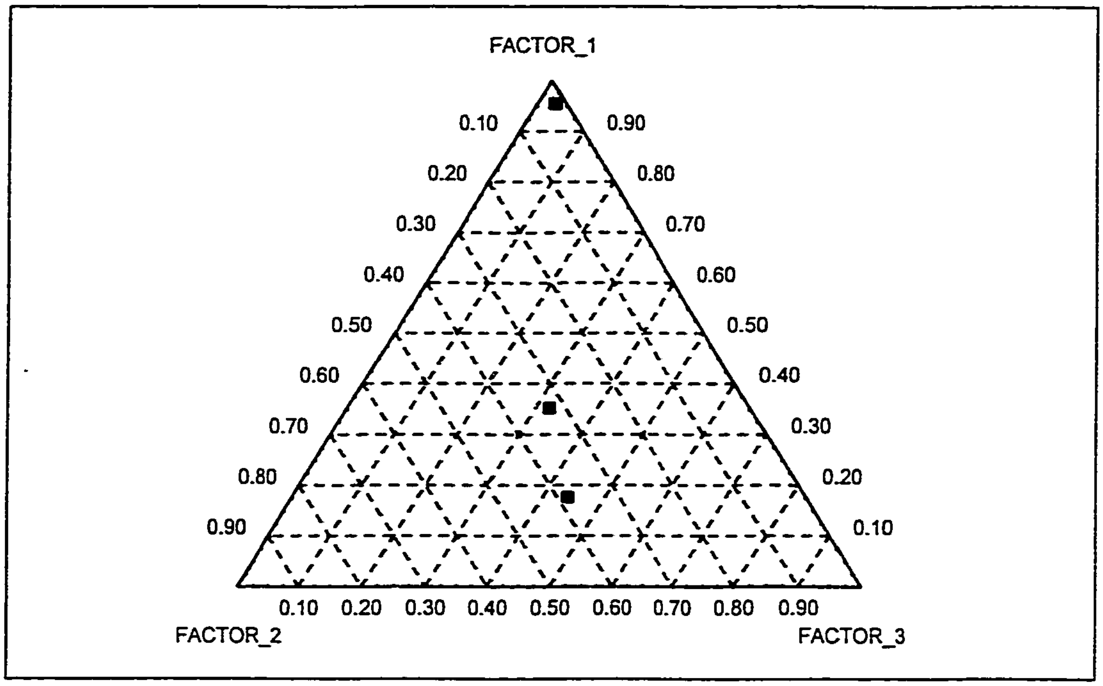

(a)

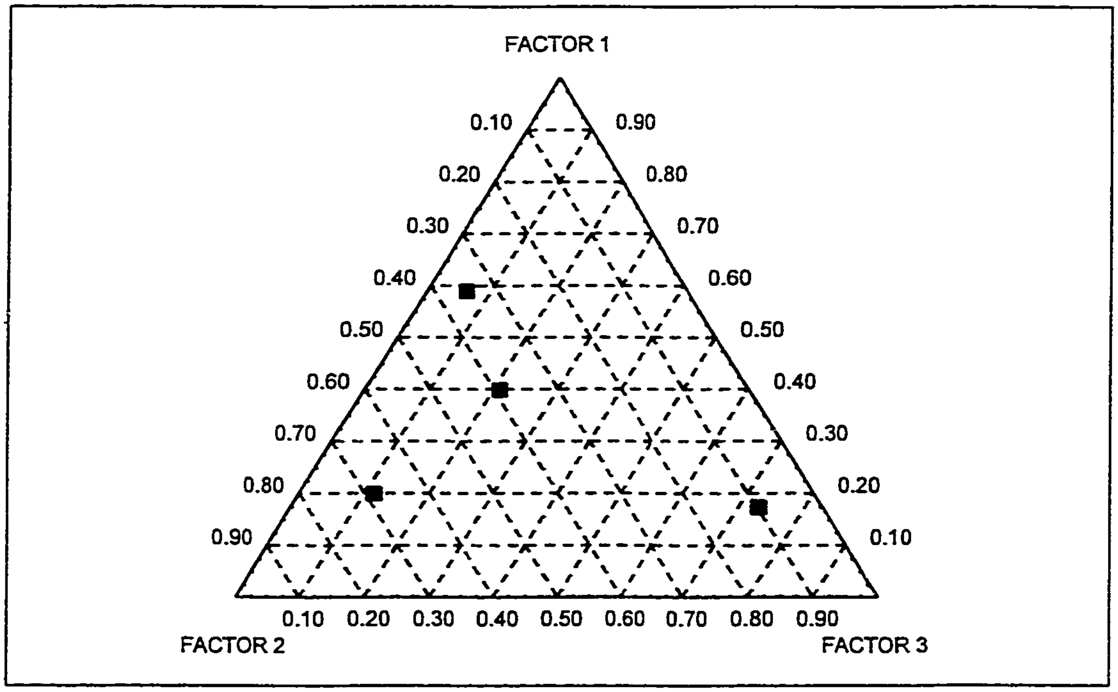

(b)

Figure 4.10. Ternary diagrams showing factor loadings for heavy minerals: (a) Ahad Rufaidah and (b) Al Habalah I.

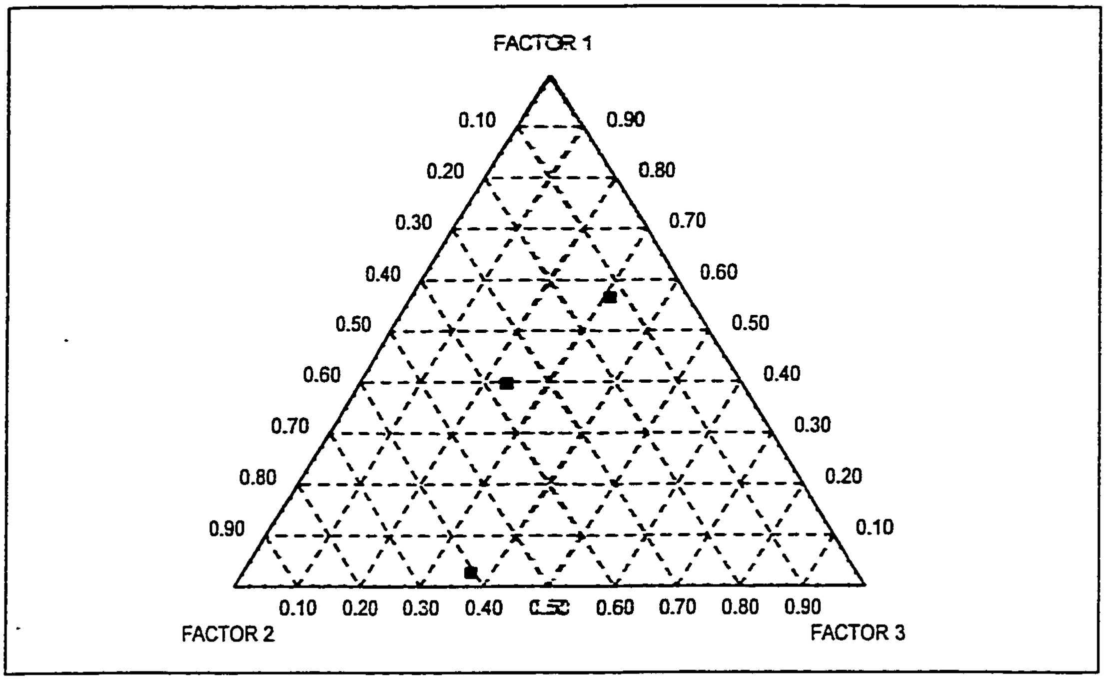

(a)

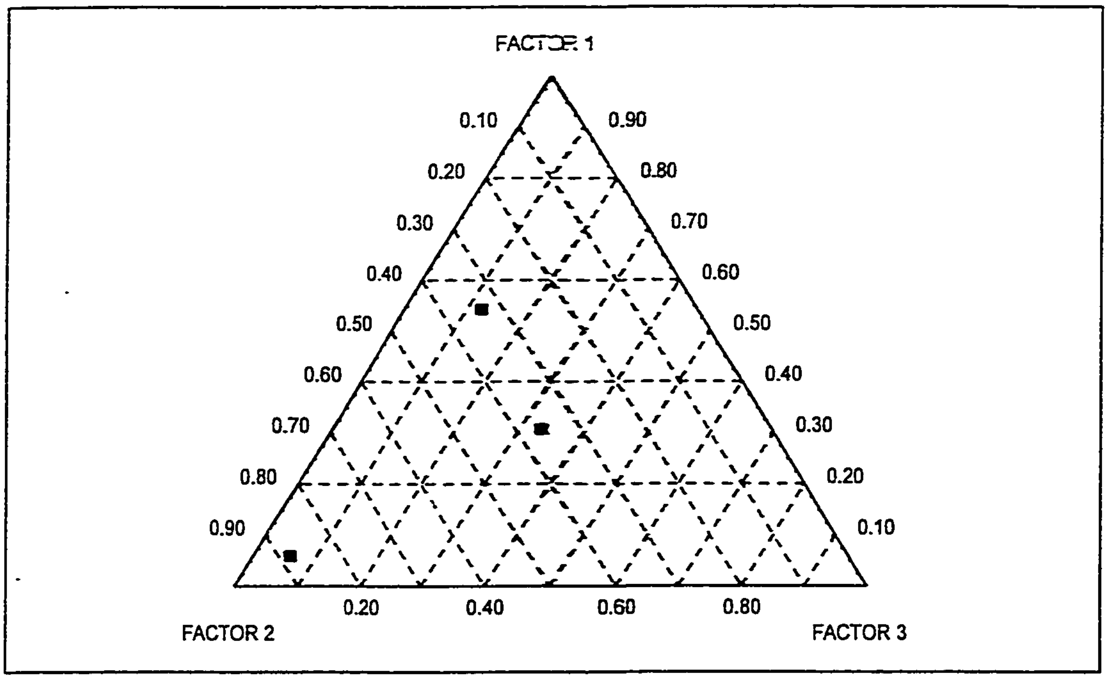

(b)

Figure 4.11. Ternary diagrams showing factor loadings for heavy minerals: (a) Al Habalah II and Al Soudah.

4.7.4.2.2. Cluster Analysis

Two main groups emerged from the cluster analysis of the heavy mineral suites in this study. These groups and their associated end members are presented in Table 4.7 and dendrograms in Figures 4.12 and 4.13.

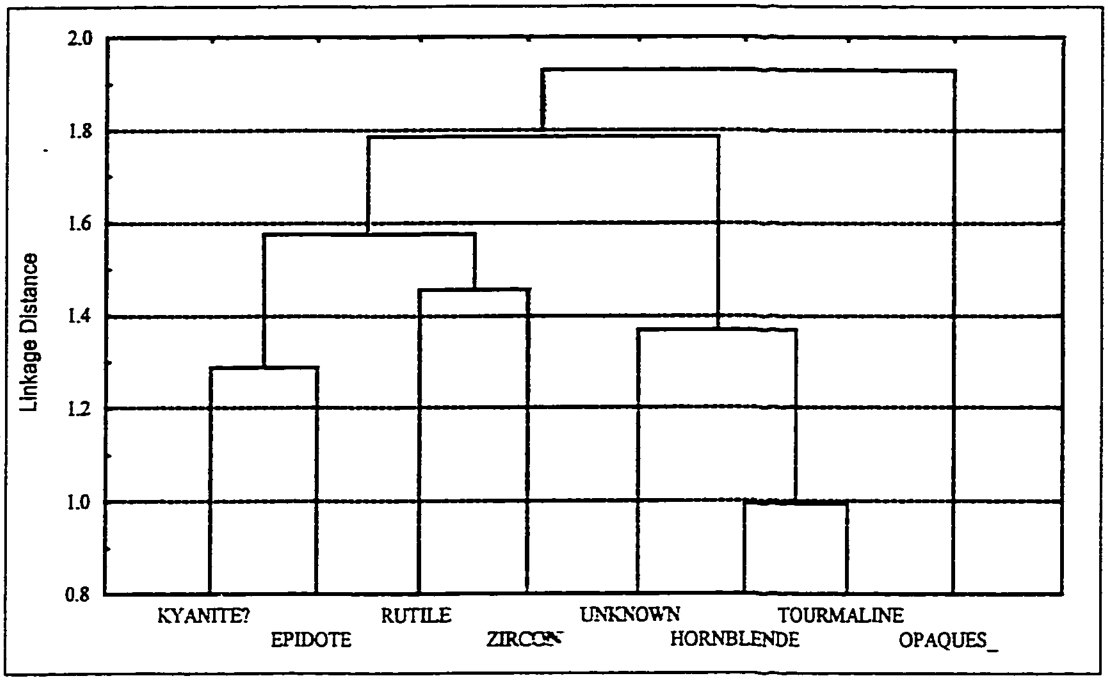

(a)

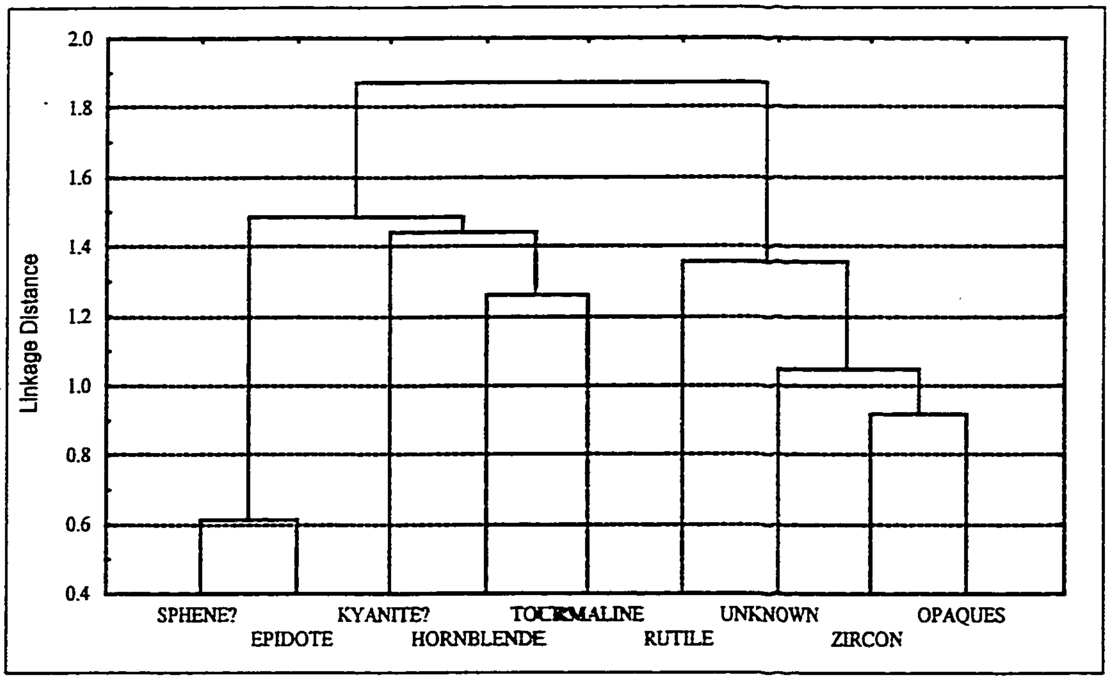

(b)

Figure 4.12. Dendrograms showing clustering of heavy minerals: (a) Ahad Rufaidah and (b) Al Habalah I.

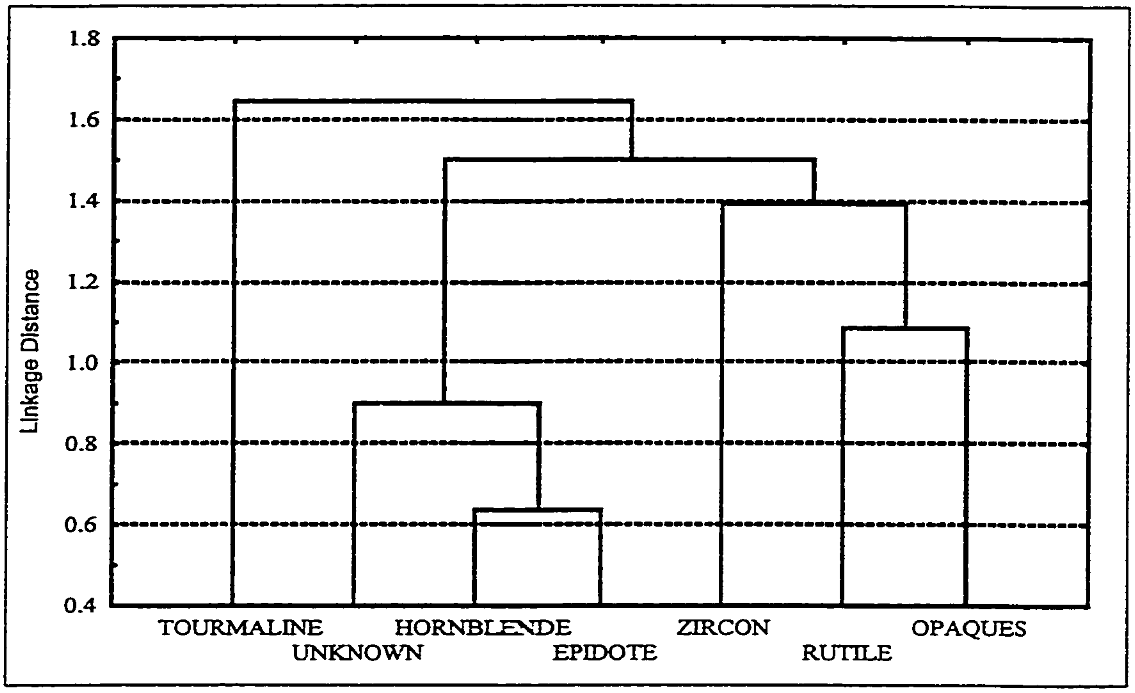

(a)

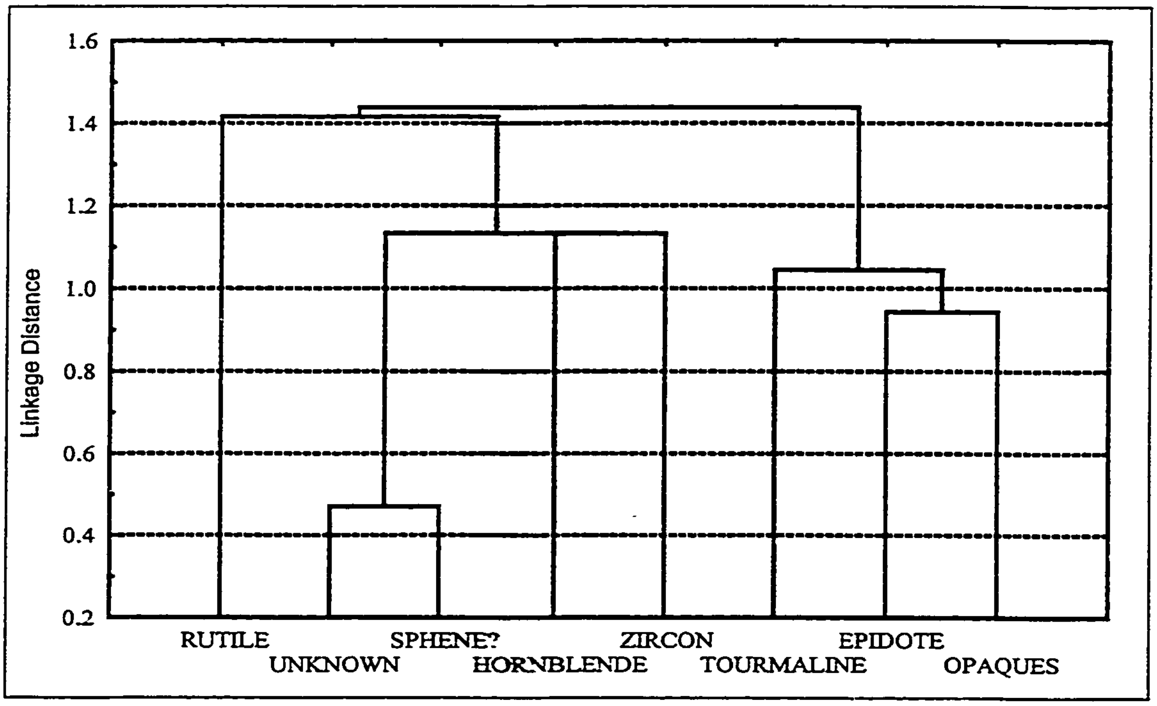

(b)

Figure 4.13. Dendrograms showing clustering of heavy minerals: (a) Al Habalah II and (b) Al Soudah.

Table 4.7. Summary of the cluster groups for the heavy mineral assemblages in the Wajid Sandstone: (a) Ahad Rufaidah, (b) Al Habalah, (c) Al Habalah II and (d) Al Soudah.

(a)

Group	Strong Linkage	Weak Positive	Outlier
A	Kyanite, Epidote, Rutile & Zircon		
B	Hornblende & Tourmaline	Opaques	

(b)

Group	Strong Linkage	Moderate Linkage	Outlier
A	Sphene & Epidote	Hornblende, Kyanite & Tourmaline	
B	Zircon, Opaques and Unknown	Rutile	

(c)

Group	Strong Linkage	Moderate Linkage	Outlier
A	Hornblende, Epidote and Unknown	None	Tourmaline
B	Rutile, Opaques and Zircon	Rutile	

(d)

Group	Strong Linkage	Moderate Linkage	Weak Linkage	Outlier
A	Sphene and Unknown	None	Zircon and Hornblende	Rutile
B	Rutile, Opaques and Zircon	Epidote, Tourmaline and Opaques		

4.7 4.3. Q-Mode Analysis of Heavy Mineral Samples

Q-mode analyses were attempted to characterize the Red Unit and Grey Unit based on their heavy mineral distribution. The factor loadings are summarized in Table 4.8 and plotted as ternary diagram in Figure 4.14

Factor Analysis

Samples from the Red Unit appear to dominate the high factor loading associations in all three factors. Only eight samples from the Grey Unit record factor loadings in excess of 0.6. Heavy mineral distribution is almost the same in the three factors of both units (Figures 4.15). Minor differences are, however, observable. These include lower concentration of opaque minerals in factor 1 of the Grey Unit than in the Red Unit. In factor 3, the distribution of opaque minerals, tourmaline and epidote are lower in Grey Unit than in the Red Unit. In the same vein, zircon and rutile are comparatively lower in the Red Unit than in the Grey Unit (Figure 4.16).

Cluster Analysis

The cluster analysis shows that the groups A and C are constituted by samples from the Red Unit while the assemblage from the group B represents the Grey Unit (Table 4.8). Samples from the Red Unit that cluster with those of Grey Unit in group B of the heavy mineral data probably represent the transitional zone between the Red and Grey Units. It is interesting to note that most of these samples were taken close to the top of the studied outcrops.

TABLE 4.8. Factor and cluster Q-mode Analyses listing associations of samples for different factors and cluster groups: Heavy mineral data

Factor Analysis

FACTOR	RED UNIT	GREY UNIT
1	AR39, AR17, AR14, AR11A, AR6, AR2, ARLC3SC, HA57, HA52, HA45, H44, HA41, HA40, HA39, HA26, HA21, HA15, HA14, HA7, HA5, HAP25, S12, S2	HAP32, HAP16, HAP11, HAP4
2	AR17, AR14, AR13, AR10, HA58, HA50, HA36, HA26, HA21, HA15,HA7, HA5	HAP22, HAP13
3	AR17, AR8,HA41, HA26, S21, S17, S8, HAP24	HAP20, HAP16, HAP7, HAP3

Cluster Analysis

GROUP	RED UNIT	GREY UNIT
A	HA36, HA50, S13, S21, S12, S8	HAP24
B	S17, AR8, AR2, AR39, , HA26, HA41, ARLC3SC, HA40, S2 HAP 25, AR11A, HA52, HA57	HAP3, HAP7B, HAP20, HAP16 HAP4, HAP32, HAP39, HAP11
C1	A17, HA7, AR6, HA14, HA21, AR14, HA5, HA44, HA45	HAP13
C2	AR13, HA15, HA15, , AR10, HA58	HAP22

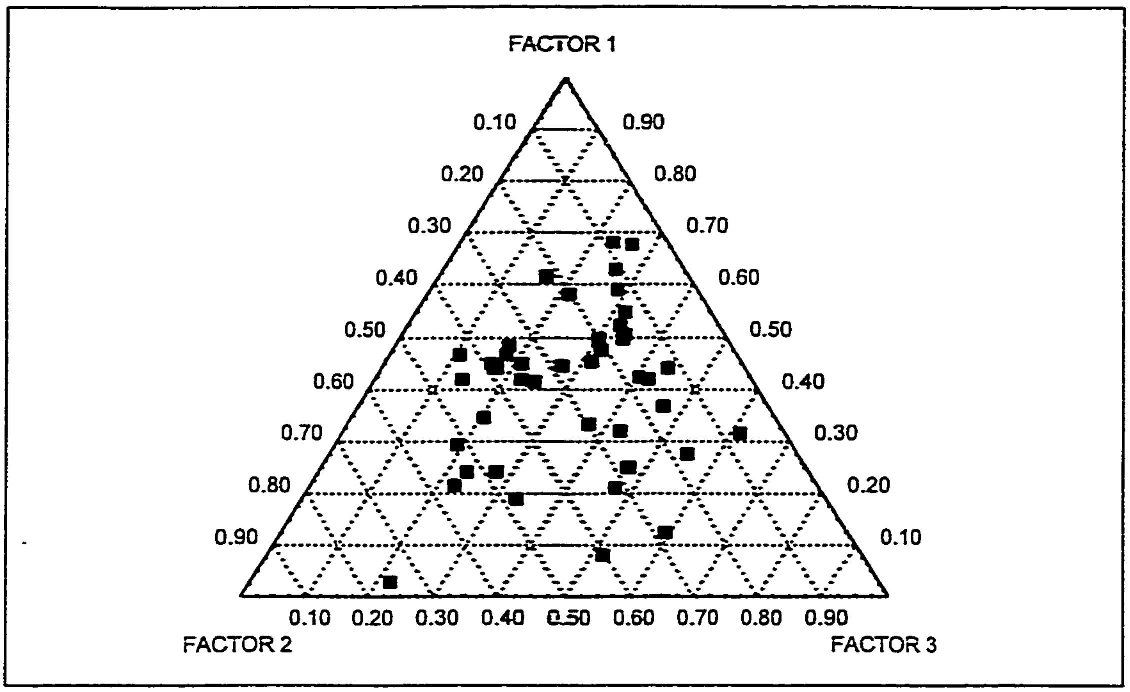

(a)

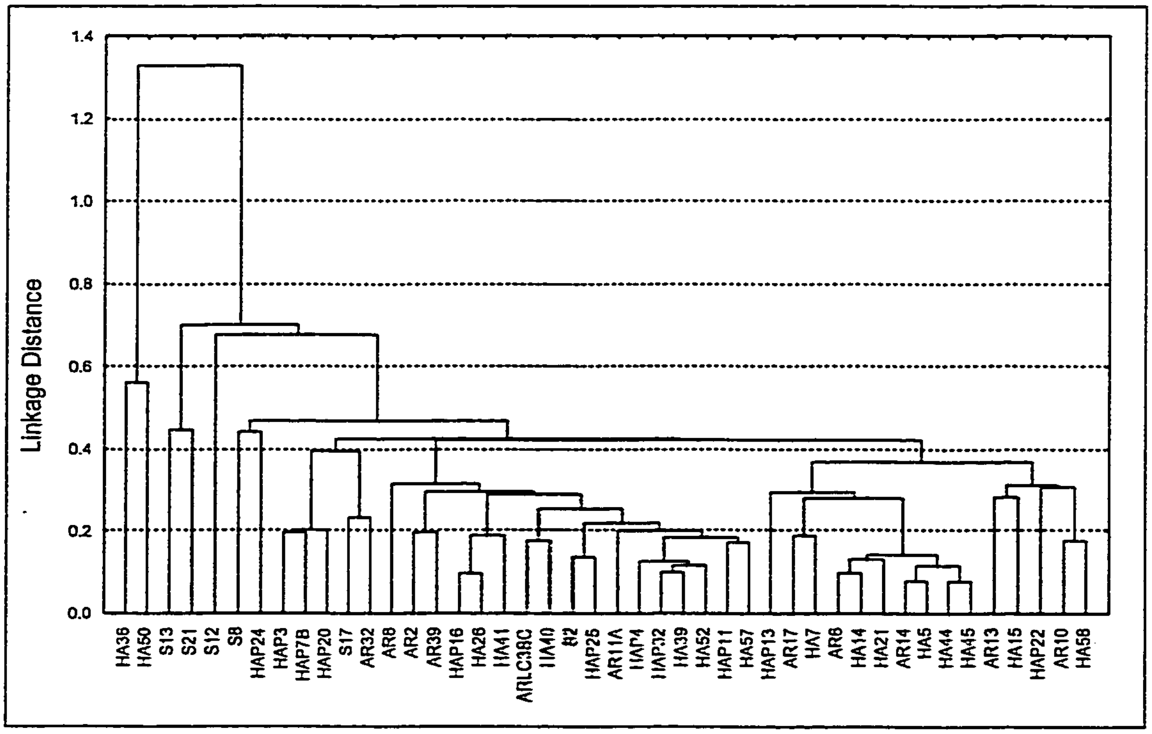

(b)

Figure 4.14. Ternary diagram and dendrogram of the Q-mode factor and cluster analyses of heavy mineral samples: (a) Ternary diagram anfd (b) Dendrogram. Mainly samples from the heavy the Red Unit dominate the extracted factors.

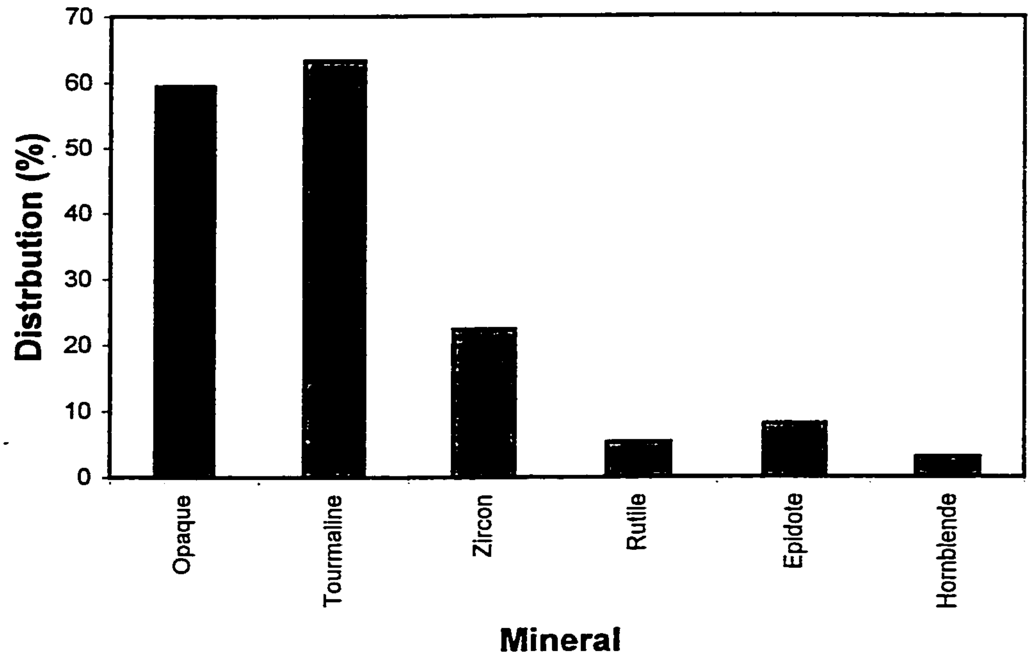

(a)

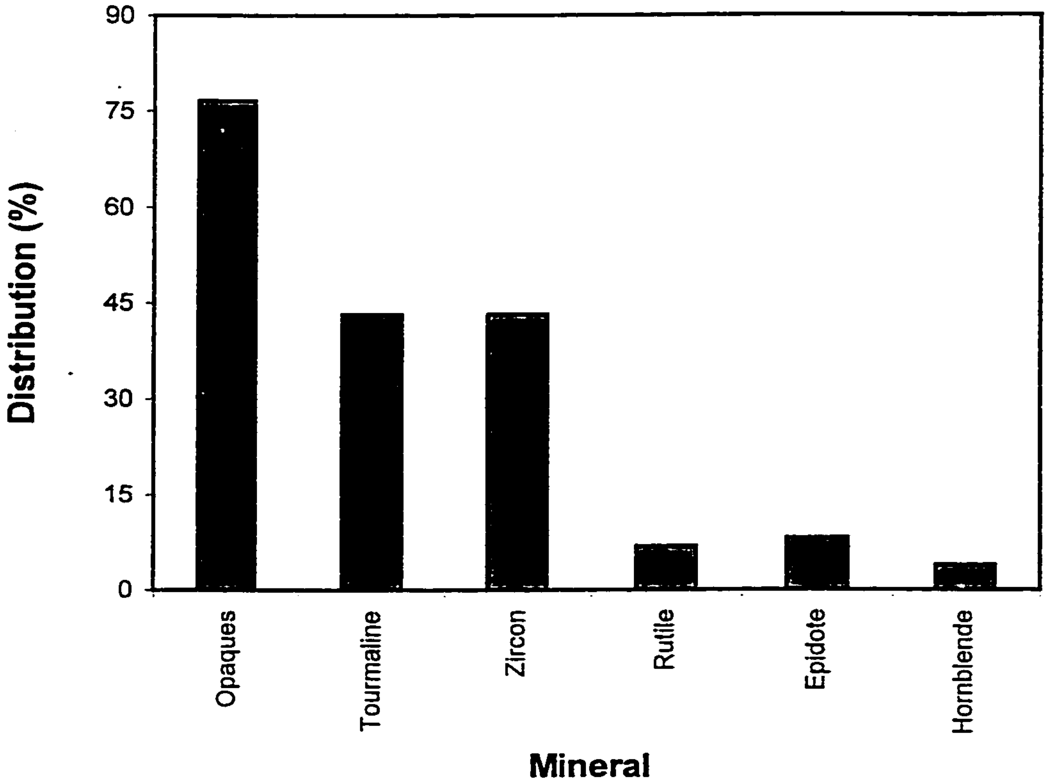

(b)

Figure 4.15. Heavy mineral distribution in the different factors as delineated by Q-mode factor analysis: (a) Factor 1 and (b) Factor 2. Opaque minerals and zircon appear slightly higher in factor 2 than in factor 1 while tourmaline is higher in factor 1 than in factor 2.

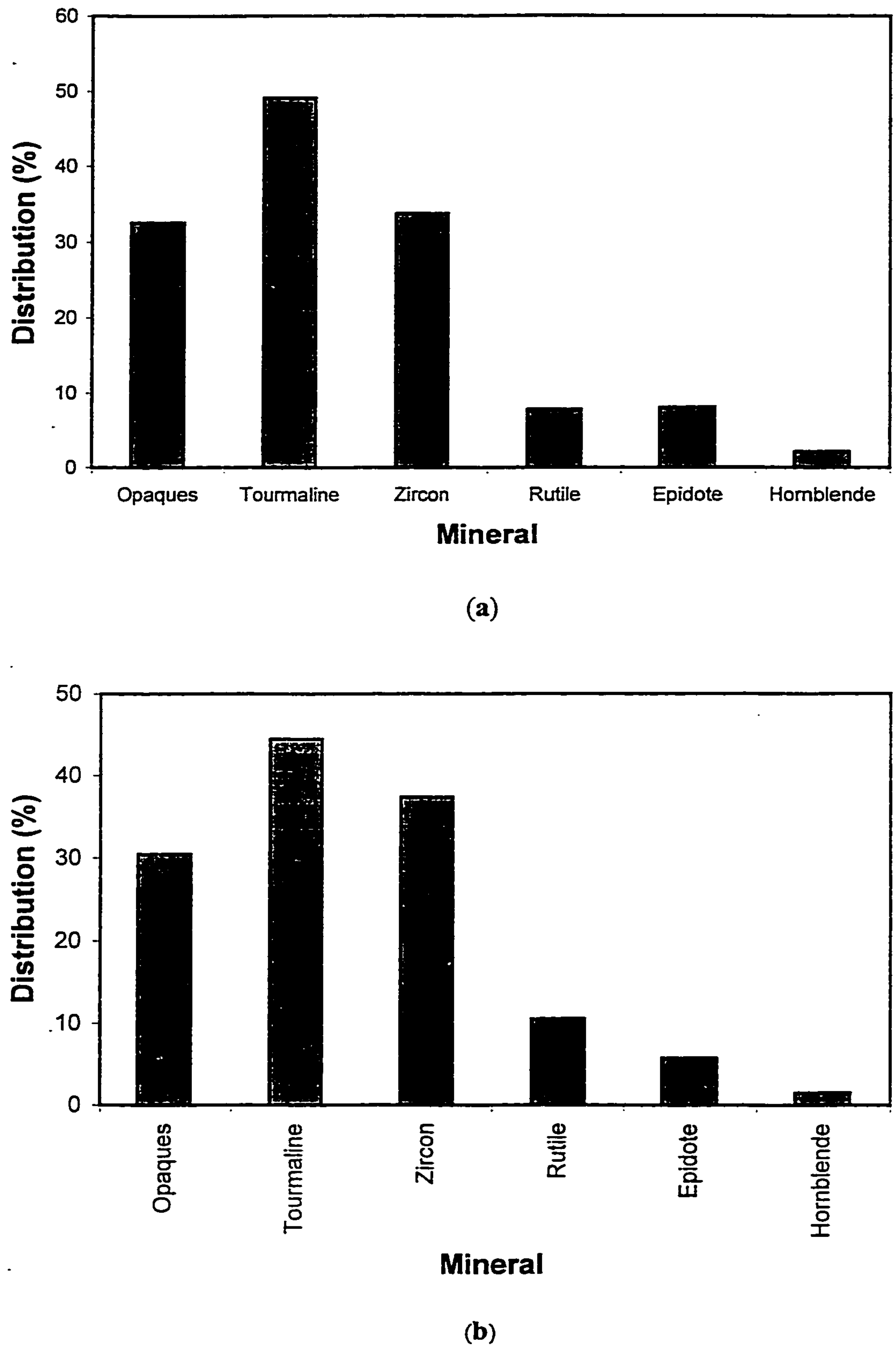

Figure 4.16. Heavy mineral distribution in factor 3 as delineated by Q-mode factor analysis: (a) Red Unit and (b) Grey Unit. The distribution of heavy mineral in factor 3 is similar in the two units.

CHAPTER FIVE

GEOCHEMISTRY

5.1 Introduction

Trace element chemistry may be used to decipher sediments provenance, paleogeographic reconstruction and unroofing tectonic history. The common preservation of chemical signatures of mafic components (e.g. Mg, Cr, Co and Ni) through weathering and diagenesis (van de Kemp and Leake, 1985) has enhanced the use of trace element geochemistry as an important tool in identifying and revealing the details of the sediments composition. It is also useful in determining the time of the movement of sediments from the source terrain (Garver and Scott, 1995). Garver and Royce (1993) interpreted anomalously high concentrations of Cr and Ni, and values of Cr/Ni ranging from 1.2 to 1.6 as indicators of ultramafic source rock. According to these authors Cr/Ni ratio in excess of this value suggests mafic volcanic source rocks. Garver and Scott (1995) used the concentrations of Cr, Ni, and V as well as ratios Cr/Ni, V/Cr, V/Ni, Ba_N/La_N and La_N/Sm_N to determine provenance and terrain accretion of the southern

Canadian Cordillera. van de Kemp and Leake (1985) put the thresholds of Co, Cr and Ni concentrations indicating ultramafic source rocks at >10, >200 and >50ppm respectively. According to Gole (1967) Cr/Ni ratio of 1.6 indicates ultramafic source.

Girty *et al* (1996) used Al_2O_3/TiO_2 index to differentiate mafic source rocks from felsic to intermediate source in the Paleozoic chert and argillites of Sierra Nevada. According to these authors, values less than ~14 indicate mafic rocks whilst higher values suggest acidic to intermediate source rocks. Discriminating diagrams of $Al_2O_3/(Al_2O_3+Fe_2O_3)$ versus Fe_2O_3/TiO_2 and $Al_2O_3/(Al_2O_3+Fe_2O_3)$ versus La_N/Ce_N. originally proposed by Murray (1994) were also used by these authors to differentiate between continental margin-island arc and mid-oceanic ridge basalt and seamount or ocean island basalt sources.

Fornelli and Piccarreta (1997) observed a positive correlation between MgO and Ni + Cr for ultramafic source terrane while low concentrations of Cr and Ni were used to indicate the absence of mafic and ultramafic sources. According to these authors, higher feldspar contents at the source are also reflected by high concentrations of K_2O, Al_2O_3, Sr, and Rb in sediments. They also noted that the association of high Al_2O_3, MgO, Fe_2O_3, Sr, Be, and V contents with low Cr and Ni reflects abundance of andesitic detritus at the source.

Holail and Moghazi (1998) inferred mafic source rocks with high concentrations of Cr, Ni and MgO for the greywacke and siltstone in Hammamat area of Egypt. Based on higher concentrations of Nb, Zr, Y and low TiO_2, Al_2O_3, MgO and CaO, they also inferred felsic igneous rocks provenance.

In the present study, elemental and whole rock chemistry was used to determine the provenance, paleogeography and tectonic history of the Wajid Sandstone.

5.2. Distribution of Elements

A total of eighty-seven (87) samples including ten (10), from the surrounding basement comlpex were analyzed for both elemental and bulk composition (Appendix IIIa).. These data were analyzed using multivariate statistical tools. Relevant provenance, chemical index of alteration, depositional environments and chemical maturity indices were determined. The major and trace elements distribution patterns are presented in Figures 5.1 and 5.2 and described in the following section. Some of the calculated parameters and indices are, summarized in Tables 5.1 and 5.2 and presented in Figures 5.3 - 5.11. The raw data are also presented in Appendix IIIa.

TABLE 5.1. Distribution of some selected trace elements in the basement samples

Sample	Ba (ppm)	Co (ppm)	Cr (ppm)	Cu (ppm)	La (ppm)	Mn (ppm)	Mo (ppm)	Ni (ppm)
B1(?gabbro)	40	21	129	30	<10	740	3	25
B2 (gabbro)	20	24	387	86	30	360	2	281
B3 (mica schist)	170	7	44	4	40	300	2	21
B4 (biotite gneiss)	70	5	52	11	40	225	3	5
B5 (pegmatite)	<10	2	154	6	<10	30	1	11
B6 (pegmatite)	10	1	77	6	<10	75	<1	3
B7 (S11-talc?)	30	<1	26	<1	50	25	1	2
B8 (granite)	10	1	75	7	60	215	3	9
B9 (S43 - schist)	30	43	93	32	<10	915	4	47
B10 (pegmatite)	<10	1	103	4	10	30	1	4
B11(schist)	20	29	123	46	<10	810	3	24
Average	**44.44**	**13.4**	**114.82**	**23.2**	**38.33**	**338.64**	**2.3**	**39.27**

TABLE 5.1. Contd.

Sample	P (ppm)	Sc (ppm)	Sr (ppm)	V (ppm)	Zn (ppm)	Cr/Ni	V/Cr	V/Ni
B1(?gabbro)	980	4	20	92	74	5.16	0.713	3.68
B2 (gabbro)	1750	17	61	36	32	1.377	0.093	0.128
B3 (mica schist)	1620	4	28	48	98	2.095	1.09	2.285
B4 (biotite gneiss)	590	3	95	41	24	10.4	0.788	8.2
B5 (pegmatite)	90	3	2	20	8	14	0.129	1.818
B6 (pegmatite)	70	<1	4	4	8	25.66	0.051	1.333
B7 (S11-talc?)	130	1	14	1	10	13	0.038	0.5
B8 (granite)	210	1	16	4	30	8.333	0.053	0.444
B9 (S43 - schist)	1310	5	24	69	92	1.978	0.74	1.468
B10 (pegmatite)	100	<1	4	8	2	25.75	0.077	2
B11(schist)	950	5	21	105	76	5.125	0.853	4.375
Average	**709.09**	**4.778**	**26.27**	**38.90**	**41.27**	**10.26**	**0.42**	**2.38**

TABLE 5.2. Distribution of some selected trace elements and indices in Wajid Sandstone

Ahad Rufaidah Locality											
Sample	Co (ppm)	Cr (ppm)	Cu (ppm)	Mn (ppm)	Ni (ppm)	P (ppm)	Sr (ppm)	V (ppm)	Cr/Ni	V/Cr	V/Ni
AR3	9	81	3	1455	12	270	15	12	6.75	0.15	1
AR6	<1	24	1	15	1	40	29	1	24	0.04	1
AR9A	17	63	3	>10000	12	1520	87	10	5.25	0.16	0.833
AR15	4	46	<1	220	13	50	7	6	3.538	0.13	0.462
AR19	3	95	3	70	5	310	20	103	19	1.08	20.6
AR20	<1	44	1	20	1	20	12	12	44	0.27	12
AR21	<1	50	3	35	3	10	27	5	16.67	0.1	1.667
AR22	1	99	6	55	6	50	16	11	16.5	0.11	1.833
AR23	<1	29	1	15	2	10	17	4	14.5	0.14	2
AR25	2	52	7	145	16	50	19	19	3.25	0.37	1.188
AR35	9	71	20	145	7	80	11	4	10.14	0.06	0.571
AR43	<1	28	3	35	1	30	20	3	28	0.11	3
AR51	7	109	13	70	9	50	44	14	12.11	0.13	1.556
ARLC4K1	<1	30	1	<5	1	20	5	8	30	0.27	8
ARLC4K2	<1	39	1	20	1	10	15	2	39	0.05	2
ARLC4K3	<1	24	1	55	3	20	59	8	8	0.33	2.667
ARLC3SC	4	180	2	40	5	80	31	133	36	0.74	26.6
Average	**6.22**	**62.59**	**4.313**	**159.67**	**5.765**	**154**	**25.53**	**20.9**	**18.6**	**0.25**	**5.1**
Habalah I Locality											
Sample	**Co (ppm)**	**Cr (ppm)**	**Cu (ppm)**	**Mn (ppm)**	**Ni (ppm)**	**P (ppm)**	**Sr (ppm)**	**V (ppm)**	**Cr/Ni**	**V/Cr**	**V/Ni**
HA2	<1	75	<1	10	4	220	44	14	18.75	0.19	3.5
HA9	<1	65	1	10	2	30	5	12	32.5	0.18	6
HA13	1	44	3	25	4	50	10	10	11	0.23	2.5
HA14	4	57	7	90	13	80	5	13	4.385	0.23	1
HA15	1	83	4	40	10	80	5	5	8.3	0.06	0.5
HA18	<1	34	3	30	4	90	15	28	8.5	0.82	7
HA20	<1	47	4	5	3	10	5	2	15.67	0.04	0.667
HA23	<1	38	2	5	3	10	1	1	12.67	0.03	0.333
HA24	4	41	11	435	13	110	4	58	3.154	1.41	4.462
HA25	<1	29	5	50	5	10	20	6	5.8	0.21	1.2
HA27	7	68	9	285	19	140	4	88	3.579	1.29	4.632
HA28	<1	15	3	10	1	80	331	2	15	0.13	2
HA30	<1	10	3	25	<1	90	243	3	11.11	0.3	3.33
HA31	<1	16	7	15	3	90	225	10	5.333	0.63	3.333
HA35	<1	54	4	25	3	20	21	3	18	0.06	1
HA36	3	39	3	45	12	340	10	23	3.25	0.59	1.917
HA38	1	133	4	20	5	40	17	10	26.6	0.08	2
HA45	3	87	8	45	13	70	5	12	6.692	0.14	0.923
HA47	1	48	3	130	4	20	2	9	12	0.19	2.25
HA51	1	48	4	35	10	40	14	15	4.8	0.31	1.5
HA52	<1	26	1	10	1	40	17	5	26	0.19	5
HA56	<1	56	1	15	2	40	5	16	28	0.29	8

TABLE 5.2. Contd.

HA59	2	61	3	20	4	30	8	8	15.25	0.13	2
HA62	<1	24	1	15	2	30	5	4	12	0.17	2
HA64	32	89	68	35	12	40	12	3	7.417	0.03	0.25
OUT5K	<1	26	1	15	2	20	8	8	13	0.31	4
OUT5I1	3	67	3	80	7	60	7	41	9.571	0.61	5.857
OUT5I2	3	105	3	105	6	100	14	77	17.5	0.73	12.83
OUT6C	1	13	4	35	4	90	342	9	3.25	0.69	2.25
OUT6I	14	81	12	130	57	100	6	108	1.421	1.33	1.895
Average	**5.06**	**52.63**	**6.379**	**59.83**	**7.86**	**72.3**	**47**	**20.1**	**12**	**0.39**	**3.1**
	Habalah II Locality										
Sample	**Co (ppm)**	**Cr (ppm)**	**Cu (ppm)**	**Mn (ppm)**	**Ni (ppm)**	**P (ppm)**	**Sr (ppm)**	**V (ppm)**	**Cr/Ni**	**V/Cr**	**V/Ni**
HAP1	3	103	7	75	9	110	8	13	11.44	0.13	1.444
HAP7	1	68	5	25	5	80	13	1	13.6	0.01	0.2
HAP9	12	120	27	50	7	80	9	1	17.14	0.01	0.143
HAP10	1	80	6	35	6	70	27	1	13.33	0.01	0.167
HAP11	1	111	4	10	4	10	8	4	27.75	0.04	1
HAP13	1	61	6	40	4	100	5	1	15.25	0.02	0.25
HAP16	6	60	13	25	6	50	6	4	10	0.07	0.667
HAP17	<1	41	3	15	2	10	10	3	20.5	0.07	1.5
HAP19	<1	22	1	10	1	10	5	4	22	0.18	4
HAP21	<1	42	1	10	2	<10	5	2	21	0.05	1
HAP23	<1	38	1	15	1	20	8	5	38	0.13	5
HAP28	4	66	8	50	11	80	6	22	6	0.33	2
HAP29	<1	39	3	20	3	40	7	1	13	0.03	0.333
HAP31	<1	80	2	<5	3	50	26	56	26.67	0.7	18.67
HAP33	<1	26	1	10	1	10	5	3	26	0.12	3
HAP37	29	95	60	30	10	170	17	3	9.5	0.03	0.3
HAP40	39	58	75	50	12	50	11	7	4.833	0.12	0.583
Average	**9.7**	**65.29**	**13.12**	**29.375**	**5.118**	**58.8**	**10.35**	**7.71**	**17.4**	**0.12**	**2.4**
					Al Soudah						
Sample	**Co (ppm)**	**Cr (ppm)**	**Cu (ppm)**	**Mn (ppm)**	**Ni (ppm)**	**P (ppm)**	**Sr (ppm)**	**V (ppm)**	**Cr/Ni**	**V/Cr**	**V/Ni**
S1	3	79	6	50	7	250	3	37	11.29	0.47	5.286
S2	<1	64	3	15	4	50	8	9	16	0.14	2.25
S5	4	42	11	110	15	230	5	28	2.8	0.67	1.867
S8	<1	76	4	20	3	30	3	1	25.33	0.01	0.333
S12	5	42	10	210	15	200	3	16	2.8	0.38	1.067
S13	2	31	6	25	10	150	4	16	3.1	0.52	1.6
S13B	2	52	6	105	7	120	7	10	7.429	0.19	1.429
S15	4	64	2	180	8	220	6	3	8	0.05	0.375
S20	4	75	6	95	13	120	3	13	5.769	0.17	1
S26	4	52	3	185	8	510	7	28	6.5	0.54	3.5
S28	2	49	1	25	3	110	4	82	16.33	1.67	27.33
S30	3	39	3	55	5	80	1	10	7.8	0.26	2
S39	4	24	1	140	9	40	<1	9	2.667	0.38	1
Average	**3.3636**	**53**	**4.769**	**93.462**	**8.6667**	**176.7**	**4.5**	**20.154**	**8.909**	**0.42**	**3.772**

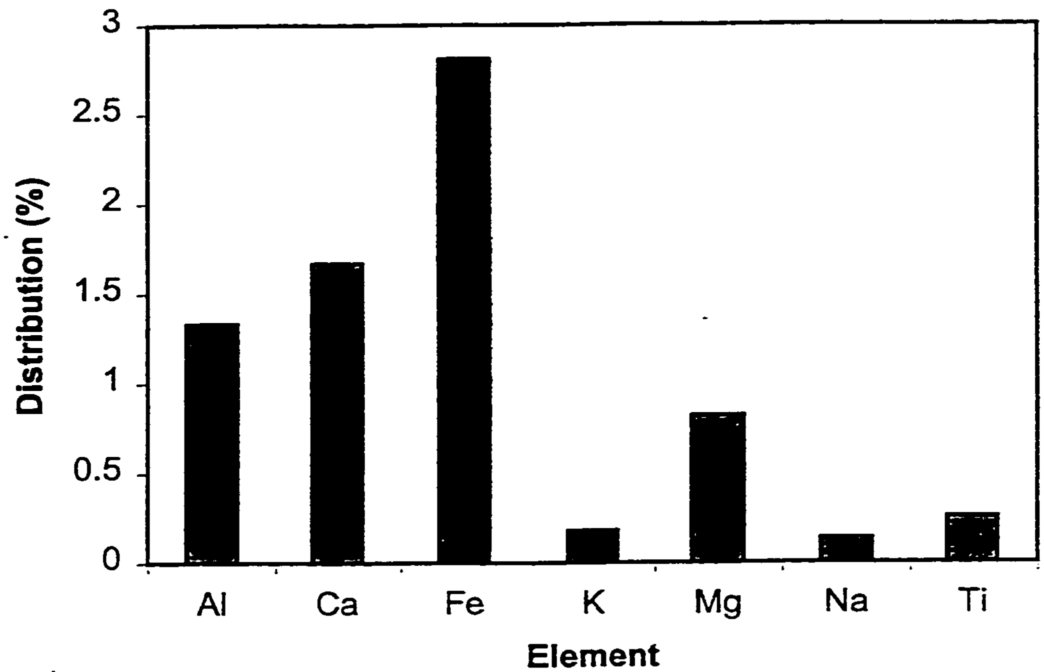

(a)

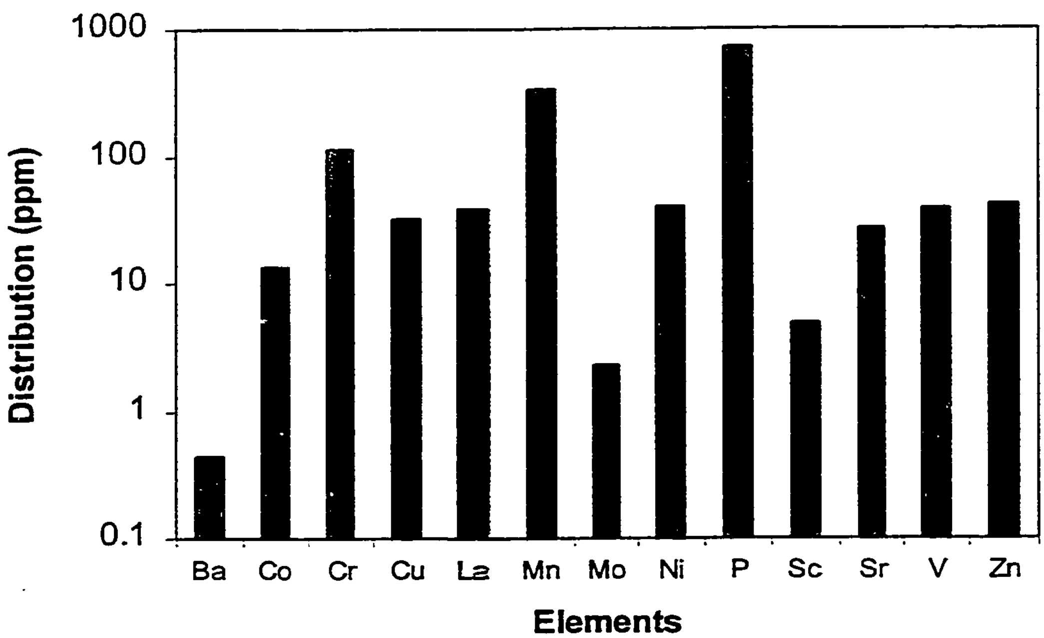

(b)

Figure 5.1: Relative distribution of different elements in the basement samples: (a) Major elements and (b) Trace elements. Note the high concentrations of Fe, Cr, Mn and P in the samples.

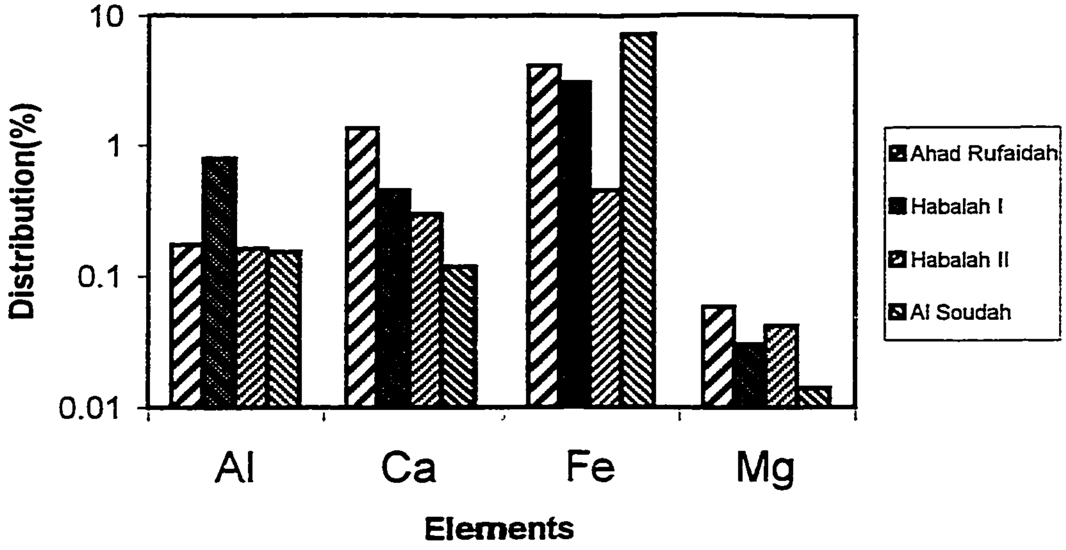

(a)

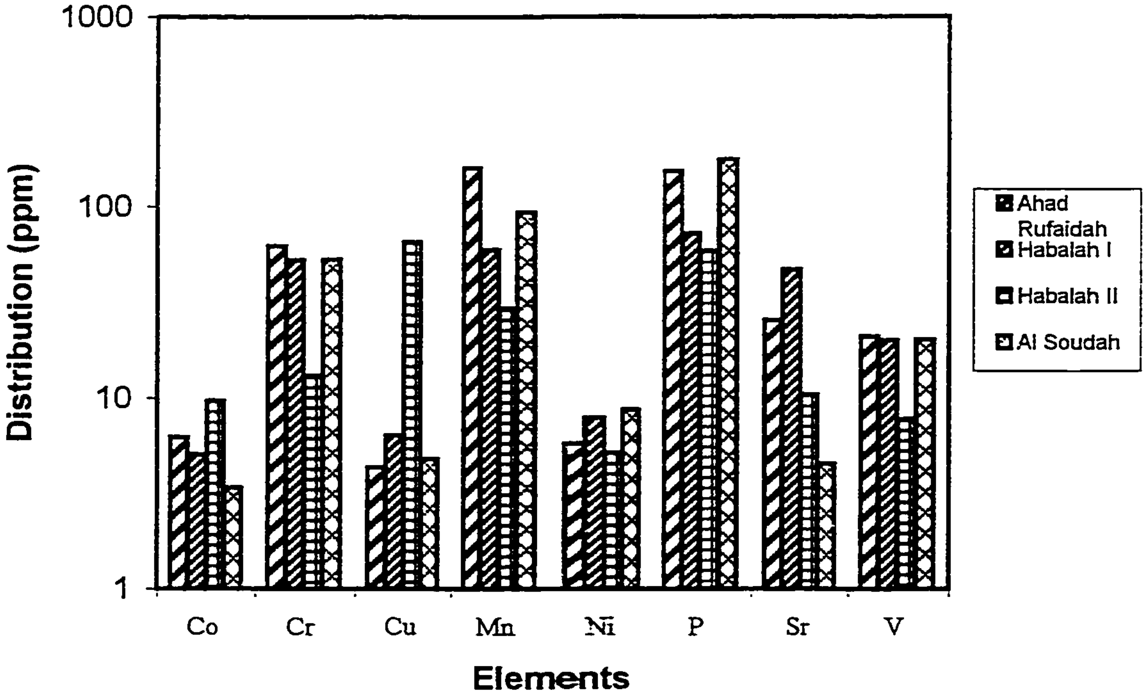

(b)

Figure 5.2. Relative distribution of different elements in Wajid Sandstone: (a) Major elements and (b) Trace elements. The distribution of Fe is higher in the Ahad Rufaidah, Al Habalah I and Al Soudah samples than in the Al Habalah II samples. Co and Cu concentrations are higher in Al Habalah II than in the other three localities.

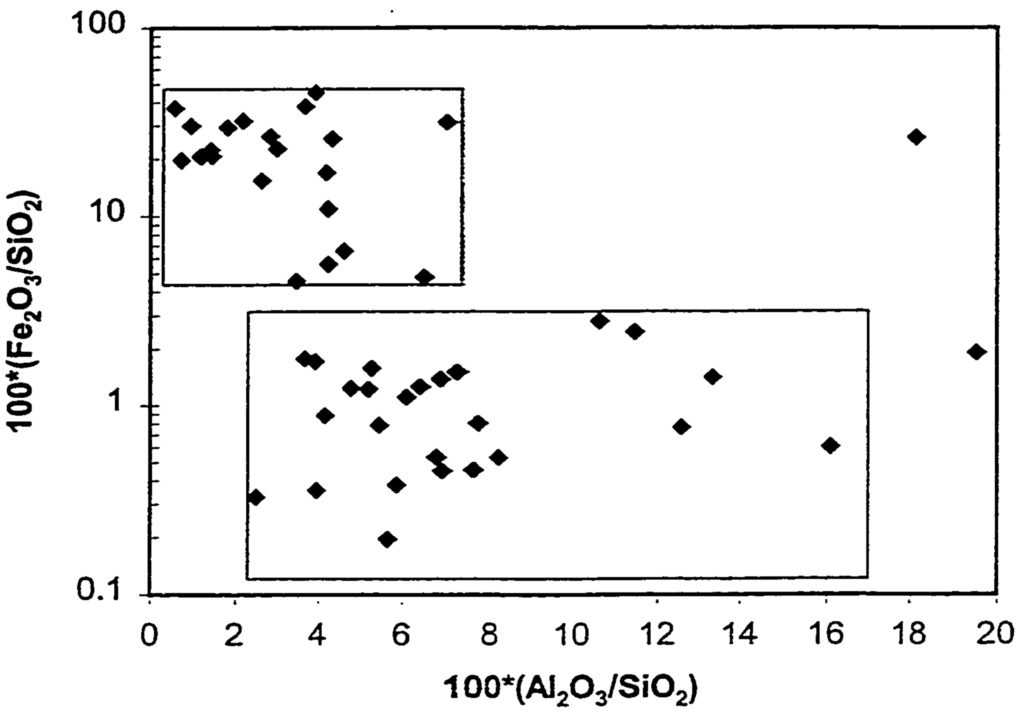

(a)

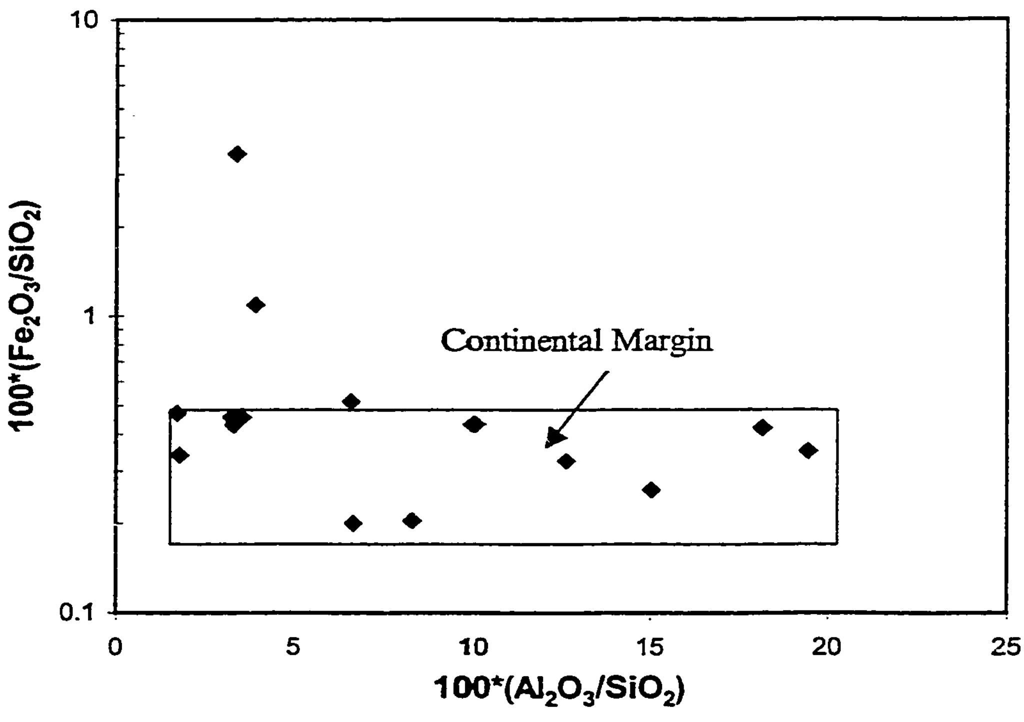

(b)

Figure 5.3. Bivariate plots of 100*(Al_2O_3/SiO_2) and 100*(Fe_2O_3) in the Wajid Sandstone: (a) Red Unit and (b) Grey Unit. The plots indicate a predominantly continental margin tectonic provenance in both the Red and Grey Units. Contribution from oceanic ridge terrane is also shown for the Red Unit.

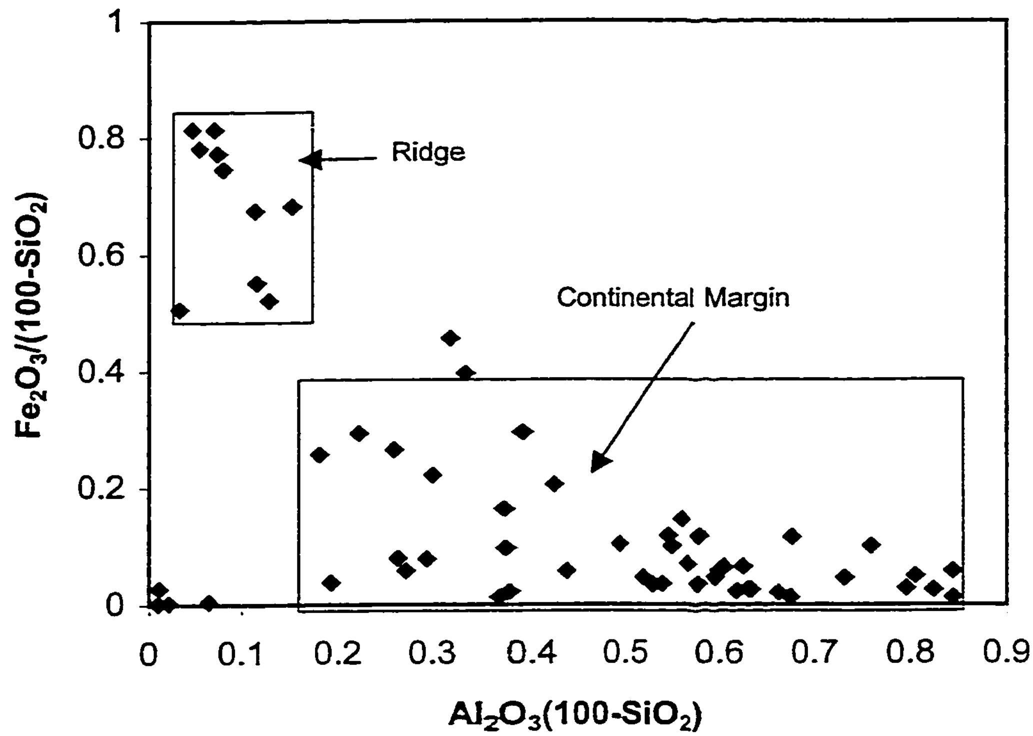

(a)

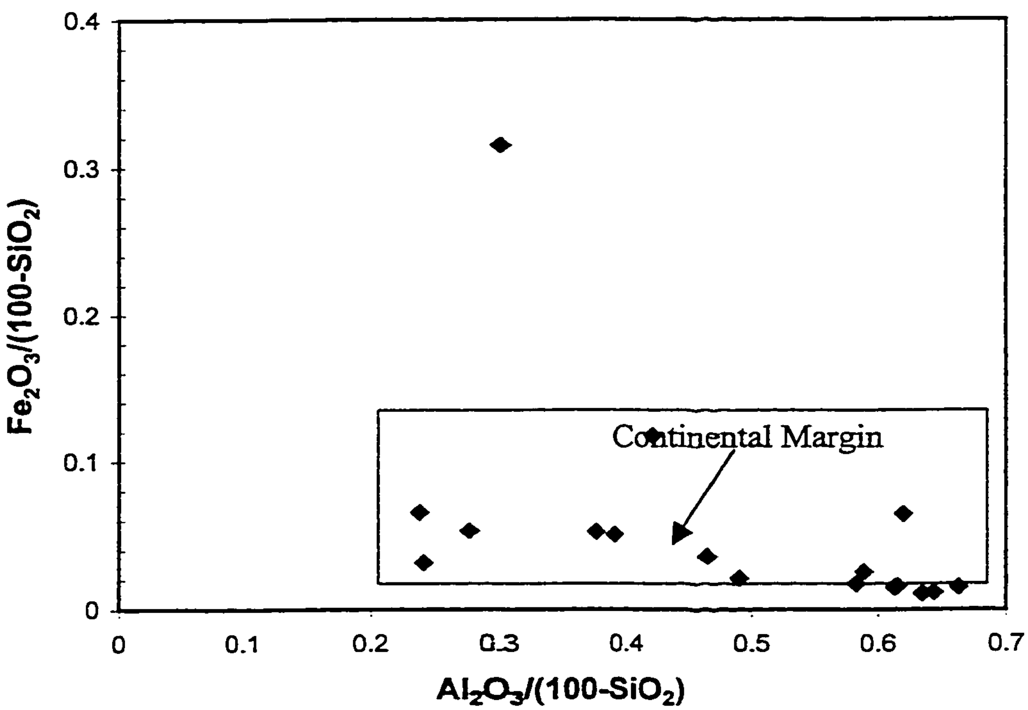

(b)

Figure 5.4. Bivariate plots of $Al_2O_3/(100\text{-}SiO_2)$ and $Fe_2O_3/(100\text{-}SiO_2)$ in the Wajid Sandstone: (a) Red Unit and (b) Grey Unit. The plots indicate a predominantly continental margin tectonic provenance in both the Red and Grey Units. Contribution from the oceanic ridge terrane is also shown for the Red Unit.

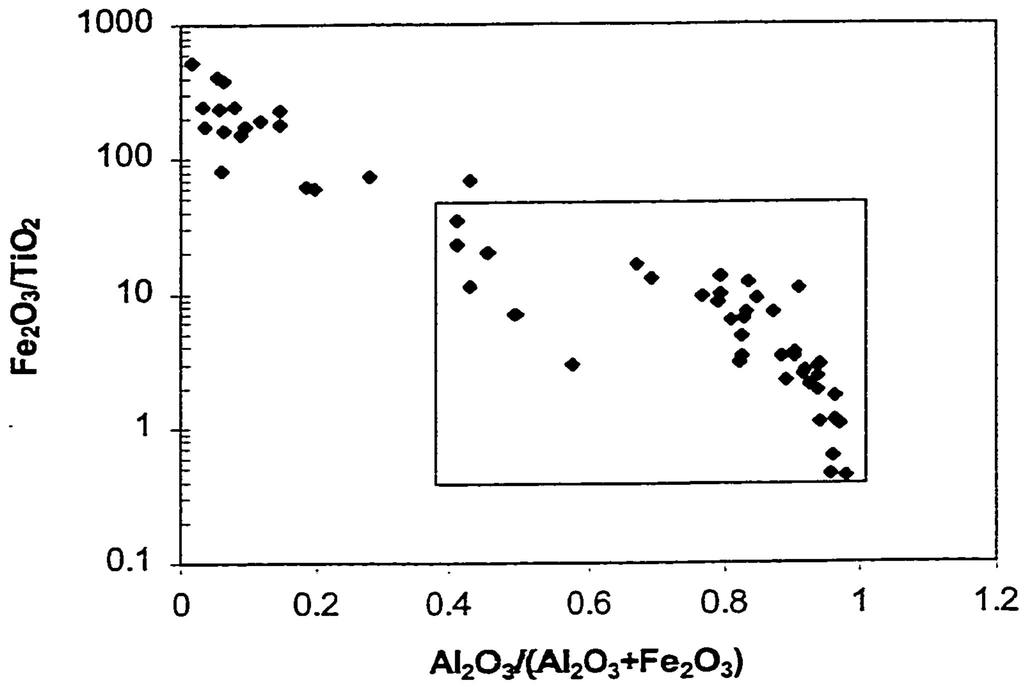

(a)

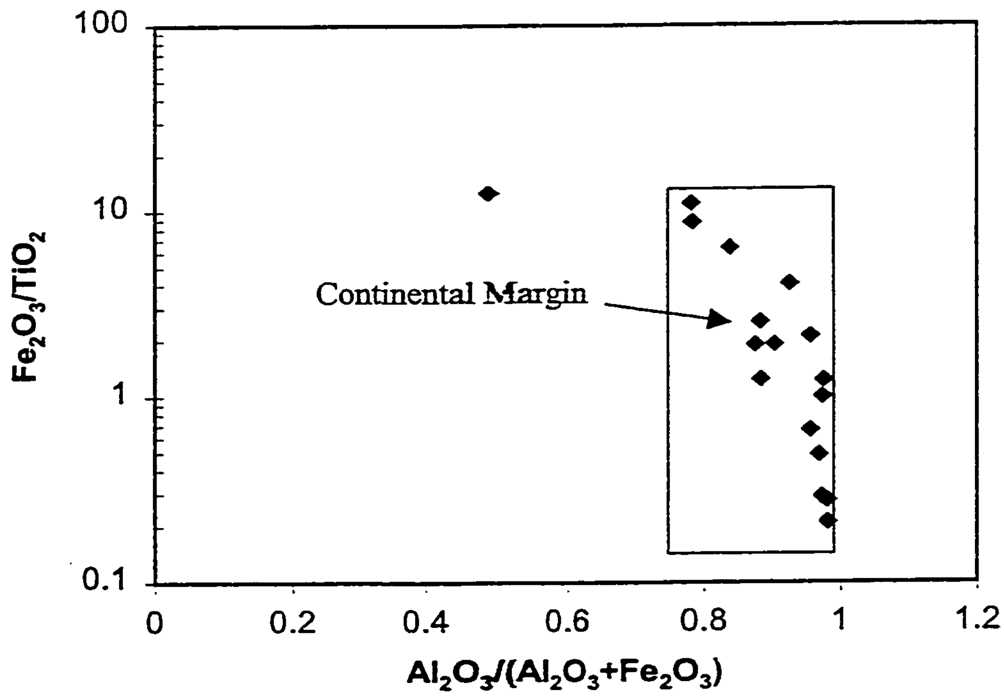

(b)

Figure 5.5. Bivariate plots of $Al_2O_3/(Al_2O_3+Fe_2O_3)$ and Fe_2O_3/TiO_2 in the Wajid Sandstone: (a) Red Unit and (b) Grey Unit. The plots indicate a predominantly continental margin tectonic provenance in both Red and Grey Units. Contribution from oceanic ridge terrane is also shown for the Red Unit.

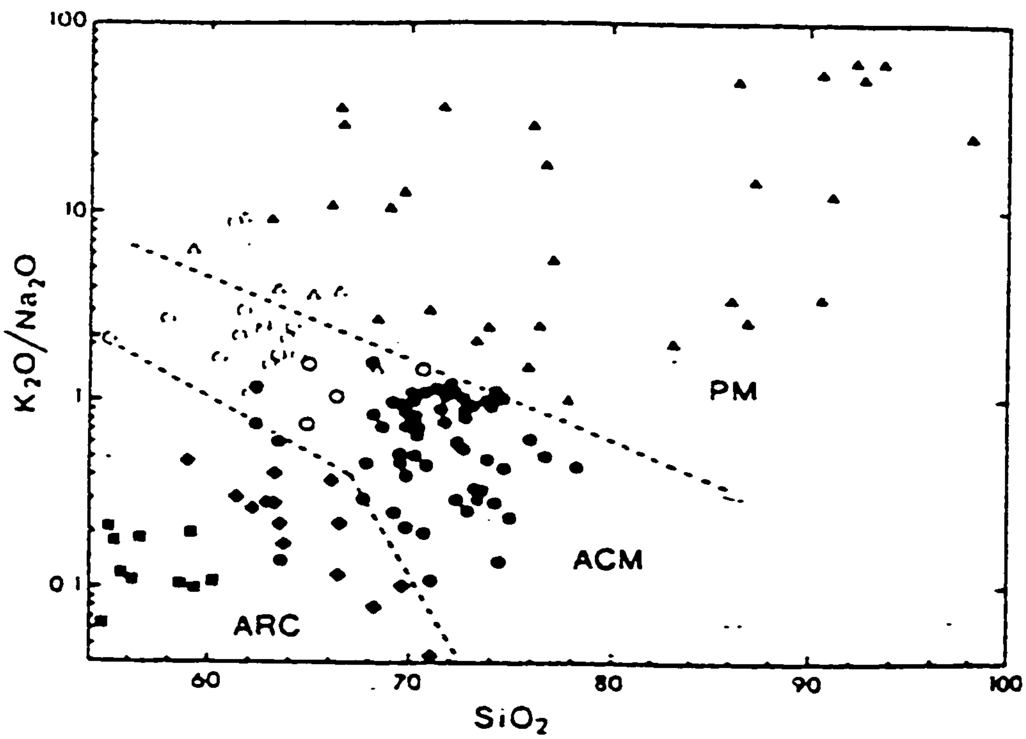

Figure 5.6. Discriminant diagram proposed by Roser and Kosch (1986) for identifying different tectonic fields of sandstones and argillites. ARC = Oceanic Island Arc, ACM = Active Continental Margin and PCM = Passive Continental Margin

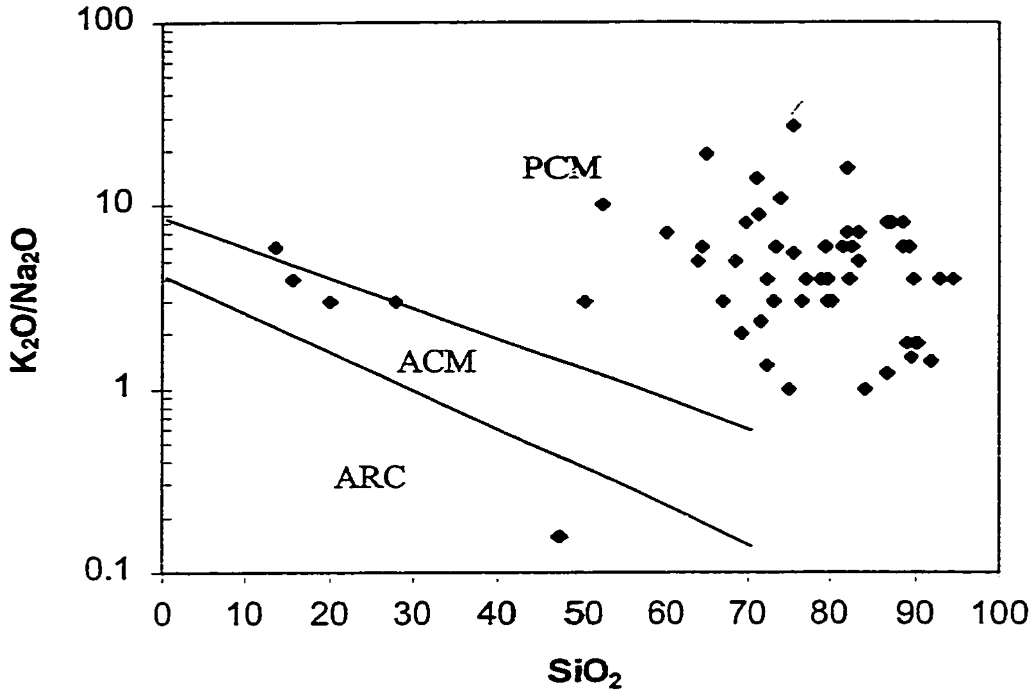

(a)

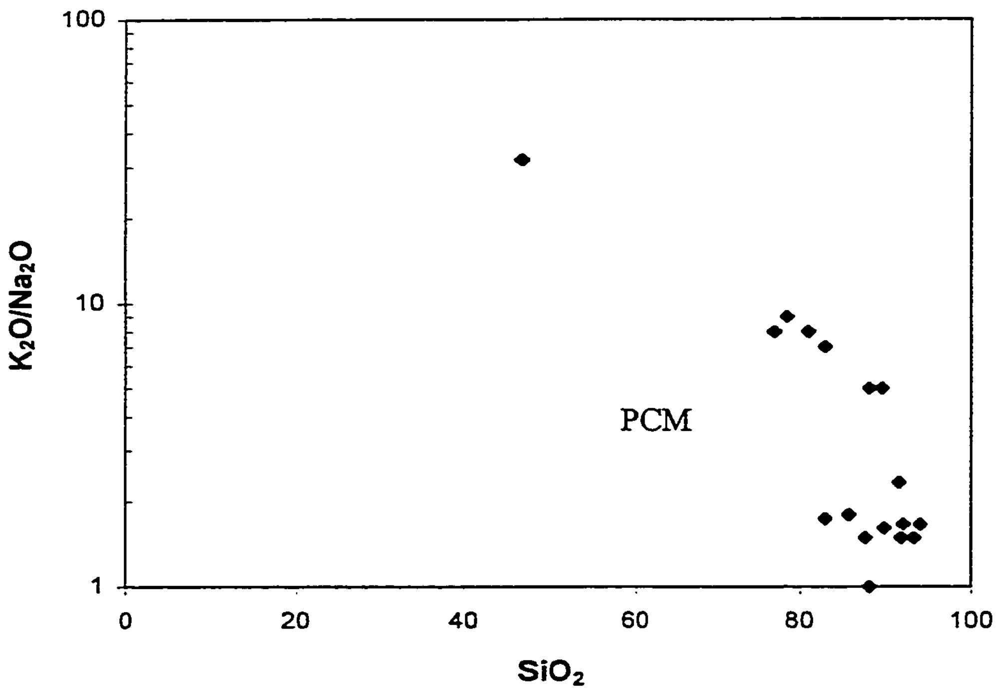

(b)

Figure 5.7. Discriminant plots of Roser and Kosch (1986) for Wajid Sandstone: (a) Red Unit and (b) Grey Unit. ARC = Oceanic Island Arc, ACM = Active Continental Margin and PCM = Passive Continental Margin. These plots indicate a dominantly passive continental margin provenance.

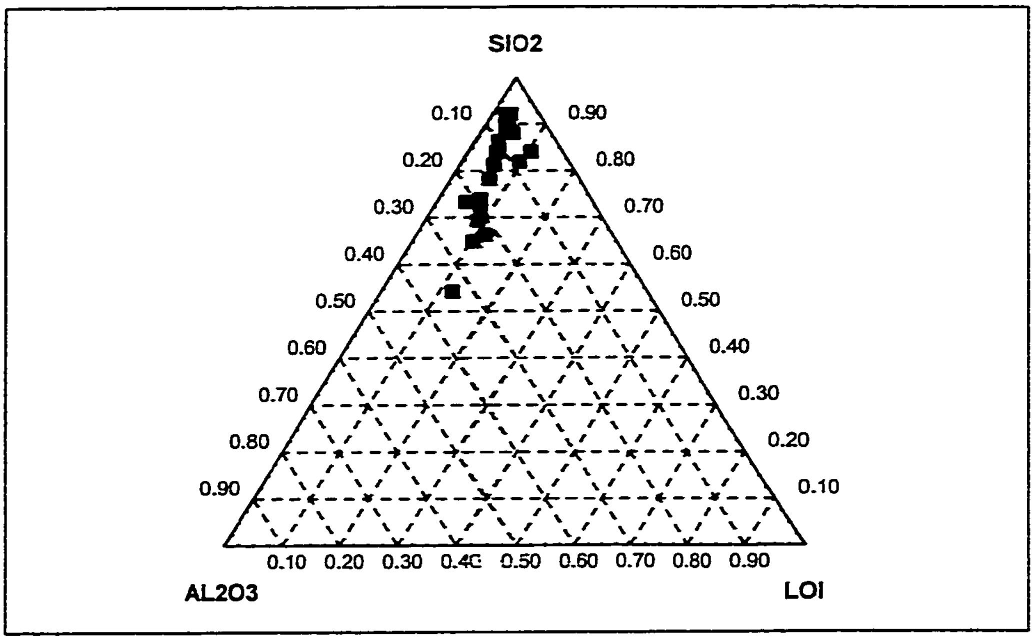

(a)

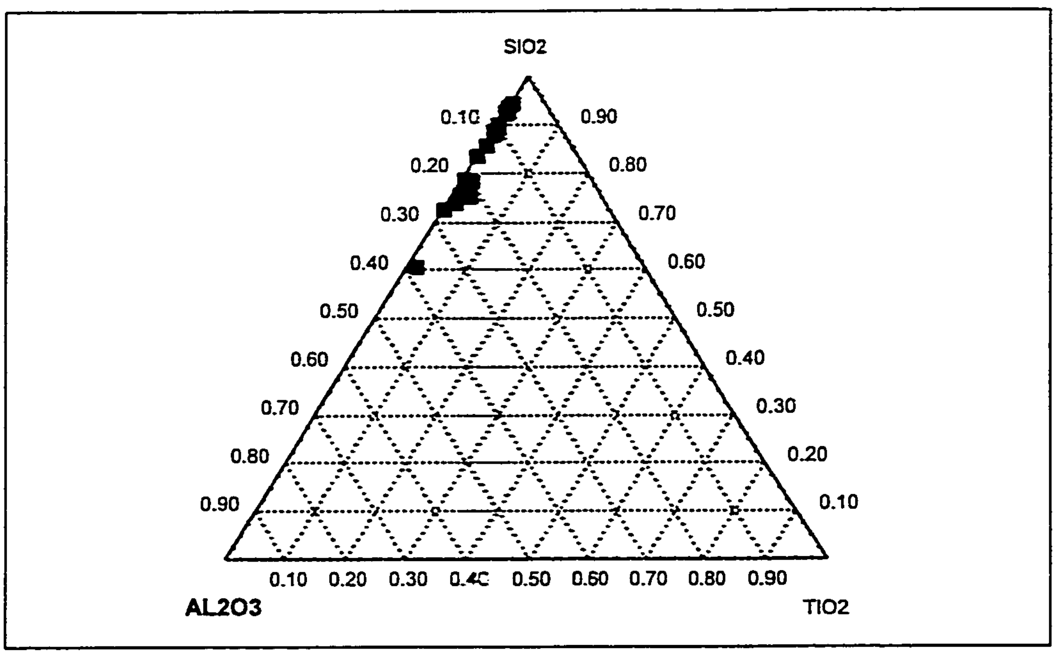

(b)

Figure 5.8. Ternary diagrams of Al_2O_3-SiO_2-LOI and Al_2O_3-SiO_2-TiO_2 for kaolinite-rich samples from the Red Unit. These plots are within the composition field of kaolin deposits derived from granitic source terrain (da Costa and Moraes, 1998).

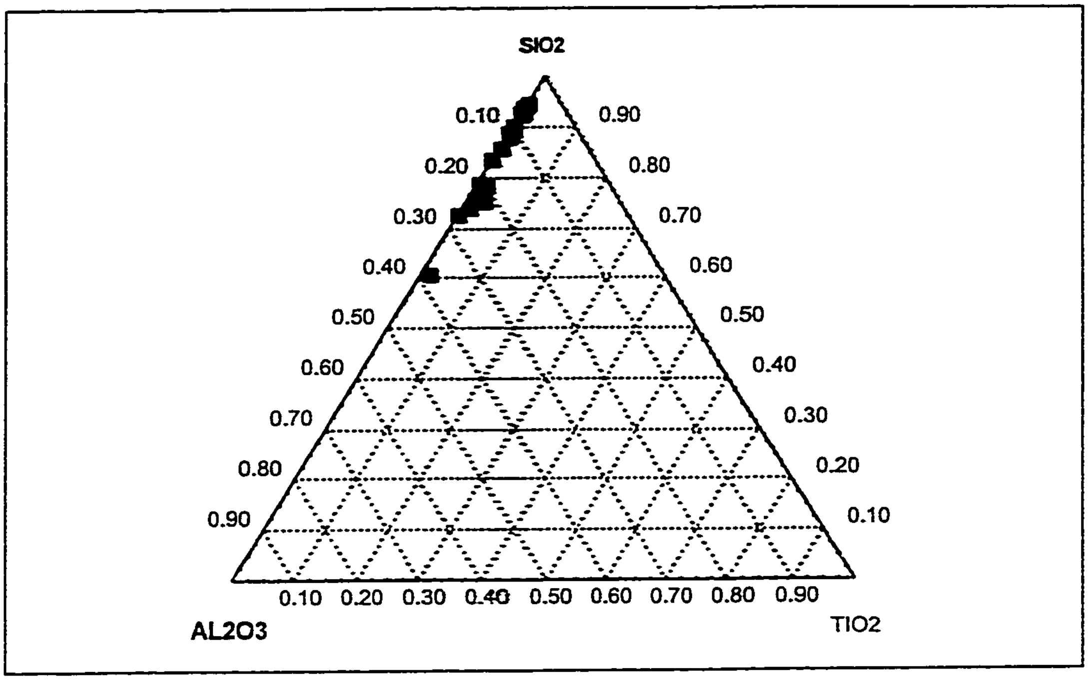

(a)

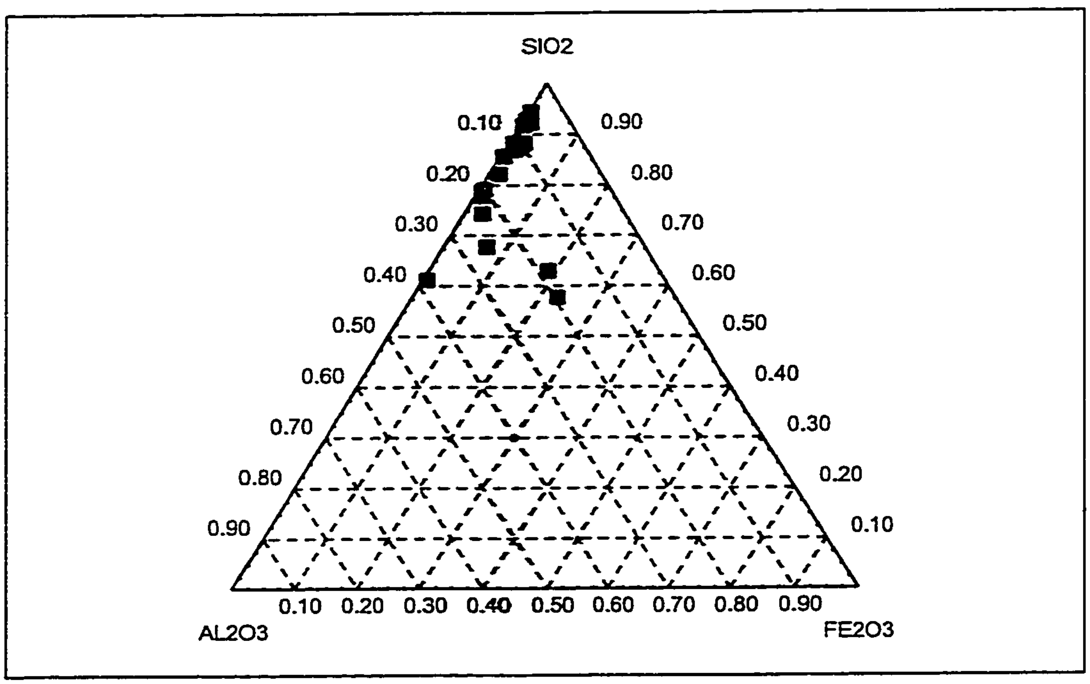

(b)

Figure 5.9. Ternary diagrams of (a) Al_2O_3-SiO_2-Fe_2O_3 and (b) Al_2O_3-SiO_2-K_2O for kaolinite-rich samples from the Red Unit. These plots are within the composition field of kaolin deposits derived from granitic source terrain (da Costa and Moraes, 1998).

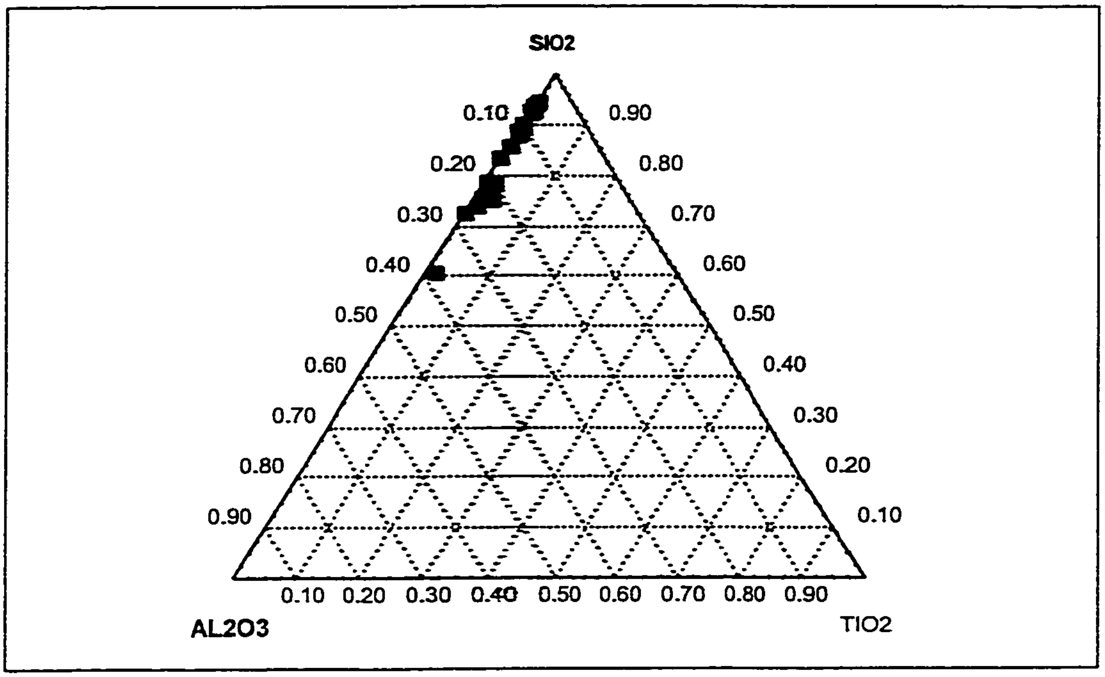

(a)

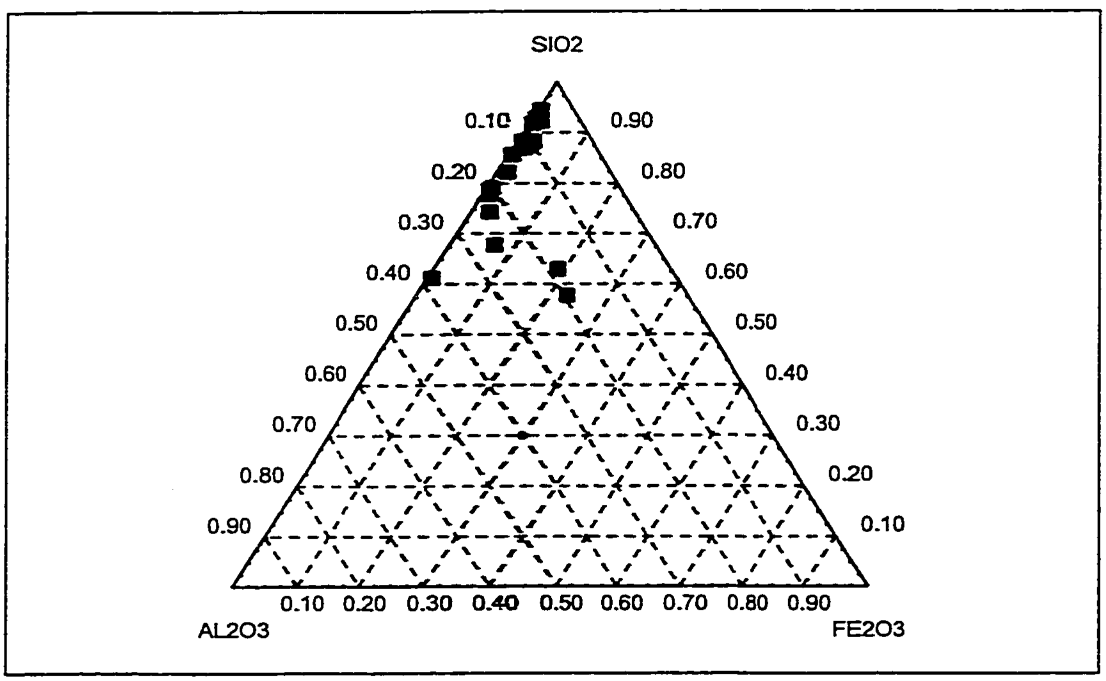

(b)

Figure 5.9. Ternary diagrams of (a) Al_2O_3-SiO_2-Fe_2O_3 and (b) Al_2O_3-SiO_2-K_2O for kaolinite-rich samples from the Red Unit. These plots are within the composition field of kaolin deposits derived from granitic source terrain (da Costa and Moraes, 1998).

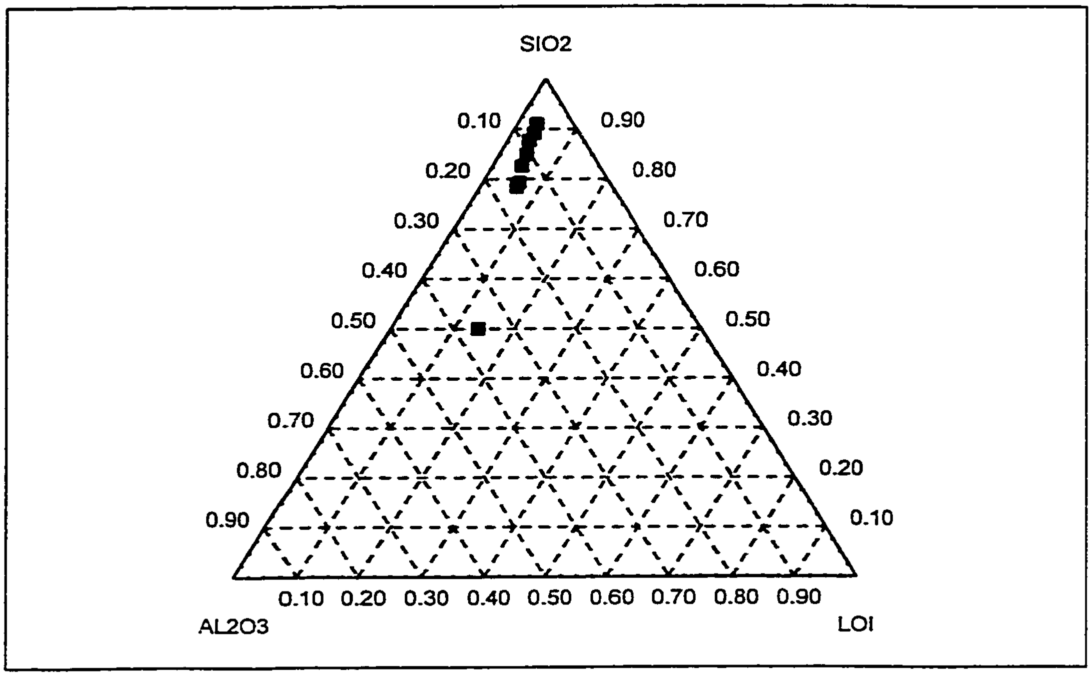

(a)

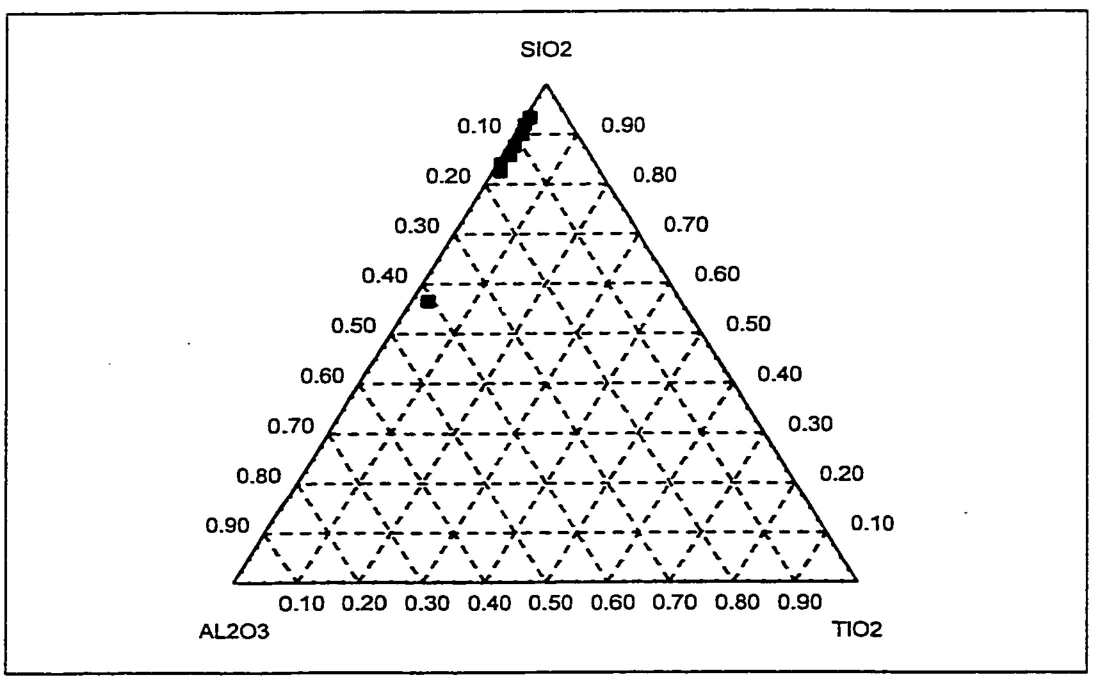

(b)

Figure 5.10. Ternary diagrams of (a) Al_2O_3-SiO_2-LIO and (b) Al2O_3-SiO_2-TiO_2 in kaolinite-rich samples from the Grey Unit. These plots are within the composition of kaolin deposits derived from granitic source terrain (da Costa and Moraes, 1998).

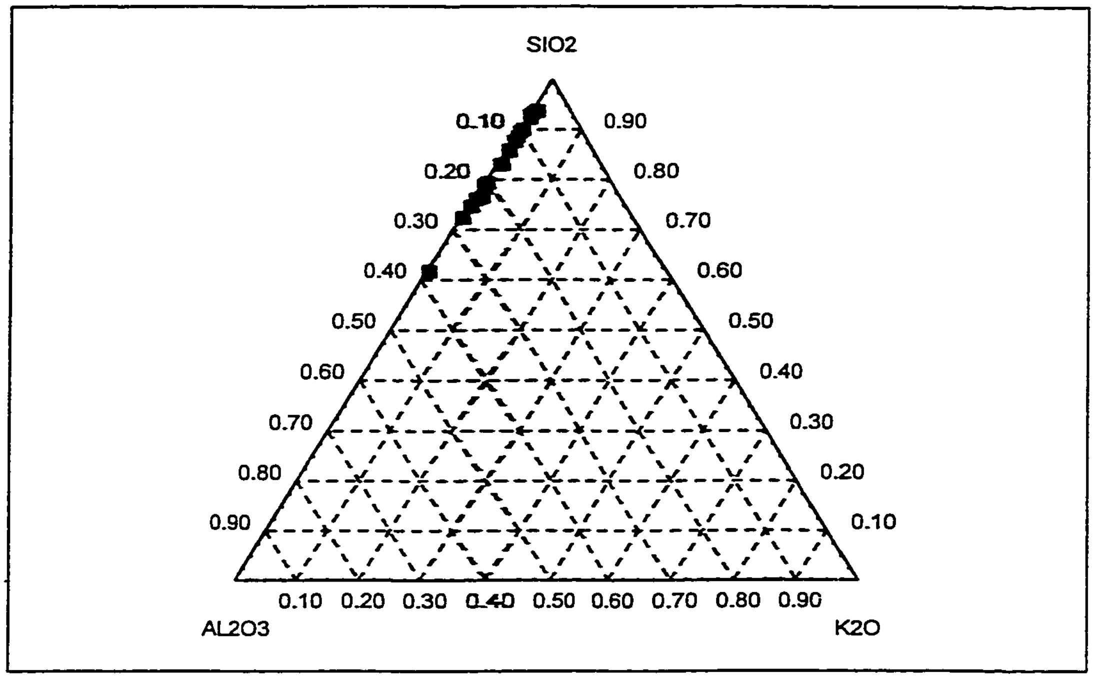

(a)

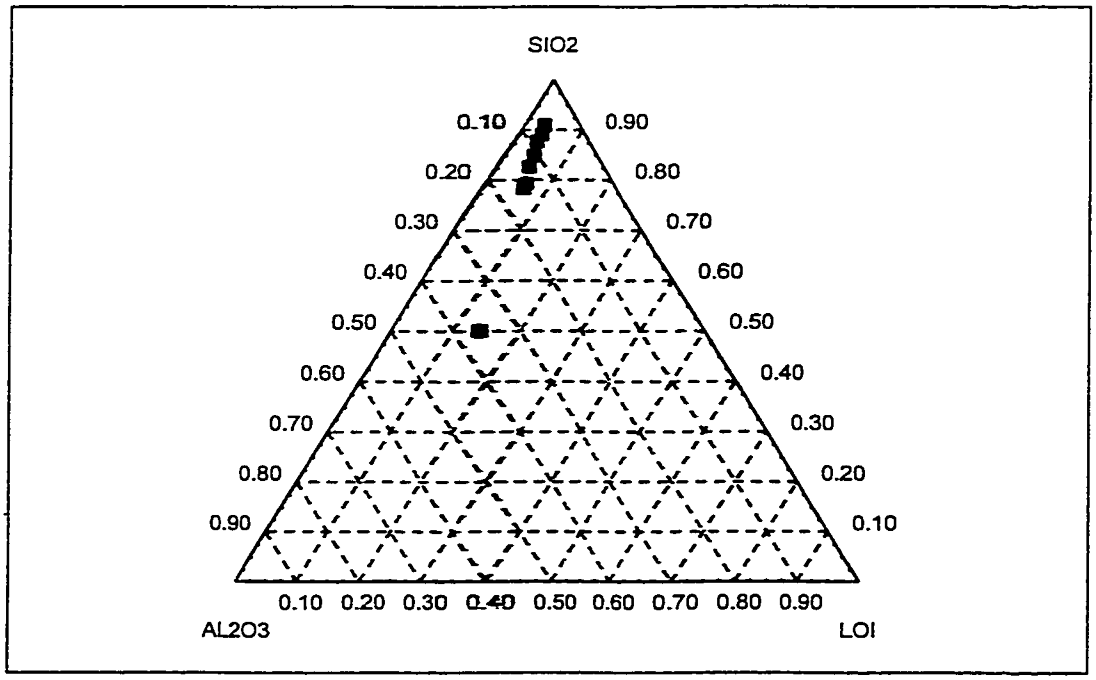

(b)

Figure 5.11. Ternary diagrams of (a) Al2O3-SiO2-Fe2O3 and (b) Al2O3-SiO2-K2O for kaolinite-rich samples from the Grey Unit. These plots are within the composition field of kaolin deposits derived from granitic source terrain (da Costa and Moraes, 1998).

5.2.1. Basement Complex Samples

Basement samples analyzed are mostly felsic igneous (granittes and pegmatites), and metamorphic. Only two samples are mafic (gabbro) igneous rocks. The relative distribution of some of the elements is shown in Figure 5.1 and briefly characterized as follows.

The major elements are generally low to moderate in these samples (Appendix IIIa). The concentrations of Al range from 0.23 to 2.75%, Fe 0.49 to 5.42% and Ca 0.07 to 11.95% respectively. Concentrations of Mg, K, Ti and Na are relatively low. Their concentrations range from 0.07 to 2.62%, 0.03 to 0.84%, <0.01 and 0.49% and <0.01 to 0.46%, respectively.

The concentrations of the trace elements including the provenance indicators Cr, Ni, Co, V and Sr range from low to moderately high concentrations of the individual elements (Table 5.1 and Appendix IIIa). The respective concentrations of these elements (Cr, Ni, Co, V and Sr) vary from 26 to 387ppm, 2 to 287ppm, 1 to 105ppm and 2 to 95ppm. The ratio of Cr/Ni ranges from 1.38 to 25.75, V/Cr from 0.038 to 1.09 and V/Ni from 0.128 to 8.2.

The whole rock chemistry shows that the concentrations of Al_2O_3 range from 7.49 to 15.71%. The concentrations of SiO_2 vary from a low 39.2% in the biotite schist sample to a high ~ 87% in the pegmatite samples. The gabbro samples recorded ~50%. The distribution of Cr_2O_3 records range from 0.85 to14.05%, CaO from 0.2 to 21.5%, K_2O from 0.32 to 13.73%, MgO from 0.11 to 13.76%), Na_2O from 0.05 to 6.88% and TiO_2 from 0.05 to 1.98% respectively.

5.2.2. Wajid Sandstone

The chemistry of the Wajid Sandstone generally follows the trends observed in the basement rock samples. The relative distribution of selected elements in the Wajid Sandstone are shown in Figure 5.2, and briefly discussed in this section. The samples from the Ahad Rufaidah locality generally record low concentrations of major elements except Fe, which is exceptionally high, 0.08 to 12.8%. The concentrations of Al average 0.18% while the concentrations of Ca and Mg average 1.35% and 0.058%, respectively. The concentrations of Na and Ti fall within a range of <0.01 to 0.08%.

The trace elements are also low in abundance in this locality. The concentrations of Cr range from 24 to 180ppm. The concentrations of Co, Ni and Sr range from <1 to 17ppm, 1 to 16ppm and 5 to 87ppm respectively. The concentrations of V generally range from 1 to 19ppm (except for a couple of samples with values above 100ppm). The ratios Cr/Ni, V/Cr and V/Ni vary from 3.25 to 39, 0.42 to 0.72 and 0.46 to 26.6, respectively (Table 5.2).

With the exception of a clay-rich sample (ARLCSC) which recorded 50%, the SiO_2 concentrations generally range from 64% to ~92%. The concentrations of Fe_2O_3 are high, 0.38 to 29% while the concentration of Al_2O_3 fall between 3.14 and 18.21%. The concentrations of K_2O, Na_2O and TiO_2 range from <0.01 - 0.34% (Appendix IIIa).

The distribution of elements in Al Habalah Area I locality is similar to that of Ahad Rufaidah (Appendix IIIa). The concentrations of Al fall between 0.04 and >15%. The concentrations of Ca are low, mostly between 0.03 and 1.47% except for the caliche-rich samples, which show values greater than 15%. The concentrations of K, Na, and Ti are virtually low. Except for few samples, the concentrations of these elements are mostly <0.01. The concentration of Fe ranges between 0.11 and 14.2%.

As shown in Figures 5.12 and 5.13, the concentrations of Cr, Co, Ni, V and Sr are generally poor in the analyzed samples. The concentrations of Cr, Ni, V and Co range from 10 to 133ppm, <1 to 51ppm, 1 to 108ppm, and 1 to 14ppm respectively. With the exception of the caliche samples that recorded 225 to 342ppm, the concentrations of Sr in this locality range between 1 and 44ppm (Table 5.2 and Appendix IIIa). The ratios Cr/Ni, V/Cr and V/Ni, respectively, range from 1.42 to 32.5, 0.026 to 1.4 and 0.25 to 12.

SiO_2 is abundant in Al Habalah Area I except for the caliche samples. The concentrations of SiO_2 are as high as ~ 95% in some of the samples and average 64%. The distribution of Al_2O_3 is relatively high, 1.14 to 32.68% while CaO concentrations range mostly between 0.04 and 7.39% (except for the caliche samples with concentrations between ~38 and ~ 46%). Fe_2O_3 is conspicuously high in samples from this locality, 0.48 to 25.38%. The concentrations of the other oxides are very low, ranging between <0.01 and 1.4% (Appendix IIIa).

Major elements in the Al Soudah locality exhibit similar trends as in the other two localities discussed above. Aluminium is low, 0.08 - 0.31% and averages 0.12%. The concentrations of Na, Mg, K and Ti are extremely low in concentrations ranging between <0.01 and 0.01%. Calcium also recorded low concentrations, 0.03 to 0.19% in this locality. Fe is particularly abundant in this locality, with a record of 0.57 to 12.8% and an average of 11.36%.

The provenance indicators such as trace elements Co, Cr, Ni, V and Sr are low in Al Soudah locality. Chromium records values ranging between 24 and 79ppm. The concentrations of Co, Ni, V and Sr at this locality are 1 to 5ppm, 3 to 15ppm, 1 to 82ppm and 1 to 8ppm, respectively. The ratios of Cr/Ni, V/Cr and V/Ni ranging from 2.8 to 25.3, 0.013 to 1.67 and 0.33 to 27.3, respectively were recorded in this locality (Table 5.2 and Appendix IIIa).

The concentrations of SiO_2 range from 69 to 94% (average ~82%). The concentrations of Al_2O_3 and Fe_2O_3 also range from 0.33 to 15.72% and 0.01 to 26% respectively. The concentrations of MgO, Na_2O and K_2O are very low ranging from <0.01 to 0.06%. The values of CaO and TiO_2 also range between 0.03 and 0.96% (Appendix IIIa).

The distribution of elements in the Grey Unit at the Al Habalah II locality follows almost the same trend as in the other three localities with only few exceptions. High iron content that is characteristic of the other localities and consequently the Red Unit is extremely low here. The concentrations of Fe fall between 0.14 and 2.27% (average 0.52%), Appendix IIIa. The concentrations of Cr, V, Co, Ni and Sr range from 22 to 120ppm, 1 to 56ppm, <1 to 39ppm, 1 to 12ppm and 5 to 27ppm, respectively. The ratios of Cr/Ni, V/Cr and V/Ni range from 4.83 to 36, 0.083 to 0.33 and 0.3 to 18.67, respectively, in this locality (Table 5.2 and Appendix IIIa).

Silica (SiO_2) values dominantly range between 76.8 and 94% and average 89.5%. The extremely abundant Fe_2O_3 of the Red Unit is low, 0.18 to 3.46% in this locality. The low concentrations of K_2O, MgO, Na_2O and TiO_2 recorded in the other three localities are also low in the Al Habalah II locality (Appendix IIIa).

5.3. Geochemical distinction between Red and Grey Units

Geochemical signatures of the two units appear to be virtually similar. The only major difference is the distribution of iron. The concentrations of iron are higher in the samples from the Red Unit than in the Grey Unit. This is in agreement with the field observation of red coloration of the basal unit (Red Unit). The concentrations of Mg, Al and Ca are also slightly higher in the Red Unit than in the Grey Unit (Fgure 5.12a). In the same vein, trace elements such as As, Ba, Bi, La, Mo, Ni, P, Pb, Sc, Mn, Sr and Zn show slightly higher average concentrations in the Red Unit compared to the Grey Unit (Figure 5.12b). The distribution of Cu and Co are, however, slightly higher in the Grey Unit than in the underlying Red Unit (Figure 5.12b). Similar trends are observable in the oxides. CaO, Fe_2O_3, MnO, MgO, MnO, Na_2O and P_2O_5 are higher in concentrations in the Red Unit than in the overlying Grey Unit (Figure 5.13).

Higher concentrations of Ca, Fe, Mn, Mg, and Ni suggest a relatively more mafic provenance for the Red Unit. However, the seemingly similar mineralogical composition of both the Red and Grey Units might be due to dissolution and leaching of the mafic minerals from the Red Unit.

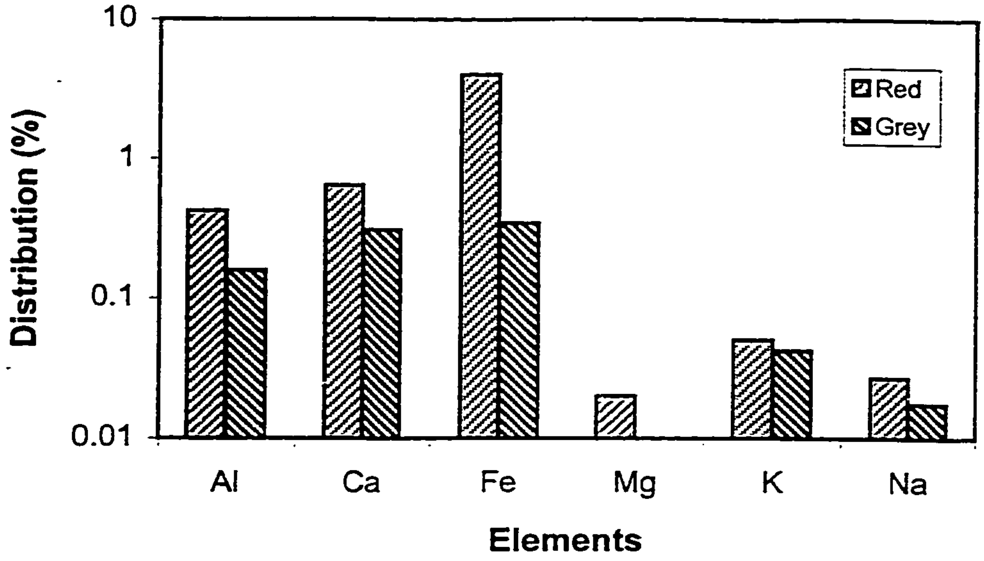

(a)

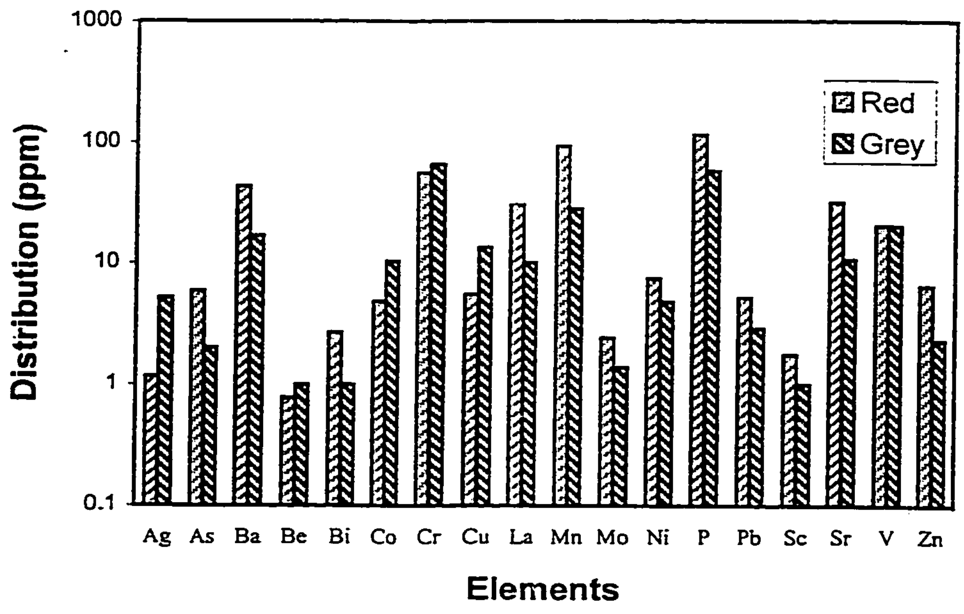

(b)

Figure 5.12. Distribution of elements in the Red and Grey Units: (a) Major elements and (b) Trace elements.

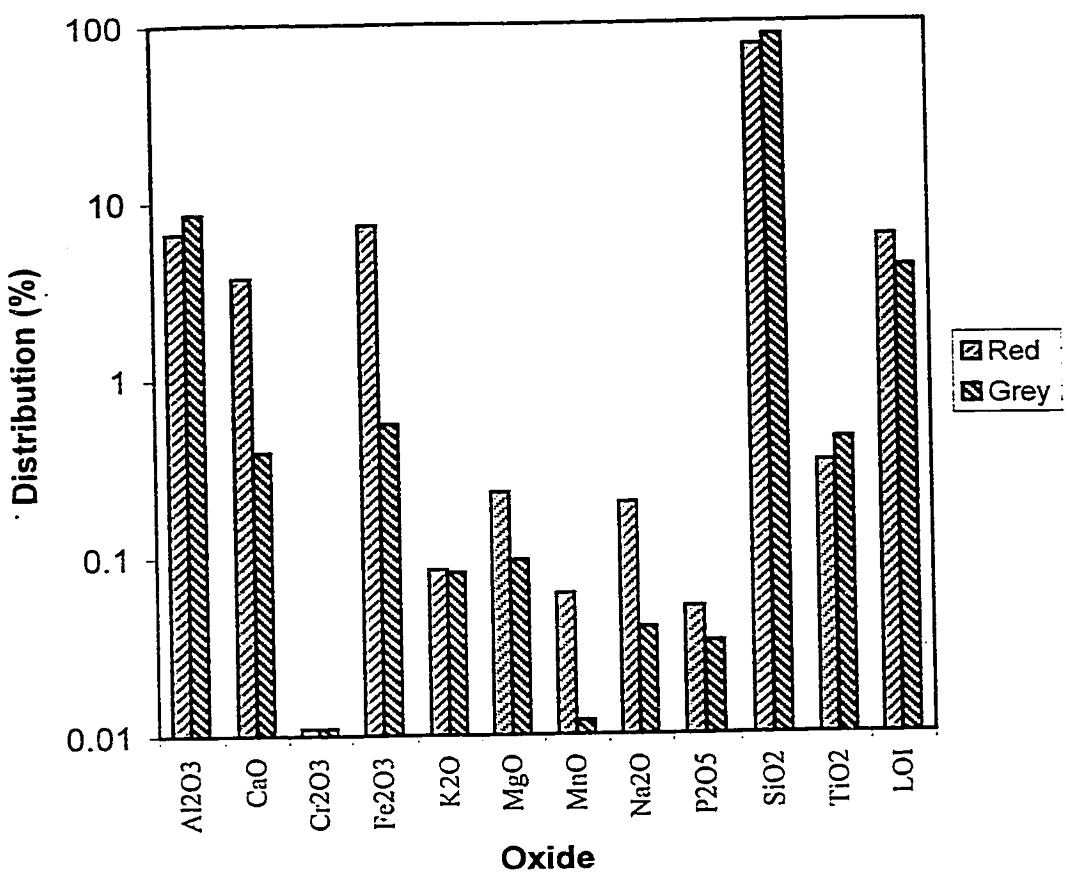

Figure 5.13. Distribution of oxides in the Red and Grey Units. The concentrations of Fe_2O_3, CaO, MgO and Na_2O are relatively higher in the Red Unit than in the Grey Unit.

5.4. Multivariate Analyses of the Geochemical Data

Multivariate techniques including factor and cluster analyses (involving both the R and Q-modes analyses) were used to analyze the geochemical data in order to further constrain the provenance of the Wajid Sandstone.

5.4.1. R-Mode Analysis

5.4.1.1. Factor Analysis

In this study, the principal component varimax rotation method was applied to extract the factor end members and their corresponding factor loadings from the variables. Factor loadings of 0.6 and above, 0.6 to 0.45, and <0.45 to 0.2 are respectively classified as strong, moderate and weak loadings (Morsy, 1993). The associated end members of the different factors are listed in the Tables 5.3 and 5.4. The factors were also plotted as ternary diagrams (Figures 14 - 17). The details of the factor loadings and their corresponding and eigenevalue are included in the Appendix IIIc.

5.4.1.1. Cluster Analysis

The cluster groups are summarized in Table 5.5 and plotted as bar graphs (Figures 5.18 - 5.21).

TABLE 5.3. Summary of the factor loadings for elements: (a) Ahad Rufaidah, (b) Al Habalah I, (c) Al Habalah II, and (d) Al Soudah.

(a)

Factor	Strong Positive (>0.6)	Moderate Positive (<0.45 - 0.6)	Weak Positive (<0.45 - 0.2)	Strong/Mod. Negative	Eigene-value	Var. (%)
Factor 1	Ag, Co, Hg, Mo, Pb & Sc	Zn, Na & Sb	U	Cr. Ni, Cu &Ti	8.98	31.34
Factor 2			Ag, Cu, & Be	Ba, K, P, & Sb	3.74	12.98
Factor 3	Cu	As, Sb		U, V, Ti &Cr	3.17	10.68

(b)

Factor	Strong Positive (>0.6)	Moderate Positive (<0.6 - 0.45)	Weak Positive (<0.45 - 0.2)	Strong/Mod. Negative	Eigene-value	Var. (%)
Factor 1	Be & Ag	Sc & Co	Hg, Pb, Ba, Sb & Zn	Fe, Mn, Ti, V, Cr & Ni	7.17	25.62
Factor 2	Ca, Mg & Sr	Ni	As, La, & Mo	V & Ti	5.22	18.66
Factor 3	Cu, Na & La		Cr & P		2.76	15.16

(c)

Factor	Strong Positive (>0.6)	Moderate Positive (<0.6 - 0.45)	Weak Positive (<0.45 - 0.2)	Eigene value	Var. (%)
Factor 1	Ni, Cr, P, Sb & Mg		Ca, Cu & Mn	7.26	29
Factor 2	Al, Fe, Mn & V		Cr, Na, Ni, Sr & Mg	4.81	19.26
Factor 3	Ag & Cd	Mg & Hg	Al, Ba, Mo & Na	2.98	11.93

(d)

Factor	Strong Positive (>0.6)	Moderate Positive (<0.6 - 0.45)	Weak Positive <0.45 - 0.2)	Eigene value	Variance (%)
Factor 1	Mn, Ni & P	Fe	Al, Mo, Na & Cu	5.39	21.56
Factor 2	As, Pb, Sc & Sr		Mo & Fe	3.86	15.32
Factor 3	Ag, Cr, Hg & Bi	Na & La	Pb, Mo & Al	3.31	13.23

TABLE 5.4: Summary of the factor loadings for the oxides: (a) Ahad Rufaidah, (b) Al Habalah I, (c) Al Habalah II and (d) Al Soudah.

(a)

Factor	Strong Positive (>0.6)	Moderate Positive (<0.6 - 0.45)	Weak Positive (<0.45 - 0.2)	Eigene value	Var. (%)
Factor 1	Al_2O_3, TiO_2 & LOI			3.0	25
Factor 2	SiO_2, MnO, & MgO		Cr_2O_3	2.45	20.47
Factor 3		P_2O_5 & K_2O	Fe_2O_3, Cr_2O_3 & MnO	1.95	16.21

(b)

Factor	Strong Positive (>06)	Weak Positive (<0.45 - 0.2)	Eigenevalue	Variance (%)
Factor 1	Ca & LOI	MnO & K_2O	3.62	30.19
Factor 2	Cr_2O_3 & Na_2O	MgO, MnO, P_2O_5 & LOI	2.88	24
Factor 3		MgO, Na_2O, CaO & P_2O_5	1.64	13.64

(c)

Factor	Strong Positive (>0.6)	Weak Positive (<0.45 - 0.2)	Eigene-value	Variance (%)
Factor 1	Fe_2O_3, K_2O, P_2O_5, LOI, Al_2O_3 & TiO_2	Cr_2O_3, MgO & Na_2O	6.77	56.4
Factor 2	Cr_2O_3, MgO, MnO & Na_2O	Al_2O_3 & TiO2	3.18	26.52

(d)

Factor	Strong Positive (>0.6)	Moderate Positive (<0.6 - 0.45)	Weak Positive (<0.45 - 0.2)	Eigenevalue	Variance (%)
Factor 1	Cr_2O_3, Fe_2O_3, MgO & Na_2O		P_2O_5	6.06	50.53
Factor 2		MnO & SiO_2	Al_2O_3, TiO_2 & LOI	2.74	22.86
Factor 3	CaO & P_2O_5		Cr_2O_3, MnO & Na_2O	1.28	10.68

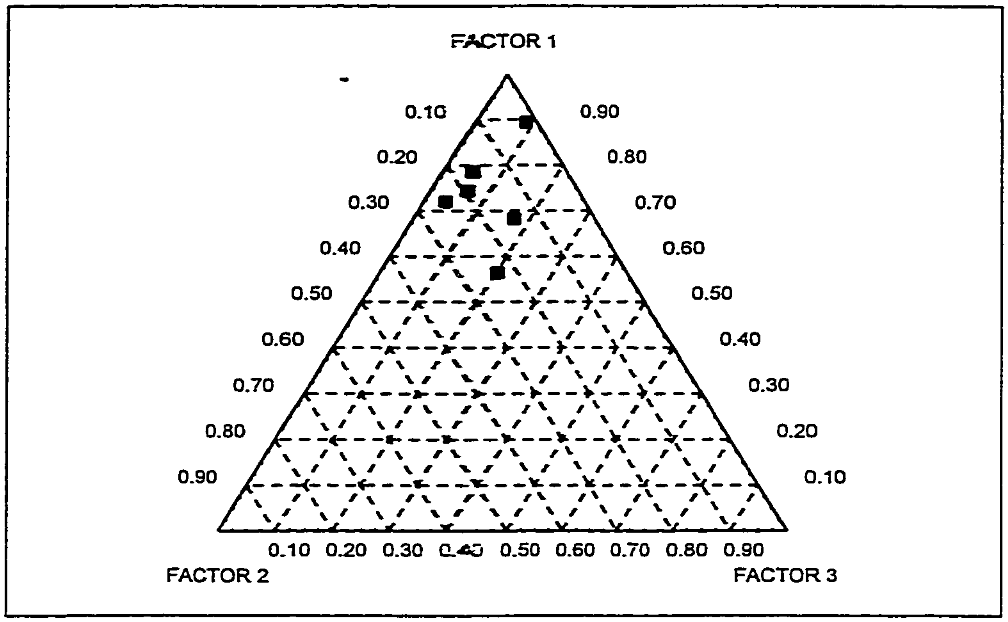

(a)

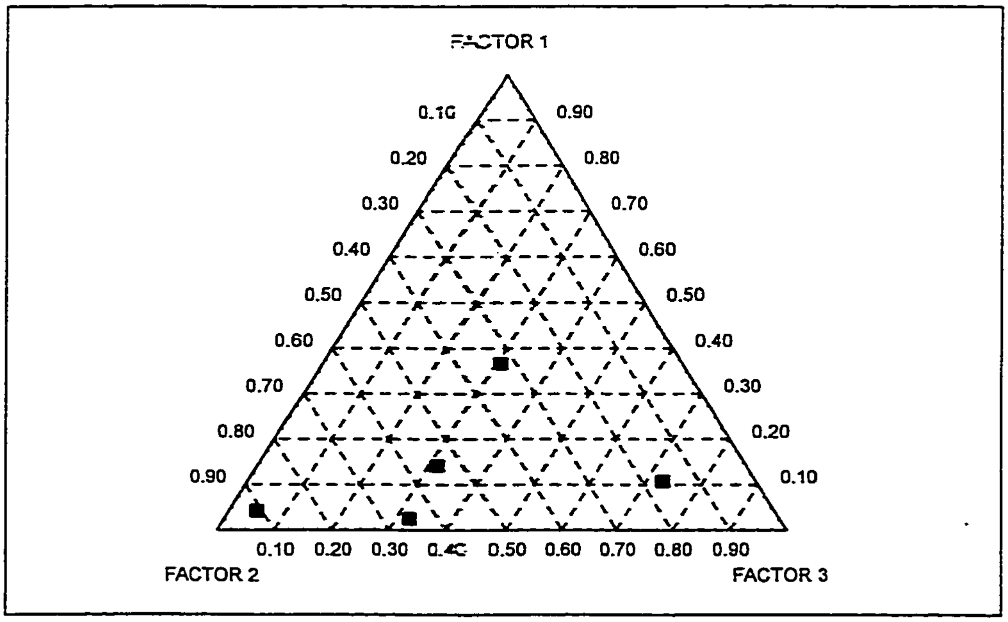

(b)

Figure 5.14. Ternary diagrams showing the distribution of different factor in samples from Ahad Rufaidah locality: (a) Elements and (b) Oxides.

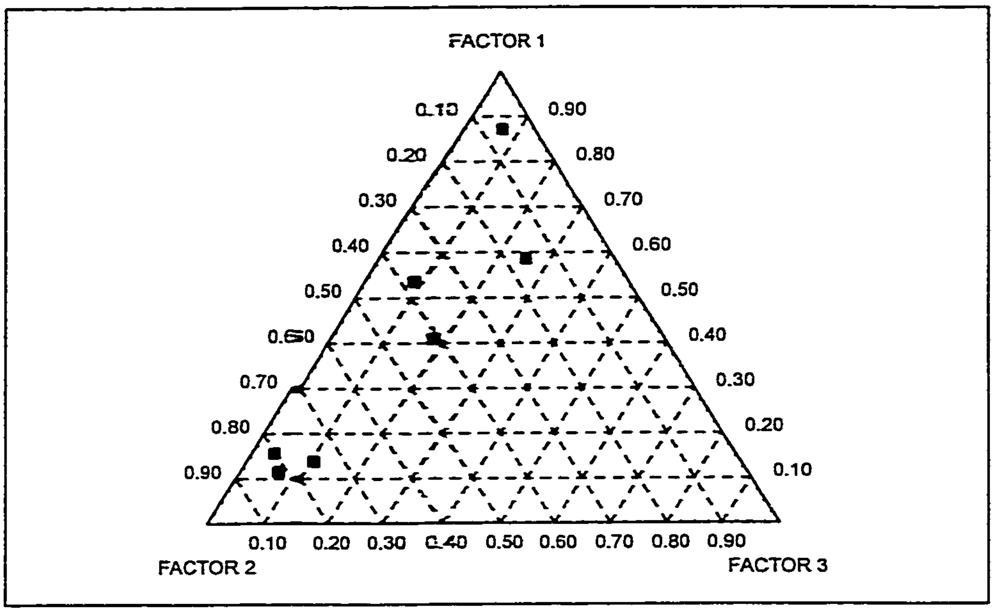

(a)

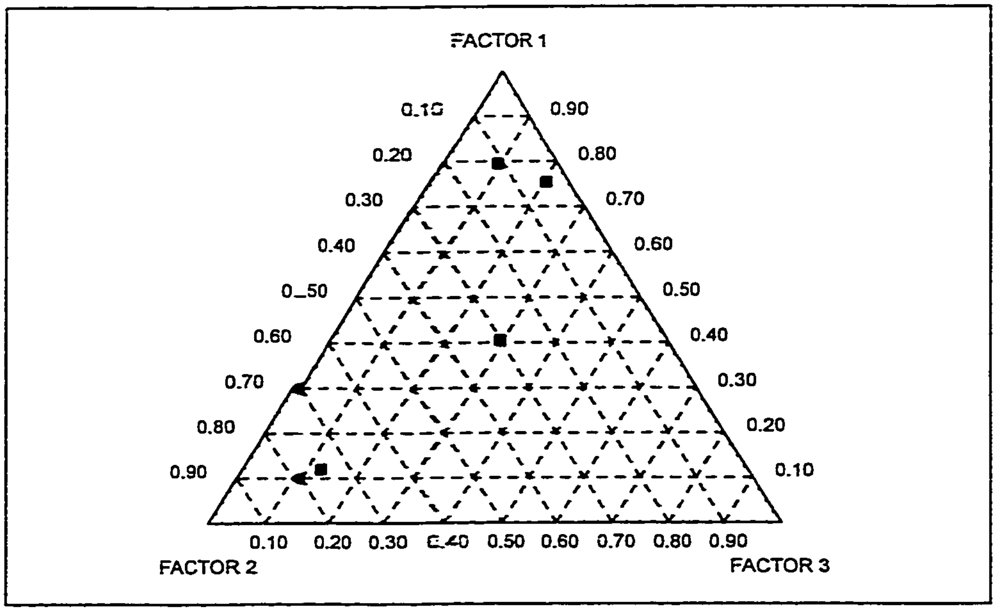

(b)

Figure 5.15. Ternary diagrams showing the distribution of different factors in samples from Al Habalah I locality: (a) Elements and (b) Oxides.

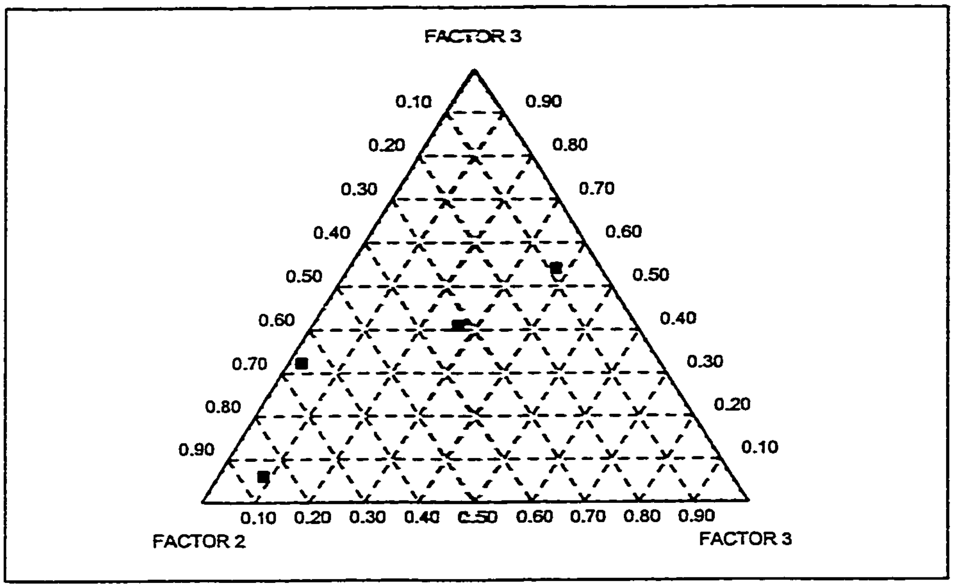

(a)

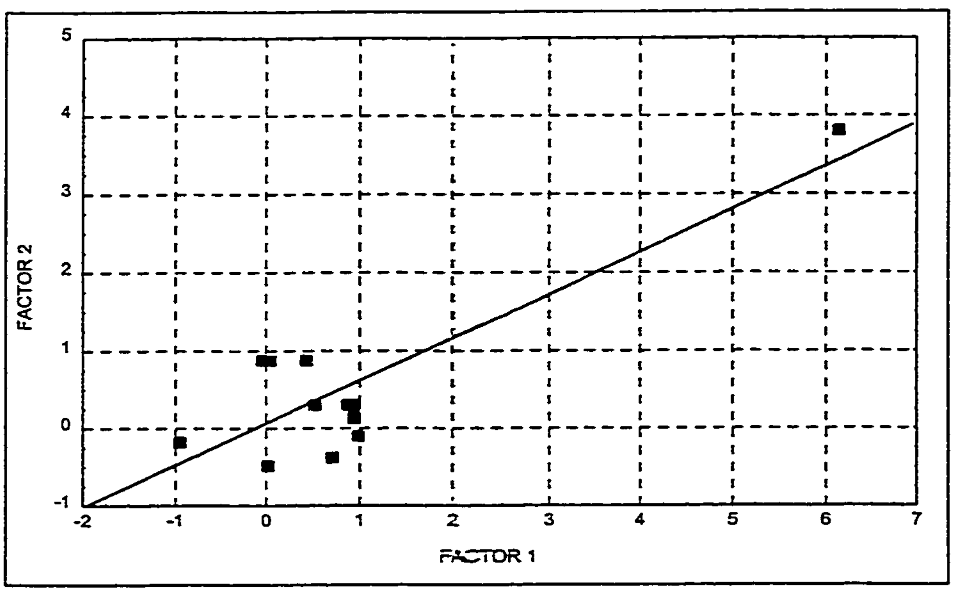

(b)

Figure 5.16. Ternary diagrams showing the distribution of different factors in Al Habalah II locality: (a) Elements and (b) Oxides.

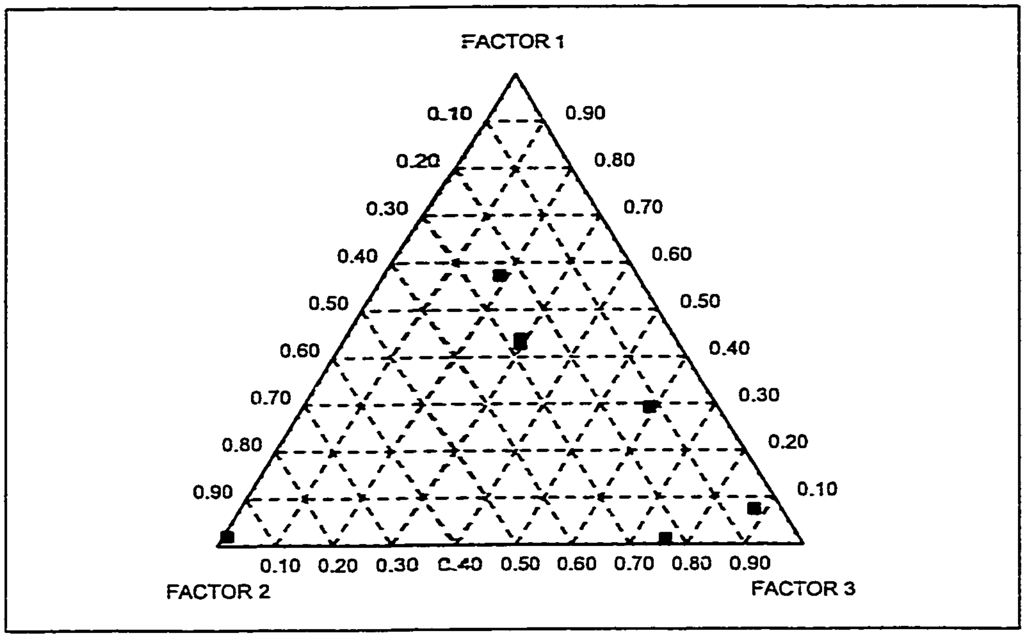

(a)

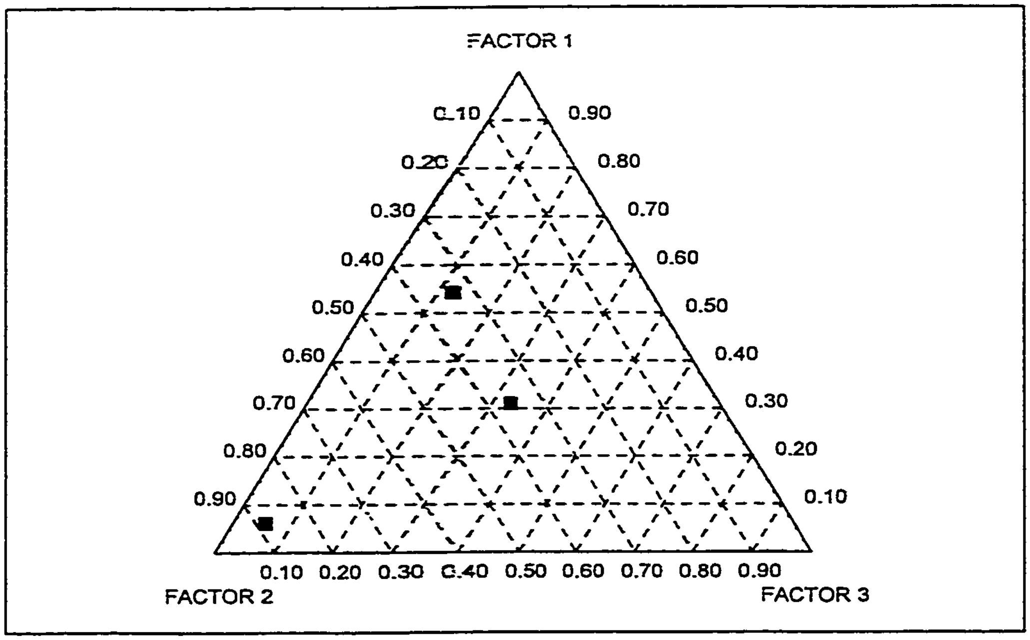

(b)

Figure 5.17. Ternary diagrams showing the distribution of different factors in samples from Al Soudah locality: (a) Elements and (b) Oxides.

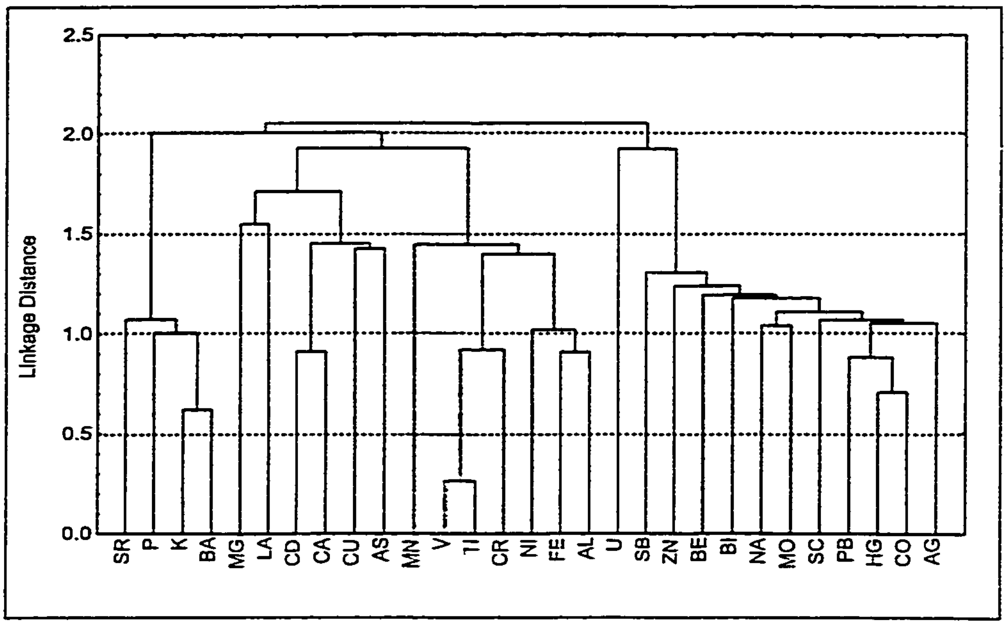

(a)

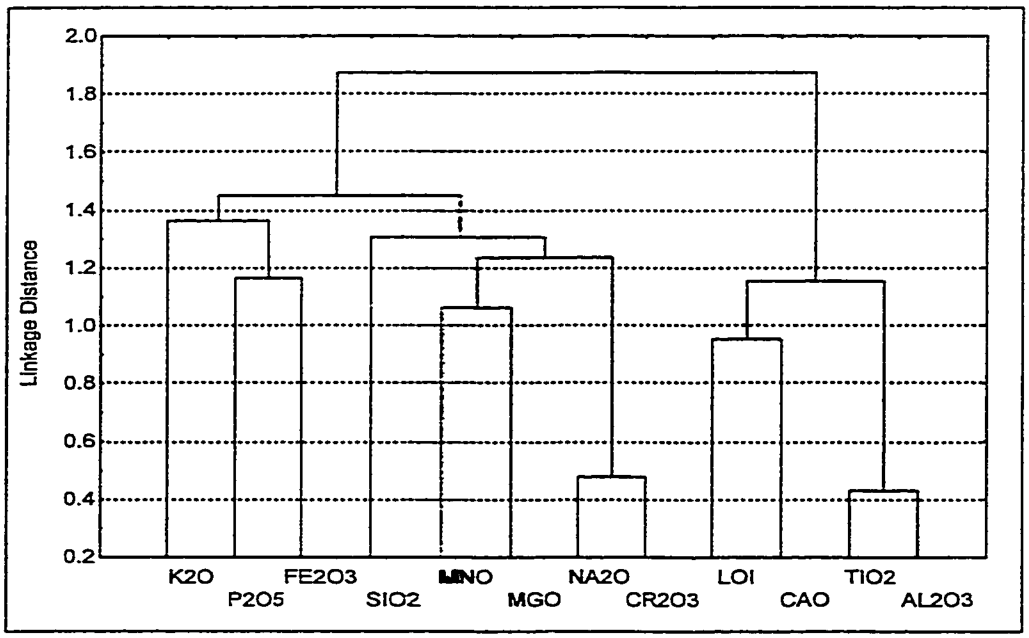

(b)

Figure 5.18. Dendrograms showing clustering among different elements and oxides in Ahad Rufaidah: (a) Elements and (b) Oxides.

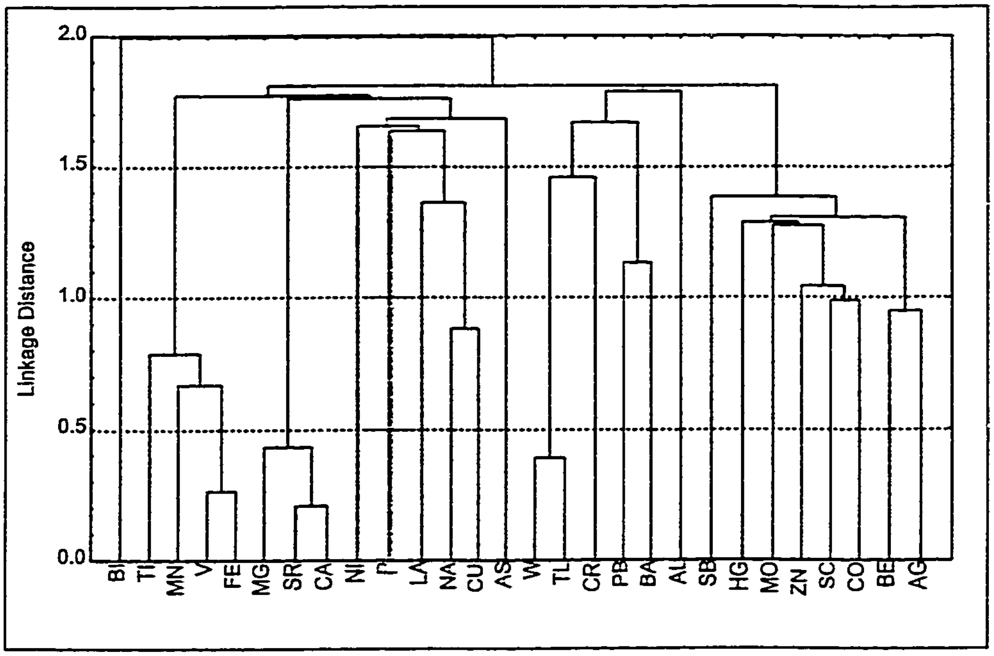

(a)

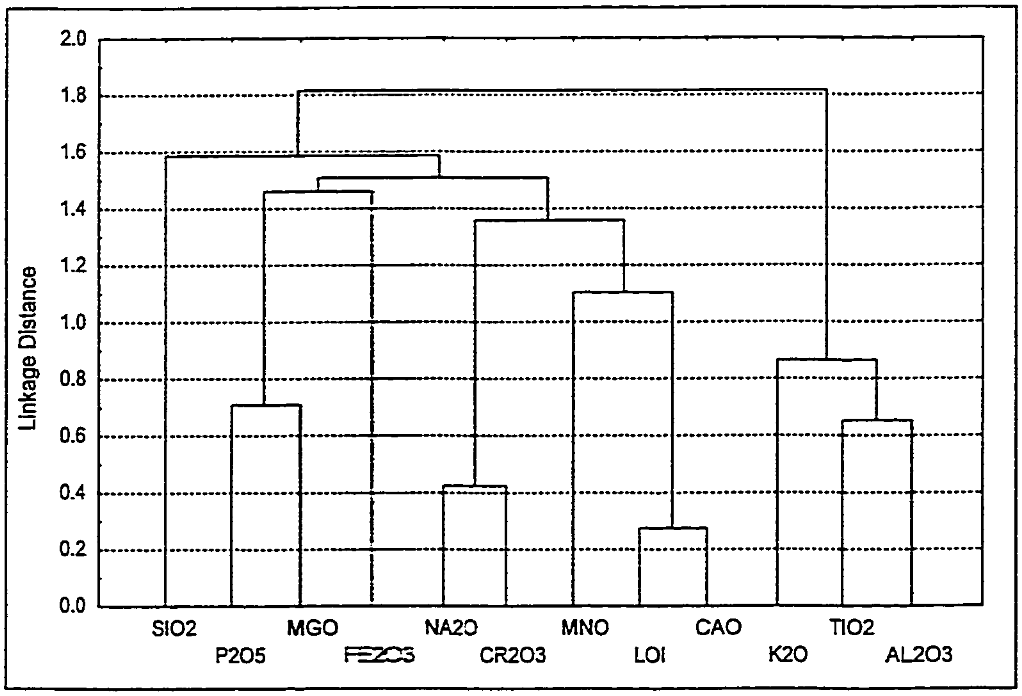

(b)

Figure 5.19 Dendrograms showing clustering among different elements and oxides in samples from Al Habalah I locality: (a) Elements and Oxides.

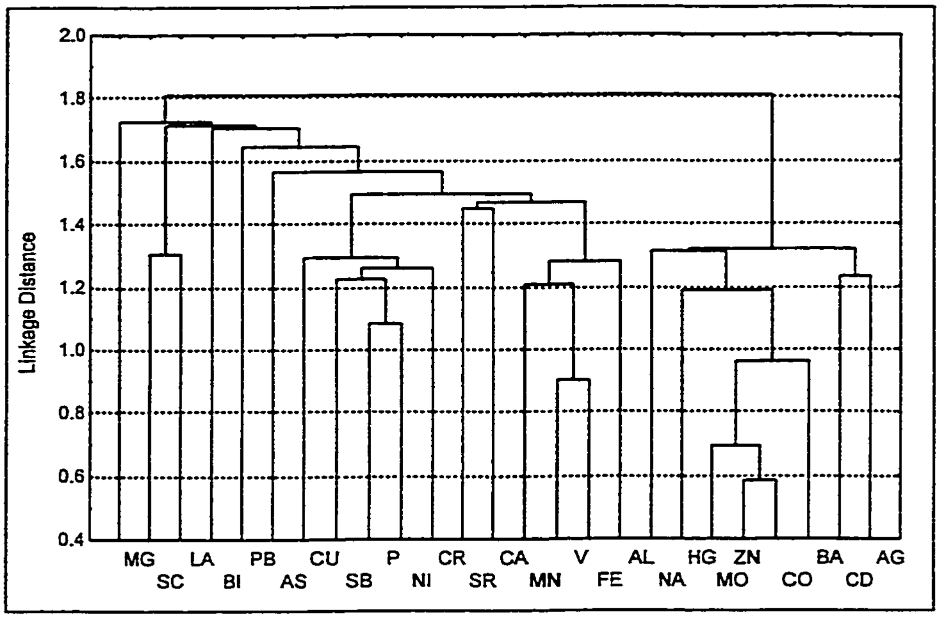

(a)

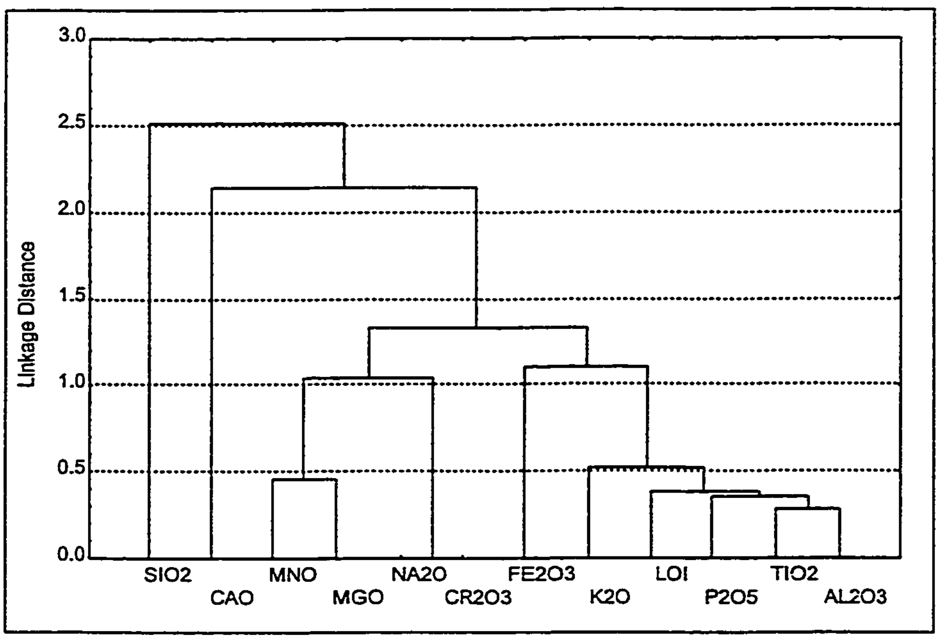

(b)

Figure 5.20. Dendrogram showing clustering among different elements and oxides in Al Habalah II locality: (a) Elements and (b) Oxides.

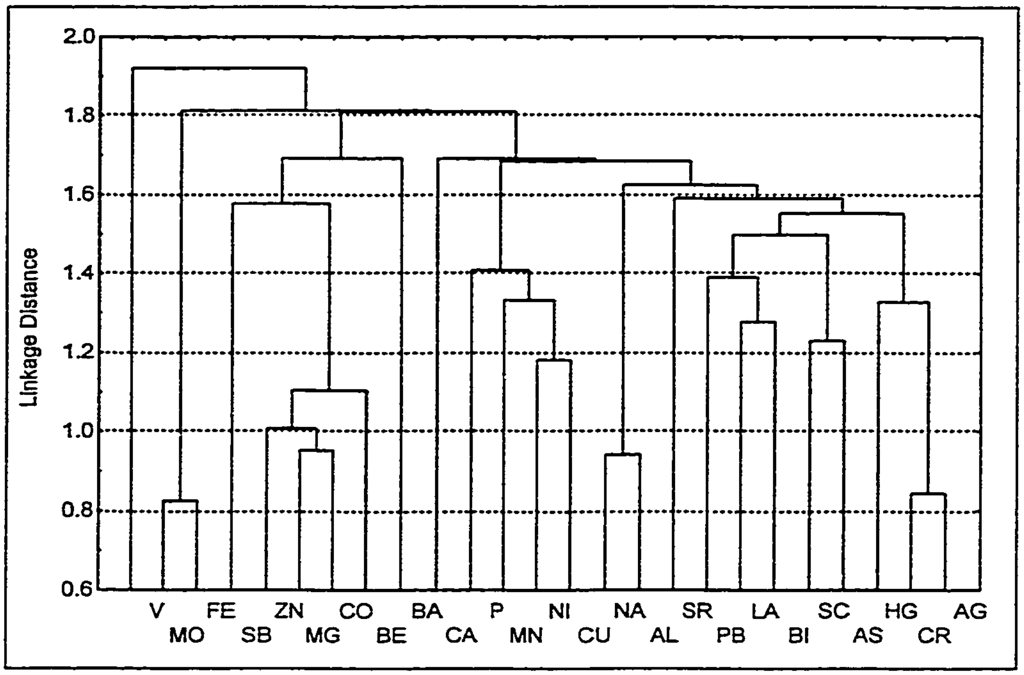

(a)

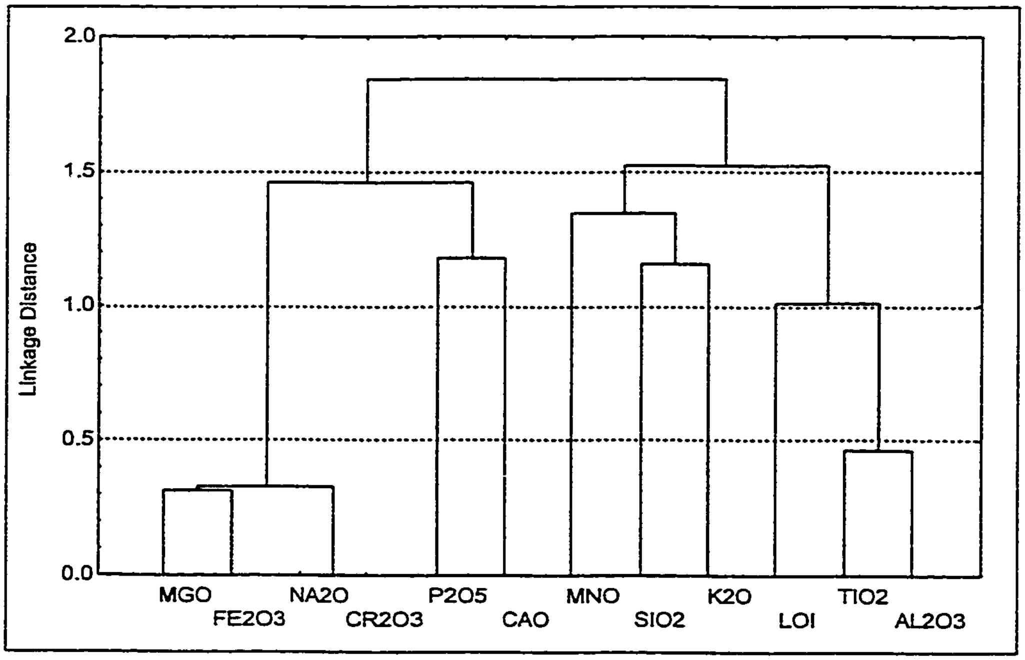

(b)

Figure 5.21. Dendrograms showing clustering among different elements and oxides in Al Soudah locality: (a) Elements and (b) Oxides.

TABLE 5.5. Linkage among different elements and oxides as determined by cluster data: (a) Ahad Rufaidah, (c) Al Habalah I, (c) Al Habalah II and (d) Al Soudah.

(a)

Group	Strong Linkage	Moderate Linkage	Weak Linkage	Outlier
		ELEMENTS		
A	K, Ba, P & Sr			
B1		Ca & Cd	Cu, As, Mg & La	
Subgroup B2 Subgroup	V, Ti & Cr		Mn	
C	Co & Hg	Pb, Ag, Sc, Zn, Na, Sb, Be, Bi, Mo		U
		OXIDES		
A	CaO & Na_2O	MgO, MnO, P_2O_5, Fe_2O_3, SiO_2 & K_2O		
B	TiO_2 & Al_2O_3	CaO & LOI		

(b)

Group	Strong Linkage	Moderate Linkage	Weak Linkage	Outlier
		ELEMENTS		
A	V & Fe		Mn & Ti	
B	Sr, Ca & Mg	Na & Cu	Ni, P & As	
C1	W & Tl		Cr, Ba & Pb	Al
C2		Be, Ag, Co, Sc & Zn	Hg, Sb & Mo	
		OXIDES		
A1		MgO, Fe_2O P_2O_5		SiO_2
A2	CaO, LOI, Cr_2O_3 & Na_2O	MnO		
B		TiO_2, Al_2O_3 & K_2O		

(c)

Group	Strong Linkage	Moderate Linkage	Weak Linkage	Outlier
		ELEMENTS		
A			La, Sc, Bi & Mg	
B1		P, Ni, Sb, Cu & Cr		
B2	V & Fe	Al & Mn	Ca & Sr	
C	Co, Zn, Mo & Ba	Hg, Cd & As	Na	
		OXIDES		
A	MgO & MnO	Na_2O & Cr_2O_3		
B	TiO_2, Al_2O_3, K_2O, LOI & P_2O_5	Fe_2O_3		SiO_2

(d)

Group	Strong Linkage	Moderate Linkage	Weak Linkage	Outlier
		ELEMENTS		
A	Fe & Mo	Co, Mg, Be & Zn	Sb & Ba	V
B		Cu & Ni,	Ca, P & Mn	
C	Cr & Ag	Al & Na	As, Bi, Hg, La Pb & Sr	
		OXIDES		
A	MgO, Na_2O, Cr_2O_3 & Fe_2O_3		P_2O_5	
B	TiO_2 & Al_2O_3	LOI	SiO_2, K_2O, & MnO	

5.4.3. Q - Mode Analyses of the Geochemical Data

In order to further constrain, the distinctions between the Red and Grey Units, Q-mode factor and cluster analyses of the samples were attempted. The extracted factors and cluster groupings are summarized in Tables 5.6 and 5.7 and represented as ternary diagrams and bar graphs (Figures 5.22 and 5.25). The details of the factor loadings, eigenevalues, and associated total variance are presented as Appendix IV.

5.4.3.1. Factor Analysis

Factor analysis shows that three factors (Table 5.7 and Figure 5.22) explain total variance of 79% and 76% for the element and oxide data respectively. The samples representing the Red Unit dominate the end members of factor 1 with only minor contribution from the Grey Unit. Factor 2 and 3 end members are composed of equal numbers of samples from both units. Samples from the Grey Unit, are fairly well represented in the factor 2 of the oxide data whilst only five each are included in factors 1 and 3.

Since most of the highly loaded samples are from the Red Unit, discriminating the units based on the chemical signatures of the samples that contribute to these factors will be subjective. However, an attempt is made to highlight the minor differences between the extracted factors rather than the units. The concentration of Al is slightly higher in factor 3 than in other two factors. Similarly, Fe and Ca are respectively higher in factors 1 and 2 compared to factor 3. The average concentrations of trace elements As, Ba, Be, Bi, La, Mn, P, Ni, Pb, Sb, Sc, V and Zn are higher in factor 1 than in other factors (Figure 5.23). The concentrations of MgO, MnO and Na_2O are higher in factor 2 than in any of the other two factors. On the other hand, Fe_2O_3 and CaO are respectively higher in factors 2 and 3 compared to factor 1 (Figure 5.24).

5.4.3.2. Cluster Analysis

In this analysis, four clusters were obtained in both the elemental and oxides data. The samples from the Red Unit cluster dominantly in A, C and D groups while those from the Grey Unit, cluster mainly in the group B. Based on oxides data, samples from the Red Unit cluster in the groups B and C while samples from the Grey Unit cluster in group A. Group D consists of a mixture of samples from both units.

TABLE 5.6. Summary of the distribution of factors derived from the Q-mode Factor Analysis of the Wajid Sandstone samples: (a) Elemental and (b) Oxide data

(a)

FACTOR	RED UNIT	GREY UNIT
1	AR3, AR9, AR15, AR19, AR22, AR23, AR25, AR35, AR51, ARLC4K1, ARLC3SC, HA2, HA9, HA13, HA14, HA18, HA23, HA24, HA27, HA36, HA38, HA45, HA47, HA51, HA52, HA56, HA59, OUT5I1, OUT5I2, OUT6C, S1, S2, S5, S8, S12, S13B, S15, S20, S26, S28, S30, S39, HAP 28	HAP13, HAP31, HAP37
2	AR26, AR21, AR43, AR51, ARLC4K3, HA28, HA30, HA31, HA35, OUT6C	HAP7, HAP9, HAP10, HAP13, HAP16, HAP17
3	HA15, HA52, HA59, HA62, HA64	HAP11, HAP17, HAP19, HAP21, HAP23, HAP33

(b)

FACTOR	RED UNIT	GREY UNIT
1	AR21,ARLC4K1, ARLC4K2, ARLC4K3, ARLC3SC, HA9, HA23, HA24, HA25, HA27, HA47, HA51, HA52, OUT5I1, S2, S5, S13B, S20, S26, S28, S30, S39	HAP17, HAP19, HAP23, HAP29, HAP33
2	AR3, AR9A, AR21, AR22, AR35, ARLC3S, HA14, HA15, HA38, HA45, HA64, OUT5K, S2, S8, S12, S13, HAP28	HAP1, HAP7, HAP9, HAP10, HAP11, HAP13, HAP16, HAP37, HAP40
3	AR20, AR23, ARLC4K2, HA2, HA23, HA28, HA50, HA51,HA52, HA56, HA62, OUT6C	HAP19, HAP21, HAP23, HAP29, HAP33

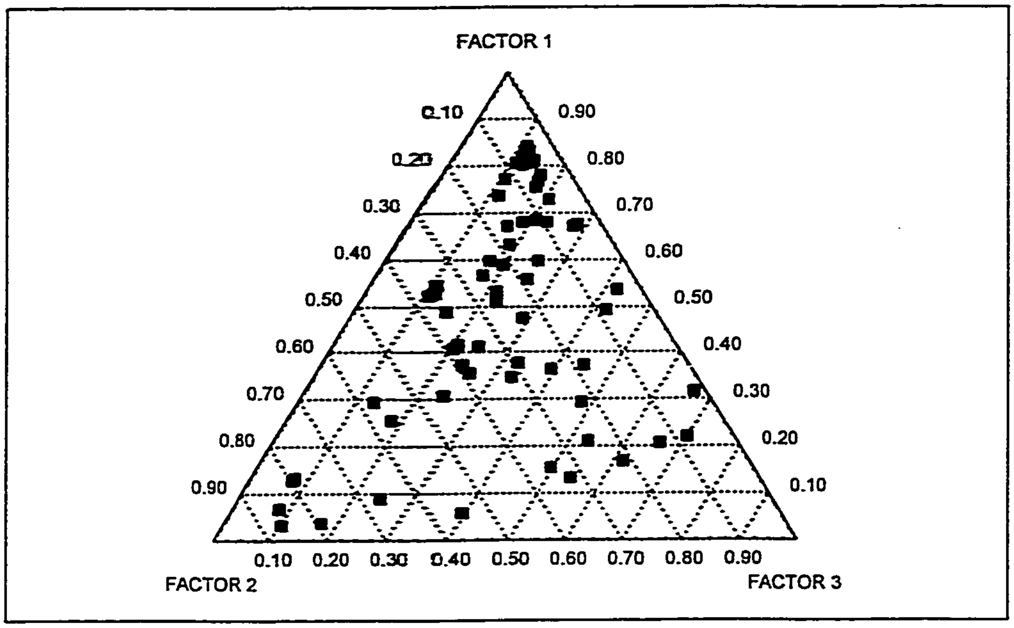

(a)

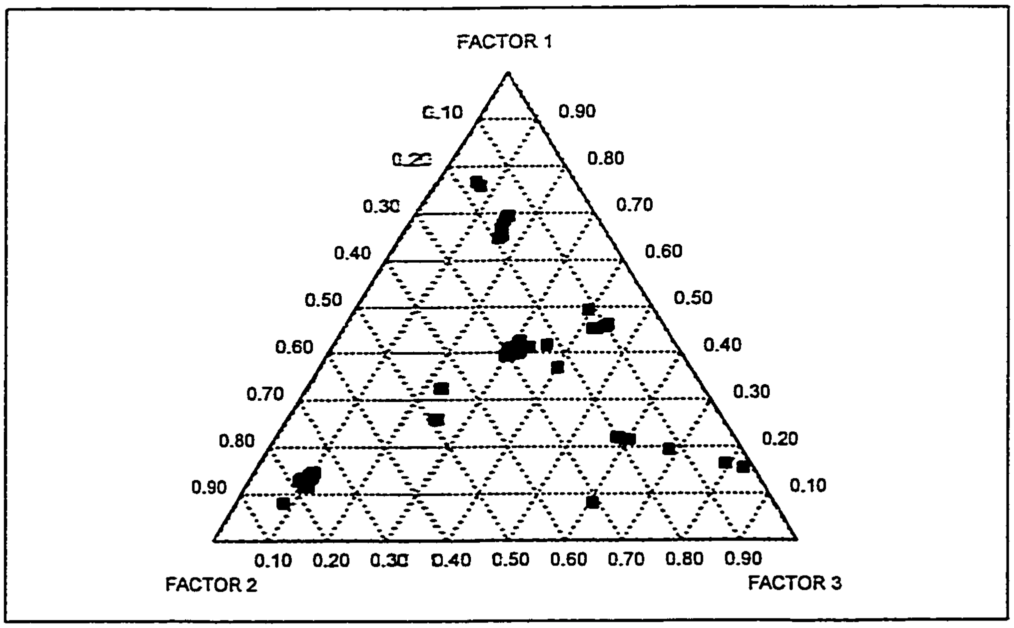

(b)

Figure 5.22. Ternary diagrams of the factor loadings for Q-mode sample analysis: (a) Elemental data and (b) Oxides data. The samples from the Red Unit dominate factor 1 in both the elemental and oxides data. The samples from Grey Unit are represented mainly in factors 2 and 3.

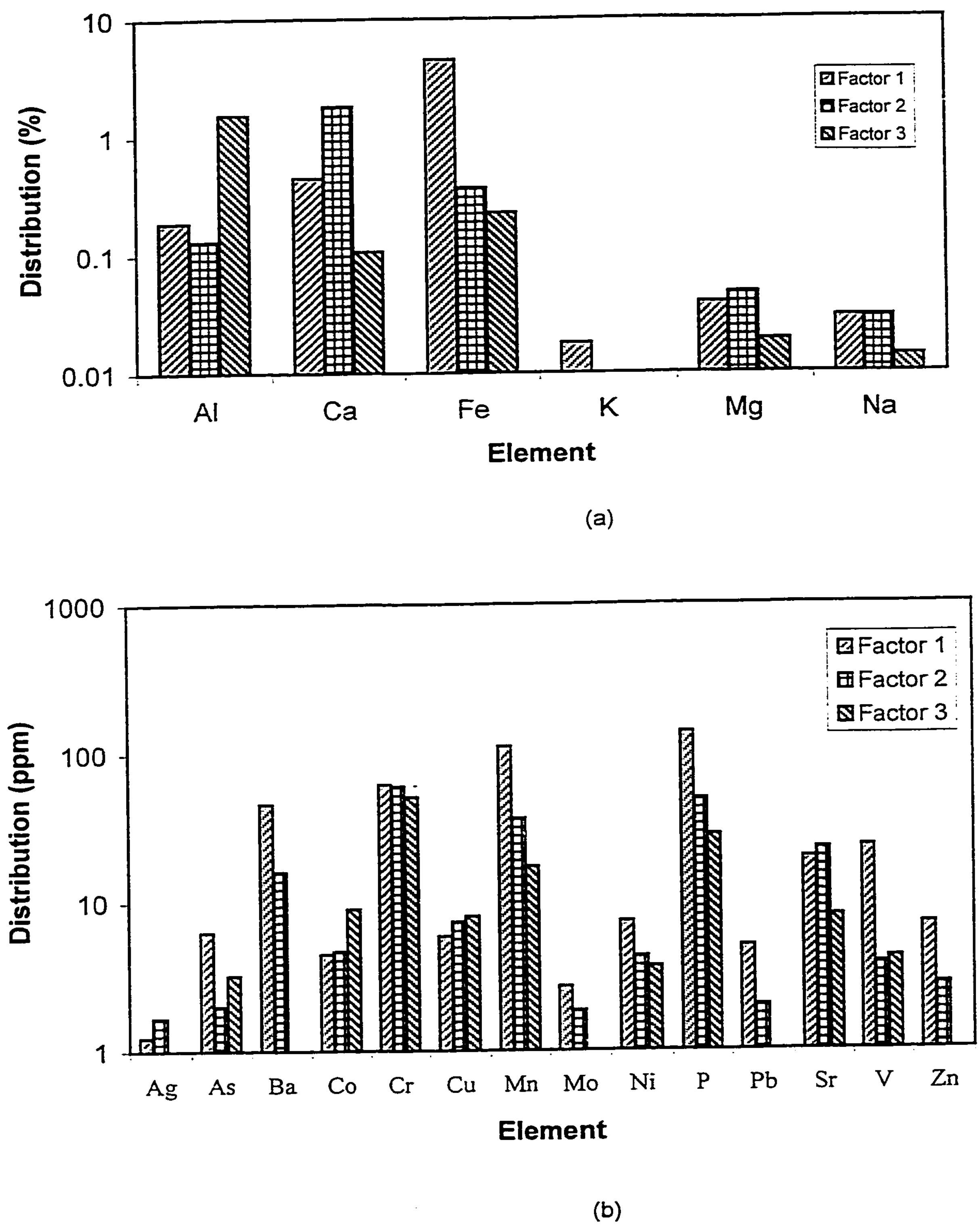

Figure 5.23. Relative distribution of elements in the samples characterized by high factor loadings in the Q-mode factor analysis. (a) Major elements and (b) Trace elements.

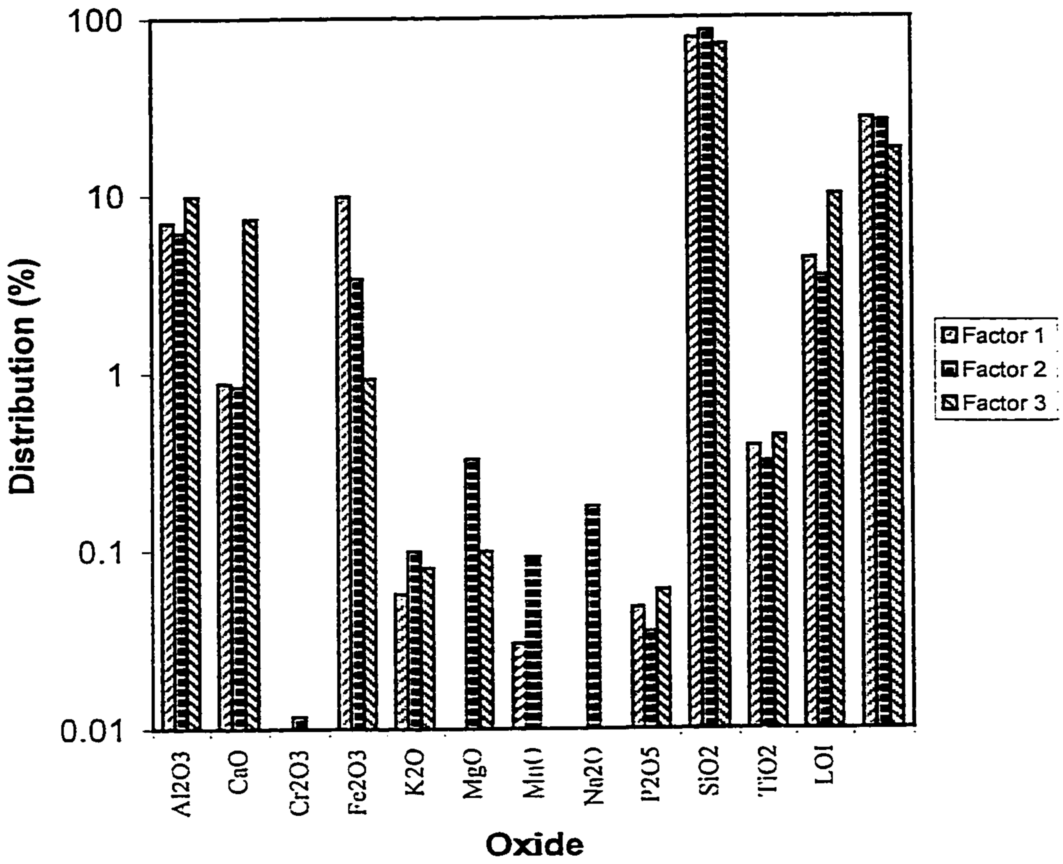

Figure 5.24. Relative distribution of oxides in the samples characterized by high factor loadings in Q-Mode factor analysis.

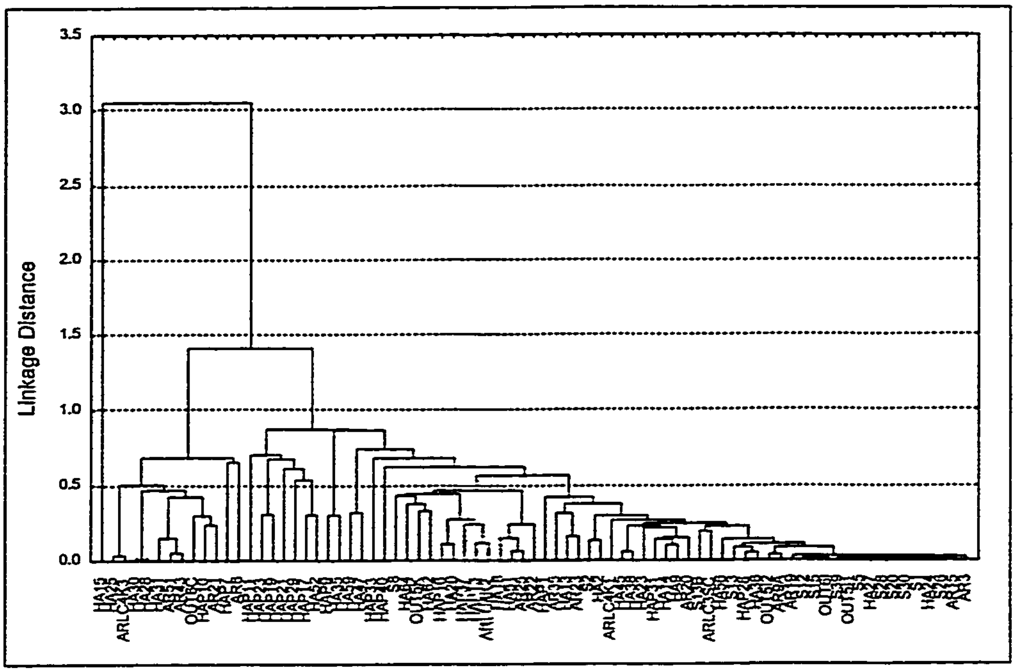

(a)

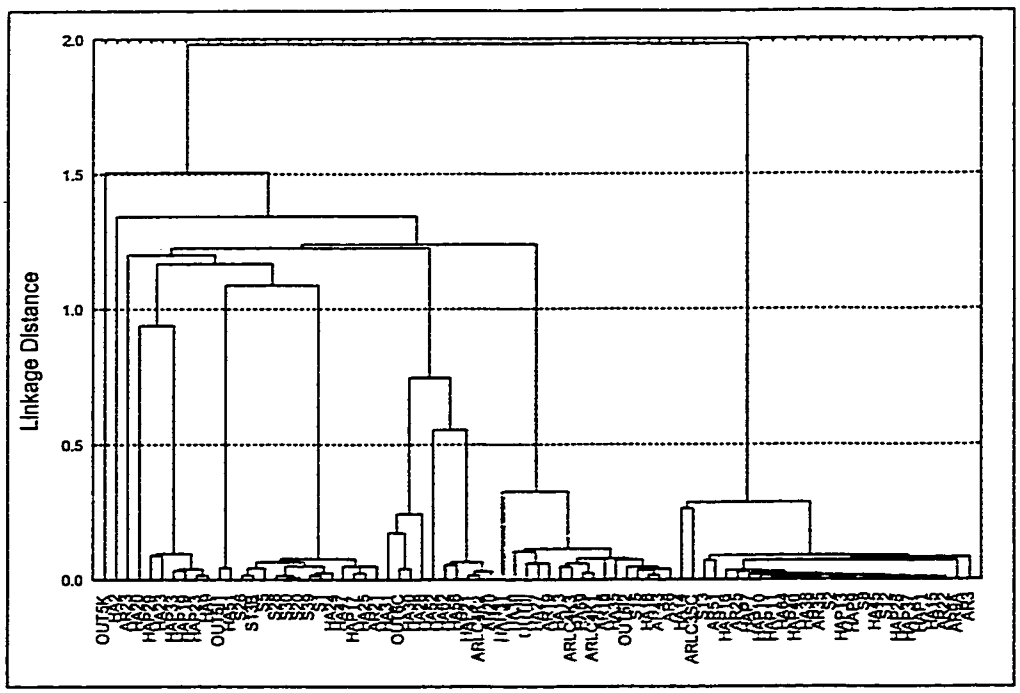

(b)

Figure 5.25. Grouping of samples based on their relative distribution in Q-mode cluster analysis: (a) Elemental and (b) Oxides data.

TABLE 5.7. Linkage of the cluster groups in Q-mode analysis of the Wajid Sandstone samples: Elemental and oxides data

GROUP	ELEMENTS DATA	OXIDES DATA
A	HA25, ARLC4K2, HA30, HA31, AR51, AR43, OUT6C, HAP10, AR21, HAP7, AR6	HA20, HAP29, HAP23, HAP33, HAP19, HAP23, HA9
B	HAP11, HAP23, HAP19, HAP21, HAP29, HAP17, HA52, HAP9, HAP35, HA59, HA47, HAP33, HAP40	OUT5I1, HA51, S26, S13B, S5, S28, S30, S20, S39, S1, HA24, HA47, HAP17, HA25, AR21
C1	S8, HA64, OUT5K, HA62, HAP 16, HA20, HAP37, HAP13, ARLC4K2, HA18, HA51, AR25, AR22	HA31, OUT6C, HA30, HA28, HA52, HA62, HA56, HAP21, ARLC4K2, AR20
C2	HAP1, AR35, HA13, AR23, S2, HA2, ARLC4K1, HA45, HA38, HA23, HA14, HA9, AR20, S13B, ARLC3SC, HA56, S13, HAP28, HA36, OUTI2, AR9A	HAP31, HA36, OUT6I, HA27, AR19, HA13, ARLC4K3, AR15, HA15, HA35, OUT5I2, S15, HA18, AR43, AR6
D	AR19, S12, S15, OUT6I, S39, OUT5I1, S5, HA27, S28, S20, S30, S1, HA24, S26, AR15, AR3	HA14, ARLSC3SC, S13, AR51, HAP16, AR25, HAP7, HAP10, HAP11, HA64, HAP40, HA38, AR35, S2, HAP13, HAP9, S8, HA45, S12, HAP28, HAP37, HAP1, HA15, AR22, AR9A, AR3

CHAPTER SIX

DISCUSSION AND CONCLUSIONS

6.1. Provenance

6.1.1. Introduction

Provenance analysis serves to reconstruct the predepositional history of sediments and sedimentary rocks including the distance and direction of transport, size and tectonic setting of the source region, climate and relief in the source area and specific types of rocks at the source terrane (Pettijohn *et al*, 1987).

In the present study, a multidisciplanry approach is employed to determine the provenance of the Wajid Sandstone. This multidisciplinary approach includes the petrological characteristics, heavy mineral assemblages, paleocurrent and the geochemical signatures of the sediments. The petrologic criteria used include textural characteristics (grain shape, sorting, and varieties), types of inclusions and composition of the sediments. Distribution, assemblages, ZTR ratio, color variation, form habits and types of inclusions constitute the heavy mineral parameters used for these interpretations. Geochemical characteristics including the distribution of trace elements Cr, Co, Ni and V, their corresponding ratios, distribution of some major elements and oxides were also utilized in the provenance study.

6.1.2. Petrofacies and Provenance

The petrofacies of the investigated Wajid Sandstone was determined on the basis of the QFL plots of Folk *et al* (1970), Dickinson and Suczek, (1979), Dickinson *et al* (1983) and Dickinson, (1983,1985). Wajid Sandstone in the studied localities is composed of mature quartz arenite. The quartz content averages between ~95 and 100%, feldspar, 0 and 3% and rock fragments, mainly cherts, 1.4 and 2.3% respectively. The mineralogical composition of the sediments is similar to those established from Wajid Sandstone elsewhere (Sable, 1982 and Dabbagh and Rogers, 1983).

Quartz-rich sandstones are products of preferential enrichment of quartz relative to destruction of the more labile, non-quartz components of sediments (Lewis and McConchie, 1994). Such sandstones are usually derived from stable cratonic setting or recycling of older quartz rich sedimentary source rocks.

The Wajid Sandstone in Abha-Khamis area was deposited on the peneplaned topography of the Precambrian basement. This eroded topography most likely provided the low relief require for the intensive chemical weathering (Johnson and Meade, 1990; Akthar and Ahmad, 1991; Franzinelli and Potter, 1983; and Fergusson *et al*, 1999) that produced the quartz-rich sediments of the Wajid Sandstone. The corroded nature of feldspar and hornblende grains, and replacement of calcite cement by hematite and kaolinitization suggest role of diagenesis (de Ros, 1998; Ehrenberg, 1991; Harris, 1989; McBride, 1987 and Schulz-Rojahn and Phillips, 1989) in modifying the composition of the Wajid Sandstone.

Considering the fact that the Wajid Sandstone consists predominantly angular to subrounded and generally poor to well-sorted quartz, a cratonic source close to the proximity of the depositional basin can be inferred. Outcrops of the Wajid Sandstone occur as outliers along the edge of the stable Arabian shield. Then the Precambrian rocks in the Arabian Shield are the likely sources of the quartz arenite.

An igneous provenance is indicated by the dominance of monocrystalline quartz in all the studied samples. These quartz grains are characterized by straight extinction and are unstrained. The presence of rutile, tourmailine and zircon as parts of the inclusions in the quartz grains suggests acidic igneous rock provenance. The presence of microcline and orthoclase grains (in the sparsely occurring feldspars) also indicates acidic composition source terrain

The occurrences of chert and some rounded quartz grains in the analyzed samples suggest contributions from sedimentary source (reworking of older sediments). Contributions from metamorphic source terrain are indicated by some of the quartz grains showing evidence of stress including undulatory extinction (Allen, 1965, Waugh, 1970).

6.1.3. Heavy Mineral Evidence

As evident by the XRD and SEM analyses hematite and goethite, which dominate the opaque fraction of the heavy minerals is largely diagenetic in nature. However, the presence of minor illmenite and chromite from SEM and XRD analyses suggests that some detrital opaque minerals are allogenic.

Thin section petrography of the bulk samples shows that the sediments are composed of quartz with very little mica, feldspars and matrix. The ZTR index of the heavy minerals is very high suggesting mineralogical maturity of the sediments (Hubert, 1962; Statteger, 1987 and Moral-Cardona *et al*, 1996). The high ZTR index is probably due to preferential depletion of unstable minerals by intense chemical weathering at source or during deposition (Hubert, 1962; Uddin and Lundberg, 1998) or intrastratal solution after deposition (Pettijohn, 1941). According to Uddin and Lundberg (1998), the association of zircon, tourmaline and rutile suggests felsic to intermediate provenance in a cratonic setting.

The abundance of tourmaline, zircon, rutile and apatite in sediments of the Red Sandstone of Europe was attributed to the stability of this assemblage, under the conditions favorable for red bed formation (Morton and Hallsworth, 1999). The Red beds were formed by extensive dissolution of ferromagnesian minerals under desert or seasonal climate. A similar condition may have probably existed during the deposition of the Wajid Sandstone especially the Red Unit. Apatite was not identified in the heavy mineral fraction of the Wajid Sandstone. The absence of apatite in the Wajid Sandstone might have resulted from dissolution by acidic groundwater (Morton, 1985; Morton and Hallsworth, 1994; 1999). A fluvial depositional environment such as the braided river system (depositional environment of part of the Wajid Sandstone; Dabbagh and Rogers, 1983) will allow circulation of groundwater and depletion of apatite.

The variations in color and form habits of heavy minerals are useful in provenance interpretations. Zircon grains observed in this study are dominantly euhedra with abundant inclusions (Plate 6 and 7). These types of zircon may be derived from a number of different source terrains including acidic to intermediate granitoid and recycled sedimentary rocks (Poldervaart, 1955 and Krumbein and Pettijohn, 1966). The color varies from colorless to pale yellow. The presence of some glossy variety suggests that some of the grains were derived from metamorphic sources (Schaffer and Dorr, 1997). The tourmaline grains are dominantly red brown, pink to green, inclusion-rich, idiomorphic, hypidiomorphic to fragmentary forms indicating predominantly acidic granitic to pegmatitic source (von Eynatten and Gaupp, 1999, Feo-Codicedo, 1956; Kerr, 1977 and Krynine, 1946). The subrounded to rounded nature of some of the tourmaline grains indicates sedimentary source (Krynine, 1946), probably from reworking of the underlying metasediments of the Precambrian to Proterozoic rocks.

Rutile is commonly derived from acidic igneous rocks or crystalline metamorphic rocks (Scholle, 1979). Epidote is dominantly associated with metamorphosed igneous rocks (Krumbein and Pettijohn, 1966). The total absence of pyroxene and other labile minerals, and sparse to common occurrences of epidote and hornblende in the Wajid Sandstone may be attributed to a number of reasons including intrastratal dissolution (Pettijohn, 1946; Statteger, 1987) and the felsic nature of the source.

The high contributions from tourmaline and hornblende in association with weak loading of rutile in factor 1 suggest an acidic source in Ahad Rufaidah. The observed negative loading for kyanite rules out a probable metamorphic influence from this factor. On the other hand, the combination of strong factor loading for epidote with weak contribution from kyanite indicates metamorphic source in factor 2 at this locality. According to Mezzadri and Saccani (1988), high loading of epidote indicates a metasedimentary source terrain. Factor 3 consisting of strong contribution from tourmaline and weak loading for hornblende suggests contribution from acidic rock terrains. Ternary plots of these factors show dominant contributions from factor 1. The presence of chromite in sample AR13 suggests contributions from an ultramafic source terrian.

Strong factor loadings for zircon in assocaition with weak contributions from rutile and opaque minerals in Al Habalah I locality indicate a acidic source rock. High positive loadings for opaque minerals, moderate contribution from zircon and weak loading from hornblende in factor 2 also suggest acidic igneous source rock. The strong negative loading of epidote (an index metamorphic mineral) and very low contribution from kyanite add support to this interpretation. High positive loading for rutile in factor 3 suggests acidic igneous provenance for the sediments exposed in Al Habalah I. Probable contributions from basic and ultramafic rocks at this locality are indicated by minor presence of ilmenite and chromite in some of the samples.

The strong association of epidote and hornblende with moderate negative loading of zircon in factor 1, suggest metamorphic source influence in the Al Habalah locality II. On the other hand, the association of zircon and rutile in factor 2 indicates acidic igneous source terrain. The observed moderate to weak association of rutile in addition to strong positive contribution from opaque minerals in factor 3 provide additional support in favor of acidic igneous source of sediments at this locality.

The strong association of epidote, rutile and opaque minerals suggests a metamorphic source terrain for factor 1 in Al Soudah area. The very strong loading for epidote (0.92) further strengthens (Mezzadri and Saccani, 1988) this inference. The observed, moderate positive contribution from touramaline in association with weak loading for opaque minerals and high negative loading for epidote indicate acidic source influence for factor 2 at Al Soudah. The strong loadings of hornblende and zircon indicate additional igneous source influence from factor 3.

6.1.4. Geochemical Evidence

The high values of the chemical index of alteration (CIA) obtained in this study suggest the effect of extensive chemical weathering at the source of the Wajid Sandstone. Values ranging from 51 to ~ 98 were recorded in Ahad Rufaidah. Samples from Al Habalah locality I (except the caliche samples) are characterized by values ranging between ~ 56 and 99. In Al Soudah locality, the values are as high as 78 to 99. The values at Al Habalah locality II range between ~58 and ~ 98 (Appendix IIIa).

According to Taylor and McLennan (1985) and McLennan (1993), the CIA values for the upper crust range from 47 to 51 while values between 45 and 55 indicate barely weathered to unweathered granite and granodiorite. Idealized muscovite, smectite and illite are characterized by values between 70 and 85 while kaolinite; chlorite; gibsite and bohemite yield values close to 100 (Nesbitt and Young, 1982; 1997 and Depetris and Probst, 1998).

The abundance of kaolinite abundance, paucity of feldspar and other labile minerals as determined from thin sections, SEM and XRD analyses. The values of Na_2O/K_2O of the Wajid Sandstone are generally low; ranging from 0.02 to 0.71 while those of Al_2O_3/Na_2O are high (not less than 39) in the samples studied (Appendix IIIa). These trends suggest chemical maturity of the sediments (Holail and Moghazi1, 1998).

Except for caliche and clay-rich samples, the concentrations of SiO_2 in are in the excess of 61% (with majority of the samples showing values ranging between 64 and 95%). The SiO_2 concentrations of intermediate rocks such as syenite, and diorite range from 57.5 to 59% while the values between 67 and 72% are typical for granodioritic and granitic (LeMaitre, 1976; Blatt and Tracy, 1996). The concentration of SiO_2 of the upper crust averages 60% (Taylor, 1964). Therefore, these relatively high concentrations of SiO_2 in this study indicate the dominance of intermediate to felsic source terrain. Murray (1994) and Murray *et al* (1991, 1992) suggested that high silica content (as found in the studied samples) might be due to diagenetic generation of silica. Thin section petrography showed that quartz overgrowth and quartz microcrystallites are common in the samples analyzed indicating diagenetic enrichment of silica.

The low concentrations of Al_2O_3, MgO, CaO, TiO_2 and Sr (Appendix IIIa) suggest acidic to intermediate source rocks with minor contributions from mafic sources (LeMaitre, 1976 and Holail and Moghazi, 1998). The extensive effect of chemical weathering as discussed earlier may explain the low concentration of these elements in the studied samples. The concentrations of these elements are lower than those obtained from the granite and pegmatite basement samples analyzed (Appendix IIIa). With only few exceptions, the concentrations of P_2O_5 range between <0.01 and 0.09%. These values are within the range of 0.02 to 0.09% reported by Stern and Gottfield (1986) from the felsic suite of Dhokan volcanic in Egypt.

The Al_2O_3/TiO_2 values range from 8 to 60 in Ahad Rufaidah with only a few samples showing values less than 14. In Al Habalah locality I, Al_2O_3/TiO_2 values are between 4 and 38 with only three samples showing values less than 14. On the other hand, the Al Soudah samples are characterized by values ranging from ~ 5 to ~ 44 with four samples showing values less than 14. Data from Al Habalah II locality indicate a range of values between 9 and 59 with five samples recording less than 14. Girty *et al* (1996) suggested that values of this ratio in the range of ~20 to 30 are common to sediments derived from andesitic to rhyolitic and/or granodioritic to tonalitic source terrains. According to LeMaitre (1976), values less than 14 indicate mafic rock composition. Therefore, the observed trends indicate that parts of the Wajid Sandstone were derived from dominantly intermediate to acidic source terranes with limited contribution from mafic terrain.

The relatively low concentrations of trace elements including Cr, Co, Ni, and V add support to the provenance interpretations (Table 5.2). The average concentrations of Cr range between ~ 52 and 62.59ppm in the investigated localities. The concentrations of Ni average between ~5 and ~9ppm. Similarly, the average concentrations of V fall between ~8 and ~21ppm. Cobalt concentrations in the samples are generally within a range of <1 to 39 with most values ranging between <1 and 7. The concentrations of these elements appear to be in the ranges of the values obtained from the basement samples analyzed (Table 5.1). These concentrations are below the average values of Cr (120ppm), Ni (100ppm), Co (50pppm) and V (240ppm) assigned to standard basalt

(Taylor, 1964, Reeves and Brooks, 1978) and the average mafic composition of volcanic rocks from the Nubian Shield (Zimmer et al, 1995). These observed trace elements concentrations are, however, within the threshold values of the granodioritic source terrains in the Colorado and Utah (van de Kamp and Leake, 1994) and felsic to intermediate Dokhan volcanics (Stern and Gottfield, 1986).

The Cr/Ni values in this study average between ~7 and ~21 (Table 5.2). A range of 1.2 to1.6 Cr/Ni indicates ultramafic source composition (Garver *et al*, 1994; Garver and Scott, 1995). The Cr/Ni, V/Cr and V/Ni ratios of the Wajid Sandstone are dominantly within the range of the values of the basement samples except the gabbro samples (Tables 5.1 and 5.2). These ratios suggest acidic to intermediate source terrain.

The cluster and factor associations obtained from the multivariate statistical analyses further enhanced provenance interpretations in this study. The influences from the different end members of the extracted factors and their corresponding cluster associations as applied to provenance are discussed below.

The combination of high contributions from Ag, Hg, Mo, Pb, Sc, Al_2O_3 and TiO_2 in factor 1 in Ahad Rufaidah is interpreted to indicate dominantly felsic source. This interpretation is supported by moderate loadings of Zn, Na, Sb; weak U and strong to moderate negative loadings for elements Cr, Al, Ni, Cu and Ti representing mafic source in the same factor. The association of Zn, Pb, Na, Mg, and Hg with U reflects more acidic than basic composition at the source. This factor accounts for virtually all the source contributions in this locality. Weak loadings for Ag, Cu, Be and strong positive contributions from SiO_2, MnO and MgO in association with strong negative loadings from Ba, K, P and Sr characterize factor 2 in this locality. This assocaition probably indicates mafic influence at the source. The negative loadings for elements (Ba, K, and Sr) derived from felsic rocks negate the dominance influence of this source terrain in this factor. However, strong contributions from MgO and MnO in combination with weak Be and Cu in factor 3 are more positive evidence of mafic influence.

The factor 1, is characterized by high to moderate association of Be, Ag, Sc, Co, CaO and weak loadings for Hg, Pb, Ba, Sb and Zn in Al Habalah I locality. The combination of this association, with strong negative loadings for Fe, Mn, Ti, V, Cr and Ni suggest a felsic composition of the source terrain for the sediments from this locality. The strong negative loadings for the mafic elements Fe, Mn, Ti, V, Cr and Ni preclude a basic source terrain. Ternary plots show that factor 1 has dominant influence on the source of the sediments at this locality. High to moderate contributions of Ca, Mg, Ni, Cr_2O_3 and weak loadings for MgO, MnO and Fe_2O_3 suggest a mafic influence from factor 2 in this locality. However, the observed high loadings for Na_2O, Sr, As, La and Mo indicate complimenting felsic influences as well. Factor 3 association composed of high loadings for Cu, Na and La and weak Cr, P, MgO, CaO and P_2O_5 indicate the dominance of metamorphosed volcanics at the source terrain. The weak loadings for Cr, P, MgO and CaO indicate the presence of at least minor mafic contributions. This factor combines with other factors to account for the source of sediments in this locality.

The factor 1 is characterized by high contributions from elements such as Ni, Cr, Mg, P and Sc that are characteristic of mafic provenance (Reeves and Books, 1983 and Morsy, 1993). The association of these elements with weak contributions from Ca, Cu and Mn suggest mafic influence from factor 1 at the source in Al Habalah II locality. The inferred mafic influence is further evident by strong positive loadings for Fe_2O_3, P_2O_5, and TiO_2 in addition to weak contribution from Al_2O_3 and negative loading from SiO_2. The characteristic strong loadings for Fe, Mn, V, Cr_2O_3, MgO, MnO and Na_2O in association with weak Cr, Na, Ni and Sr suggest a dominantly mafic source composition for factor 2 at this locality. The strong negative loadings from La, Pb, As and Bi further support this interpretation. Strong factor loadings for Ag and Cd in association with moderate contributions from Mg, Hg and weak loadings for Al, Ba, Mo and Na in factor 3 of this locality suggest mafic influence at the source.

High contributions from Mn, Ni, P; moderate loading for Fe; weak loadings for Al, Mo, Na and Cu in association with strong negative Zn, Be, Co, Mg and Ba suggest mafic influence for factor 1 in Al Soudah locality. This deduction is supported by high contributions of Cr_2O_3, Fe_2O_3, MgO and Na_2O. According to Morsy (1993), strong loadings for Fe and Mn indicate secondary environmental influence. Strong loadings for As, Pb, Sc, Sr, MnO and SiO_2 in association with weak loadings of Mo, Hg, Cr_2O_3 and Na_2O indicate felsic influence from factor 2 at the Al Soudah locality. High contributions from Ag, Cr, Hg, Bi, CaO, P_2O_5; moderate La and Na and weak Al, Mo, Pb, Cr_2O_3, and Na_2O are characteristic of factor 3 in Al Soudah Locality. This association suggests mixed sediment sources with Cr, Bi, La, CaO, Cr_2O_3 and MnO indicating mafic influence. On the other hand, the combination of high Na, Hg with low Al, Mo, Pb and Na_2O suggests felsic influence.

6.2. Tectonic Setting and Sedimentation

The composition of the sedimentary rocks in an area is largely controlled by the tectonic setting (Dickinson, 1983). Many authors including Dickinson and Suczek (1979), Ingresoll and Suczek (1979), Dickinson (1983, 1985), Dickinson and Valloni (1980) and Basu, (1985) used composition data of sandstones to recognize the tectonic provenance of depositional basin and source terrain.

The Wajid Sandstone, which is dominantly quartz arenite, plots within the stable cratonic domain of Dickinson and Suczek (1979). The craton derived quartz arenites are products of weathering and denudation of low-lying granites and gnessis rocks supplemented by recycling of associated flat lying platform sediments (Dickinson, 1985).

The heavy mineral assemblages of the Wajid Sandstone are dominantly composed of ZTR minerals. According to Uddin and Lundberg (1998), an association of ultrastable minerals including zircon, tourmaline and rutile suggests felsic to intermediate provenance in a stable cratonic setting. Mature passive continental margins are characterized by high percentage of zircon, tourmaline, epidote, and amphibole as well other less common minerals of metamorphic and felsic intrusive origin (Nechaev and Isphoring, 1993, von Eynatten and Gaupp, 1999). Most of these minerals were identified in the Wajid Sandstone

The concentrations of Al and Ti are commonly high in terrigenous sediments while iron occurs abundantly in metaliferous ridge proximal sediments (Murray, 1994).

The abundance of these elements indicates continental and hydrothermal input at oceanic spreading centers Murray, 1994). On the basis that Al and Ti are relatively immobile elements, Murray (1994) employed the variations in Al_2O_3, TiO_2 and Fe_2O_3 concentrations in sediments to establish chemical criteria to identify different tectonic environments. A great majority of the samples analyzed plots in the continental margin field of the Murray (1994), Figures 5.3 - 5.5.

The K_2O/Na_2O values of the studied samples range from 1 to 16 (only few samples recorded higher values). The K_2O/Na_2O values of geosynclinal greywacke are usually less than while values greater than 1 are characteristic of stable continental setting (Middleton, 1960). Crook (1974) noted that the quartz-rich sandstones with SiO_2 average concentration of 89 and K_2O/Na_2O values greater than 1 are derived from passive continental margin and plate interior. According to Maynard et al (1982), SiO_2 and K_2O/Na_2O of passive margin derived sands, average 77.9% and 1.05, respectively. Based on bivariate relationship between SiO_2 contents and K_2O/Na_2O of ancient sandstone, argillite/shale, Roser and Korsch (1986) identified different tectonic environments. As outlined by these authors, the values of K_2O/Na_2O and amount of SiO_2 for the oceanic island arc field range between 0 and 2, and 0 to 75%, respectively. For active and passive continental margins, these parameters range between 0.4 and 8, and 0 and 88%, respectively (Figure 5.6). As shown in Figure 5.7, the bivariate plots of K_2O/Na_2O ratio with SiO_2 concentrations in Wajid Sandstone fall within the passive continental margin field.

The Wajid Sandstone crops out near the edge of the stable Arabian craton. The derivation of this Sandstone from the shield area is very likely. However, the dominantly northern orientation of the cross beds, indicates a southern source, probably, the highlands in Yemen. The contribution from the shield area to the west is likely to be minor. This paleocurrent trend is consistent with the trends reported elsewhere (Sable, 1982 and Dabbagh and Rogers, 1983).

The Asir and the Afif terranes of the southern and eastern parts of the Arabian Shield in Saudi Arabia, extend all the way to Yemen. In the central and eastern parts of Yemen, are the Abas gneiss, Al Bayda Island Arc, Al-Mahfid and Al-Mukailla gneiss terranes (see Widley *et al*, 1996). The Asir terrane is composed of alternating beds of greenschists-grade volcanic and sedimentary rocks and high-grade gneisses. The Andean-type continental margin Afif terrane is characterized by monotonous orthogneisses intercalated with arc-type pillow basalts, andesite and rhyolites and plutonic granitoid and gabbroic suites. Rocks of the Abas terrane are gneiss and metamorphosed supracrustal rocks. Greenschists-grade rhyolites, andesites, basalts and tuffs representing arc-type volcanics characterize the Al-Bayda terrane (Widley *et al*, 1996). Plutonic rocks of this terrane include hornblende bearing granodiorites, granites and gabbros. These plutonic rocks are later intruded by pegmatites and hornblende andesite dykes. Al-Mafid terrane is composed of migmatized orthogneiss rocks of older supracrustal belts. This terrane contains a lot of amphibolite dykes, granitic veins and swarms of tourmaline bearing aplite-pegmatite sheets. This terrane is overlain by suite of supracrustal belt consisting of greenschists-grade, rhyolites, basaltic andesites, marbles and thin conglomerate beds of the Masha'ar Group of Ishakin and Degtyariov (1990). The Al-Mukailla terrane is composed of tuffs, feldspar porhyry lavas, volcanic breccias, rhyolites, basalts and quartz-porphyry dykes found typically in an island arc setting.

Based on the mineralogical composition, the sediments of the Wajid Sandstone were probably derived from Afif terrane with minor contributions from the other terranes. An island arc and supracrustal provenance is also possible. However, if the sediments were derived from such provenance, then the effects of chemical weathering at the source must have profoundly modified the composition of these sediments, since attributes of such sources are not represented.

The presence of rounded quartz and ZTR grains in both the light and heavy mineral suites suggests derivation of sediments from of older sediments. The Ghabar Group, which includes pebbly coarse sandstone units, can serve as a probable provenance of the sediments of the Wajid Sandstone.

6.3. Depositional Environments

The overall geometry (vertical stacking of blocky sand bodies) and facies associations indicate that the Wajid Sandstone was deposited in a fluvial depositional setting. The Sandstone is composed of poor to well-sorted, medium to coarse grained, pebbly sands. The general sedimentological characteristics observed in the Wajid sandstone resemble those of modern braided stream channel system (Doeglas, 1962, Leopold *et al*, 1964 and Allen, 1965). Braided river system usually occurring in the upstream, high energy part of the river system is characterized by rapid discharge, high slope, heavy load of coarse sediments and more readily erodible boundaries (Walker and Cant, 1984). The dominantly large scale, low angle tabular to planar cross- bedding characteristic of the studied succession may have been formed on the downstream of the braided bars and as chute pool deltas (Mcgowen and Garner, 1969 and Selley, 1972). Such features may also develop due to migration of the slip face of sand waves and sandbars (Ward and Mcdonnald, 1979). On the other hand, the minor trough-like cross stratification observed in few outcrops might be the result of infilling of chute channels during period of waning discharge (cf Selley, 1972).

The predominance of unidirectional paleocurrent trend, coupled with the observed large-scale cross stratifications (mainly planar and trough), regular and lateral continuity of the beds and the absence of any fossils indicate a braided stream system. Based on similar parameters, Dabbagh and Rogers (1983) recognized the Wajid Sandstone south of the study area (Al Soudah inclusive), as a braided river sequence.

The presence of bi-directional cross beds in the Grey Unit may suggest a coastal plain deposit or nearshore depositional environment. However, the absence of any fossils, however, makes this interpretation subjective. Laboun (1999; personal communication) observed similar type of bi-directional cross bedding in the basal part of the Khussayyan Formation of the Wajid sandstone at Wadi ad Dawasir. According to this author, Khussayyan Formation was deposited in a braided river to eolian setting.

The massive sand bodies, which occur frequently in the Wajid Sandstone, may have been deposited by gravity flow. Hussain (1999; personal communication) recognized slump structures in the massive sand bodies in the Wajid Sandstone exposed in the Najran area. Channel-type massive sand bodies, as observed in Wajid Sandstone have been interpreted elsewhere as products of subaqueous gravity flow (Jones and Rust, 1983, Rust and Jones, 1987, Turner and Monro, 1987 and Wizevich, 1992) and also as braided bar incision product (Hodgson, 1978). Such sand bodies are believed to be deposits of highly concentrated sediments/water mixture, which lies in the continuum of cohesionless sediment flow (Martin and Turner, 1998).

The occasional fining upward sequence in the kaolinite-rich horizons might be the product of gradual infilling of the braided channel during the waning stage of flow in the channel (Kelling, 1968 cited in Selley, 1972). Claystone or silty sediments may accumulate on the floodplain levees overbank of a meandering river system. Such vertical accretion of the fine-grained sediments is less common in a braided stream (Walker and Cant, 1984). Khitzsch *et al* (1979) and Ward and Mcdonald (1979), ascribed kaolinitic sandstone occurring in the braided river basal clastic unit in the cretaceous Nubian Formation to interchannel flood plain deposit.

The occurrences of intraformational clasts and quartz pebbles in the kaolinite-rich lenses indicate fluctuating intensity of the transporting medium. Selley (1972) attributed the occurrence of siltstone in channels to erosion of the main channel complex followed by catastrophic abandonment such that the main channel bedload supply is cut off and only the suspended fine sediments are deposited. This phenomenon which is commonly associated with meandering river system has, however, been reported in braided sequence as well (Doeglas, 1962 and Selley, 1969). In a braided river system, channel abandonment could probably result from channel choking and switching (Doeglas, 1962) or rapid headward channel erosion in the unconsolidated detritus (Denny, 1967).

Geochemical evidence suggesting fluvial depositional environment in Wajid Sandstone is the high values of CaO/(CaO+MgO) of the studied samples, which are largely between 0.77 and 0.99. This criterion is on the basis that chemical mobility is minimal in iron-rich and manganese-rich sediments during diagenesis and low metamorphism (Dasgupta *et al*, 1999). The Wajid sediments particularly the basal parts of the studied section are iron and manganese rich. The CaO/(CaO+MgO) values are usually higher than 0.7 in freshwater lakes and rivers and much lower in marine setting, usually less than 0.5 (Dasgupta *et al*, 1999). The record of values mostly higher than the 0.7 thresholds suggests that the Wajid Sandstone in the investigated localities were predominantly deposited in a freshwater setting. This is in favor of a braided river system.

In this study, intense chemical weathering at the source is inferred as a major contributor to the compositional maturity of the Wajid Sandstone. The effects of this process are evident by the near to total depletion of feldspar, lithic grains and other labile constituents and abundance of kaolinite as well as the exceptionally high CIA values.

Plate tectonic reconstruction showed that the Arabian plate along with Turkey and other adjacent plates constitute part of the northern passive margin of the Gondwanaland bordering the PaleoTethys ocean in the Proterozoic to Late Paleozoic (Beydoun, 1991). This landmass forms the southern Tethyan geosyncline. At the Early Paleozoic, the block of the Gondowanaland was within the 30°S and 60°S latitudes in the Southern Hemisphere. This indicates that this landmass and its plate components, the Arabian-Nubian plate inclusive were within the temperate paleolatitude at this period. The characteristic sedimentary sequence was dominantly clastics with minor episodic carbonate deposits.

According to Beydoun (1991), temperate climatic conditions prevailed in the Early Paleozoic. These climatic conditions must have been humid (Miall, 1980 to facilitate high level of chemical disintegration of labile components at the source and explain the compositional maturity of the Wajid Sandstone. Humid climatic conditions and adequate precipitation are also required for a braided river stream depositional system under which the Wajid Sandstone was deposited.

Close association of caliche with the ferruginous materials and kaolinite in the basal Red Unit, may have resulted from leaching and reprecipitation of calcareous components of the sediments. Rust and Koster (1984) ascribed the abundance of calcrete and red coloration in the Cannes de Roche fan deposits to a relatively dry paleoclimate. The presence of these sediments in the Wajid Sandstone indicates episodes of drier climatic regimes in an otherwise humid setting of the region.

6.4. Origin of the Ferruginous Horizons

The abundance of angular to subrounded grains in the ferruginous horizons indicates a short distance of transportation of the sediments. The Precambrian rocks exposed in the vicinity are possible sources of iron in the investigated Wajid sequence. Gabbro, biotite schists, granites, pegmatite and other iron bearing rocks outcrop abundantly within the vicinity of the Wajid sequence in the study area. The paleocurrent direction, however, suggests a predominantly southerly source of sediments. It is possible that the iron was derived from leaching of the mafic minerals from this southern source. Another possible sources of iron are the younger mafic rocks (Tertiary columnar basalts) in the Najran and Dhahran Junub areas. However, the absence of iron horizons in the upper Grey Unit (showing the same trend of paleocurrent) rules out a probable contribution from these sources.

The absence of iron in the Grey Unit may be due to depletion of iron at the source when the unit was deposited. There may have also been a change in the sediment source. It is also possible that there was a change in the atmospheric chemistry when the Grey Unit was deposited. A more oxidizing condition that does not allow efficient transportation of iron may have also prevailed at the time the Grey Unit was deposited. The occurrence of hematite mainly as pore-filling cement observed in the thin sections suggests that an authigenic origin of the iron minerals in the Wajid Sandstone (Plate1, Figure a, Plate 2 Figure 1, and Plate 3, Figures b-d). This deduction is supported by the preservation of well-formed euhedra delicate textural morphologies as observed in SEM photomicrographs (Plate2, Figures b and c). Wilson (1971) used similar textural morphologies to identify authigenic hematite and goethite in the Old Red Sandstone of Scotland.

The modes of incorporation of iron in the Wajid Sandstone may be one of the following. (i) Leaching of iron out of the ferruginous minerals at the source by intensive chemical weathering and transportation as Fe^{2+} in colloidal solution into the basin where it was subsequently oxidized and incorporated into the sediments. The maturity of the framework minerals, high CIA and ZTR index recorded in this study indicate intensive weathering at the source. (ii) Another scenario is that the iron material probably occurred primarily as goethite/limonite cement (van Houten, 1964; 1968; 1972, and 1973 and Berner, 1969) and later converted to hematite by in-situ diagenesis. (iii) Postdepositional intrastratal dissolution of iron-rich mafic minerals including hornblende, biotite, pyroxene, olivene and epidote (Walker, 1967, 1973, and Walker *et al*, 1967) might have also taken place. The state of degradation of feldspars and hornblende grains as observed in thin sections favors such conclusion. The absence of other labile minerals such as pyroxene, olivine and low concentration of epidote and hornblende may be due to both intrastratal alteration and weathering.

6.5. Origin of the Kaolinitic Claystone

The close association of the kaolinitic claystone, silt and fine sand in the outcrops indicates that it was partly allogenic in nature. On the other hand, monomineralic composition (kaolinite only) and the pore-filling nature of the clay suggest an authigenic origin. The delicate euhedral book-stack, blocky, pseudohexagonal plates and granular or vermicular textures of the kaolinite as observed in SEM study (Plate2, Figures d - f) also support the authigenic (Keller, 1978, Morgan *et al*, 1979; Zalba, 1981 and Welton, 1984) mode of occurrence of this clay mineral in the Wajid Sandstone.

Kaolinite may be derived from surface weathering and hydrothermal alteration (Fan, 1979), weathering of granitic rocks or in-situ alteration of arkosic sand (Murray and Partridge, 1981) or due to leaching by circulating acidic groundwater (Morgan *et al* 1979). Murray and Heckroodt (1979) attributed the alteration of feldspars to kaolinite without intermediate stage smectite to superficial weathering probably during humid era or when chemical weathering dominated mechanical weathering. The absence of smectite in the analyzed samples suggests this condition in the development of kaolinite in the Wajid Sandstone. The compositional maturity and high CIA values of the investigated sediments suggest intensive weathering of the parent rocks. The high SiO_2 concentrations in the studied samples indicate that the parent rock is acidic igneous rock. The low concentrations of K_2O and Na_2O in the analyzed samples indicate depletion of feldspars, mica and other minerals rich in these elements in the parent rocks due to weathering at source or in-situ alteration at the depocenter. Ternary plots of SiO_2-Al_2O_3-LOI, SiO_2-Al_2O_3-TiO_2, SiO_2-Al_2O_3-Fe_2O_3 and SiO_2-Al_2O_3-K_2O (Figures 5.8 - 5.11) show fields similar to those of the Central African kaolins and some of the kaolin deposits in the Amazon region. According to da Costa and Moraes (1998), the central African and Amazon region kaolin deposits, consisting dominantly of pure kaolinite were derived from granitic source terrain.

6.6. Conclusions

- Petrologic characteristics (mainly unstrained monocrystalline quartz); heavy minerals data including color, types of inclusions, crystal types and associations; whole rock and trace element chemistry indicate that the Wajid Sandstone, was dominantly derived from intermediate to felsic source terrain.

- The QFL plots of the Wajid Sandstone suggest a stable cratonic provenance.

- Based on the tectonic provenance discriminant criteria developed by Roser and Kosch (1986) and Murray (1994), a passive continental margin provenance with some oceanic island arc influences is inferred in this study.

- Paleocurrent distribution suggests that the Wajid Sandstone was derived from mainly southern source terrain, probably from highlands in Yemen.

- Gross textural attributes, sedimentary structure, paleocurrent orientation and overall facies geometry indicate a braided river depositional setting. The associated kaolinitic claystone lenses were probably deposited during the slack stage of the river.

- The results from SEM and XRD studies show that the iron minerals of the Red Unit are mainly authigenic hematite and goethite. The clay mineral content of claystone and fine sandstone was identified as authigenic kaolinite.

REFERENCES

Akhtar, K. and Ahmad, A.H.M., 1991, Single-cycle cratonic quartzarenites produced by tropical weathering: the Nimar Sandstone (Lower Cretaceous), Narmada Basin, India. *Sedimentary Geology, 71*: 23 - 32.

Alabouvette, B. and Villemur, J.R., 1973, Reconnaissance of the Wajid Sandstone: *(France) Bureau des Recherches Geologiques et Mineres Open File Report 73-JED-3*: 22p.

Al-Laboun, A. A., 1993, Lexicon of the Paleozoic and Lower Mesozoic of Saudi Arabia: Nomenclature Review. *Al-Hudhud Publishers, Riyadh, Saudi Arabia*: 511p.

Allen, J.R.L., 1965, Upper Old Red Sandstone (Farlovian) Paleogeography in South Wales and the Welsh borderland. *Journal of Sedimentary Petrology, 35:* 167 - 195.

Basu, A., 1985, Influence of climate and relief on composition of sand released at source areas. *In: Zuffa, G.G. (ed.), Provenance of arenites, NATO Series, Series C: mathematical and Physical Sciences, 148*: 1 - 18.

Berner, R.A., 1969, Goethite stability and the origin of Red Beds. *Geochimica et Cosmochimica Acta, 33*: 267 - 273.

Beydoun, Z.R., 1982, The Gulf of Aden and northeast Arabian Sea. *In: The Ocean Basins and Margins, Volume 6. The Indian Ocean, Nairn, A.E.M. and Stehli, F.G. (editors). Plenum Publishing Corporation, New York, Chapter 6*: 253 – 313.

Beydoun, Z.R., 1991, Arabian plate hydrocarbon geology and potential: a plate tectonic approach. *American Association of Petroleum Geologists Studies in Geology, 33*: 77p.

Blatt, H., 1967, Provenance determinations and recycling of sediments. *Journal of Sedimentary Petrology, 37*: 1031 1044.

Blatt, H. and Tracy, R.J., 1996, Petrology: Igneous, Sedimentary and Metamorphic. *W.H. Freeman & Company, Second edition: 529p.*

Briggs, L.I., 1965, Heavy mineral correlation and provenances. *Journal of Sedimentary Petrology, 35*: 939 - 955.

Bostrom, R., 1970, Submarine volcanism as a source of iron. *Earth Planetary Science Letter, 9*: 348 - 354.

Brown, G.F., 1970, Eastern Margin of the Red Sea and Coastal structures in Saudi Arabia. *Phil. Trans. Roy. Soc. London, A267*: 75 –87.

Brown, G.F. and Jackson, R.D., 1959, Geologic map of the Asir quadrangle, Kingdom of Saudi Arabia: US Geological survey Miscellaneous Geological Investigation Map 1-217 A, Scale 1:500000.

Brown, G.F. and Jackson, R.O., 1960, The Arabian Shield. *21st International Geological Congress Report, Copenhagen*: 69 –77.

Brown, G.F., Schmidt, D.L. and Huffman (Jr.), A.C., 1989, Geology of the Arabian Peninsula Shield Area of the western Saudi Arabia. *US Geological Survey Professional Paper 560 A*: A188p.

Beyth, M., 1973, Correlation of Paleozoic-Mesozoic sediments in northern Yemen and Tigre, northern Ethiopia. *American Association of Petroleum Geologist Bulletin* 57: 2240 - 2443.

Button, A., Brock, T.D., Cook, P.J., Eugster, H.P., Goodwin, A.M., James, H.L., Margulis, I., Nealson, K.H, Nriagu, J.O., Trendall, A.F and Walter, M.R., 1982, Sedimentary iron deposits, evaporites and phosphorites. *In H.D. Holland and M. Schidlowski (eds.), Mineral deposits and evolution of biosphere. Springer-Verlag, New York*: 259 - 273.

Carver, R.E., 1971, Heavy Mineral separation. *In Carver, R.E. (ed.), Procedures insedimentary Petrology. Wiley-Interscience, New York*: 427 - 452.

Chork, C.Y. and Salminen, R., 1993, Interpreting exploration geochemical data from Outokumpu, Finland: a MVE-robust factor analysis. *Journal of Geochemical Exploration, 48*: 1 - 20.

Coleman, R.G., 1973a, Reconnaissance geology of the Khaybar Quadrangle (18/42), Kingdom of Saudi Arabia: *Saudi Arabian Directorate General of Mineral Resources Geologic Map GM-4, scale 1:00000, Text*, 5p.

Coleman, R.G., 1973b, Reconnaissance geology of the Khamis Mushayt Area - A Preliminary Report, *Jiddah, USGS Saudi Arabia Project Report PR-227: 14p.*

Crook, K.A, W., 1974, Lithogenesis and geotectonics: the significance of composition variation in flysch arenites (greywackes). *In Dott, R.H. and Shaver, R.H. (eds.), Modern and ancient geosynclinal sedimentation SEPM special Publication, 19*: 304 – 310.

da Costa, M.L. and Moraes, E.L., 1998, Mineralogy, geochemistry and genesis of kaolins from the Amazon region. *Mineralium Deposita*, 33: 283 - 297.

Dabbagh, M.E. and Rogers, J.J.W., 1983, Depositional environments and tectonic significance of the Wajid Sandstone of Saudi Arabia. *Journal of African Earth sciences, 1*: 47 – 57.

Dasgupta, H.C., Sambasiva Rao, V.V. and Krisha, C., 1999, Chemical environments of deposition of ancient iron- and manganese-rich sediments and cherts. *Sedimentary Geology, 125*: 83 - 98.

Doeglas, D.J., 1962, The structure of sedimentary deposits of braided rivers. *Sedimentology, 1*: 167 - 190.

Denny, C.S., 1967, Fans and Peidments. *American Journal of Science, 265*: 81 - 105.

De Ros, L.F., 1998, Heterogeneous generation and evolution of diagenetic quartzarenites in the Silurian-Devonian Furnas Formation of Parana Basin, southern Brazil. *Sedimentary Geology, 116*: 99 - 128.

Depetris, P.J. and Probst, J.L., 1998, Variability of chemical index of alteration (CIA) in the Parana River suspended load. *Mineralogical Magazine, 62A*: 366-367.

Dickinson, W.R., 1985, Interpreting provenance relations from detrital modes of sandstones. *In: Zulfa, G.G. (ed.), Provenance of Arenites. NATO ASI Series, Series C, Vol. 148; Riedel, Dordrecht*: 333 - 361.

Dickinson, W.R., Beard, L.S., Brakenridge, G.R., Erjavel, J.L., Ferguson, R.C., Inman, K.F, Knepp, R.A., Lindberg, F.A., and Ryberg, P.T., 1983, Provenance of North American Phanerozoic sandstones in relation to tectonic setting. *Geological Society of America Bulletin, 94*: 222-235.

Dow, D.B., Beyth, M. and Hailu, T., 1971, Paleozoic glacial rocks recently discovered in northern Ethiopia. *Geologic Magazine 108(1)*: 53 – 60.

Dickinson, W.R. and Suczek, C.A., 1979, Plate tectonics and sandstone composition. *American Association of Petroleum Geologists Bulletin, 63*: 2164 - 2182.

Dickinson, W.R. and Valloni, R., 1980, Plate settings and provenance of sands in modern ocean basins: *Geology, 8*: 82 – 86.

Drever, J.I., 1974, Geochemical model for the origin of Precambrian banded iron formations. *Bulletin Geological Society of America, 85*: 1099 - 1106.

Ehrenberg, S.N., 1991, Kaolinized, potassium leached zonesin the contacts of Garn Formation, Haltenbanken, mid-Norwegian continental shelf. *Marine Petroleum Geology, 8*: 250 - 269.

Ewa, I.O.B, Oladipo, O.A., and Dim, L.A., 1992, Cluster analysis of elemental concentrations of cored Nigerian river sediments. *Journal of Environmental Science and Health A27(1)*: 1-11

Fan, P.F., 1979, Clays and clay minerals of hydrothermal origin. *In Mortland, M.M., and Farmer, V.C., (eds.), Proceedings of the VI International Clay Conference 1978, Oxford; Developments in Sedimentology, 27*: 369 - 374.

Feo-Codecido, G., 1956, Heavy mineral techniques and their application to Venezuelan stratigraphy. *American Association of Petroleum Geologists Bulletin, 40*: 984 – 1000.

Fergusson, C.L. and Tye, S.C., 1999, Provenance of early Paleozoic sandstones, southeastern Australia, Part 1: vertical changes through the Bengal fan-type deposit. *Sedimentary Geology, 125*: 135 - 151.

Folk, R.L, 1968, Petrology of Sedimentary Rocks. *Hemphill's*: 170p.

Folk, R.L., Andrews, P.B. and Lewis, D.W., 1970, Detrital sedimentary rock classification and nomenclature for use in New Zealand. *New Zealand Journal of Geology and Geophysics, 13*: 937 - 968.

Fornelli, A. and Piccarreta, G., 1997, Mineral and chemical provenance indicators in some early Miocene sandstones of the Southern Apennines (Italy): *European Journal of Mineralogy, 9*: 433 - 447.

Frazinelli, E., and Potter, P.E., 1983, Ptrology, chemistry and texture of modern river sands: Amazon River System. *Journal of Geology, 91*: 23 - 39.

Garver, J.I. and Scott, T.J., 1995, Trace elements in shale as indicator of crustal provenance and terrane accretion in the southern Canadian Cordillera. *Geological Society of America Bulletin, 107*: 440 - 453.

Garver, J.I. and Royce, P.R., 1993, Chromium and nickel in shale of the foreland deposits of the Ordovician Taconic Orogen using shale as a provenance indicator for ultramafic rock. *Geological Society of Amrica Abstracts with Program, 25*: 17.

Garver, J.I. and Royce, P.R., and Scott, T.J., 1994, The presence of ophiolites in tectonic highlands deytermined by chromium and nickel anomalies in synorogenic shale: Two examples from North America. *Geologiya i Geofizika, 35*: 3 - 11

Girty, G.H, Ridge, D.L, Knaack, C., Johnson, D. and Al-Riyami, R.K., 1996, Provenance and depositional setting of Paleozoic chert and argillite, Sierra Nevada, California. *Journal of Sedimentary Research, 66*: 107 –118.

Goldstein, J.L., 1992, Scanning electron microscopy and X-ray microanalysis. *Plenum Press, New York, USA.*

Goles, G.C., 1967, Trace elements in ultramafic rocks. *In: Willie, P.J., ed. Ultramafic and related rocks, Wiley, New York*: 222 - 238.

Greenwood, W.R., 1985, Explanation notes to the geologic map of the Abha Quadrangle, Sheet 18F, Kingdom of Saudi Arabia. *Ministry of Petroleum and Mineral Resources, Deputy Ministry for Minerals Resources*: 27p.

Greenwood, W.R., Stoesser, D.B., Fleck, R.J., and Stacey, J.S., 1982, Late Proterozoic island arc complex and tectonic belts in the southern part of Arabian Sheld, Kingdom of Saudi Arabia. *Saudi Arabia Deputy Ministry for Mineral Resources Open File Report, USGS-OF-02-8*: 46p.

Hadley, D.G. and Schmidt, D.L., 1975, Nonglacial origin for conglomerate beds in the Wajid Sandstone of Saudi Arabia. *In: Campbell, K.S.W (editor), Gondowana Geology, Papers presented at the third Gondowana Symposium, Canberra 1973, Australia National University Press*: 357 – 371.

Harris, N.B., 1989, Diagenetic quartzarenite and destruction of secondary porosity: An example from the Middle Jurassic Brent Sandstone of Northwest Europe. *Geology, 17*: 361 - 364.

Helal, A.H., 1964, On the occurrence and stratigraphic position of Permo-Carboniferous tillites in Saudi Arabia. *Geologishe Rdsch., 54*: 193 – 207.

Hemer, D.O., 1968, Diagnostic palynologic fossils from Arabia: *American Institute of Mining Engineers Regional Technical Symposium, 2d Dhahran, Saudi Arabia, 1968 Report*: 311 – 315.

Hodgson, A.V., 1978, Braided river bedforms and related sedimentary structures in the Fell Sandstone Group (Lower Carboniferous) of North Northumberland, *Pro. Yorks. Geological Society, 41*: 509 - 532.

Holail, H.M. and Moghazi, A.M., 1998, Provenance, tectonic setting and geochemistry of greywackes and siltstones of Late Precambrian Hammat Group, Egypt. *Sedimentary Geology, 116*: 227 - 250.

Houseknecht, D.W., 1988, Intergranular pressure solution in four quartzose sandstones. *Journal of Sedimentary Petrology, 58*: 228 - 246.

Hubert, J. F., 1962, A zircon-tourmaline-rutile maturity index and the interdependence of the composition of heavy mineral assemblages with gross composition and texture of sandstones. *Journal of Sedimentary Petrology, 32*: 440 - 450.

Hubert, J. F., 1971, Analysis of Heavy-Mineral Assemblages. *In Carver, R.E. (ed.), Procedures in sedimentary Petrology, Wiley Interscience, New York*: 453 - 479.

Hussain, M., Khandaker, N.I. and Bu-Khamseen, R.H., 1997: The Wajid Sandstone in the Asir Region: An example of petrologically immature braided river system on the Arabian Shield. *Proceedings, the fourth Meeting of the Saudi Society for Earth Sciences, October 13 – 16, 1997, Jeddah.*

Imam, M.B., 1986, Scanning electron microscopy study of the quartz overgrowths within Neogene sandstones of Bengal Basin, Bangladesh. *Journal of Geological Society of India, 28*: 407 - 413.

Imbrie, J., and van Andel, T.H., 1964, Vector Analysis of Heavy Mineral Data. *Geological Society of America Bulletin, 75*: 1131 - 1156.

Ingresoll, R.V., and Sueczek, C.A., 1979, Petrology and provenance of Neogene from Nicobar and Bengal fans, DSDP sites 211 and 218. *Journal of Sedimentary Petrology,* 1217 – 1228.

Institute of Applied Geology Research Series, 1978, A review of the I.A.G Research activities (1970 - 1978 AD or 1390 – 1398H). *King AbdulAziz University Jeddah. Kingdom of Saudi Arabia. I.A.G. Research Series No 8*: 140p.

Ishakin, M.M. and Degtyariov, V.S., 1990, Explanation note to the geologic map of the People' Democratic Republic of Yemen, Al-Mahfid sheet, D70: *Moscow, USSR Ministry of Geology for Ministry of Energy and Minerals, Aden, People Democratic Republic of Yemen*: 24p.

Intaconsult, 1969, Water and Agricultural Development surveys for Areas II and III: Geological investigations (Rome). *Final Report for the Ministry of Agriculture and Water, Riyadh.*

Jackson, R.O., Bogue, R.G., Brown, G.F. and Gierhart, R.D., 1963, Geologic Map of the southern Najd quadrangle, Saudi Arabia. *US Geological Survey Miscellaneous Geological investigation Map I – 211A.*

Jones, B.G. and Rust, B.R., 1983, Massive sandstone facies in the Hawkesbury Sandstone, a Triassic fluvial deposit near Sydney, Australia. *Journal of Sedimentary Petrology, 53*: 1249 - 1261.

Johnson, M.M., stix, J., Tacxe, L., Cervency, P.F., and Tahirkheli, R.A.K., 1985, Paleomagnetic chronology, fluvial process and tectonic implications of Siwalick deposits near Chinji Village, Pakistan. *Journal of Geology, 93*: 27 - 40.

Johnsson, M.J. and Meadre, R.B., 1990, Chemical weathering of fluvial sediments during alluvial storage: The Macuanim Island Point bar, Solimoes, River, Brazil. *Journal of Sedimentary Petrology, 60*: 827 - 842.

Karlsson, W., Vollset, J., Bjorlykke, K and Jorgensen, P., 1979, Changes in mineralogical composition of Tertiary sediments from North Sea wells. *In Mortland, M..M. and Farmer, V.C (eds.), Developments in Sedimentology, 27. Proceedings of the International Conference 1978, Oxford. Elsevier, Amsterdam*: 281 - 289.

Keller, W.D., 1978, Classification of kaolins exemplified by the textures in scanning electron micrographs. *Clays and Clay Minerals 26*: 1 - 20.

Keller, W.D., 1988, Authigenic kaolinite and deckite associated with meta-sulfides - probable indicators of a regional thermal event. *Clays and Clay Minerals, 36*: 153 - 158.

Kellog, K.S., Fourniguet, J., Janjou, J and Minoux, L., 1986, Geologic Map of the Wadi Tathlith quadrangle, Sheet – 20G, Saudi Arabia. *Saudi Arabian Deputy Ministry for Mineral Resources, Map G.M - 103C.*

Kelling, G., 1968, Patterms of sedimentation in Rhondia beds of South Wales. *American Assocaition of Petroleunm Geologists Bulletin, 52*: 2369 - 2386.

Kerr, P.F., 1977, Optical Mineralogy. *Third Edition McGraw-Hill Book Company, New York*: 492p.

Klitzsch, J.C., Harms, A., Lejal-Nicol and List, F.K., 1979, Major subdivisions and depositional environments of Nubia strata Southwestern Egypt. *American Association of Petroleum Geologists Bulletin, 63*: 967 - 974.

Klovan, J.E., 1966, The use of factor anlysis in determining depositional environments from grain-size distributions. *Journal of Sedimentary Petrology, 36(1)*: 115 - 125.

Kimberley, M.M., 1979, *Origin of oolitic iron formation. The Society of Economic Paleontologists and Mineralogists, 79*: 111 - 131.

Krumbein and Pettijohn, F.J., 1966, Manual of sedimentary Petrography. *Appleton-Century-Crofts, Inc., New York*: 412 - 464.

Krynine, P.D., 1942, Provenance versus Mineral stability as a controling factor in the composition of sediments. *Geological Society of America Bulletin, 53*: 1850 - 1851.

Krynine, P.D., 1946, The tourmaline group in sediments. *The Journal of Geology, LIV*: 65 - 87.

Le Maitre, R.W., 1976, The chemical variabilty of some common igneous rocks. *Journal of Petrology, 17*: 589-637.

Leopold, L.B., Wolman, M.G and Miller, J.P., 1964, Fluvial Processes in Geomorphology. *Freeman, San Francisco*: 522p.

Lewis, D. W. and McConchie, D., 1994, Practical Sedimentology. *Second Edition, Chapman and Hall, New York*: 213p.

Louail, J., Esteoule, J. and Esteoule-Choux, J., 1979, The origin of clay minerals in Cenomnianlittoral deposits around the Armorican Massif. *In Mortland, M.M. and Farmer, V.C (eds.), Developments in Sedimentology, 27. Proceedings of the International Conference 1978, Oxford. Elsevier, Amsterdam*: 291 - 300.

Mange, M.A. and Maurer, H.F.W., 1994, Heavy minerals in colour. *Chapman and Hall, London*: 147p.

Martin, C.A.L and Turner, B.R., 1998, Origins of massive-type sandstones in braided river systems. *Earth Science Reviews, 44*: 15 -38.

Maynard, J.B., Valloni, R. and Yu, H.S., 1982, Composition of modern deep-sea sands from arc related basins. *In: Leggett, J.K. (ed.), Trench-forearc geology, sedimentation and tectonics on modern and ancient active plate margins. Geological Society of London Special Publication 10*: 551 - 561.

McBride, E.F., 1987, Diagenesis of the Maxon sandstone (Early Cretaceous), Marathon region, Texas: a diagenetic quartzarenite. *Journal of Sedimentary Petrology, 57*: 98 - 107.

McClure, H.A., 1980, Permian-Carboniferous glaciation in the Arabian Peninsula. *Geological Society of America Bulletin, 91*: 707 - 712.

McClure, H.A., Hussey, E.M. and Kaill, I.J., 1988, Permian-Carboniferous glacial deposits in southern Saudi Arabia. *Geogisches Jahrbuch, B68*: 3 –31, 1 fig., 10 plates.

McGowen, J.H. and Garner, L. E., 1970, Physiographic features and stratification types of coarse-grained point bars: modern and ancient examples. *Sedimentology, 14*: 77 - 111.

McLeannan, S. M., 1993, Weathering and Global Denudation. *The Journal of Geology, 101*: 295 - 303.

Mezzadri, G. and Saccani, E., 1989, Heavy Mineral distribution in Late Quaternary sediments of the Southern Aegean Sea: Implications for provenance and sediment dispersal in sedimentary basins at active margins. *Journal of Sedimentary Petrology, 59, 3*: 412 - 422.

Miall, A.D., 1980, Cyclicity and the facies model concept in fluvial deposits. *Canadian Petroleum Geologists Bulletin, 28*: 59 - 80.

Middleton, G.V., 1960, Chemical composition of sandstone. *Geological Society of America Bulletin, 71*: 1011 - 1026.

Minatome (1984): Extract from Confidential Report MSA-CR-04-1, Geology of Exploration work in the Al-Qasim and Wajid areas. *Saudi Arabian Deputy Ministry for Mineral Resources (Unpublished Report).*

Moody-Stuart, M., 1966, High and low-sinuosity stream deposits, with examples from the Devonian of Spitsbergen. *Journal of Sedimentary Petrology, 36(4)*: 1102 - 117.

Moral-Cardona, J.P., Bellon, A.S., Lopez-Aguayo and Aballero, M.A., 1996, The analysis of quartz grain surface features as a complementary method for studying their provenance: the Guadalete River Basin (Cadiz, SW Spain). *Sedimentary Geology, 106*: 155 - 164.

Morgan, D.J., Highley, D.E., and Bland, D.J, 1979, A montimorillonite, kaolinite association in Lower Cretaceous of south-east England. *In Mortland, M.M and Farmer, V.C., (eds.), Proceedings of the VI International Clay Conference, Oxford 1978, Developments in Sedimentology 27*: 301 - 310.

Morsy, M.A., 1993, An example of application of Factor Analysis on geochemical stream sediment survey in Umm Khariga Area, Eastern Desert, Egypt. *Mathematical Geology, 25*: 833 - 850.

Moshrif, M.A., 1988, Fluvial environment of the southern part of Wajid Sandstone (Cambrian – Ordovician) deduced by textural analysis. *Iraqi Journal of Science. The University of Baghdad, Jadiriya, Baghdad, Iraq.*

Morton, A.C., 1985, Heavy Minerals in Provenance Studies. *In Zulfa, G.G. (ed.), Provenance of Arenites*: 249 - 277.

Morton, A.C. and Hallsworth, C.R., 1994, Identifying provenance-specific features of detrital heavy mineral assemblages in sandstone. *Sedimentary Geology, 90*: 241 - 256.

Morton, A.C. and Hallsworth, C.R., 1999, Processes controlling the composition of heavy mineral assemblages in sandstones. *Sedimentary Geology, 124*: 3 - 29.

Morton, A.C. and Johnson, M.J., 1993, Factors influencing the composition of detrital heavy mineral suites in Holocvene sands of Apure River drainage basin, Venezuel. *In: Johnsson, M.J and Basu, A. (eds.), Processes Controlling the composition of clastic sediments*: 171 - 185.

Murray, L.J. and Heckroodt, 1979, South African kaolins. *In: Mortland, M.M. and Farmer, V.C. (eds.), Developments in Sedimentology. Proceedings of the International Conference, 1978, Oxford. Elsevier, Amsterdam*: 601 - 608.

Murray, R.W., 1994, Chemical criteria to identify depositional environments of chert: general principles and application. *Sedimentary Geology, 90*: 213 - 232.

Murray, R.W., Brink, M.R.B., Gerlach, D.C., Russ III, G.P and Jones, D.L., 1991, Rare earth, major and trace elements in chert from the Fransciscan Complex and Monterey Group, California: Assessing REE sources to fine-grained marine sediments. *Geochimica et Cosmochimica Acta, 55*: 1875 - 1895.

Murray, R.W., Brink, M.R.B., Gerlach, D.C., Russ III, G.P and Jones, D.L., 1992, Rare earth, major and trace element composition of Monterey and DSDP chert and assocaited host sediment: Assessing the influence of chemical fractionation during diagenesis. *Geochimica et Cosmochimica Acta, 56*: 2657-2671.

Murray, H.H. and Partridge, P., 1981, Genesis of Rio jari Kaolin. *In: Olphen, H.V and Veniale (eds.), Developments in Sedimentology, 35. International Conference, 1981. Elsevier*: 279 - 291.

Nechaev, V.P. and Isphording, W.C., 1993, Heavy mineral assemblages of continental margins as indicator of plate-tectonic environments. *Journal of Sedimentary Petrology, 63*: 1110 - 1117.

Nesbitt, H.W and Young, G.M., 1982, Early Proterozoic climates and plate motions inferred from major element chemistry. *Nature 299*: 715 -717.

Nesbitt, H.W and Young, G.M., 1997, Sedimentation in the Venezuela Basin, Circulation in the Caribbean Sea, and Onset of Northern Hemisphere Glaciation. *Journal of Geology, 105*: 531 - 544.

Pallister, J.S., 1982, Reconnaissance geology of the Jabal Al-Ilman quadrangle, Sheet 18/44A. *Saudi Arabian Deputy ministry for Mineral Resources, Open File Report USGS-OF-02-90*: 61p.

Pettijohn, F.J., 1941, Persistence of Heavy Minerals and Geologic age. *Geology, 46:* 610-625.

Pettijohn, F.J., Potter, P.E., and Siever, R., 1987, Sand and sandstones. *Second Edition, New York, Springer-Verlag*: 533p.

Piper, D.Z., 1975, An iron-rich deposit from the Northeastern Pacific. Earth and *Planetary Science Letter*, 26: 114 -120.

Pittman, E.D., 1979, Porosity, diagenesis and productive capability of sandstone reservoirs. *In Aspects of Diagenesis. SEPM Special Publicatio, 26*: 159 – 173.

Poldervaart, A., 1955, Zircons in rocks 1 Sedimentary rocks. *American Journal of Science, 253*: 433 - 451.

Powers, R.W., Ramirez, L.F., Redman, C.D. and Elberg (Jr.), E.L., 1966, Geology of the Arabian Peninsula – Sedimentary Geology of Saudi Arabia. *US Geological Survey Professional Paper 560-D, Washington*: 147p.

Prinz, W.C., 1975, Reconnaissance geology of the Jabal 'Aya quadrangle sheet 18/42 A, Kingdom of Saudi Arabia with a section on aeromagnetic studies by G.E. Andreasen: *Saudi Arabia directorate General of Mineral Resources Geologic Map GM-17, scale 1:100000, Text 9p.*

Rattle, J.C and Andreasen, G.E., 1974, Reconnaissance geology and magnetic intensity map of the Jabal Sawdah Quadrangle Sheet 18\42C, Kingdom of Saudi Arabia. *Saudi Arabian Directorate General of Mineral Resources, Geologic map GM-16, Scale 1: 100,000,* text 8p.

Reeves, R.D. and Brooks, R.R., 1978, Trace Element Analysis of Geological Materials. *John Wiley and Sons, New York*: 421p.

Roedder, E., 1990, Fluid inclusion analysis–prologue and epilogue. *Geochemica et Cosmochemica Acta, 54*: 495 – 507.

Rooney, C.B. and Basu, A., 1994, Provenance analysis of muddy sandstones. *Journal of Sedimentary Research, A64*: 2 – 7.

Rotovtseva, Yu V., and Shapiro, M.N., 1998, Provenance of the Paleocene-Eocene clastic rocks of the Komandorsky Islands. *Sedimentology, 45*: 201 - 216.

Rust, B.R. and Jones, G.G., 1987, The Hackesbury Sandstone south of Sydney, Qaustralia, Triassic analogue for deposit of a large braided river. *Journal of Sedimentary Petrology, 57*: 222 - 233.

Roser, B.P. and Korsch, R.J., 1986, Determination of tectonic setting of sandstone-mudstone suites using SiO_2 content and K_2O/Na_2O ratio. *Journal of Geology, 94*: 635 - 650.

Rust, B.R and Koster, E.H., 1984, Coarse Alluvium Deposits. *In Walker, R.G. (ed.), Facies Model, Second Edition, Canadian Geosciences Series* : 53 - 69.

Sable, E.G., 1982, Reconnaissance geology of the Jabal Shaqran quadrangle, sheet 17/44B, Kingdom of Saudi Arabia. *Ministry of Petroleum and Mineral Resources, Deputy Ministry for mineral Resources, Jeddah, Technical Record USGS-TR-02-1*: 17p.

Schafer, J and Dorr, W., 1997, Heavy mineral analysis and topology of detrital zircon – A new approach to provenance Study (Saxothuringian Flysch, Germany). *Journal of Sedimentary Research, 67*: 451 - 461.

Scholle, P.A., 1979, A color illustrated Guide to Constituents, Textures, Cements and porosities of Sandstones and Associated Rocks. *American Association of Petroleum Geologists Memoir 28*: 201p.

Schulz-Rojhan, J.P. and Phillips, J.P., 1989, Diagenetic alteration of Permian reservoir sandstones in the Nappamerri Trough and adjacent areas, southern Cooper Basin. *Australia. Proc. Petroleum society of Australia, Society of Petroleum Engineers, Ausralian Society of Exploration Geophysicists, Adelaide*: 629 - 645.

Selley, R.C., 1972, Diagnosis of marine and non-marine environments from Cambro - Ordovician sandstone of Jordan. *Journal of Geological Society, 128*: 135 - 150.

Selley, R.C., 1969, Torridonian alluvium and quicksands. *Scott. Journal of Geology, 5*: 328 - 346.

Seyfert, C.K. and Sirkin, L.A., 1973, Earth History and Plate tectonics: an introduction to historical geology. *Harper and Row, New York*: 504p.

Simmons, G.C., 1980, Reconnaissance geology of the Madha quadrangle, sheet 18/43A, Kingdom of Saudi Arabia: *Saudi Arabia Directorate of Mineral Resources Geologic Map GM-55, scale 1:100000; Text 13p.*

Simmonson, B.M. (1985): Sedimentological constraints on origin of Precambrian iron formations. *Geological Society of America Bulletin, 96*: 224 - 252.

Steineke, M., Bramkamp, R.A. and Sanders, N.J., 1958, Stratigraphic relations of Arabian Jurassic Oil. *In: Weeks, L.G. (editor), Habitat of Oil. American Association of Petroleum Geologists, Tulsa, Oklahoma, U.S.A.: 1294 - 1329.*

Stattegger, K., 1986, Heavy Minerals and provenance of sands: Modeling of lithological end members from river sands of northern Austria and from sandstones of Austroalpine Gosau Formation (Late cretaceous). *Journal of Sedimentary Petrology, 57*: 301 - 310.

Stern, R.J. and Gottfried, D., 1986, Petrogenesis of a Late Precambrian (575-600 Ma) bimodal suite in Northeastern Africa. *Contributions to Mineralogy and Petrology, 92*: 492 - 501.

Stoesser, D.B., 1984, Reconnaissance geology of the Wadi Tarib quadrangle, sheet 18/43 C, Kingdom of Saudi Arabia: *Saudi Arabian Deputy Ministry for Mineral Resources Technical Record USGS-TR-04-4, scale 1:100,000, Text, 77p.*

Stump, T.E. and van der Eem, J.G., 1994, Overview of the stratigraphy, depositional environments and periods of deformation of the Wajid outcrop belt, southwestern Saudi Arabia. *Proceedings Geo Arabia Conference 1994*: 867 – 876.

Stump, T.E. and van der Eem, J.G., 1995, The stratigraphy, depositional environments and periods of deformation of the Wajid outcrop belt, southwestern Saudi Arabia. *Journal of African Earth Sciences, 21*: 421 - 441.

Taylor, S.R., 1964, Trace element abundance and the chrondite earth model. Geochimica *et* Cosmochimica *Acta*, 28: 189 -198.

Taylor, K.G and Curtis, C.D., 1995, Stability and facies association of ealy diagenetic iron mineral assemblages: an example from a Jurassic ironstone-mudstone succession, U.K. *Journal of Sedimentary Research, A65*: 358 - 368.

Taylor, S.R. and McLennan, S.M., 1985, The continental Crust: Its composition and evolution. *Oxford, Blackwell*: 312p.

Turner, B.R. and Munro, M., 1987, Channel formation and migration by mass flow processe in the Lower Carboniferous fluviatile Fell Sandstone Group, North-East England. *Sedimentology, 34*: 1107 - 1122.

Uddin, A., and Lundberg, N., 1998, Unroofing history of the Eastern Himalaya and the Indo-Burman Ranges: Heavy Mineral study of Cenozoic sediments from the Bengal Basin, Bangladesh. *Journal of Sedimentary Research, 68*: 465 - 472.

van Andel, T.H., 1959, Reflections on the interpretation of heavy Mineral analysis. *Journal of Sedimentary Petrology, 29*: 153 - 163.

van der Kemp, P.E. and Leake, B.E., 1985, Petrography and geochemistry of feldspathic and mafic sediments of the norteastern Pacific Margin: *Transaction of the Royal Society of Edinburg, 76*: 411 - 449.

van der Kemp, P.E. and Leake, B.E., 1994, Petrology, geochemistry, provenance and alteration of Pennsylvanian – Permian arkose, Colorado and Utah. *Geological Society of America Bulletin, 105*: 1571 – 1582.

van Houten, F.B., 1964, Origin of red beds - some unresolved problems, *In: Nairn, A.E.M, (ed.) Problems in paleoclimatology, Proceedings of NATO paleoclimates Conference, 163: New York, Interscience Pubs., Inc*: 647 - 661.

van Houten, F.B., 1968, Iron oxides in red beds. *Geological Society America Bulletin, 79*: 399 - 416.

van Houten, F.B., 1972, Iron and clay in tropical savanna alluvium, northern Colombia: a contribution to the origin of red beds. *Bulletin Gelogical Society of America, 83*: 2761 - 2772.

Van Houten, F.B., 1973, Origin of red beds: A review - 1961 - 1972. *Annual Review of Earth and Planetary Science, 1*: 39 - 61.

Vaslet, D., 1989, Late Ordovician glacial deposits in Saudi Arabia: A lithostratigraphic revision of the Early Paleozoic succession, *Kingdom of Saudi Arabian Ministry for Petroleum and Mineral Resources, Deputy Ministry for Mineral Resources, Jeddah, Professional Paper 3*: 44p.

Vaslet, D., 1990, Upper Ordovician glacial deposition in Saudi Arabia. *Episodes 13*: 147 - 161.

von Eynatten, H. and Gaupp, R., 1999, Provenance of Cretaceous synorogenic sandstones in the Eastern Alps: constrains from framework petrography, heavy minerals and mineral chemistry. *Sedimentary Geology, 124*: 81 - 111.

Walker, R.G. and Cant, D.J., 1984, Sandy Fluvial Systems. *In: Walker, R.G (ed.), Facies Model, Second edition, Canada Geoscience Series*: 71 - 89.

Walker, T.R., 1967, Formation of red beds in modern and ancient deserts. *Bulletin Geological Society of America, 78*: 353 - 368.

Walker, T.R., 1973, Intrastratal alterations in the Fountain Formation (Pennsylvanian age), Denver area, Colorado. *Geological Society of America, Abs. With programs (Southwestern Section), 5*: 521 - 522.

Walker, T.R., 1974, Formations of Red Beds in Moist Tropical Climates: A Hypothesis. *Geological Society of America Bulletin, 85*: 633 - 638.

Walker, T.R., and Honea, R.M., 1969, Iron content of modern deposits in the Sanoran Desert: a contribution to the origin of red beds. *Geological Society of America Bulletin, 80*: 535 - 544.

Ward, W.C. and McDonald, K.C., 1979, Nubian Formation of Central Eastern Desert, Egypt-Major subdivisions and depositional setting. *American Association of Petroleum Geologists Bulletin, 63*: 975 - 983.

Waugh, B., 1970, Petrology, provenance and silica diagenesis of the Penrith Sandstone (Lower Permian) of Northeast England. *Journal of Sedimentary Petrology, 40*: 1226 - 1240.

Welton, J.E., 1984, SEM Petrology Atlas. *Methods in Exploration Series, American Association of Petroleum Geologists*: 236p.

Widley, B.F., Whitehouse, M.J and Babttat, M.A.O., 1996, Early Precambrian gneiss terranes and Pan African island arcs in Yemen: Crustal accretion of eastern Arabian Shield. *Geology, 24*: 131 - 134.

Wilson, M.J., 1971, Clay Mineralogy of the Old Red Sandstone (Devonian) of Scotland. *Journal Sedimentay Petrology, 41*: 995 - 1007.

Wizevick, M.C., 1992, Sedimentology of Pennsylvanian quartzose sandstones of Lee Formation, Central Appalachian Basin: fluvial interpretation based on lateral profile anlysis. *Sedimentary Geology, 78*: 1 - 47.

Zalba, P.E., 1981, Scanning electron micrographs of clay deposits of Buenos Aires. *In: Olphen, H.V. and Veniale, F. (eds.), Developments in Sedimentology, 35. Internal Conference 1981, Elsevier*: 513 - 528.

Zimmer, M., Kroner, A., Jochum, K.P., Reiscchmann, T. and Todt, W., 1995, The Gebel Gerf Complex: a Precambrian N-MORB ophiolite in the Numbian Shield, NE Africa. *Chemical Geology, 123*: 21 - 51.

Zuffa, G. G., 1985, Provenance of Arenites: *North Atlantic Treaty Organization (NATO) Advanced Study Institute, Series C, Mathematical and Physical Sciences, Boston, D. Riedel Pub. Co*: 139 – 164.

APPENDIX I

STRATIGRAPHIC COLUMNS AND LITOLOGIC DESCRIPTION

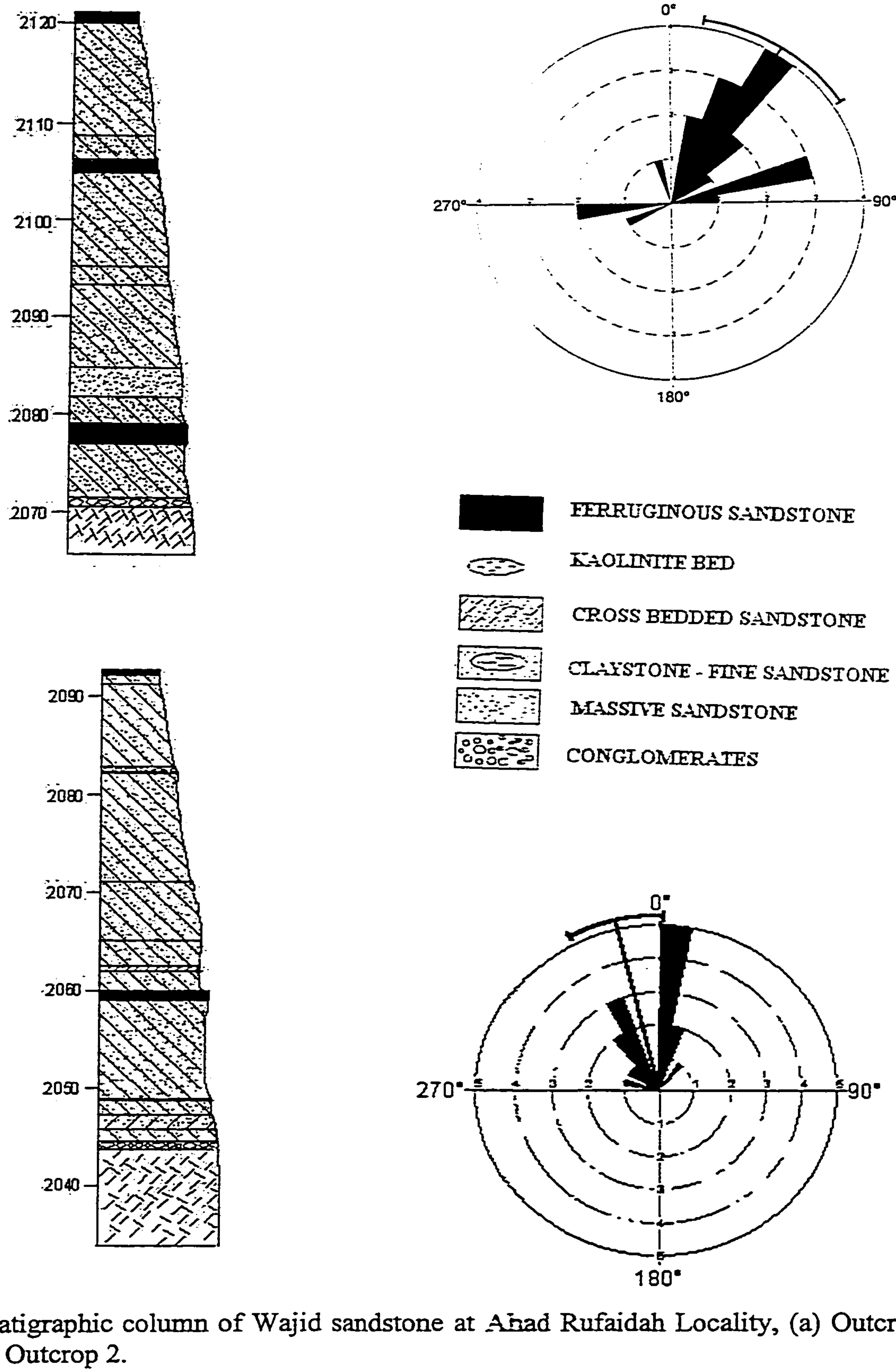

Stratigraphic column of Wajid sandstone at Ahad Rufaidah Locality, (a) Outcrop 1 and (b) Outcrop 2.

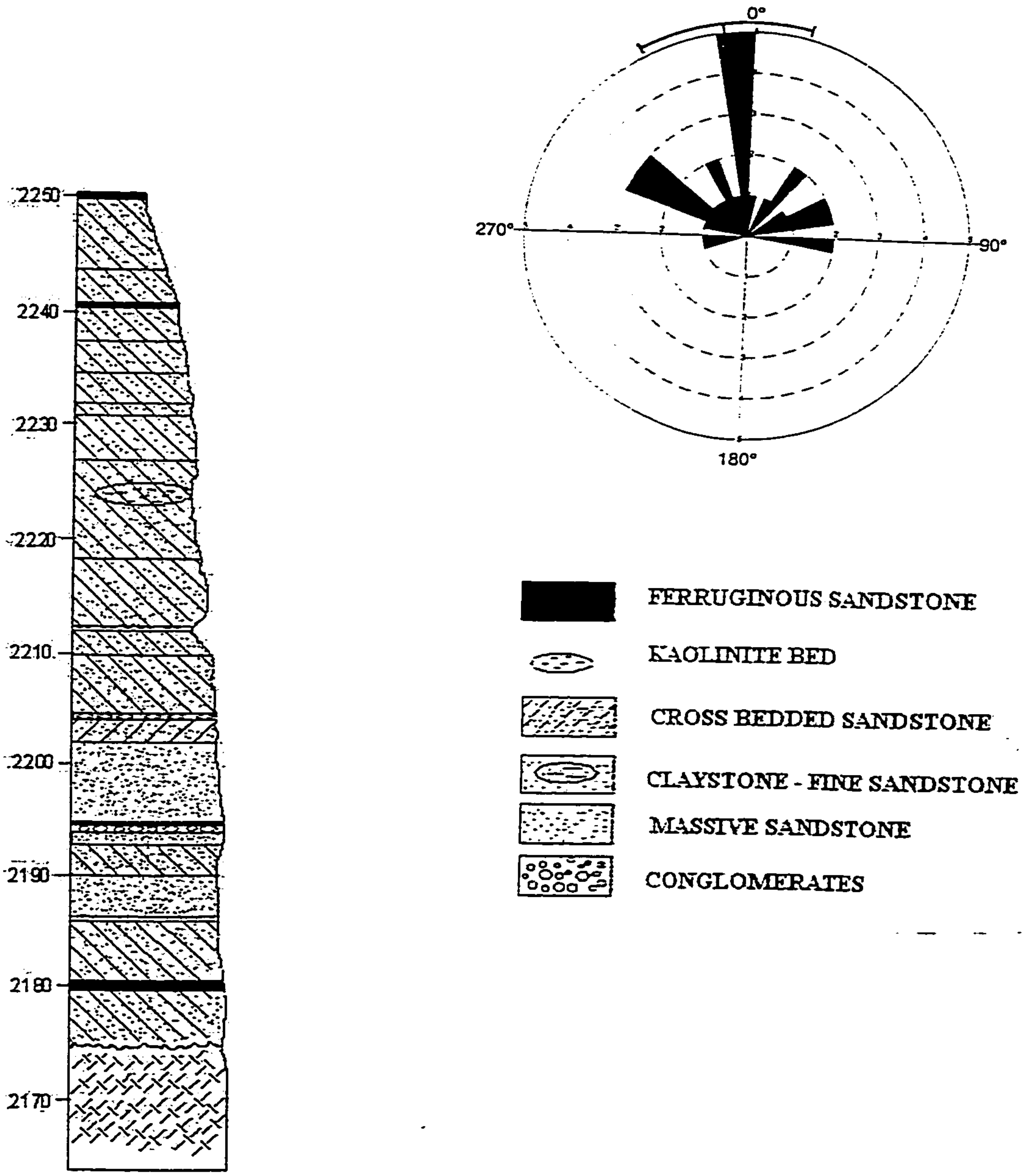

Stratigraphic column of the Wajid Sandstone at Ahad Rufaidah Locality, Outcrop 3.

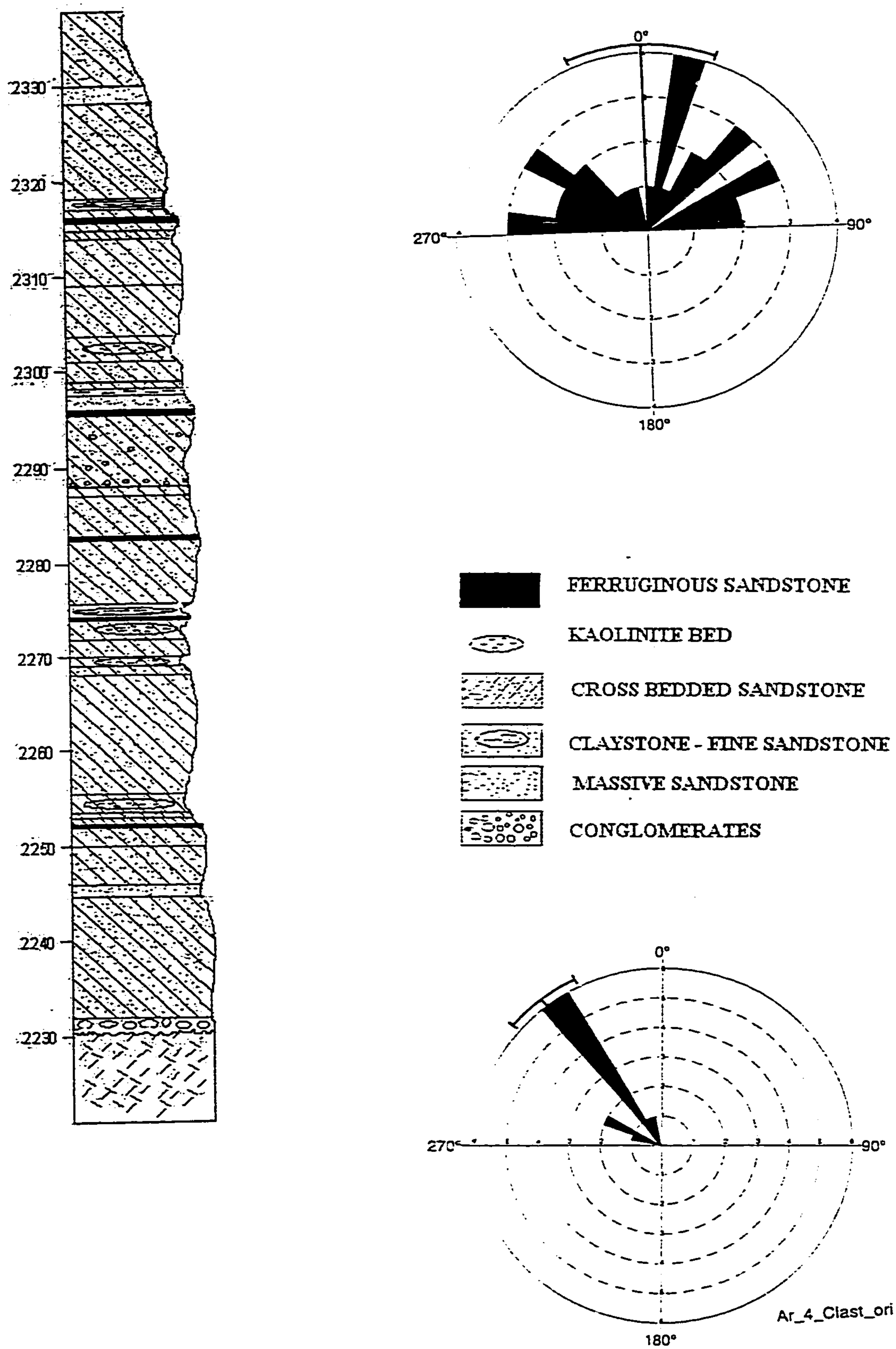

Stratigraphic column of the Wajid Sandstone at Ahad Rufaidah Area, Outcrop 4.

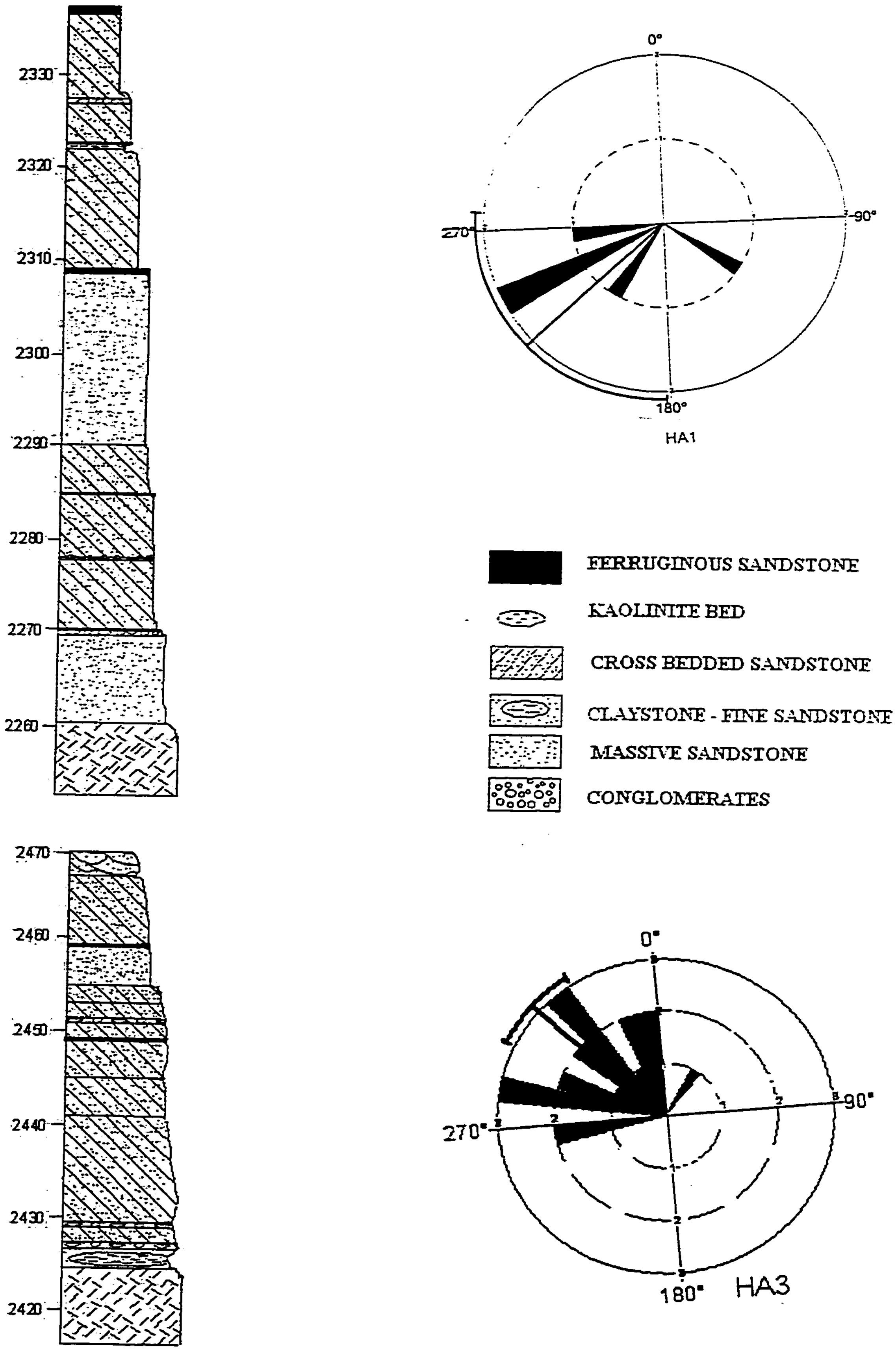

Stratigraphic column of the Wajid Sandstone at Al Habalah Area, (a) Outcrop 1 and (b) Outcrop 3.

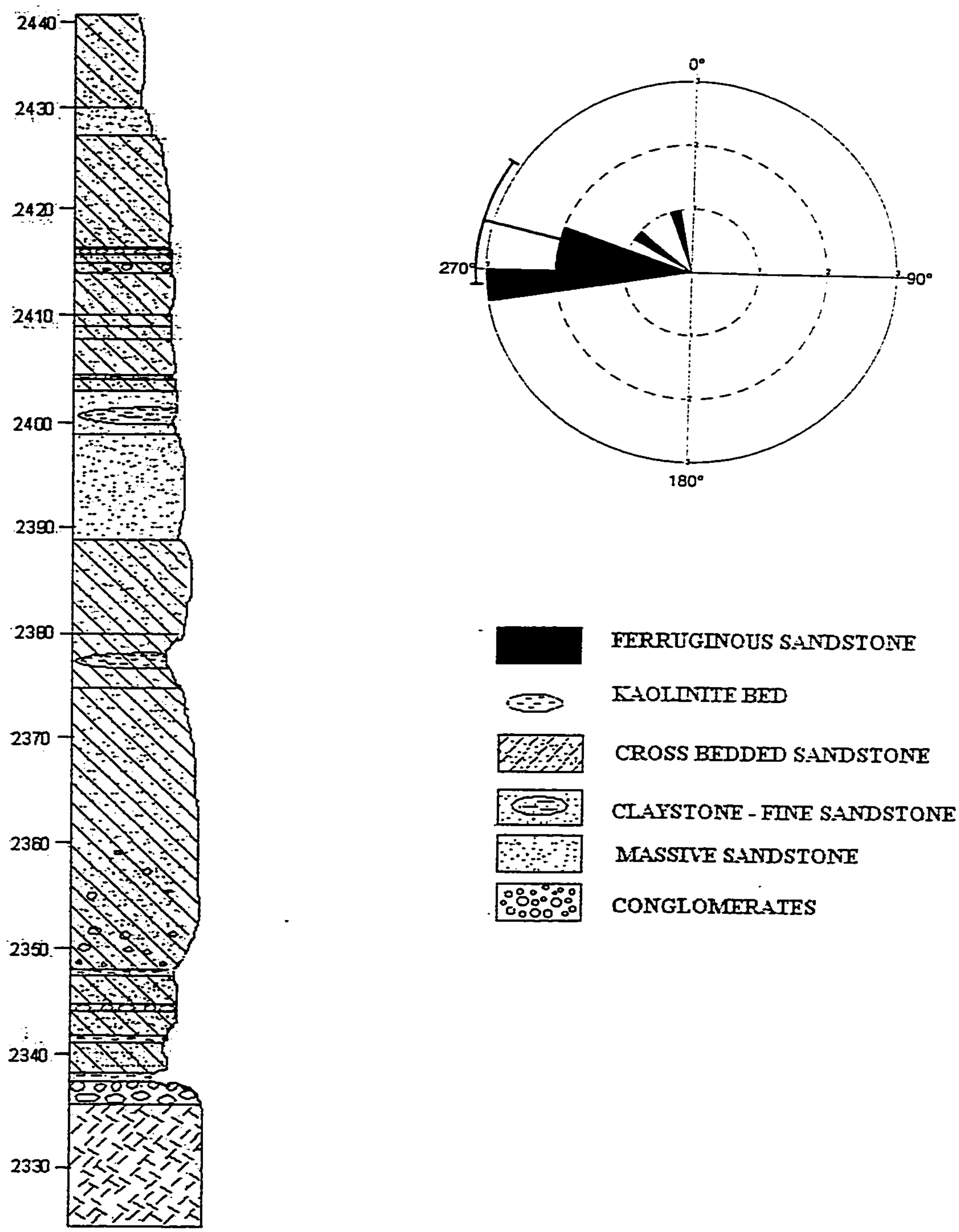

Stratigraphic column of the Wajid Sandstone at Al Habalah Area, Outcrop 2.

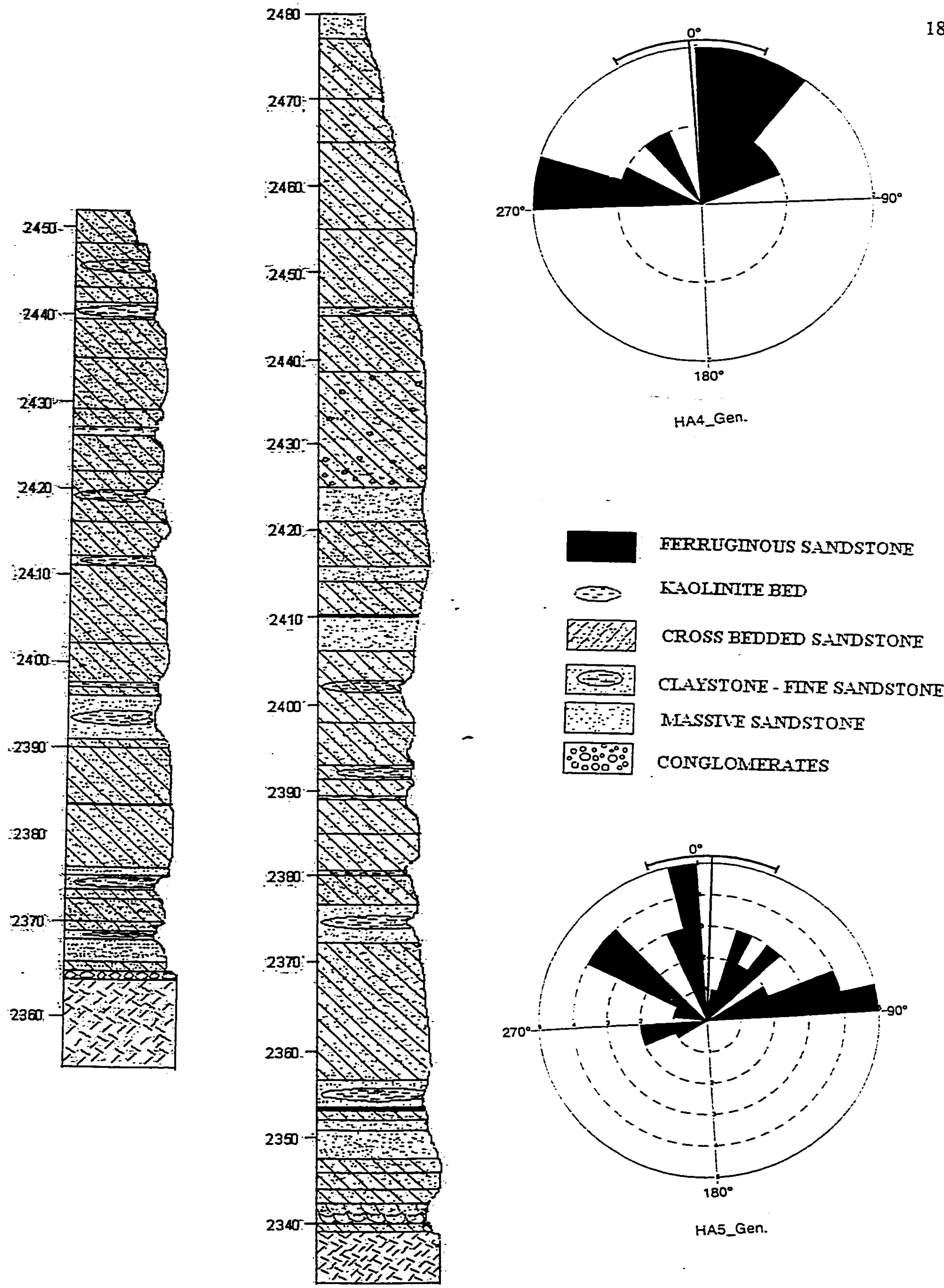

Stratigraphic column of the Wajid Sandstone at Al Habalah Area, (a) Outcrop 4 and (b) Outcrop 5.

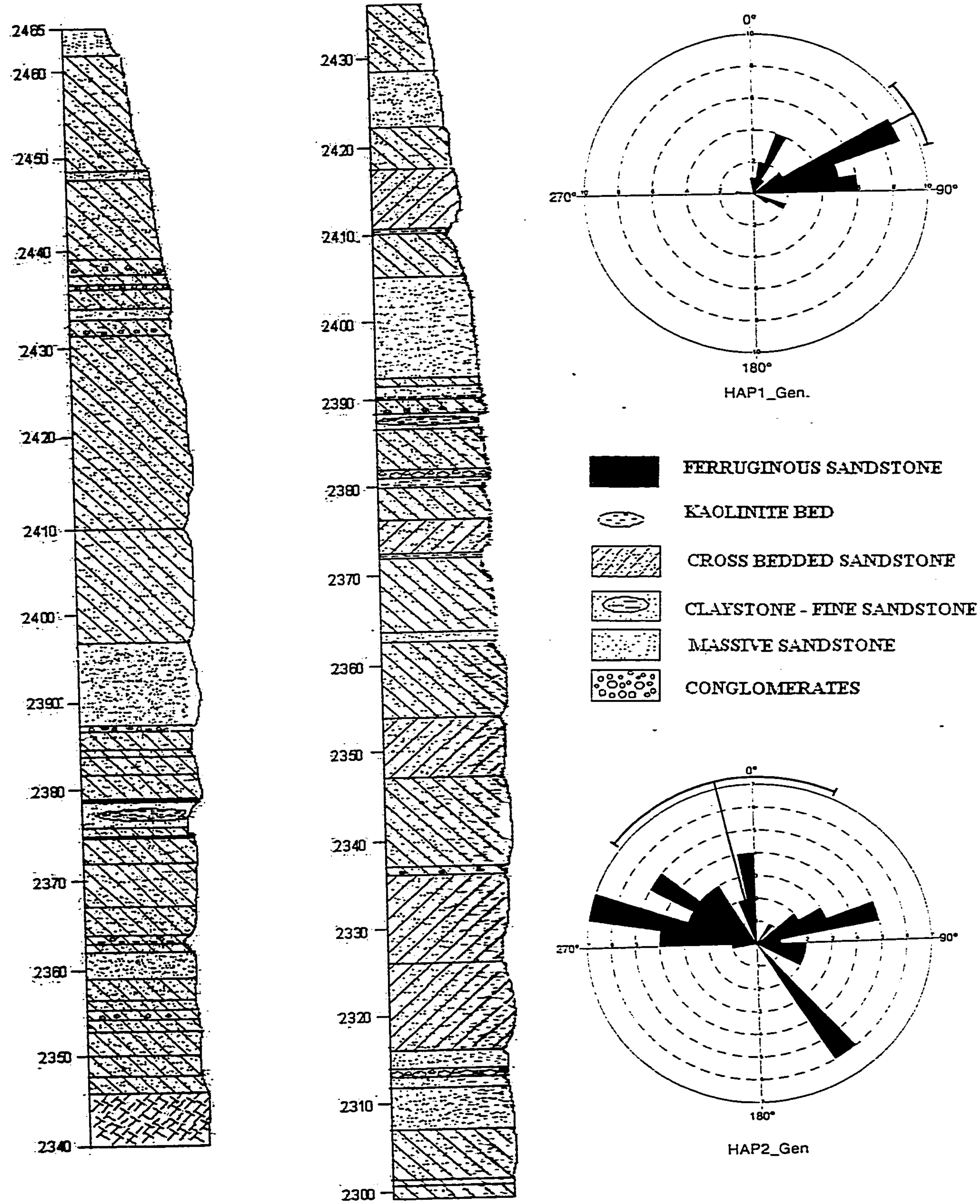

Stratigraphic column of the Wajid Sandstone at Al Habalah Area, (a) Outcrop 6 and (b) Outcrop 7.

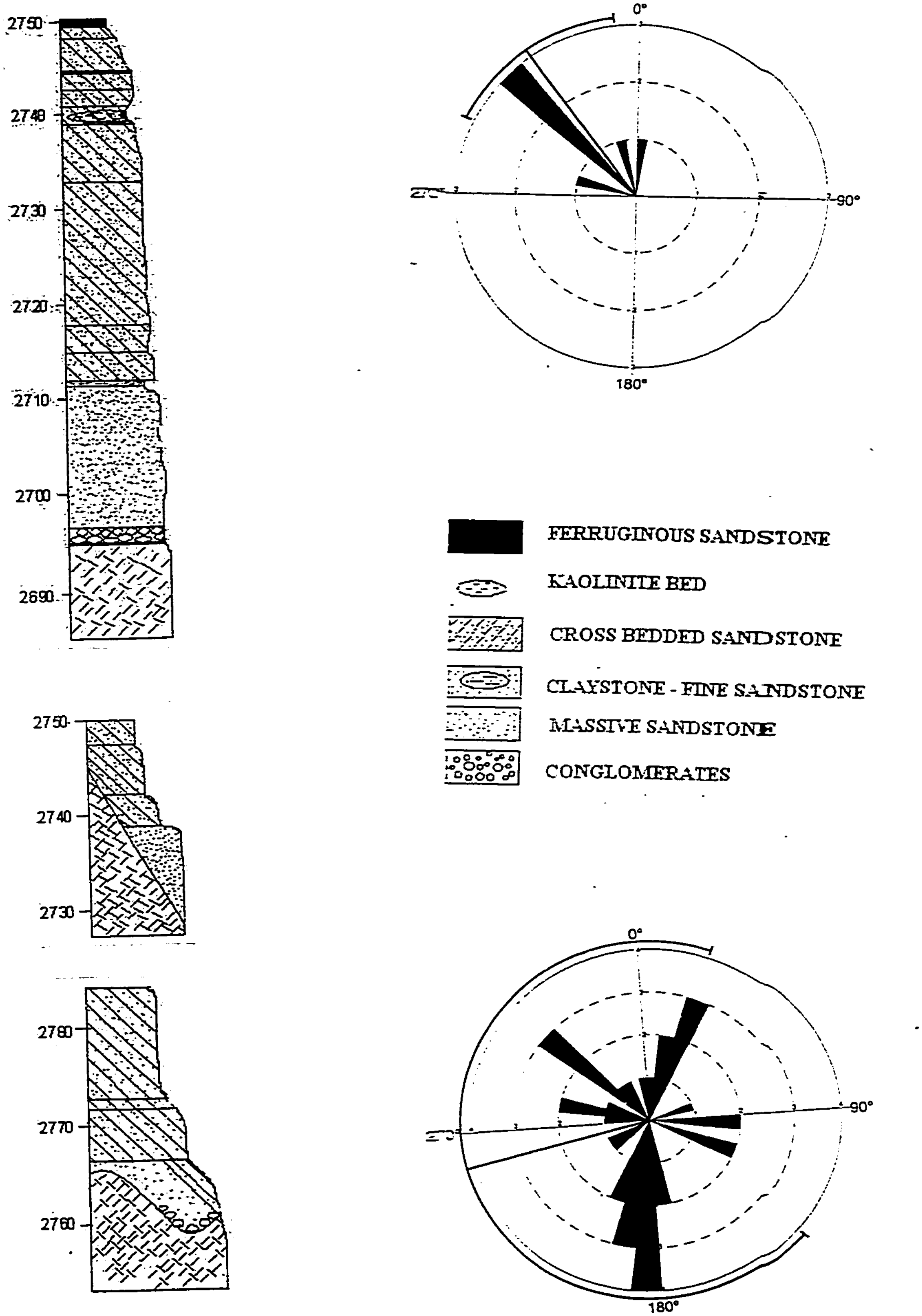

Stratigraphic column of Wajid Sandstone at Al Soudah Area, (a) Outcrop 1 and (b) Outcrop 2 and (c) Outcrop 3.

LITHOLOGIC DESCRIPTION

AHAD RUFAIDAH

Outcrop 1

Interval (m)	Lithology	Description
2120-2121	Ferruginous Horizon	
2107.5-2120	Light Grey Sandstone	Light grey, pebbly coarse to fine grained, poorly sorted cross bedded sandstone, more blocky than lower interval, lightly coated by ferruginous materials, capped by about 1m thick ferruginous bed.
2106-2107.5	Brown–Red Sandstone	Brown-red, pebbly coarse grained, well-sorted, iron rich, indurated, cross-bedded sandstone
2105.25 – 2106	Ferruginous Horizon	
2095.25 – 2105.25	Light Grey Sandstone	Light grey, pebbly coarse-fine grained, poorly sorted, friable, finely cross-bedded
2093.25 – 2095.5	Red-Brown Sandstone	This interval commences with a 50cm thick ferruginous bed. It is coarse to medium grained, moderately sorted, friable and cross bedded
2085 – 2093.25	Grey-Brown Sandstone	Light grey-brown, pebbly coarse, well-sorted, indurated, cross-bedded sandstone. Cosets, separated by ferruginous bands.
2082.75 – 2085	Red-Brown Sandstone	Coarse to medium grained, indurated, rich in iron, massive sandstone. It is bounded at the base and top by thin layers of ferruginous material.
2079.75 – 2082.75	Light Grey Sandstone	Light grey, medium to fine grained, moderately sorted, friable, cross-bedded sandstone.
2077 – 2079.25	Ferruginous Horizon	
2071.5 – 2077	Grey-White Sandstone	Grey-white, pebbly coarse grained, well sorted, friable, lightly coated by ferruginous materials, cross-bedded sandstone.
2071-2071.5	Conglomerate	About 50cm thick conglomerate commences the sequence in this outcrop. It is composed of quartz and rock fragment pebbles.
Below 2071	Basement rocks	Biotite-schists, granite and pegmatite.

Outcrop 2

Interval (m)	Lithology	Description
2091 - 2093.5	Grey -Brown:	White to brown, medium to fine grained, friable,

		capped by thin iron band, cross-bedded sandstone
2083 - 2091	Brown Sandstone	Brown, coarse grained, friable, cross-bedded, sandstone
2082.5 - 2083	Conglomerates	About 50cm of conglomerates
2070.5 - 2082.5	Red -Brown Sandstone	Red to brown, coarse to medium, friable, cross bedded sandstone. It commrences with about 10cm thick ferruginous bed.
2065.25 - 2070.5	Light Grey Sandstone	Light grey, coarse to fine grained, poorly sorted, friable, thinly cross bedded, sandstone. It is bounded at the base and top by ferruginous beds.
2060 - 2065.25	Light Grey Sandstone	Light grey, medium to fine grained, moderately sorted, friable, cross-bedded sandstone. A Thin intervening red unit occurs within this interval.
2059 - 2060	Ferruginous Horizon	
2049 - 2059	Light Grey Sandstone	Light grey, coarse to medium grained, moderately sorted, friable, cross-bedded sandstone. It is capped by about 1m thick ferruginous bed.
2046 - 2049	Brown Sandstone	Brown, pebbly coarse, well sorted, friable, cross bedded, with foresets dipping opposite to the adjacent beds. It is capped by thin ferruginous bed.
2045 - 2049	White - Grey Sandstone	White to grey, coarse grained, well sorted, friable, cross-bedded sandstone.
2045 - 2046	Conglomerates/Claystone	About 1m thick conglomerate, pebbles of quartz and rock fragments. Thin claystone overlies this conglomerate. This interval marks the regional surface of unconformity.
Below 2044	Basement	Schist and granite.

Outcrop 3

Interval (m)	Lithology	Description
2244.5 - 2250.5	Brick Red Sandstone	Commences with a thin layer of claystone, medium to fine grained, more of fine, poorly cross bedded characterized by lots of ferruginous encrustation and fractures filled by iron. Capped by a 30-40cm thick ferruginous band.
2237 - 2244.5	Red-Pink Sanstone	Medium to fine- grained, thinly cross bedded, foresets thickness ranges between 2 and 3cm, and rich in ferruginous materials occurring as bands of thin beds.
2235 - 2237	Grey-White Sandstone:	Clayey, coarse grained, thinly cross-bedded with

		foresets dipping NE. Has lots of iron bands and clay.
2232 - 2235	Pink Sandstone	Coarse to medium grained, thickly cross-bedded and indurated.
2231 - 2232	Grey-white Sandstone	Coarse grained, indurated, cross-bedded, bounded both the base and top by ferruginous horizons. It has some clay materials.
2227 - 2231	Red Sandstone	Coarse grained, friable, thickly cross-bedded.
2218 - 2227	Grey claystone-fine Sandstone	The sequence becomes fine to clayey at 2218m, an upward coarsening trend is apparent It is indurated and cross bedded.
2212 - 2218	Red Sandstone	Thin kaolinite commences this thinly cross-bedded, coarse grained, well- sorted iron rich sandstone.
2210 - 2212	Red-Pink Sndstone	The sequence becomes more iron rich, highly indurrated, bounded, both at the base and top. It commences with a thin kaolinite. The interval tends to coarse upward.
2204 - 2210	Grey Sandstone	Pebbly, coarse to fine-grained, poorly sorted sandstone. Lots of conglomerates were observed at base of the unit (2204m). It is thinly cross-bedded (cross -laminated essentially).
2202 - 2204	Grey Sandstone	The sequence becomes cross bedded, coarse to fine grained, friable, generally fines upward.
2194 - 2202	Brick Red Sandstone	Coarse-fine grained, poorly sorted, massive sandstone, rich in ferruginous material, indurrated, commences with thin conglomerate surface at 2194m (the pebbles are polymitic). At the top of this conglomerate surface is a 50cm thick ferruginous horizon. The interval becomes more iron rich from the base to the top.
2193 2194	Grey-Pink Sandstone	Coarse grained, well-sorted, thickly bedded, highly indurated sandstone
2190 - 2193	Claystone	Clay to fine grained sandstone, well-sorted, thinly cross-bedded unit
2186.5 - 2190b	Brick Red Sandsone	Coarse to medium, moderately sorted indurated, massively bedded, iron rich, capped by thin iron band at 2190m.
2186 - 2186.5	Pink Sanstone	Highly indurated, massive, fine to medium-grained, moderately sorted.
2180 - 2186	Grey-White Sandstone	A 50cm thick ferruginous band commences at the base. This is followed by about 20cm kaolinite lense. The sandstone is thinly cross-bedded, fine to medium

		grained, moderately sorted and friable
2175 - 2180	Sandstone:	Highly indurated, ferruginous rich, grey, coarse grained, well- sorted sandstone which commences the successions of this outcrop overlies the basement (pegmatite) unconformably.
Below 2175	Basement	Mainly Pegmatite

Outcrop 4

Interval (m)	Lithology	Description
2330 - 2337	Grey-Pink Sandstone	Medium-fined grained, moderately sorted, indurated sandstone. About 3m thick lense of white cross-bedded claystone occurs laterally within this interval. Ferruginous bed capped the interval at 23338m.
2328 - 2330	Massive Sandstone	Medium to fine grained, clayey fairly well sorted, friable, massive sandstone.
2325 - 2328	Brown Sandstone	Coarse grained, well sorted, friable, cross-bedded sandstone.
2324 - 2325	Pink Sandstone	Relatively more clayey than underlying interval, medium to fine grained (more of fines), moderately sorted, friable, cross-bedded sandstone.
2318 - 2324	Red-Pink Sandstone	Coarse to medium grained, moderately sorted, indurrated, thinly cross-bedded sandstone
2317 - 2318	Claystone-Fine Sandstone:	Finely laminated claystone, fine sandstone, capped by thin ferruginous bed at 2318m.
2315 - 2317	Brown Sandstone	Pebbly, coarse-fine grained, poorly sorted, indurated, thinly cross-bedded sandstone. About 50cm thick ferruginous bed was observed at 2316m. The interval is also rich in clay.
2314 - 2315	Claystone-Fine Sandstone	This is pink to white claystone-fine sandstone horizon. The sediment is indurated and finely cross-bedded.
2309 - 2314	Red-Brown Sandstone	This is a red, pink to brown, pebbly, coarse to medium, moderately sorted, indurated sandstone. It is cross bedded, has a lot of ferruginous encrustation.
2303.75 - 2309	Pink-White Sandstone	Coarse -fine grained, friable, clayey, cross-bedded sandstone.
2301 - 2303.75	Pink Claystone-Fine Sandstone	Highly indurrated, cross bedded claystone-fine sandstone.

2298.5 - 2299	Red-Pink Sandstone	Thin bed (~10cm) of ferruginous material commences this interval. The sandstone is coarse to fine grained, poorly sorted, friable, thinly cross-bedded. It has a lot of claystone clasts and is very rich in iron. The ferruginous horizon thickens up the interval. The sediment show an a fine upward sequence.
2298.5.- 2299	Grey Sandstone	Coarse to medium, moderately sorted, cross-bedded sandstone.
2298 - 2298.5	Claystone Fine Sandstone	Finely laminated clay rich fine sandstone.
2296 - 2298	Grey -White Sandstone	Coarse-medium, friable, thickly bedded sandstone.
2288 - 2296	Brick Red Sandstone	This interval commences with a thin ferruginous bed. It is pebbly, coarse grained, well sorted, cross bedded, lots of intraformational claystone clasts. Conglomerate surfaces abound within the interval. It grades laterally to pink-grey claystone and is bounded by a 20cm thick ferruginous layer at 2996m.
2287 - 2288	Grey-Pink Sandstone	Coarse grained, well-sorted, sandstone
2275.75 - 2287	Grey-Brown Sandstone	Coarse-medium, indurated, thinly cross-bedded sandstone. Fining upward sequence is apparent within this interval.
2274 - 2275.75	Claystone	This interval starts with a thin ferruginous bed (30-40cm) overlain by a 30cm thick coarse grained, friable sandstone. It fines upward to about 1m thick claystone. The claystone is finely laminated.
2272 - 2274	White Claystone-Fine Sandstone	Cross-bedded, friable claystone-fine sandstone. Local occurrence of medium grained sand is observed within this interval.
2270 - 2272	Grey Sandstone	The claystone-fine sandstone of the underlying interval grades upward to a coarse-medium cross bedded sandstone at this interval.
2269 - 2270	Grey Claystone-Fine Sandstone	Finely cross-bedded laminated claystone to fine sandstone. It is bounded by thin ferruginous band (`10cm) at the base and top.
2268 - 2269	Grey Sandstone	Coarse to medium grained, moderately well sorted, friable, rich in ferruginous materials and cross-bedded.
2255.5 - 2268	Brick Red Sandstone	Commences with a thin bed of conglomerates, rich in iron, pebbly coarse grained, thinly cross bedded. The pebbles include claystone clasts.
2254 - 2255.5	Claystone-Fine Sandstone	Cross laminated claystone-fine sandstone, has a lot of intraformational claystone clasts (rip off clasts).

2253 - 2254	Grey-White Sandstone	Fine grained, clayey rich, indurated, cross bedded sandstone.
2252 - 2253	Grey-Pink Sandstone	The interval begins with thin ferruginous bed and claystone, coarse to medium, indurated and thinly cross bedded. Local occurrence of conglomerate is observed.
2250 - 2252	Grey Sandstone	Pebbly coarse to medium grained, iron rich, highly indurated, ross bedded.
2246 - 2250	Grey-Pink Sandstone	Coarse grained, iron rich, thinly cross bedded (cross-lamination more or less) sandstone.
2245 - 2246	Grey Sandstone	Pebbly coarse grained, thickly bedded sandstone
2232 - 2245	Light Brown-Pink Sandstone	Coarse to medium grained sandstone, commences with thin lense of kaolinite (20cm). Has some iron encrustation.
2231 - 2232	Conglomerate	Characterized the regional surface of unconformity. Quartz pebbles and claystone clasts are present.
Below 2231	Basement	

AL HABALAH

Outcrop 1

Interval (m)	Lithology	Description
2327.5 - 2337.25	Brick Red Sandstone	This interval commences with a thin conglomerate and kaolinite horizon. It is brick red, iron rich, coarse to fine grained, shows an upward fining trend, thickly cross-bedded sandstone. A 50cm thick ferruginous bed caps it.
2309.3 - 2327	Red Sandstone	Medium to fine grained, highly indurated, thinly cross-bedded sandstone. Thin kaolinite horizon (50cm) occurs at 2322m.
2309 - 2309.3	Ferruginous Bed	
2290 - 2309	Red Massive sandstone	Red, coarse to medium, indurated, rich in iron, thickly-bedded to massive sandstone. A 30cm ferruginous bed caps it.
2285 - 2290	Pink Sandstone	Coarse to fine grained, poorly sorted, thinly cross-bedded, fractured sandstone.
2278 - 2285	Red Sandstone	Coarse to fine grained, fines upward, poorly sorted, thinly cross bedded sandstone. It commences with about 25cm thick conglomerate bed.

2270.5 - 2278	Grey-White Sandstone	Grey to white, medium to fine grained, localy pebbly, cross-bedded, rich in iron, fractureed, fractures are healed by iron.
2270 - 2270.5	Conglomerate bed	Conglomerate with a thin layer of kaolinite.
2260 - 2270	Quartzite	Highly indurated sandstone
Below 2260	Basement	Bedded granite and some pegmatite veins. The granite is higly weathered. Xenoliths of older basement rocks are observed.

Outcrop 2

Interval (m)	Lithology	Description
2430 - 2441	Brick Red Sandstone	The sequence becomes deeply red at 2430, coarse fine grained, poorly sorted, friable, more thickly cross-bedded than the underlying interval. Intraformational conglomerates with sizes ranging from few mm to 5cm show imbrication at 2431m.
2427 2430	Grey - Pink Massive Sandstone	This is grey to pink, pebbly to fine , kaolinite-rich massive sandstone. The pinkish part is iron rich. Ferruginous band occurs at 2427m.
2423 - 2427	Red Pebbly Sandstone	Pebbly, coarse, well-sorted, friable, red, rich in iron.
2416.5 2423	Pinkish Sandstone	The interval commences with a thin ferruginous bed (40cm) overlying a 50cm conglomerate surface. It is pinkish, medium to fine grained, calcareous, thinly cross-bedded. Caliche and kaolinite occur at 2417m.
2416 - 2416.5	Conglomerate	
2415 - 2416	Pink Sandstone	The sequence becomes fine grained, well sorted, fraible, generally fines upward and cross bedded.
2414 - 2415	Red Pebbly Sandstone	This interval is composed of red, pebbly coarse, indurated, thinly cross-bedded, iron rich sandstone
2410 - 2414	Red - Pink Sandstone	Red to pink, coarse to fine grained, friable, thinly cross bedded sandstone. It has some caliche and erosional surfaces.
2409 - 2410	Pink-Brown Sandstone	Pink to brown, coarse to fine grained, poorly sorted, friable, cross-bedded sandstone.
2408 - 2409	Red Sandstone	Medium to fine grained, moderately sorted, friable, thinly cross-bedded sandstone.
2404.3 - 2408	Pink Sandstone-Claystone	The interval commences with intraformational

		conglomerates. A 2m thick lens of kaolinite rich claystone to fine sandstone overlies the conglomerate surface. The sandstone is pink, coarse to fine grained, friable and cross-bedded.
2404 - 2404.3	Conglomerate	
2403 - 2404	Red-Pink Sandstone	Red to pink, pebbly coarse to medium, moderately sorted, friable, cross bedded, iron rich sandstone.
2399 - 2403	Claystone-Fine Sandstone	Kaolinite rich calystone to fine sand, friable and thinly laminated.
2389 - 2399	Grey Sandstone	Grey, coarse grained, well-sorted, thickly bedded to massive, has thin layer of ferruginous bed capping it at 2399m
2380 - 2389	Red-Pink Sandstone	Red to pink, coarse to fine grained, poorly sorted, friable, cross-bedded sandstone.
2375 - 2380	Claystone-Fine Sandstone	Kaolinite-rich claystone to fine sandstone, friable, and cross-bedded. It is capped by thin (10cm thick) ferruginous bed.
2348 - 2375	Red-Pink Sandstone	Red to pink, pebbly, coarse to fine, poorly sorted, indurated, iron rch, iron materials occur as bands and fracture infils and nodules. The pebbles are angular to rounded.
2347.5 - 2348	Claystone	
2344.4 - 2347.5	Pink Sandstone	Pink, coarse to fine grained, fines upward, friable, cross-bedded sandstone. It is overlain by a 50cm thick kaolinite rich claystone.
2344 - 2344.4	Conglomerate	
2341.5 - 2344	Red - Pink Sandstone	Medium to fine grained, friable, moderately sorted, thinly cross-bedded sandstone.
2341.5 - 2341	Claystone:	
2339.5 - 2341	Red-Pink Sandstone	Red to pink, coarse to fine grained, poorly sorted, friable, locally pebbly, cross bedded sandstone. It is overlain by a 50cn thick kaolinite rich claystone to fine sandstone.
2335 - 2339.5	Conglomeratic Claystone	The sequence commences with a surface of unconformity composed of quartz boulders, cobbles and pebbles ranging up to 10cm in length. It is overlain by about 1m thick kaolinite rich claystone to fine sandstone.
Below 2335	Basement:	Mica schists, banded gneiss, granite, diorite and pegmatite. Abundant exfoliation surfaces, were observed on the granite.

Outcrop 3

Interval (m)	Lithology	Description
2459 - 2470	Red Coarse Sandstone	This unit commences with a thin ferruginous horizon at 2459m. It is reddish, coarse grained, thinly cross bedded sandstone. It shows trough-like cross bed and u-sahped tube-like trace fossil (ophiomorpha?). It laterally changes to a more or less massive greyish sequence at 2463. Southeast trending fractures were noticed at 2453.
2455 - 2459	Red Sandstone	A thickly bedded medium to fine grained indurated red unit associated with some lateral occurrences of grey-white horizons.
2453 - 2455	Grey Sandstone	This interval commences with grey, medium to fine grained beds and changes to red up the section with a lot of pebbles on the surface.
2451 - 2453	Red Sandstone	Coarse grained, cross bdded capped by iron horizon.
2449 - 2451	Red - White Sandstone	The sediments of this interval occurs as more or less an alternating sequence of white/grey . It grades upward to essentially coarse to medium grained, indurrated, capped at the top by conglomerate bed at 2451m. It is cross bedded.
2445 - 2447.75	Grey-White Sandstone	The underlyinmg grey-white intervals persists to this interval. It is, however, more thinly cross bedded, coarse-medium grained. It has lots of ferruginous encrustation.
2441 - 2445	Grey-White Sandstrone	Coarse to fine grained, indurated, thickly cross bedded. It shows some red beds and is capped by ferruginous horizon.
2429 - 2445	Red Sandstone	About 50cm thick conglomerate commences this thickly cross bedded, medium grained sandstone The sandstone is pebbly on the surface.
2427 - 2429	Grey-Brown	Commences with thin layer of conglomerate (monmitic and polymitic), coarse grained, grey, brown to pink, thickly cross bedded sandstone.
2425 - 2427	Claystone (Kaolinite)?	White-baked horizon, likely kaolinite.
Below 2425	Basement	

Outcrop 4

Interval (m)	Lithology	Description
2448 -2452	Red - Pink Sandstone	Red to pink, coarse to medium, friable sandstone with a lot of ferruginous encrustation. It is thinly cross-bedded. Iron anmaterials occur fractue infils and caps (~50-60cm). It also has intraformational clasts.
2443 -2448	Red Claystone-Fine Sandstone	About 5cm thick iron bed commences this red, thinly cross bedded, kaolinitic claystone to fine garined sandstone.
2441 - 2443	Grey-Brown Sandstone	The sediments of this interval are coarse to fine grained, grey, brown to pink and cross bedded.
2439 - 2441	Claystone/fine Sandstone	This white claystone-fine sandstone commenced with about 5cm thick ferrugnous bed. It is friable.
2429 - 2439	Brown Sandstone	The sequence becomes thinly cross-bedded, brownish with lateral variation to reddish, rich in ferruginous materials, coarse to medium grained. The foresets are about 2-3cm thick and NE. The interval is capped by iron bed at 2439m.
2427 - 2429	Brown - Grey sandstone	Overlying a 50cm claystone is a thin ferruginous bed at 2427m. This is followed by a pebbly coarse brownish (soil color) to grey friable cross bedded claystone clasts bearing interval.
2426 - 2427	Brown Sandstone	A 6-10cm thick ferrugninous bed commences this interval. The sediments of the interval are brownish, medium to fine grained sandstone. About 60cm thick claystone occurs at 2426.5m.
2422 - 2426	Red - Pink Sandstone	About 10cm thick iron bed at 2422m begins this coarse to medium grained, pink to red, friable, cross bedded sandstone.
2416 - 2422	Red Claystone -Fine Sandstone	This unit commences with about 10cm thick ferrugious bed. Following this is a red kaolinitic claystone to fine sandstone. It is thinly cross-bedded, rich in rock fragments on the surface. A thin iron bed (10cm) capped the unit at 2422m.
2412 - 2416	Grey-Pink Sandstone	Sediments of this interval are coarse to fine grained, grey, pink to red, thinly cross bedded and fine upward. It is rich intraforamtional clasts (claystone). The sand is friable and clasts generally dip southwest.
2411 - 2412	Claystone-Fine Sandstone	Finely cross-bedded, pinches southward.
2402 - 2411	Brick-like Sandstone	It commences with a thin claystone. It is pebbly, coarse to medium grained, and rich in

		intraformational clasts; thinly cross bedded and has ferruginous bands. The interval shows a well-defined erosional surface at 2403m. Claystone (30cm) rich in iron nodules follow this thin ferruginous bed.
2397 - 2402	Light Brown Sandstone	About 30cm thick claystone begins this coarse to medium grained, light brown sandstone. Caliche and claystone clasts bearing interval are present within.
2396 - 2397	Grey - brown Sandstone	The sediments of this interval are coarse to medium grained, friable, cross bedded and clast rich.
2391 - 2396	Claystone - Fine Sandstone	This kaolinitic claystone/fine sandstone is indurated, rich in ferruginous material, caliche and clasts.
2390 - 2391	Red -Pink Sandstone	Medium to fine graineed, cross laminated to cross bedded, sandstone.
2383.5 - 2391	Red -Pink Sandstone	Coarse to fine grained, laminated, rich in ferruginous material.
2377 - 2383.5	Red to Pink Sandstone	Essentially medium to fine grained, cross laminated to thinly cross bedded, rich in ferruginous material. The iron occurs as frature infill.
2376 - 2377	Massive Sandstone	Medium to fine grained, friable, massive sandstone. It has caliche and ferruginous encrustation.
2374 - 2376	Claystone to Fine Sandstone	Friable kaolinitic claystone to fine grained sandstone
2373 - 2374	Yellow - Red Sandstone	Medium to fine grained, friable, cross bedded yellow to red sandstone.
2370 - 2373	Light Brown Sandstone	Fine grained, friable, ferruginous, cross-bedded sandstone.
2369 - 2370	Red - Pink Sandstone	Medium to fine grained, indurrated , rich in iron and fractures that are healed by iron.
2368 - 2369	Pink Claystone	Kaolinite rich claystone to fine sandstone
2365 - 2368	Massive White Sandstone	Medium to fine grained, white indurrated massive sandstone
2364 - 2365	Grey - Brown Sandstone	Medium to fine, indurrated, cross bedded, light grey to brown sandstone.
2364 - 2364	Basal Conglomerate	Conglomerate bed marking the regional surface of unconformity. The conglomerates consist of quartz and rock fragments.
Below 2364	Basement	

Outcrop 5

Interval (m)	Lithology	Description
2477 - 2480	Quartzite	Highly compacted sandstone. It is grey.
2470 - 2477	Grey - Pink Sandstone	Grey to Pink, commences with a thin claystone horizon at 2470m
2465 - 2470	Brown - White Sandstone	The sequence becomes thinly cross bedded, brown, medium to fine grained, friable at 2465m and grades to white coarse grained upward.
2456 - 2465	Light Brown Sandstone	Thickly cross bedded, rich in ferruginous material, fractured with fractures trending NW and are as long as 10cm close to the top of the interval.
2446 - 2456	White Sandstone	Coarse to fine, poorly sorted, cross bedded, friable sandstone.
2445 - 2446	Claystone - Fine Sandstone	White laminated friable kaolinitic claystone to fine sandstone.
2439 - 2445	White - Grey Sandstone	Coarse to fine, poorly sorted white to grey, friable, cross-bedded sandstone.
2425 - 2439	Grey - Brown Sandstone	Coarse to medium grained, grades upwards to pebbly coarse grained sandstone. It is friable and cross-bedded.
2421 - 2425	Grey - Brown Sandstone	This interval is thickly bedded to massive, coarse grained, friable sandstone.
2416 - 2421	Grey - Brown Sandstone	The sequence grades to cross laminated - thinly cross bedded grey to brown, coarse to fine grained, poorly sorted, fractured sandstone. The fractures trend NE and NE/SW.
2414 - 2416	White-Grey Sandstone	Transition to mainly white-grey sequence at 2414m. Between 2414 and 2415m lies an alternating sequence of coarse to medium grained sediment. The interval is generally a medium to fine grained, fiable, finely laminated to massive sandstone.
2410 - 2414	Red Sandstone	About 40cm ferruginous horizon which capped the underlying interval forms the basal part of this essentially coarse to medium grained, red cross bedded unit
2406 - 2410	Sandstone	The interval commences with a 50cm thick locally pebbly, coarse sand sediments. It is overlain by claystone to fine grained sandstone lens. A thin

		ferruginous band occurs at 2408m. The ferruginous band bears some conglomerates on the surface.
2403.5 - 2406	Red Claystone - Fine Sandstone	Sediments of this interval are essentially red cross-laminated kaolinitic claystone to fine sandstone.
2398.5 - 2403.5	Red Claystone/Fine Sandstone	The sequence transits to essentially reddish compacted to fine sandstone claystone, finely cross-laminated. About cm thick iron band occurs at 2403m.
2393 - 2398.5	Grey Sandstone	The sequence becomes grey, coarse grained, thinly cross bedded with foresets thickness 1-3cm. The foresets dip east-west.
2391- 2393	Grey-Pink Sandstone	Very coarse grained, thinly cross bedded. Claystone reddish occurs within the sand body. Iron band at 2393m caps the interval.
2389 - 2391	Red - Pink Sandstone	A thin claystone (20cm) begins this interval. It is coarse to fine grained, it coarseens upward and cross bedded. The foresets dip NE. Major fractures trend NE.
2385 - 2389	Grey - Light Brown Sandstone	Very thin ferruginous band (5 -10cm) that caps the underlying interval is overlain by grey, light brown, friable, pebbly coarse grained cross bedded sandstone. Very thin claystone and iron band occur at 2388m. Foresets dip NW.
2380 - 2385	Red - Pink Sandstone	The sequence grades to red, pink, coarse to medium grained, friable sandstone. It has some intraformational conglomerates (claystone) on the surface. It is thinly cross-bedded. About 50cm thick red claystone to fine snadstone crops out at 2383m.
2373 - 2380	Red - Brown Claystone - Fine Sandstone	This interval is composed of red kaolintic claystone to fine grained sandstone.
2357 - 2373	Red Sandstone	The interval commences with a very thin ferruginous band (10cm). The sediments that follow the iron bed are coarse to medium grained. Fractures on the interval trend NW and dip SE. The interval is cross - bedded and indurrated.
2353 - 2357	White - Pink Claystone - Fine Sandstone:	About 35 to 40cm thick ferruginous bed commences this white to pink kaolinitic claystone to fine sandstone at 2353m.
2352 - 2353	Red Sandstone	Thinly cross bedded sandstone It is highly fractured with ferruginous filled.
2351 - 2352	Grey - Brown Massive Sandstone	Massive to thickly bedded, coarse, highly indurated sandstone.

2347.5 - 2351	Grey Sandstone	The interval begins with white kaolinitic claystone. This is overlain by massive, pebbly, coarse to medium sandstone. It shows a generally upward fining trend.
2346 - 2347.5	Brown (Soil-like)	Coarse medium grained, fines upward, friable, thickly cross bedded brown sandstone.
2344 - 2346	Red - Grey Sandstone	Thinly cross bedded, red to grey sandstone.
2342.5 - 2344	Yellow Sandstone	Generally, a yellow with lateral gradation to bown. It is coarse to medium grained sandstone.
2340 - 2342.5	Very Reddish (Brick Red)	Coarse grained, friable, cross bedded with trough-like cross beds. It grades upward, grey to red with iron encrustation.
2339 - 2340	Yellow Sandstone	Yellow with some shades of brow and red, medim to fine, thickly cross bedded and indurated sandstone. Its cross bed foresets dip NW.

Outcrop 6

Interval (m)	Lithology	Description
2462 - 2465	Quartzite	Highly indurated quartzite, individual grains still distinct, coarse to medium grained, moderate to well-sorted.
2453.75 - 2462	Brown-Grey Sandstone	Coarse to fine grained, poorly sorted, thickly cross-bedded, foresets thickness averages 10cm, highly fractured, fractures trend mainly N-S.
2448 - 2449	Brownish-Grey Massive Sandstone	Coarse to fine, fines upward, highly eroded.
2439 - 2448	Light Brown-Grey Sandstone	Medium to fine grained, moderately sorted, cross-bedded, foresets dip NW.
2437 - 2439	Pebbly Sandstone	Pebbly, coarse-fine grained, poorly sorted, cross bedded, pebbles are mainly well rounded quartz.
2436 - 2437	Light Brown-Grey Sandstone	This interval overlies a conglomerate surface at 2436m. The sediments are coarse grained, thickly cross-bedded, foresets thicknes averages 5-6cm.
2434 - 2436	Fine Sandstone	Fine, well-sorted, indurated, cross bedded sandstone. It is capped by polymitic and monomitic conglomerates at 2436m, pebbles are up to 10cm long and 4cm in width.
2433 - 2434	Light Grey Massive Sandstone	Coarse grained, sorted, less pebbly than underlying interval, massive sandstone.

2431 - 2433	Light Grey Pebbly Sandstone	Pebbly coarse grained, well sorted, cross bedded, foresets dip NW. Both quartz pebbles and claystone intraclasts are present on the surface of the sediments of this interval.
2410 - 2431	Light Grey Sandstone	Medium to fine grained, moderate to well-sorted, thinly cross bedded, foresets are about 2cm thick and dips NW. Thin kaolinite lens lies between 2417.5 to 2418m.
2397 - 2410	Grey-Light Brown Sandstone	The sequence becomes cross bedded at 2397m. It is medium to fine grained, moderate to well sorted, generally fines upward, and cross bedded.
2387 - 2397	Grey-White Sandstone	A thin bed of quartz pebbles and intraformational conglomerates (granite fragments and claystone clasts) marking the transitional zone between the red and grey unit occurs at 2387m. The pebbles are large, ranging up to 40cm long and 10cm wide. White - grey, coarse grained, thickly bedded sediments disconformably overly this conglomerate bed. The sediments are friable and show a fining upward sequence.
2385 - 3387	Red Sandstone	Coarse to medium, moderately sorted, thinly cross bedded, friable sandstone
2384 - 2385	White-Red Sandstone	Coarse to fine, poorly sorted, friable, thickly cross - bedded, overlies a thin ferruginous bed.
2382 - 2384	Red-Grey Sandstone	Coarse to fine, poorly sorted, indurated, thinly cross-bedded, has some caliche and encrusted by ferruginous materail at 2384m.
2379 - 2382	Red Sandstone	Coarse to fine grained, poorly sorted, friable, thickly cross bedded sandstone.
2376 - 2379	Claystone-Fine Sandstone	This interval is capped by a 40cm thick ferruginous bed at 2376m. The ferruginous horizon is fractured and the iron material heals the fractures.
2372 - 2376	Red-Pink Sandstone	Coarse grained, well sorted, thickly cross bedded, about 20cm thick ferruginous bed and some caliche occurs at 2375m.
2367 -2372	Pink Sandstone	Medium to fine grained, moderately sorted, indurated, thinly cross- bedded, iron and caliche encrustation is noticed at 2370 and 2372m.
2364 - 2372	Red Sandstone	Coarse-fine grained, poorly sorted, iron rich, indurated, and well cross-bedded. Local intercalation of white/grey sediments is observed.
2363 - 2364	Red-Brown Sandstone	The upper brownish part is coarse and has intraformational conglomerates. Sediment fines upward to mediun to fine sequence.

2362 - 2363	Pink Sandstone	Medium to fine, moderately sorted, highly indurated, capped by locally red, indurated claystone (10-15cm thick).
2359 - 2362	Red Sandstone	Essentially red, coarse grained, well sorted, thickly-bedded, angular to rounded pebbles are characteristic of this interval. Iron encrustation is observed at 2361m.
2356 - 2359	Grey-Pink Sandstone	Medium to fine grained, moderately sorted, thickly cross-bedded, local occurrence of claystone at 2359m, claystone capped by thin bed (~10cm) of pebbly iron rich sediment.
2355 - 2356	Brick Red Sandstone	Iron rich, medium to fine, cross bedded deeply red sandstone.
2354 - 2355	Pink-Grey Sandstone	Commences with a thin bed of iron rich sediments. It is coarse-medium grained, poor to moderately sorted, grades to medium-fine, more reddish and iron rich in the upper part of the sequence. It has intraformational conglomerates.
2353 - 2354	Grey-Red Sandstone	Begins with essentially fine sediments and grades to coarse sediments up the sequence. It is thinly cross bedded. The coarse upper part is red to pink colored.
2350 - 2353	Pink-Red Sandstone:	Coarse to fine grained, poor ly sorted, rich in intraformation clasts and thinly cross-bedded.
2348 - 2350	Grey-Red Sandstone	The sequence becomes coarse, well sorted, rich in intraformational conglomerates, and caliche. The interval is thinly cross-bedded.
2346 - 2348	Grey-Red Sandstone	Alternating sequence of grey and red, medium to fine grained, friable cross bedded sandstone. It has some iron encrustation.

Outcrop 7

Interval (m)	Lithology	Description
2428 - 2436	Grey-White Sandstone	The sequence becomes well cross bedded at 2428, medium to fine, grades to very fine close to the top, moderately sorted, friable and cross bedded with foresets dipping NE. Fractures observed within this interval trend E-W
2422 - 2428	Grey-White Sandstone	Coarse-fine grained, poorly sorted, friable, massive, fractured, the fractures trend E-W.
2417 - 2422	Grey-White Sandstone	Coarse to fine grained, friable, thinly cross-bedded, foresets dip opposite to the underlying interval (NE).

2410 - 2417	Grey-White Sandstone	Commences with a 40cm thick kaolinite-very fine sandstone. It is coarse to fine, essentially thinly cross-bedded, foresets are 2-4cm thick and generally dip NW, bidirectional to adjacent intervals.
2405 - 2410	Grey Sandstone	Medium to fine grained, moderately sorted, well cross-bedded, forsets dip NE. It is overlain by 40cm claystone-fine sandstone.
2393 - 2405	Massive Sandstone	Coarse to fine, poorly sorted, fines upward, internally laminated massive sandstone
2392 - 2393	Coarse Sandstone	Coarse grained, well-sorted, friable, grey to white cross bedded sandstone
2390 - 2392	Grey -White Sandstone	Medium to fine grained, moderately sorted, indurated, massive sandstone.
2388.5 - 2390	Pebbly sandstone	Commences with conglomerate rich thin bed, coarse to fine, poorly sorted, fines upward, cross bedded, overlain by a 30cm thick kaolinite rich claystone.
2387 - 2388.5	Claystone-Fine Sandstone	White, friable, kaolinite rich claystone to fine sandstone.
2381.8- 2387	Pink-Brown Sandstone	Medium to fine grained, locally pebbly on the surface, cross bedded (more of cross lamination, foresets 2-3cm thick).
2381 - 2381.8	Conglomerate	About 80cm thick molomitic and polymitic conglomerate bed overlies the underlying claystone-fine sandstone interval.
2380 - 2381	Claystone-Fine Sandstone	Kaolinite rich claystone and fine sandstone. Intraformational claystone clasts are present within this interval.
2376 - 2380	Light Brown Sandstone	Pebbly, coarse-fine grained, friable, cross-bedded sandstone, foresets dip NW opposite to the underlying interval.
2372 - 2376	Grey-White Sandstone	Commences with fine grained sediments and coarsens upward, cross bedded, foresets dip NE. Fractures observed in the interval dip NE as well.
2364 - 2372	Grey Sandstone	Coarse to fine, poorly sorted, highly eroded, fractured, cross bedded with foresets dipping NW and overlain by a 40cm thick kaolinitic claystone at 2372m.
2363 2364	Grey-Brown Sandstone	Coarse-fine grained, poorly sorted, highly fractured and eroded blocky to massive sandstone.

2354 - 2363	Grey Sandstone	Pebbly, coarse grained, well sorted, indurated, thinly cross bedded, foresets are about 2cm thick, dips opposite to the underlying interval (NW).
2347 - 2354	Grey-White Sandstone	Coarse to fine grained, poorly sorted, friable, cross bedded sandstone
2337 - 2337.75	Pebbly Sandstone	Commences with a 50cm thick conglomerate bed, cross- laminated, shows bi-directional cross bedding compared with adjacent intervals.
2326 - 2337	Light Grey-White Sandstone	The sequence becomes more thinly cross bedded with foresets being 2-4cm thick, shows general coarsening upward sequence.
2316 - 2326	Light Grey Sandstone	Coarse to fine grained,poorly sorted, thickly cross-bedded, forsets range from 5 to 8cm thick and dips NE.
2314 - 2316	Light Grey Sandstone	Coarse grained, well sorted, thickly bedded to massive sandstone.
2313 - 2314	Conglomerate	About 90cm thick conglomerate bed, consists of quartz pebbles, rock fragments and claystone clasts. This interval marks the surface of unconformity between the Red and Grey Units.
2311.5 - 2312.5	Light Grey Sandstone	Fine grained, well-sorted, friable, thickly bedded to massive sandstone
2307 - 2311.5	Light Grey Sandstone	Pebbly Coarse to fine grained, poorly sorted, thickly bedded to massive, calcareous, grossly eroded sandstone.
2301.5 - 2307	Red-Pink Sandstone	Coarse to fine, poorly sorted, friable cross-bedded sandstone.
2301 - 2301.5	Grey Sandstone	Coarse to medium grained, indurated, cross-bedded.
2299 - 2300	Red-Pink Sandstone	Very coarse to medium, local ferruginous coating at 2300m. A lot of well-rounded conglomerates were observed within the interval.

AL SOUDAH

Outcrop 1

Interval (m)	Lithology	Description
2748 - 2750	Red Sandstone	Coarse grained, well sorted, friable, capped by about 1m thick ferruginous horizon. The ferruginous bed is also cross-bedded.
2745 - 2748	Grey Sandstone	Pebbly coarse to fine, poorly sorted, friable sandstone.

2743 - 2745	Grey-Red Sandston0e	Commences with light grey, fine grained, cross-bedded, and grades upward to coarse grained red, iron rich sediments. It is capped by a about 20cm thick ferruginous bed.
2741 - 27431	Red Sandstone	Pebbly Coarse to medium grained, moderately sorted, cross-bedded
2739 - 2741	Kaolinitic Claystone	White, friable, kaolinite rich claystone to fine grained sandstone
2733 - 2739	Light Grey Sandstone	Weathered, pebbly coarse to medium grained sandstone, cross bedded, cosets are saparated by ferruginous bands.
2718 - 2733	Grey sandstone	Coarse to fine, poorly sorted, friable, cross bedded sandstone.
2715 - 2718	Red -Brown Sandstone	Coarse to fine, poorly sorted, cross bedded, the cross beds are planar to trough like, ferruginous bands separate the cross beds cosets.
2712 - 2715	Grey-White Sandstone	Coarse to fine grained, poorly sorted, friable, cross bedded, some iron rich beds, local occurrence of conglomerates observed at 2713m.
2695 - 2712	Grey Massive Sandstone	Basal pebbly, coarse grained highly weathered, massive sand. The base of this interval is composed of about 1m thick conglomerate overlain by a thin kaolinite bed.
Below 2690	Basement	Schist and some veins of quartzite.

Outcrop 2

Interval (m)	Lithology	Description
2750	White-Red Sandstone	The interval is composed of alternating white and red sediments. The Sand grains are fine, well sorted, friable and cross-bedded. The transition to red is barupt and it is capped by thin iron bed.
2748 - 2750	White Sandstone	The sequence transists to essentailly white, pebbly sediments at 2748m.
2742 - 2748	Red Sandstone:	Pebbly coarse grained cross bedded sandstone.
2739 - 2742	Red Sandstone	Red friable, cross bedded Sandstone. Thin ferruginous band occurs within. The interval, is capped by about 10cm thick ferruginous bed at 2742m.

2725 2739	Quartzite	This is a 14m thick of highly indurated quartzite. The presence of pebbles and cobbles within the quartzite indicate it sedimentary origin. Some ferrugnous coatings are observed within fractures of this interval. The interval is in justaposition with white, powdery metasediments (talc?).

Outcrop 3

Interval (m)	Lithology	Description
2773 - 2785	Red Sandstone	This interval is composed of red, coarse to fine grained, cross bedded sandstone. Lenticular cross bedding is prominent here. The interval is highly ferruginated with abundant iron coatings on the surface, foresets and fractures are also present. A probable normal fault is suspected to be present within the topmost part of thisinterval.
2772 - 2773	Brown - Red Sandstone	Thin ferruginous bed commences this interval. It coarse to fine grained, friable, cross-bedded. It shows an upward coarsening trend.
2770 - 2772	Grey Sandstone	Coarse to medium, friable, cross bedded sandstone. The interval is capped by thin ferruginous bed.
2765 - 2770	Red Sandstone	Overlying the channel filled interval is an interval of coarse to medium grained, friable, iron rich cross bedded sandstone
2760 - 2765	Red - Grey Sandstone	The interval is composed of channel filled sediments cutting through the basement. It is essentially massive coarse to fine grained, friable and ferruginous. It alternately transits to cross-bedded sandstone laterally.
2759 - 2760	Conglomerate	Basal conglomerate made up of quartz and rock fragment pebbles are present where the cahannel does not cut across the basement. The pebbles are angular to rounded and are as long as 10cm.

APPENDIX II

Factor Loadings distributions for heavy Minerals in Wajid Sandstone.

Ahad Rufaidah

	Factor 1	Factor 2	Factor 3
Opaques	0.008659	-0.993865	0.01677
Tourmaline	0.628572	-0.19609	0.71092
Zircon	-0.61536	-0.292816	-0.708
Rutile	0.269274	0.145529	-0.8426
Epidote	-0.29467	0.7854435	-0.0385
Hornblende	0.922975	0.0183903	0.02376
Kyanite	-0.75501	0.3695711	-0.0043
Unknown	0.276725	0.5938576	0.67241
Expl.Var	2.431681	2.2396482	2.17125
Prp.Totl	0.30396	0.279956	0.27141

Eigenvalues

Factor		% total	Cumul.	Cumul.
	Eigenval	Variance	Eigenval	%
1	3.189606	39.870069	3.18961	39.87
2	2.389345	29.866808	5.57895	69.737
3	1.263633	15.79541	6.84258	85.532

Habalah I			
	Factor 1	Factor 2	Factor 3
Qpaques	0.209843	0.7342243	0.12355
Tourmaline	-0.79946	-0.278529	-0.3293
Zircon	0.813255	0.4777735	0.08773
Rutile	0.220809	0.1240294	0.92064
Epidote	-0.07649	-0.901253	-0.0385
Hornblende	-0.83016	0.2439942	-0.0298
Kyanite	-0.06011	0.1533864	-0.027
Sphene	-0.03006	-0.79762	0.02075
Unknown	0.620319	0.2416987	-0.5843
Expl.Var	2.477628	2.450247	1.32397
Prp.Totl	0.275292	0.2722497	0.14711

Eigenevalues

Factor	Eigenval	% Variance	Eigenval	% Cum.
1	3.514418	39.049085	3.51442	39.04
2	1.702566	18.917403	5.21698	57.95
3	1.286274	14.291934	6.50326	72.24

Habalah II			
	Factor 1	Factor 2	Factor 3
Opaques	-0.10191	0.0878354	0.93607
Tourmaline	-0.04532	-0.99461	-0.0545
Zircon	-0.58008	0.7157243	-0.2784
Rutile	0.039785	0.7912693	0.4742
Epidote	0.955152	0.0085884	-0.1583
Hornblende	0.7617	-0.175418	-0.184
Unknown	0.738804	0.1659336	0.39696
Expl.Var	2.388851	2.1937111	1.39806
Prp.Totl	0.341264	0.3133873	0.19972

Eigenevalues

Factor	Eigeneval.	% Variance	Cum Eigenval	% Cum.
1	2.68343	38.33472	2.68343	38.335
2	2.114146	30.202087	4.79758	68.537
3	1.183044	16.900624	5.98062	85.437

Al Soudah

	Factor 1	Factor 2	Factor 3
Opaques	0.727806	-0.308204	-0.5765
Tourmaline	0.090424	-0.578975	-0.7911
Zircon	-0.57613	0.4318651	0.6689
Rutile	0.767068	0.4634011	0.20972
Epidote	0.877524	-0.123412	-0.1228
Hornblende	0.002663	-0.044875	0.94496
?Sphene	-0.16099	0.9106465	0.1805
Unknown	0.069483	0.9768855	0.07631
Expl.Var	2.258996	2.6322768	2.39603
Prp.Totl	0.282374	0.3290346	0.2995

Eigenvalues

Factor	Eigenval	% Variance	Cum Eigenval	% Cum.
1	4.191147	52.389336	4.19115	52.389
2	2.145518	26.81898	6.33667	79.208
3	1.197739	14.971743	7.5344	94.18

Heavy mineral Q-Mode Factor Distribution

	Factor 1	Factor 2	Factor 3
HA58	0.329926	0.849485	0.334785
HA57	0.890668	0.155481	0.365286
HA52	0.786254	0.240007	0.521916
HA50	0.034996	0.920257	0.26928
HA45	0.763233	0.544548	0.273088
HA44	0.741684	0.568263	0.276592
HA41	0.680703	0.184498	0.675947
HA40	0.898523	0.076009	0.348384
HA39	0.804449	0.237016	0.491531
HA36	-0.0058	0.957257	0.139665
HA26	0.660727	0.257533	0.662775
HA21	0.730457	0.554534	0.332817
HA15	0.297739	0.755711	0.515037
HA14	0.686726	0.560129	0.40088
HA7	0.711532	0.650161	0.156503
HA5	0.705165	0.61011	0.278569
AR39	0.8932	0.319192	0.232817
AR32	0.558302	0.500105	0.617779
AR17	0.651309	0.69681	0.21024
AR14	0.714729	0.610478	0.259007
AR13	0.387364	0.773385	0.437923
AR11A	0.76706	0.31337	0.466519
AR10	0.367197	0.810909	0.350322
AR8	0.573864	0.25687	0.720363
AR6	0.690302	0.581949	0.365301
AR2	0.864457	0.299937	0.315095
ARLC3SC	0.915136	0.11567	0.303483
HAP32	0.775516	0.255218	0.523868
HAP25	0.765576	0.336376	0.502249
HAP24	0.421035	0.260174	0.832223
HAP22	0.453705	0.80374	0.288425
HAP20	0.339856	0.508121	0.747541
HAP16	0.675389	0.279606	0.645226
HAP13	0.551152	0.714124	0.323529
HAP11	0.862518	0.180003	0.412907
HAP7B	0.403899	0.451928	0.75066
HAP4	0.829898	0.199168	0.474461
HAP3	0.405054	0.444527	0.755602
S21	0.181794	0.413935	0.856796
S17	0.532216	0.422257	0.701096
S13	0.113997	0.580801	0.739583
S12	0.810426	0.512504	-0.00355
S8	0.446741	0.099391	0.861746
S2	0.740763	0.384439	0.50197
Expl.Var	18.35471	11.72732	11.26155
Prp.Totl	0.417153	0.26653	0.255944

Eigenevalues

	Eigenval	% Variance	Cum. Eigenval	% Cum.
1	34.75723	78.9937	34.75723	78.9937
2	3.918165	8.90492	38.67539	87.8986
3	2.668181	6.064048	41.34358	93.9627

APPENDIX III

Distribution of Element in the Basement Samples

SAMPLE	Ag (ppm)	Al (%)	As (ppm)	Ba (ppm)	Be (ppm)	Bi (ppm)	Ca (%)	Cd (ppm)	Co (ppm)	Cr (ppm)	Cu (ppm)	Fe (%)	Ga (ppm)	Hg (ppb)	K (%)	La (ppm)
B1(?gabbro)	<.2	2.61	<2	40	<.5	<2	1	<.5	21	129	30	5.04	10	10	0.1	<10
B2 (gabbro)	<.2	1.69	<2	20	0.5	<2	1.33	<.5	24	387	86	2.97	<10	10	0.02	30
B3 (mica schist)	<.2	1.76	<2	170	<.5	<2	0.61	<.5	7	44	4	2.74	10	<10	0.84	40
B4 (biotite gneiss)	<.2	0.99	<2	70	<.5	<2	11.95	<.5	5	52	11	1.7	<10	<10	0.23	40
B5 (pegmatite)	<.2	0.23	6	<10	<.5	2	0.03	<.5	2	154	6	4.92	<10	<10	0.03	<10
B6 (pegmatite)	<.2	0.32	<2	10	<.5	2	0.06	<.5	1	77	6	0.49	<10	10	0.04	<10
B7 (S11-talc?)	<.2	0.7	2	30	0.5	2	0.13	<.5	<1	26	<1	0.52	<10	<10	0.22	50
B8 (granite)	8	0.37	<2	10	<.5	<2	1.4	<.5	1	75	7	1.23	<10	40	0.14	60
B9 (S43 - schist)	<.2	2.9	6	30	<.5	<2	0.88	<.5	43	93	32	5.27	<10	10	0.09	<10
B10 (pegmatite)	<.2	0.32	2	<10	<.5	2	0.07	<.5	1	103	4	0.62	<10	<10	0.03	10
B11(schist)	<.2	2.75	6	20	<.5	<2	0.86	<.5	29	123	46	5.42	10	10	0.29	<10

SAMPLE	Mg (%)	n (pp	Mo (ppm)	Na (%)	Ni (ppm)	P (ppm)	Pb (ppm)	Sc (ppm)	Sr (ppm)	Ti (%)	V (ppm)	Zn(ppm)	Cr/Ni	V/Cr	V/Ni
B1(?gabbro)	1.44	740	3	<.01	25	980	<2	4	20	0.49	92	74	5.16	0.713178	3.68
B2 (gabbro)	2.62	360	2	0.05	281	1750	<2	17	61	0.16	36	32	1.3772	0.093023	0.128114
B3 (mica schist)	0.87	300	2	0.01	21	1620	<2	4	28	0.18	48	98	2.0952	1.090909	2.285714
B4 (biotite gneiss)	0.73	225	3	0.46	5	590	6	3	95	0.15	41	24	10.4	0.788462	8.2
B5 (pegmatite)	0.01	30	1	<.01	11	90	<2	3	2	<.01	20	8	14	0.12987	1.818182
B6 (pegmatite)	0.08	75	<1	0.04	3	70	6	<1	4	<.01	4	8	25.667	0.051948	1.333333
B7 (S11-talc?)	0.07	25	1	0.01	2	130	<2	1	14	<.01	1	10	13	0.038462	0.5
B8 (granite)	0.13	215	3	0.25	9	210	<2	1	16	0.04	4	30	8.3333	0.053333	0.444444
B9 (S43 - schist)	1.54	915	4	<.01	47	1310	<2	5	24	0.28	69	92	1.9787	0.741935	1.468085
B10 (pègmatite)	0.03	30	1	<.01	4	100	2	<1	4	<.01	8	2	25.75	0.07767	2
B11(schist)	1.51	810	3	<.01	24	950	2	5	21	0.5	105	76	5.125	0.853659	4.375

Distribution of Oxides in the basement samples

SAMPLE	Al_2O_3	CaO	Cr_2O_3	Fe_2O_3	K_2O	MgO	MnO	Na_2O	P_2O_5	SiO_2	TiO_2	LOI	TOTAL	K_2O/Na_2O	Al_2O_3/Na_2O	Al_2O_3/TiO_2	CIA
B1(Diorite?)	13.99	7.72	0.02	13.15	0.51	6.26	0.21	3.73	0.18	49.54	1.98	2.59	99.88	0.136729	3.75067	7.065657	53.91
B2 (gabbro)	8.29	9.2	0.11	9.03	0.95	13.76	0.14	1.52	0.36	50	1.19	6.29	100.85	0.625	5.453947	6.966387	41.53
B3 (mica schist)	15.6	2.7	0.01	3.89	3.73	1.5	0.05	4.03	0.35	64.58	1.32	2.05	99.8	0.925558	3.870968	11.81818	59.86
B4 (biotite gneiss)	10.5	21.5	0.01	3.59	1.67	1.86	0.06	3.26	0.12	39.21	0.47	18.05	100.3	0.51227	3.220859	22.34043	28.43
B5 (pegmatite)	2.23	0.05	0.02	7.01	0.25	0.08	0.01	0.04	0.01	89	0.05	1.52	100.25	6.25	55.75	44.6	86.77
B6 (pegmatite)	15.71	0.2	0.01	0.85	1.88	0.19	0.01	6.88	0.01	73.18	0.1	1.01	100	0.273256	2.28343	157.1	63.68
B7 (S11-talc?)	12.92	0.19	0.01	1.12	6.19	0.31	0.06	0.09	0.01	76	0.15	3.36	100.4	68.77778	143.5556	86.13333	66.63
B8 (granite)	13.13	2.45	0.01	1.79	5.16	0.22	0.05	3.87	0.04	71.6	0.16	2.46	100.95	1.333333	3.392765	82.0625	53.35
B9 (S43 - schist)	15.42	7.91	0.01	13.02	0.77	5.32	0.22	2.44	0.27	48.93	1.96	3.53	99.8	0.315574	6.319672	7.867347	58.1
B10 (pegmatite)	7.49	0.09	0.01	1.12	0.32	0.11	0.01	0.05	0.01	86.6	0.11	3.02	98.94	6.4	149.8	68.09091	94.21
B11(schist)	13.75	7.39	0.02	14.05	0.55	6.32	0.24	3.51	0.19	47.05	2.03	3.24	98.34	0.156695	3.917379	6.773399	54.56

Appendix IIIa: Distribution of Elements in Ahad Rufaidah.

SAMPLE	Ag (ppm)	Al (%)	As (ppm)	Ba (ppm)	Be (ppm)	Bi (ppm)	Ca (%)	Cd (ppm)	Co (ppm)	Cr (ppm)	Cu (ppm)	Fe (%)	Ga (ppm)	Hg (ppb)	Hg (ppm)	K (%)	La (ppm)	Mg (%)
AR3	<.2	0.41	14	20	0.5	2	0.13	<.5	9	81	3	12.8	<10	10	0.01	<.01	<10	0.06
AR6	<.2	0.15	2	40	<.5	<2	0.24	<.5	<1	24	1	0.08	<10	<10	<0.01	0.05	<10	0.04
AR9A	0.2	0.23	24	740	0.5	<2	0.35	<.5	17	63	3	8.9	<10	50	0.05	0.06	80	0.04
AR15	0.2	0.26	<2	10	0.5	2	0.14	<.5	4	46	<1	11.7	<10	10	0.01	<.01	<10	0.01
AR19	0.2	0.18	2	30	1	<2	0.34	<.5	3	95	3	15	<10	60	0.06	<.01	<10	0.06
AR20	<.2	0.1	2	10	<.5	<2	0.18	<.5	<1	44	1	0.94	<10	<10	<0.01	<.01	<10	0.05
AR21	<.2	0.11	<2	<10	<.5	<2	2.66	<.5	<1	50	3	0.51	<10	<10	<0.01	<.01	<10	0.03
AR22	<.02	0.17	2	10	<.5	<2	0.73	<.5	1	99	6	1.17	<10	<10	<0.01	<.01	<10	0.07
AR23	<.2	0.1	6	<10	<.5	<2	0.17	<.5	<1	29	1	0.41	<10	<10	<0.01	<.01	<10	0.03
AR25	<.2	0.14	12	10	<.5	2	1.92	<.5	2	52	7	3.21	<10	10	0.01	<.01	<10	0.2
AR35	1.8	0.2	<2	30	<.5	<2	0.21	<.5	9	71	20	0.49	<10	10	0.01	<.01	10	0.05
AR43	<.2	0.11	2	<10	<.5	<2	2.33	<.5	<1	28	3	0.22	<10	<10	<0.01	<.01	<10	0.04
AR51	1.2	0.21	<2	10	<.5	2	6.67	<0.5	7	109	13	0.6	<10	10	0.01	<.01	<10	0.04
ARLC4K1	<.2	0.1	2	<10	<.5	<2	0.08	<.5	<1	30	1	0.37	<10	<10	<0.01	<.01	10	<.01
ARLC4K2	<.2	0.07	<2	<10	<.5	<2	0.18	<.5	<1	39	1	0.24	<10	10	0.01	<.01	<10	0.05
ARLC4K3	<.2	0.13	2	<10	<.5	<2	4.81	<.5	<1	24	1	1.34	<10	<10	<0.01	<.01	<10	0.13
ARLC3SC	0.2	0.27	10	10	0.5	4	1.81	<.5	4	180	2	12.65	<10	10	0.01	<.01	<10	0.03

Appendix IIIa: Distribution of Elements in Ahad Rufaidah Contd.

SAMPLE	Mn (ppm)	Mo (ppm)	Na (%)	Ni (ppm)	P (ppm)	Pb (ppm)	Sb (ppm)	Sc (ppm)	Sr (ppm)	Ti (%)	Tl (ppm)	U (ppm)	V (ppm)	W (ppm)	Zn(ppm)	Cr/Ni	V/Cr	V/Ni
AR3	1455	4	<.01	12	270	8	2	1	15	<.01	<10	<10	12	<10	8	6.75	0.15	1
AR6	15	<1	0.03	1	40	2	<2	<1	29	<.01	<10	<10	1	<10	6	24	0.04	1
AR9A	>10000	6	<.01	12	1520	14	<2	<1	87	<.01	<10	<10	10	<10	8	5.25	0.16	0.83
AR15	220	1	<.01	13	50	6	<2	1	7	<.01	<10	10	6	<10	10	3.538	0.13	0.46
AR19	70	2	0.01	5	310	6	<2	2	20	0.03	<10	<10	103	<10	4	19	1.08	20.6
AR20	20	1	0.04	1	20	<2	<2	<1	12	<.01	<10	<10	12	<10	<2	44	0.27	12
AR21	35	1	<.01	3	10	<2	<2	<1	27	<.01	<10	<10	5	<10	2	16.67	0.1	1.67
AR22	55	4	0.03	6	50	2	<2	<1	16	<.01	<10	<10	11	<10	2	16.5	0.11	1.83
AR23	15	<1	0.08	2	10	<2	<2	<1	17	<.01	<10	<10	4	<10	<2	14.5	0.14	2
AR25	145	4	<.01	16	50	2	2	1	19	0.02	<10	<10	19	<10	12	3.25	0.37	1.19
AR35	145	1	<.01	7	80	4	<2	1	11	<.01	<10	<10	4	<10	2	10.14	0.06	0.57
AR43	35	<1	<.01	1	30	<2	<2	<1	20	<.01	<10	<10	3	<10	2	28	0.11	3
AR51	70	4	<.01	9	50	2	<2	<1	44	<.01	<10	<10	14	<10	<2	12.11	0.13	1.56
ARLC4K1	<5	1	<.01	1	20	<2	<2	<1	5	<.01	<10	<10	8	<10	<2	30	0.27	8
ARLC4K2	20	<1	0.04	1	10	<2	<2	<1	15	<.01	<10	<10	2	<10	<2	39	0.05	2
ARLC4K3	55	<1	<.01	3	20	2	<2	<1	59	<.01	<10	<10	8	<10	<2	8	0.33	2.67
ARLC3SC	40	3	<.01	5	80	2	6	1	31	0.05	<10	<10	133	<10	6	36	0.74	26.6

Appendix IIIa: Distribution of Elements in Al Habalah I.

SAMPLE	Ag (ppm)	Al (%)	As (ppm)	Ba (ppm)	Be (ppm)	Bi (ppm)	Ca (%)	Cd (ppm)	Co (ppm)	Cr (ppm)	Cu (ppm)	Fe (%)	Ga (ppm)	Hg (ppb)	Hg (ppm)	K (%)	La (ppm)	Mg (%)
HA2	<.2	0.26	6	<10	<.5	<2	0.43	<.5	<1	75	<1	1.4	<10	<10	<0.01	<.01	160	0.03
HA9	<.2	0.14	2	<10	<.5	<2	0.1	<.5	<1	65	1	0.84	<10	<10	<0.01	<.01	10	0.01
HA13	<.2	0.22	6	<10	<.5	<2	0.37	<.5	1	44	3	0.84	<10	10	0.01	0.01	<10	0.04
HA14	<.2	0.23	6	10	<.5	<2	0.11	<.5	4	57	7	1.17	<10	30	0.03	<.01	<10	<.01
HA15	<.2	15	4	<10	<.5	2	0.25	<.5	1	83	4	0.82	<10	<10	<0.01	<.01	<10	0.01
HA18	<.2	0.13	<2	<10	<.5	<2	1.47	<.5	<1	34	3	2.75	<10	<10	<0.01	<.01	20	0.04
HA20	<.2	0.09	2	<10	<.5	<2	0.2	<.5	<1	47	4	0.23	<10	<10	<0.01	<.01	<10	0.01
HA23	<.2	0.04	2	<10	<.5	<2	0.06	<.5	<1	38	2	0.24	<10	<10	<0.01	<.01	<10	<.01
HA24	0.2	0.21	6	50	0.5	<2	0.06	<.5	4	41	11	12.2	<10	10	0.01	<.01	<10	<.01
HA25	<.2	0.09	4	<10	<.5	<2	3.33	<.5	<1	29	5	0.91	<10	<10	<0.01	<.01	<10	0.02
HA27	0.2	0.28	8	30	0.5	<2	0.09	<.5	7	68	9	14.2	<10	50	0.05	<.01	<10	0.01
HA28	<.2	0.06	<2	10	<.5	<2	15	<.5	<1	15	3	0.11	<10	<10	<0.01	<.01	<10	0.18
HA30	<.2	0.09	<2	10	<.5	2	15	<.5	<1	10	3	0.11	<10	20	0.02	<.01	<10	0.16
HA31	<.2	0.08	<2	10	<.5	<2	15	<.5	<1	16	7	1.12	<10	<10	<0.01	<.01	<10	0.14
HA35	0.2	0.14	<2	<10	<.5	<2	1.13	<.5	<1	54	4	0.75	<10	<10	<0.01	<.01	<10	0.12
HA36	<.2	0.35	<2	<10	<.5	<2	0.14	<.5	3	39	3	3.82	<10	10	0.01	0.01	30	0.05
HA38	<.2	0.24	2	10	<.5	<2	0.03	<.5	1	133	4	0.88	<10	10	0.01	0.01	<10	<.01
HA45	0.2	0.35	2	10	<.5	<2	0.06	<.5	3	87	8	1.33	<10	20	0.02	0.01	<10	0.03
HA47	<.2	0.19	6	10	<.5	<2	0.03	<.5	1	48	3	0.33	<10	<10	<0.01	<.01	<10	0.01
HA51	<.2	0.2	<2	<10	<.5	<2	2.09	<.5	1	48	4	3.59	<10	<10	<0.01	<.01	<10	0.04
HA52	<.2	0.24	2	<10	<.5	<2	0.05	<.5	<1	26	1	0.13	<10	30	0.03	<.01	10	<.01
HA56	<.2	0.22	2	<10	<.5	<2	0.07	<.5	<1	56	1	1.45	<10	<10	<0.01	<.01	10	<.01
HA59	<.2	0.22	6	<10	<.5	<2	0.06	<.5	2	61	3	0.35	<10	40	0.04	<.01	10	0.01
HA62	<.2	0.15	<2	<10	<.5	<2	0.18	<.5	<1	24	1	0.24	<10	<10	<0.01	<.01	<10	0.06
HA64	8.2	0.22	<2	<10	<.5	2	0.17	<.5	32	89	68	0.3	<10	20	0.02	<.01	<10	0.01
OUT5K	<.2	0.18	6	<10	<.5	<2	0.2	<.5	<1	26	1	0.31	<10	<10	<0.01	<.01	<10	0.01
OUT5I1	<.2	0.09	<2	10	0.5	<2	0.09	<.5	3	67	3	7.82	<10	<10	<0.01	<.01	<10	0.01
OUT5I2	0.2	0.11	<2	30	0.5	<2	0.42	<.5	3	105	3	9.6	<10	<10	<0.01	<.01	<10	0.03
OUT6C	<.2	0.24	2	10	<.5	<2	15	<.5	1	13	4	0.27	<10	10	0.01	<.01	<10	0.21
OUT6I	0.2	0.48	10	<10	1.5	<2	0.16	<.5	14	81	12	11.05	<10	40	0.04	<.01	<10	0.05

* = Caliche Samples

Appendix IIIa: Distribution of Elements in Al Habalah I Contd.

SAMPLE	Mn (ppm)	Mo (ppm)	Na (%)	Ni (ppm)	P (ppm)	Pb (ppm)	Sb (ppm)	Sc (ppm)	Sr (ppm)	Ti (%)	Tl (ppm)	U (ppm)	V (ppm)	W (ppm)	Zn(ppm)	Cr/Ni	V/Cr	V/Ni
HA2	10	2	0.07	4	220	<2	<2	1	44	<.01	<10	<10	14	<10	<2	18.75	0.19	3.5
HA9	10	<1	<.01	2	30	<2	<2	<1	5	<.01	<10	<10	12	<10	<2	32.5	0.18	6
HA13	25	<1	<.01	4	50	<2	8	1	10	<.01	<10	<10	10	<10	2	11	0.23	2.5
HA14	90	3	<.01	13	80	<2	2	1	5	<.01	<10	<10	13	<10	2	4.385	0.23	1
HA15	40	1	<.01	10	80	<2	<2	1	5	<.01	<10	<10	5	<10	2	8.3	0.06	0.5
HA18	30	4	<.01	4	90	2	<2	1	15	0.01	<10	<10	28	<10	2	8.5	0.82	7
HA20	5	1	<.01	3	10	<2	<2	<1	5	<.01	<10	<10	2	<10	<2	15.67	0.04	0.67
HA23	5	<1	<.01	3	10	<2	<2	<1	1	<.01	<10	<10	1	<10	<2	12.67	0.03	0.33
HA24	435	1	<.01	13	110	2	<2	3	4	0.03	<10	<10	58	<10	<2	3.154	1.41	4.46
HA25	50	1	<.01	5	10	<2	<2	<1	20	<.01	<10	<10	6	<10	2	5.8	0.21	1.2
HA27	285	<1	<.01	19	140	<2	<2	5	4	0.02	<10	<10	88	<10	6	3.579	1.29	4.63
HA28	10	<1	0.01	1	80	8	<2	<1	331	<.01	10	<10	2	10	<2	15	0.13	2
HA30	25	<1	<.01	<1	90	12	<2	<1	243	<.01	10	<10	3	10	<2	11.11	0.3	3.33
HA31	15	<1	<.01	3	90	8	<2	<1	225	<.01	<10	<10	10	10	<2	5.333	0.63	3.33
HA35	25	1	<.01	3	20	<2	2	<1	21	<.01	<10	<10	3	<10	2	18	0.06	1
HA36	45	<1	0.01	12	340	<2	2	3	10	0.01	<10	<10	23	<10	22	3.25	0.59	1.92
HA38	20	1	<.01	5	40	<2	<2	1	17	<.01	<10	<10	10	<10	6	26.6	0.08	2
HA45	45	1	<.01	13	70	2	<2	2	5	0.01	<10	<10	12	<10	6	6.692	0.14	0.92
HA47	130	<1	<.01	4	20	<2	<2	<1	2	<.01	<10	<10	9	<10	<2	12	0.19	2.25
HA51	35	3	<.01	10	40	2	<2	1	14	0.01	<10	<10	15	<10	2	4.8	0.31	1.5
HA52	10	<1	<.01	1	40	2	<2	<1	17	<.01	<10	<10	5	<10	<2	26	0.19	5
HA56	15	<1	<.01	2	40	<2	<2	<1	5	<.01	<10	<10	16	<10	<2	28	0.29	8
HA59	20	<1	0.01	4	30	<2	<2	<1	8	<.01	<10	<10	8	<10	<2	15.25	0.13	2
HA62	15	<1	<.01	2	30	<2	<2	<1	5	<.01	<10	<10	4	<10	<2	12	0.17	2
HA64	35	1	0.01	12	40	<2	<2	<1	12	<.01	<10	<10	3	<10	2	7.417	0.03	0.25
OUT5K	15	<1	0.01	2	20	<2	<2	<1	8	<.01	<10	<10	8	<10	<2	13	0.31	4
OUT5I1	80	<1	<.01	7	60	2	<2	<1	7	<.01	<10	<10	41	<10	2	9.571	0.61	5.86
OUT5I2	105	1	<.01	6	100	10	<2	2	14	0.01	<10	<10	77	<10	6	17.5	0.73	12.8
OUT6C	35	<1	0.03	4	90	12	<2	<1	342	<.01	10	<10	9	10	<2	3.25	0.69	2.25
OUT6I	130	<1	<.01	57	100	2	2	4	6	0.05	<10	<10	108	<10	18	1.421	1.33	1.89

Appendix IIIa: Distribution of Elements in Al Habalah II.

SAMPLE	Ag (ppm)	Al (%)	As (ppm)	Ba (ppm)	Be (ppm)	Bi (ppm)	Ca (%)	Cd (ppm)	Co (ppm)	Cr (ppm)	Cu (ppm)	Fe (%)	Ga (ppm)	Hg (ppb)	Hg (ppm)	K (%)	La (ppm)	Mg (%)
HAP1	<.2	0.21	2	30	<.5	2	0.2	<.5	3	103	7	0.72	<10	<10	<0.01	<.01	<10	0.26
HAP7	<.2	0.21	2	<10	<.5	<2	0.69	<.5	1	68	5	0.2	<10	<10	<0.01	<.01	<10	0.1
HAP9	2.6	0.12	<2	10	<.5	<2	0.53	<.5	12	120	27	0.32	<10	10	0.01	<.01	10	0.04
HAP10	<.2	0.11	<2	10	<.5	<2	1.62	<.5	1	80	6	0.25	<10	20	0.02	<.01	<10	0.06
HAP11	<.2	0.27	<2	<10	<.5	<2	0.03	<.5	1	111	4	0.19	<10	<10	<0.01	<.01	<10	<.01
HAP13	<.2	0.07	2	10	<.5	<2	0.19	<.5	1	61	6	0.24	<10	10	0.01	<.01	<10	0.02
HAP16	1.2	0.12	<2	<10	<.5	<2	0.24	<.5	6	60	13	0.27	<10	10	0.01	<.01	<10	0.01
HAP17	<.2	0.16	2	<10	<.5	<2	0.05	<.5	<1	41	3	0.09	<10	<10	<0.01	<.01	<10	0.01
HAP19	<.2	0.13	2	<10	<.5	<2	0.11	<.5	<1	22	1	0.08	<10	<10	<0.01	<.01	<10	0.01
HAP21	<.2	0.13	<2	<10	<.5	<2	0.08	<.5	<1	42	1	0.09	<10	<10	<0.01	<.01	<10	0.04
HAP23	<.2	0.15	<2	<10	<.5	<2	0.11	<.5	<1	38	1	0.08	<10	<10	<0.01	<.01	<10	0.01
HAP28	0.2	0.22	<2	<10	<.5	<2	0.11	<.5	4	66	8	2.27	<10	<10	<0.01	0.01	<10	<.03
HAP29	<.2	0.17	2	<10	<.5	<2	0.08	<.5	<1	39	3	0.09	<10	<10	<0.01	<.01	<10	0.01
HAP31	<.2	0.27	2	<10	<.5	<2	0.3	<.5	<1	80	2	2	<10	10	0.01	<.01	10	0.01
HAP33	<.2	0.15	<2	<10	<.5	<2	0.09	<.5	<1	26	1	0.14	<10	<10	<0.01	<.01	<10	0.01
HAP37	7.4	0.11	<2	10	<.5	<2	0.21	0.5	29	95	60	0.3	<10	20	0.02	<.01	<10	0.01
HAP40	9.4	0.15	<2	30	<.5	<2	0.37	0.5	39	58	75	0.32	<10	30	0.03	0.01	<10	0.03

Appendix IIIa: Distribution of Elements in Al Habalah II Contd.

SAMPLE	Mn (ppm)	Mo (ppm)	Na (%)	Ni (ppm)	P (ppm)	Pb (ppm)	Sb (ppm)	Sc (ppm)	Sr (ppm)	Ti (%)	Tl (ppm)	U (ppm)	V (ppm)	W (ppm)	Zn(ppm)	Cr/Ni	V/Cr	V/Ni
HAP1	75	1	<.01	9	110	2	<2	<1	8	>.01	<10	<10	13	<10	2	11.44	0.13	1.44
HAP7	25	2	<.01	5	80	<2	<2	<1	13	<.01	<10	<10	1	<10	2	13.6	0.01	0.2
HAP9	50	1	<.01	7	80	<2	<2	<1	9	<.01	<10	<10	1	<10	4	17.14	0.01	0.14
HAP10	35	1	<.01	6	70	<2	<2	<1	27	<.01	<10	<10	1	<10	2	13.33	0.01	0.17
HAP11	10	<1	<0.01	4	10	2	<2	<1	8	<.01	<10	<10	4	<10	<2	27.75	0.04	1
HAP13	40	2	<.01	4	100	<2	<2	<1	5	<.01	<10	<10	1	<10	2	15.25	0.02	0.25
HAP16	25	2	<.01	6	50	<2	<2	<1	6	<.01	<10	<10	4	<10	2	10	0.07	0.67
HAP17	15	<1	0.03	2	10	2	2	<1	10	<.01	<10	<10	3	<10	<2	20.5	0.07	1.5
HAP19	10	<1	<.01	1	10	<2	2	<1	5	<.01	<10	<10	4	<10	<2	22	0.18	4
HAP21	10	<1	0.01	2	<10	<2	<2	<1	5	<.01	<10	<10	2	<10	<2	21	0.05	1
HAP23	15	<1	<.01	1	20	<2	2	<1	8	<.01	<10	<10	5	<10	<2	38	0.13	5
HAP28	50	1	<.01	11	80	<2	<2	1	6	0.01	<10	<10	22	<10	4	6	0.33	2
HAP29	20	<1	<.01	3	40	<2	<2	<1	7	<.01	<10	<10	1	<10	<2	13	0.03	0.33
HAP31	<5	<1	0.02	3	50	6	2	1	26	<.01	<10	<10	56	<10	<2	26.67	0.7	18.7
HAP33	10	<1	0.01	1	10	<2	<2	<1	5	<.01	<10	<10	3	<10	<2	26	0.12	3
HAP37	30	1	<.01	10	170	<2	<2	<1	17	<.01	<10	<10	3	<10	<2	9.5	0.03	0.3
HAP40	50	1	<.01	12	50	2	<2	<1	11	<.01	<10	<10	7	<10	2	4.833	0.12	0.58

Appendix IIIa: Distribution of Elements in Al Soudah.

SAMPLE	Ag (ppm)	Al (%)	As (ppm)	Ba (ppm)	Be (ppm)	Bi (ppm)	Ca (%)	Cd (ppm)	Co (ppm)	Cr (ppm)	Cu (ppm)	Fe (%)	Ga (ppm)	Hg (ppb)	Hg (ppm)	K (%)	La (ppm)	Mg (%)
S1	<.2	0.16	16	<10	2.5	<2	0.03	<.5	3	79	6	9.91	<10	<10	<0.01	<.01	<10	<.01
S2	<.2	0.08	2	<10	<.5	<2	0.19	<.5	<1	64	3	0.57	<10	<10	<0.01	<.01	<10	0.03
S5	<.2	0.12	6	<10	0.5	<2	0.06	<.5	4	42	11	6.59	<10	10	0.01	<.01	10	0.01
S8	<.2	0.15	<2	<10	<.5	<2	0.08	<.5	<1	76	4	0.18	<10	10	0.01	<.01	<10	<.01
S12	3	0.15	16	30	0.5	<2	0.03	<.5	5	42	10	3.19	<10	30	0.03	<.01	<10	<.01
S13	4.2	0.19	<2	<10	<.5	6	0.05	<.5	2	31	6	2.37	<10	20	0.02	<01	10	0.01
S13B	<.2	0.09	<2	10	0.5	<2	0.64	<.5	2	52	6	6.52	<10	<10	<0.01	<.01	20	0.01
S15	<.2	0.31	<2	10	0.5	<2	0.1	<.5	4	64	2	7.84	<10	<10	<0.01	<.01	<10	0.01
S20	<.2	0.12	<2	10	2.5	<2	0.03	<.5	4	75	6	10.6	<10	<10	<0.01	<.01	<10	<.01
S26	<.2	0.2	8	30	0.5	<2	0.16	<.5	4	52	3	9.7	<10	10	0.01	<.01	<10	<.01
S28	<.2	0.16	<2	<10	0.5	<2	0.04	<.5	2	49	1	12.45	<10	10	0.01	<.01	<10	<.01
S30	0.2	0.18	<2	<10	0.5	<2	<.01	<.5	3	39	3	10.6	<10	<10	<0.01	<.01	<10	<.01
S39	0.2	0.08	<2	<10	0.5	<2	0.01	<.5	4	24	1	12.8	<10	10	0.01	<.01	<10	<.01

SAMPLE	Mn (ppm)	Mo (ppm)	Na (%)	Ni (ppm)	P (ppm)	Pb (ppm)	Sb (ppm)	Sc (ppm)	Sr (ppm)	Ti (%)	Tl (ppm)	U (ppm)	V (ppm)	W (ppm)	Zn(ppm)	Cr/Ni	V/Cr	V/Ni
S1	50	<1	<.01	7	250	2	<2	3	3	<.01	<10	<10	37	<10	10	11.29	0.47	5.29
S2	15	1	0.01	4	50	<2	<2	1	8	<.01	<10	<10	9	<10	<2	16	0.14	2.25
S5	110	<1	<.01	15	230	2	2	1	5	<.01	<10	<10	28	<10	10	2.8	0.67	1.87
S8	20	1	<.01	3	30	<2	<2	<1	3	<.01	<10	<10	1	<10	<2	25.33	0.01	0.33
S12	210	6	<.01	15	200	8	<2	1	3	0.01	<10	<10	16	<10	8	2.8	0.38	1.07
S13	25	1	<.01	10	150	2	<2	2	4	0.01	<10	<10	16	<10	4	3.1	0.52	1.6
S13B	105	3	<.01	7	120	2	<2	<1	7	<.01	<10	<10	10	<10	8	7.429	0.19	1.43
S15	180	<1	<.01	8	220	<2	<2	3	6	<.01	<10	<10	3	<10	10	8	0.05	0.38
S20	95	<1	<.01	13	120	<2	2	<1	3	<.01	<10	<10	13	<10	12	5.769	0.17	1
S26	185	11	<.01	8	510	18	2	1	7	<.01	<10	<10	28	<10	8	6.5	0.54	3.5
S28	25	<1	<.01	3	110	6	<2	3	4	<.01	<10	<10	82	<10	<2	16.33	1.67	27.3
S30	55	<1	<.01	5	80	<2	2	<1	1	<.01	<10	<10	10	<10	10	7.8	0.26	2
S39	140	<1	<.01	9	40	<2	<2	<1	<1	<.01	<10	<10	9	<10	10	2.667	0.38	1

Appendix IIIa: Distribution of Oxides in Ahad Rufaidah.

SAMPLE	Al_2O_3	CaO	Cr_2O_3	Fe_2O_3	K_2O	MgO	MnO	Na_2O	P_2O_5	SiO_2	TiO_2	LOI	TOTAL	Fe_2O_3/TiO_2	$Al_2O_3/(Al_2O_3+Fe_2O_3)$	K_2O/Na_2O	Fe_2O_3+MgO	Al_2O_3/TiO_2
AR3	3.14	0.3	0.01	18.6	0.04	0.12	0.2	0.03	0.05	72.5	0.08	3	98.93	232	0.144700461	1.3333	18.68	39.25
AR6	4.92	0.3	<.01	0.17	0.46	0.13	0	<.01	0.02	86.6	0.1	2.8	95.5	1.7	0.966601179	46	0.3	49.2
AR9A	3.16	0.5	0.01	12.8	0.22	0.07	1.6	0.04	0.24	75.5	0.21	3.8	98.09	60.90476	0.198119122	5.5	12.86	15.047619
AR15	2.09	0.3	<.01	19.5	0.11	0.04	0.1	<.01	0.03	73.9	0.11	3.5	99.58	177.2727	0.096804076	11	19.54	19
AR19	2.53	0.6	<.01	29	0.06	0.12	0	<.01	0.09	64.4	0.12	2.3	99.18	241.6667	0.08024104	6	29.12	21.083333
AR20	6.32	0.3	<.01	1.32	0.08	0.02	<.01	<.01	0.01	87.2	0.2	3.1	98.52	6.6	0.827225131	8	1.34	31.6
AR21	3.61	3.4	<.01	0.77	0.08	<.01	0	<.01	0.01	86.7	0.23	4.3	99.07	3.347826	0.824200913	8	0.78	15.695652
AR22	3.38	1	0.01	1.64	0.07	0.12	0	0.05	0.01	92	0.1	2.5	100.9	16.4	0.673306773	1.4	1.76	33.8
AR23	10.3	0.4	<.01	0.63	0.16	<.01	<.01	0.01	0.04	82.1	0.21	4.9	98.85	3	0.942570647	16	0.64	49.238095
AR25	3.56	2.7	0.01	4.7	0.04	0.34	0	0.04	0.01	84	0.42	4.2	100	11.19048	0.430992736	1	5.04	8.4761905
AR35	6.87	0.3	0.01	0.72	0.07	0.11	0	0.04	0.03	89	0.2	3.3	100.7	3.6	0.90513834	1.75	0.83	34.35
AR43	6.34	3.1	<.01	0.38	0.05	0.06	0	<.01	0.01	83.2	0.34	5.2	98.7	1.117647	0.943452381	5	0.44	18.647059
AR51	4.82	9.4	0.01	0.95	0.05	0.08	0	0.05	0.01	75	0.08	9.2	99.67	11.875	0.835355286	1	1.03	60.25
ARLC4K1	18.2	0.2	<.01	0.78	0.14	0.03	0	<.01	0.04	71.1	1.72	6.7	98.91	0.453488	0.95892575	14	0.81	10.587209
ARLC4K2	6.13	0.3	<.01	0.4	0.08	0.01	<.01	<.01	0.05	88.7	0.21	3.3	99.13	1.904762	0.938744257	8	0.41	29.190476
ARLC4K3	7.82	6.8	<.01	2.07	0.06	0.19	0	<.01	0.03	73.4	0.24	8.5	99.15	8.625	0.790697674	6	2.26	32.583333
ARLC3SC	16.7	2.8	0.03	19.8	0.09	0.11	0	0.03	0.01	50	0.98	8.8	99.45	20.22449	0.457877462	3	19.93	17.081633

Appendix IIIa: Distribution of Oxides in Ahad Rufaidah Contd.

SAMPLE	Al_2O_3/Na_2O	CIA	$CaO+Na_2O$	$CaO+Na_2O+K_2O$	Na_2O/K_2O	$100*(Al_2O_3/SiO_2)$	$100*(Fe_2O_3/SiO_2)$	$Al_2O_3/(100-SiO_2)$	$Fe_2O_3/(100-SiO_2)$	$CaO/(CaO+MgO)$
AR3	104.6667	88.95	0.35	0.39	0.75	4.33103448	25.6	0.114181818	0.674909091	0.727272727
AR6	492	86.63	0.32	0.78	0.02174	5.67932587	0.196236869	0.367988033	0.012715034	0.704545455
AR9A	79	81.23	0.51	0.73	0.18182	4.18709421	16.94713131	0.128821851	0.521402364	0.87037037
AR15	209	84.95	0.26	0.37	0.09091	2.82967777	26.40129976	0.079954093	0.745983168	0.862068966
AR19	253	79.06	0.61	0.67	0.16667	3.92979186	45.04504505	0.071027513	0.814149354	0.833333333
AR20	632	94.89	0.26	0.34	0.125	7.24853768	1.513935084	0.493364559	0.103044496	0.925925926
AR21	361	51.2	3.36	3.44	0.125	4.1623429	0.887812752	0.2720422	0.058025622	0.99702381
AR22	67.6	75.11	1.05	1.12	0.71429	3.67391304	1.782608696	0.4225	0.205	0.892857143
AR23	1034	94.43	0.45	0.61	0.0625	12.5928632	0.767263427	0.577976523	0.035215204	0.977777778
AR25	89	56.42	2.71	2.75	1	4.23809524	5.595238095	0.2225	0.29375	0.887043189
AR35	171.75	94.76	0.31	0.38	0.57143	7.71910112	0.808988764	0.624545455	0.065454545	0.710526316
AR43	634	66.59	3.13	3.18	0.2	7.61744563	0.456566142	0.378056052	0.022659511	0.981132075
AR51	96.4	33.66	9.45	9.5	1	6.42666667	1.266666667	0.1928	0.038	0.991561181
ARLC4K1	1821	98.27	0.18	0.32	0.07143	25.6118143	1.097046414	0.630103806	0.026989619	0.85
ARLC4K2	613	94.59	0.27	0.35	0.125	6.91483362	0.451212634	0.540088106	0.035242291	0.962962963
ARLC4K3	782	53.34	6.78	6.84	0.16667	10.6510488	2.81939526	0.29420617	0.077878104	0.972701149
ARLC3SC	558	85.02	2.86	2.95	0.33333	33.48	39.64	0.3348	0.3964	0.962585034

CIA (Chemical Index of Alteration) = $[Al_2O_3/(Al_2O_3+CaO+K_2O+Na_2O)]*100$

Appendix IIIa: **Distribution of Oxides in Al Habalah I.**

SAMPLE	Al_2O_3	CaO	Cr_2O_3	Fe_2O_3	K_2O	MgO	MnO	Na_2O	P_2O_5	SiO_2	TiO_2	LOI	TOTAL	Fe_2O_3/TiO_2	$Al_2O_3/(Al_2O_3+Fe_2O_3)$	K_2O/Na_2O	Fe_2O_3+MgO
HA2	19.9	0.67	<.01	2.44	0.2	0.03	<.01	0.01	0.38	64.9	1.09	8.42	98.03	2.238532	0.890925346	19	2.47
HA9	10.9	0.12	<.01	1.16	0.1	<.01	<.01	<.01	0.02	81.9	0.34	4.39	98.95	3.411765	0.904132231	7	1.17
HA13	14.7	0.5	<.01	1.44	0.3	0.04	0.01	<.01	0.03	75.4	0.13	6	98.58	11.07692	0.911001236	27	1.48
HA14	13.8	7.39	0.02	14.1	0.6	6.32	0.24	3.51	0.19	47.1	2.03	3.24	98.34	6.921182	0.494604317	0.1567	20.37
HA15	3.55	0.14	0.01	1.56	0.1	0.04	0.01	0.04	0.04	90.5	0.12	2.3	98.34	13	0.694716243	1.75	1.6
HA18	5.35	2.01	<.01	3.94	0	0.04	0.01	<.01	0.04	82.2	1.31	4.14	99.06	3.007634	0.575888052	4	3.98
HA20	3.68	0.28	<.01	0.33	0	<.01	<.01	<.01	<.01	92.9	0.13	1.73	99.11	2.538462	0.917705736	4	0.34
HA23	2.37	0.08	<.01	0.31	0	<.01	<.01	<.01	0.01	94.6	0.09	1.16	98.62	3.444444	0.884328358	4	0.32
HA24	4.81	0.11	<.01	21.5	0.1	<.01	0.07	<.01	0.04	68.5	0.34	3.64	99.04	63.20588	0.182889734	5	21.5
HA25	4.41	4.53	<.01	1.32	0.1	<.01	0.01	<.01	0.01	83.3	0.14	5.41	99.18	9.428571	0.769633508	7	1.33
HA27	2.46	0.16	<.01	25.6	0	0.01	0.05	<.01	0.04	66.9	0.17	3.73	99.14	150.2941	0.087825777	3	25.56
HA35	4.25	1.45	<.01	1.1	0.1	0.14	0.01	<.01	0.01	88.6	0.11	2.98	98.75	10	0.794392523	6	1.24
HA36	22.5	0.2	<.01	5.85	0.1	0.1	0.01	<.01	0.12	59.8	0.44	9.64	98.77	13.29545	0.793941529	7	5.95
HA38	6.15	0.04	0.01	1.24	0.2	0.03	0.01	0.04	0.05	89.4	0.17	3.22	100.6	7.294118	0.832205683	6	1.27
HA45	5.5	0.08	0.01	1	0.1	0.09	0.01	0.04	0.01	90	0.11	2.06	100.6	9.090909	0.846153846	1.75	1.09
HA47	6.1	0.06	<.01	0.48	0	<.01	0.03	<.01	0.01	89.8	0.23	2.44	99.15	2.086957	0.927051672	4	0.49
HA51	3.68	2.85	<.01	5.24	0	<.01	0.01	<.01	<.01	79.6	0.23	7.41	99.07	22.78261	0.412556054	4	5.25
HA52	32.3	0.07	<.01	0.6	0.1	0.04	<.01	<.01	0.13	52.1	1.39	11.8	98.55	0.431655	0.981762918	10	0.64
HA56	9.48	0.11	<.01	2.04	0.1	0.01	<.01	<.01	0.02	82.7	0.66	3.75	98.78	3.090909	0.822916667	6	2.05
HA59	19	0.11	<.01	0.78	0.1	0.03	0.01	<.01	0.09	69.9	1.28	7.36	98.7	0.609375	0.960645812	8	0.81
HA62	12.8	0.27	<.01	0.48	0.1	0.12	<.01	<.01	0.03	79.3	0.42	5.35	98.84	1.142857	0.963773585	6	0.6
HA64	7.1	0.2	0.01	0.46	0.1	0.05	0.01	0.05	0.01	86.6	0.19	3.86	98.59	2.421053	0.939153439	1.2	0.51
OUT5K	19	0.28	<.01	0.58	0.1	0.01	0.01	0.01	0.04	71.3	0.55	7.39	99.25	1.054545	0.970332481	9	0.59
OUT5I1	0.94	0.15	<.01	16.5	0	<.01	0.02	<.01	<.01	79.8	0.04	1.54	98.96	411.5	0.054022989	3	16.47
OUT5I2	1.14	0.67	<.01	16.4	0	0.04	0.03	<.01	0.03	79	0.1	1.69	99.15	164	0.064994299	4	16.44
OUT6I	11.6	0.24	<.01	16.6	0.1	0.07	0.03	<.01	0.05	63.7	0.48	6.82	99.57	34.47917	0.411450925	5	16.62
*HA28	1.53	37.9	<.01	0.22	0	0.25	<.01	<.01	0.03	27.9	0.03	31.1	98.98	7.333333	0.874285714	3	0.47
*HA30	0.81	45.9	<.01	0.19	0	0.21	<.01	<.01	0.03	15.5	0.03	36.7	99.41	6.333333	0.81	4	0.4
*HA31	0.85	42.4	<.01	2.19	0	0.18	<.01	<.01	0.05	20.1	0.03	33.8	99.6	73	0.279605263	3	2.37
*OUT6C	5.64	43.1	<.01	0.48	0.1	0.26	<.01	<.01	0.04	13.5	0.18	36.1	99.32	2.666667	0.921568627	6	0.74

Appendix IIIa: Distribution Oxides in Al Habalah I Contd.

SAMPLE	Al_2O_3/TiO_2	Al_2O_3/Na_2O	CIA	$CaO+Na_2O$	$CaO+Na_2O+K_2O$	Na_2O/K_2O	$Al_2O_3/(100-SiO_2)$	$Fe_2O_3(100-SiO_2)$	$100*(Al_2O_3/SiO_2)$	$100*(Fe_2O_3/SiO_2)$	$CaO/(CaO+MgO)$
HA2	18.2844	1993	95.8	0.68	0.87	0.05263	0.567321378	0.069456305	30.72298443	3.761368892	0.957142857
HA9	32.1765	1094	98.2	0.13	0.2	0.14286	0.604754008	0.064123825	13.35612257	1.4161885	0.923076923
HA13	113.385	1474	95	0.51	0.78	0.03704	0.599674532	0.058584215	19.54388756	1.909307876	0.925925926
HA14	6.7734	3.917379	54.6	10.9	11.45	6.38182	0.259678942	0.265344665	29.22422954	29.8618491	0.539022611
HA15	29.5833	88.75	93.4	0.18	0.25	0.57143	0.37250787	0.163693599	3.923952691	1.724328507	0.777777778
HA18	4.08397	535	72.2	2.02	2.06	0.25	0.300224467	0.221099888	6.510099781	4.794353857	0.980487805
HA20	28.3077	368	91.8	0.29	0.33	0.25	0.519774011	0.046610169	3.96039604	0.35514421	0.965517241
HA23	26.3333	237	94.8	0.09	0.13	0.25	0.435661765	0.056985294	2.506345178	0.327834179	0.888888889
HA24	14.1471	481	96.6	0.12	0.17	0.2	0.152649952	0.682005712	7.022923054	31.37684333	0.916666667
HA25	31.5	441	48.9	4.54	4.61	0.14286	0.263755981	0.078947368	5.295389049	1.585014409	0.997797357
HA27	14.4706	246	92.5	0.17	0.2	0.33333	0.074410163	0.772837266	3.674932776	38.16850911	0.995772663
HA35	38.6364	425	73.7	1.46	1.52	0.16667	0.374119718	0.096830986	4.79467509	1.240974729	0.911949686
HA36	51.2273	2254	98.8	0.21	0.28	0.14286	0.560696517	0.145522388	37.69230769	9.782608696	0.666666667
HA38	36.1765	153.75	95.1	0.08	0.32	0.16667	0.579096045	0.116760829	6.880733945	1.387334974	0.571428571
HA45	50	137.5	96.7	0.12	0.19	0.57143	0.55	0.1	6.111111111	1.111111111	0.470588235
HA47	26.5217	610	98.2	0.07	0.11	0.25	0.595703125	0.046875	6.795900178	0.534759358	0.857142857
HA51	16	368	55.9	2.86	2.9	0.25	0.180480628	0.25698872	4.622534857	6.582087677	0.996503497
HA52	23.2374	3230	99.4	0.08	0.18	0.1	0.674321503	0.012526096	61.99616123	1.151631478	0.636363636
HA56	14.3636	948	98.1	0.12	0.18	0.16667	0.546397695	0.117579251	11.47005445	2.468239564	0.916666667
HA59	14.875	1904	99	0.12	0.2	0.125	0.632978723	0.025930851	27.23112128	1.115560641	0.785714286
HA62	30.4048	1277	97.4	0.28	0.34	0.16667	0.618102614	0.023233301	16.09528611	0.604991177	0.692307692
HA64	37.3684	142	95.8	0.25	0.31	0.83333	0.529850746	0.034328358	8.198614319	0.531177829	0.8
OUT5K	34.4909	1897	19.4	0.29	0.38	0.11111	0.661436541	0.020223152	26.59842961	0.813236119	0.965517241
OUT5I1	23.5	94	83.2	0.16	0.19	0.33333	0.046488625	0.8140455	1.17824016	20.63173728	0.9375
OUT5I2	11.4	114	61.3	0.68	0.72	0.25	0.054311577	0.78132444	1.442855335	20.75686622	0.943661972
OUT6I	24.1042	1157	97.5	0.25	0.3	0.2	0.318820612	0.456048498	18.16041438	25.97708366	0.774193548
*HA28	51	153	3.87	37.89	37.92	0.33333	0.021226415	0.003052164	5.479942693	0.787965616	Not computed
*HA30	27	81	1.73	45.92	45.96	0.25	0.009585799	0.002248521	5.225806452	1.225806452	Not computed
*HA31	28.3333	85	1.96	42.41	42.44	0.33333	0.010636967	0.027405832	4.230960677	10.90094574	Not computed
*OUT6C	31.3333	564	11.6	43.1	43.16	0.16667	0.06518724	0.00554785	41.83976261	3.560830861	Not computed

* = Caliche Samples

Appendix IIIa: Distribution of Oxides in Al Habalah II.

SAMPLE	Al_2O_3	CaO	Cr_2O_3	Fe_2O_3	K_2O	MgO	MnO	Na_2O	P_2O_5	SiO_2	TiO_2	LOI	TOTAL	Fe_2O_3/TiO_2	$Al_2O_3/(Al_2O_3+Fe_2O_3)$	K_2O/Na_2O	Fe_2O_3+MgO	Al_2O_3/TiO_2
HAP1	3.59	0.25	0.01	1	0.07	0.41	0.01	0.03	0.02	91.5	0.09	2.3	99.2	11.111111	0.782135076	2.33333	1.41	39.8889
HAP7	8.34	0.92	0.01	0.36	0.07	0.16	0.01	0.04	0.01	83	0.17	4.96	98.03	2.1176471	0.95862069	1.75	0.52	49.0588
HAP9	1.6	0.67	0.01	0.44	0.06	0.06	0.04	0.04	0.01	93.3	0.05	2.19	98.48	8.8	0.784313725	1.5	0.5	32
HAP10	2.91	2.03	0.01	0.38	0.06	0.1	0.01	0.06	0.01	88	0.15	4.45	98.15	2.5333333	0.88449848	1	0.48	19.4
HAP11	8.53	0.03	0.02	0.37	0.09	0.03	0.01	0.05	0.01	85.5	0.56	3.4	98.61	0.6607143	0.958426966	1.8	0.4	15.2321
HAP13	1.67	0.21	0.01	0.32	0.05	0.03	0.01	0.03	0.01	94	0.05	1.52	97.9	6.4	0.83919598	1.66667	0.35	33.4
HAP16	2.99	0.28	0.01	0.42	0.05	0.05	0.01	0.03	0.01	92	0.22	2.22	93.3	1.9090909	0.876832845	1.66667	0.47	13.5909
HAP17	10.5	0.08	<.01	0.27	0.07	<.01	0.01	<.01	0.05	82.9	0.93	4.21	99.06	0.2903226	0.974953618	7	0.28	11.3011
HAP19	14.9	0.16	<.01	0.27	0.08	<.01	<.01	<.01	0.03	76.8	0.97	5.73	98.98	0.2783505	0.982248521	8	0.28	15.4021
HAP21	6.03	0.11	<.01	0.18	0.05	0.04	<.01	<.01	0.04	89.7	0.37	2.6	99.08	0.4864865	0.971014493	5	0.22	16.2973
HAP23	12.2	0.16	<.01	0.21	0.08	<.01	<.01	<.01	0.04	80.9	0.99	4.69	99.18	0.2121212	0.983023444	8	0.22	12.2828
HAP28	3.03	0.14	0.01	3.17	0.08	0.08	0.02	0.05	0.01	90	0.25	2	98.79	12.68	0.488709677	1.6	3.25	12.12
HAP29	7.36	0.11	<.01	0.18	0.05	<.01	<.01	<.01	0.04	88	0.18	3.07	98.99	1	0.976127321	5	0.19	40.8889
HAP31	33.2	0.46	<.01	3.46	0.32	0.09	0.01	<.01	0.17	46.4	1.81	12.7	98.68	1.9116022	0.905722071	32	3.55	18.3646
HAP33	14.3	0.15	<.01	0.33	0.09	<.01	<.01	<.01	0.03	78.4	0.27	5.65	99.25	1.2222222	0.977428181	9	0.34	52.9259
HAP37	3.24	0.23	0.01	0.42	0.06	0.03	0.01	0.04	0.03	91.7	0.34	2.33	98.43	1.2352941	0.885245902	1.5	0.45	9.52941
HAP40	5.82	0.41	0.01	0.45	0.06	0.06	0.01	0.04	0.01	87.5	0.11	4.06	98.51	4.0909091	0.928229665	1.5	0.51	52.9091

Appendix IIIa: Distribution of Oxides in Al Habalah II Contd.

SAMPLE	Al_2O_3/Na_2O	CIA	$CaO+Na_2O$	$CaO+Na_2O+K_2O$	Na_2O/K_2O	$Al_2O_3/(100-SiO_2)$	$Fe_2O_3/(100-SiO_2)$	$100*(Al_2O_3/SiO_2)$	$100*(Fe_2O_3/SiO_2)$	$CaO/(CaO+MgO)$
HAP1	119.667	91.11	0.28	0.35	0.42857	0.422352941	0.117647059	3.923497268	1.092896175	0.378787879
HAP7	208.5	89.01	0.96	1.03	0.57143	0.490588235	0.021176471	10.04819277	0.43373494	0.851851852
HAP9	40	67.51	0.71	0.77	0.66667	0.23916293	0.065769806	1.714714393	0.471546458	0.917808219
HAP10	48.5	57.51	2.09	2.15	1	0.2425	0.031666667	3.306818182	0.431818182	0.953051643
HAP11	170.6	98.05	0.08	0.17	0.55556	0.589088398	0.025552486	9.974275023	0.432647334	0.5
HAP13	55.6667	85.2	0.24	0.29	0.6	0.278333333	0.053333333	1.776595745	0.340425532	0.875
HAP16	99.6667	89.25	0.31	0.36	0.6	0.375156838	0.052697616	3.248940563	0.456372922	0.848484848
HAP17	1051	98.5	0.09	0.16	0.14286	0.615700059	0.015817223	12.67333896	0.325575787	0.888888889
HAP19	1494	98.35	0.17	0.25	0.125	0.643965517	0.011637931	19.453125	0.3515625	0.941176471
HAP21	603	97.26	0.12	0.17	0.2	0.583172147	0.017408124	6.725407093	0.200758421	0.733333333
HAP23	1216	97.98	0.17	0.25	0.125	0.634986945	0.010966057	15.0401979	0.25974026	0.941176471
HAP28	60.6	91.81	0.19	0.27	0.625	0.301492537	0.315422886	3.368538077	3.5241801	0.636363636
HAP29	736	97.74	0.12	0.17	0.2	0.613333333	0.015	8.363636364	0.204545455	0.916666667
HAP31	3324	97.67	0.47	0.79	0.03125	0.620264975	0.064564284	71.62249515	7.455289808	0.836363636
HAP33	1429	98.28	0.16	0.25	0.11111	0.662801484	0.015306122	18.21774605	0.420703723	0.9375
HAP37	81	90.75	0.27	0.33	0.66667	0.390361446	0.05060241	3.533260632	0.458015267	0.884615385
HAP40	145.5	91.94	0.45	0.51	0.66667	0.4656	0.036	6.651428571	0.514285714	0.872340426

Appendix IIIa: Distribution of Oxides in Al Soudah.

SAMPLE	Al_2O_3	CaO	Cr_2O_3	Fe_2O_3	K_2O	MgO	MnO	Na_2O	P_2O_5	SiO_2	TiO_2	LOI	TOTAL	Fe_2O_3/TiO_2	$Al_2O_3/(Al_2O_3+Fe_2O_3)$	K_2O/Na_2O	Fe_2O_3+MgO
S1	0.95	0.06	<.01	24.99	0.03	<.01	0.01	<.01	0.1	69.99	0.06	2.98	99.17	416.5	0.036622976	3	24.99
S2	1.52	0.2	0.01	0.01	0.1	0.06	0.02	0.04	0.01	94	0.34	1.22	98.31	0.02941	0.993464052	2.5	0.07
S5	0.57	0.11	<.01	15.81	0.03	<.01	0.03	<.01	0.1	80.14	0.09	2.27	99.15	175.667	0.034798535	3	15.82
S8	5.27	0.1	0.01	0.34	0.06	0.01	0.04	0.04	0.01	89.6	0.12	3.06	98.65	2.83333	0.939393939	1.5	0.35
S12	3.1	0.02	0.01	4.1	0.06	0.02	0.07	0.04	0.04	89.5	0.06	2.06	99.15	68.3333	0.430555556	1.5	4.12
S13	15.72	0.05	0.01	3.3	0.07	0.05	0.01	0.03	0.04	71.5	0.68	6.67	98.11	4.85294	0.826498423	2.3333	3.35
S13B	1.08	0.96	<.01	17.09	0.03	<.01	0.03	<.01	0.08	76.65	0.21	3.07	99.2	81.381	0.059438635	3	17.1
S15	2.14	0.17	<.01	12.54	0.06	0.01	0.03	<.01	0.07	81.43	0.07	2.78	99.3	179.143	0.145776567	6	12.55
S20	0.69	0.06	<.01	22.02	0.03	<.01	0.02	<.01	0.03	73.28	0.09	2.9	99.12	244.667	0.030383091	3	22.03
S26	2.31	0.25	<.01	17.44	0.04	<.01	0.04	<.01	0.17	77.03	0.09	2.27	99.64	193.778	0.116962025	4	17.45
S28	1.58	0.08	<.01	23.18	0.04	<.01	0.01	<.01	0.05	72.52	0.06	1.74	99.26	386.333	0.063812601	4	23.19
S30	1.33	0.03	<.01	21.57	0.03	<.01	0.01	<.01	0.04	73.22	0.09	2.91	99.23	239.667	0.058078603	3	21.58
S39	0.39	0.04	<.01	25.87	0.02	<.01	0.03	<.01	0.03	69.35	0.05	3.34	99.12	517.4	0.014851485	2	25.88

SAMPLE	Al_2O_3/TiO_2	Al_2O_3/Na_2O	CIA	$CaO+Na_2O$	$CaO+Na_2O+K_2O$	Na_2O/K_2O	$Fe_2O_3/(100-SiO_2)$	$Al_2O_3/(100-SiO_2)$	$100*(Al_2O_3/SiO_2)$	$100*(Fe_2O_3/SiO_2)$	$CaO/(CaO+MgO)$
S1	15.833333	95	91.26	0.06	0.09	0.3333	0.832722426	0.031656115	1.357336762	35.70510073	0.857142857
S2	4.4705882	38	81.72	0.24	0.34	0.4	0.001666667	0.253333333	1.617021277	0.010638298	0.769230769
S5	6.3333333	57	78.17	0.12	0.15	0.3333	0.796072508	0.028700906	0.711255303	19.72797604	0.916666667
S8	43.916667	131.75	96.34	0.14	0.2	0.6667	0.032692308	0.506730769	5.881696429	0.379464286	0.909090909
S12	51.666667	77.5	96.27	0.06	0.12	0.6667	0.39047619	0.295238095	3.463687151	4.581005587	0.5
S13	23.117647	524	99.05	0.08	0.15	0.4286	0.115789474	0.551578947	21.98601399	4.615384615	0.5
S13B	5.1428571	108	51.92	0.97	1	0.3333	0.731905782	0.046252677	1.409001957	22.29615134	0.989690722
S15	30.571429	214	89.91	0.18	0.24	0.1667	0.675282714	0.115239634	2.62802407	15.39972983	0.944444444
S20	7.6666667	69	87.34	0.07	0.1	0.3333	0.824101796	0.025823353	0.941593886	30.04912664	0.857142857
S26	25.666667	231	88.51	0.26	0.3	0.25	0.759251197	0.100565956	2.998831624	22.64052966	0.961538462
S28	26.333333	158	92.39	0.09	0.13	0.25	0.843522562	0.057496361	2.178709322	31.96359625	0.888888889
S30	14.777778	133	95	0.04	0.07	0.3333	0.80545183	0.049663928	1.816443595	29.45916416	0.75
S39	7.8	39	84.78	0.05	0.07	0.5	0.844045677	0.012724307	0.562364816	37.3035328	0.8

Appendix IIIb: Ahad Rufaidah

	Factor 1	Factor 2	Factor 3
AG	0.706876	0.267662	-0.134
AL	-0.82178	-0.06411	-0.02919
AS	-0.21688	0.137767	0.586394
BA	0.003142	-0.92225	0.117248
BE	0.779427	0.262873	0.036857
BI	0.733653	-0.33324	0.081007
CA	0.015881	0.024429	-0.24115
CD	-0.14094	0.015831	0.015552
CO	0.879196	0.023019	0.079723
CR	-0.64446	0.05756	-0.48618
CU	-0.48559	0.232088	0.719917
FE	-0.80317	-0.10628	-0.14863
HG	0.799858	0.068384	-0.02168
K	0.006351	-0.83697	0.076147
LA	-0.05098	0.035915	-0.28
MG	-0.03825	0.099473	-0.42279
MN	-0.43778	0.134368	0.001335
MO	0.629736	-0.04681	-0.04161
NA	0.545181	0.115242	0.032374
NI	-0.77681	-0.10765	0.130192
P	-0.29863	-0.89447	0.031316
PB	0.691815	0.150937	0.1683
SB	0.527936	-0.25763	0.532605
SC	0.800708	-0.33508	0.084814
SR	-0.07331	-0.83445	-0.20258
TI	-0.46536	0.123763	-0.65447
U	0.422781	-0.21299	-0.69054
V	-0.4801	0.071382	-0.6249
ZN	0.522142	0.13525	0.041669
Expl.Var	8.981302	3.738668	3.167596
Prp.Totl	0.3097	0.12892	0.109227

Eigenevalues

Factor	Eigenval	% Variance	Cum. Eigenval	Cumul %
1	9.089229	31.34217	9.089229	31.34
2	3.740833	12.89943	12.83006	44.32
3	3.098543	10.68463	15.9286	55.00

Oxides in Ahad Rufaidah

	Factor 1	factor 2	Factor 3
AL2O3	0.978049	0.118568	-0.01991
CAO	0.01161	-0.03496	-0.92746
CR2O3	0.063026	0.240497	0.138379
FE2O3	-0.05901	-0.87572	0.216628
K2O	0.075657	0.117694	0.523079
MGO	0.023424	0.531257	0.029514

MNO	0.021612	0.60136	0.298323
NA2O	-0.01748	0.007816	0.039098
P2O5	-0.09228	-0.39501	0.537952
SIO2	-0.54093	0.752457	0.130019
TIO2	0.913894	-0.07166	0.046585
LOI	0.61765	-0.0771	-0.70083
Expl.Var	2.489031	2.23108	2.091306
Prp.Totl	0.207419	0.185923	0.174275

Eigenevalues

Factor	Eigenval	% Variance	Cum. Eigenval	% Cum.
1	3.004503	25.03752	3.004503	25.03
2	2.4565	20.47083	5.461003	45.5
3	1.946217	16.21847	7.407219	61.76

Habalah I

	Factor 1	Factor 2	Factor 3
AG	0.678183	0.058308	-0.10856
AL	0.193179	-0.04418	0.013998
AS	0.03219	0.40769	-0.05071
BA	0.258147	-0.58808	-0.01758
BE	0.909107	0.035146	-0.00584
BI	-0.25291	-0.31384	-0.07657
CA	0.18257	0.933132	0.04744
CO	0.493586	0.034616	0.035737
CR	-0.26878	-0.45394	0.222838
CU	0.057113	-0.13603	0.883324
FE	-0.94945	-0.07946	0.039191
HG	0.387948	-0.20136	0.058355
LA	-0.12108	0.205154	0.602054
MG	0.127916	0.892687	0.072892
MN	-0.80746	-0.05409	0.036135
MO	-0.0282	0.269719	-0.38915
NA	0.112863	-0.00815	0.908048
NI	-0.29294	0.515697	-0.03112
P	-0.33009	0.159127	0.44959
PB	0.409042	-0.54939	0.076016
SB	0.22624	0.062797	0.096787
SC	0.489573	0.195426	-0.30384
SR	0.170897	0.920669	0.122057
TI	-0.78261	-0.00487	0.007855
TL	-0.13861	-0.88947	-0.04761
V	-0.94009	-0.07063	0.029969
W	-0.15941	-0.94067	-0.04492
ZN_PPM_	0.266938	0.189025	0.041164
Expl.Var	5.850629	5.874839	2.536627
Prp.Totl	0.208951	0.209816	0.090594

Eigenvalues				
Factor	Eigenval	% Variance	Cum. Eigenval	Cumul.%
1	7.173113	25.61826	7.173113	25.62
2	5.224806	18.66002	12.39792	44.28
3	2.760569	9.859174	15.15849	54.13

Oxides in Al Habalah I

	Factor 1	Factor 2	Factor 3
AL2O3	-0.13117	0.055281	-0.88422
CAO	0.934053	0.053183	0.249996
CR2O3	0.131547	0.931667	-0.0455
FE2O3	-0.04526	0.155473	0.007721
K2O	0.002464	-0.50099	-0.55385
MGO	-0.47508	0.445744	0.422125
MNO	0.418017	0.344353	-0.03996
NA2O	0.14475	0.888959	0.143667
P2O5	-0.32941	0.322891	0.390117
SIO2	-0.95368	-0.12657	0.150184
TIO2	-0.05397	-0.06604	-0.87607
LOI	0.940646	0.131931	0.107854
Expl.Var	3.236159	2.398613	2.307515
Prp.Totl	0.26968	0.199884	0.192293

Eigenvalues

Factor	Eigenval	% Variance	Cum. Eigenval	Cum. %
1	3.62296	30.19133	3.62296	30.19
2	2.882197	24.01831	6.505157	54.20
3	1.636891	13.64076	8.142048	67.84

Habalah II

	Factor 1	Factor 2	Fcator 3
Ag	-0.29296	-0.12362	0.837044
Al	-0.04408	0.74614	0.256692
As	0.034505	-0.19383	-0.62963
Ba	-0.62698	0.19731	0.235976
Bi	-0.64317	-0.2373	-0.45778
Ca	0.333054	-0.20418	0.103021
Cd	-0.17811	0.020002	0.722407
Co	-0.81027	0.020761	0.166786
Cr	0.622477	0.31284	-0.10234
Cu	0.302964	-0.01191	-0.77035
Fe	0.071275	0.866851	-0.1282
Hg	-0.21927	-0.03518	0.470889
La	0.113934	-0.50594	0.02159
Mg	0.748315	0.11872	0.508175
Mn	0.37757	0.758391	0.022379

Mo	-0.81148	0.04758	0.343149
Na	-0.52043	0.262905	0.234711
Ni	0.71067	0.270074	-0.56548
P	0.625187	0.011206	-0.28006
Pb	-0.07208	-0.55826	-0.16983
Sb	0.652326	-0.25941	-0.28761
Sc	0.154525	-0.83919	0.12617
Sr	0.023285	0.312147	0.030007
V	-0.17129	0.906187	0.052466
Zn	-0.76012	0.015703	0.100177
Expl.Var	5.83037	4.58974	3.802037
Prp.Totl	0.233215	0.18359	0.152081

Eigenvalues (elements)

Factor	Eigenval	Variance (%)	Cum. Eigenval	Cumul. %
1	7.262701	29.0508	7.262701	29.05
2	4.815691	19.26276	12.07839	48.31
3	2.981909	11.92764	15.0603	60.23

Oxides data in Al Habalah II

	Factor 1	Factor 2
Al_2O_3	0.930851	0.312302
CaO	0.00922	-0.47382
CR_2O_3	0.429823	0.880723
Fe_2O_3	0.697405	-0.38123
K_2O	0.984152	-0.09759
MgO	0.022378	0.898092
MnO	-0.05408	0.899878
Na_2O	0.429837	0.880706
P_2O_5	0.934306	0.170646
SiO_2	-0.969	-0.17182
TiO_2	0.862131	0.314243
LOI	0.94026	0.127036
Expl.Var	6.13367	3.818094
Prp.Totl	0.511139	0.318175

Eigenevalues

Factor		% total	Cumul.	Cumul.
	Eigenval	Variance	Eigenval	%
1	6.769025	56.40854	6.769025	56.40854
2	3.18274	26.52283	9.951765	82.93137

Al Soudah

	Factor 1	Factor 2	Factor 3
Ag	-0.20599	-0.4541	0.6356076
Al	0.31771	-0.15354	0.3509009
As	0.014893	0.711296	0.0032634
Ba	-0.6	0.011811	-0.4871632
Be	-0.75641	0.016072	-0.2288845
Bi	0.053944	0.035779	0.6261241
Ca	0.023122	-0.0218	0.1701893
Co	-0.83268	0.046793	0.1954498
Cr	-0.29169	-0.24176	0.736472
Cu	0.330001	-0.4488	-0.3390282
Fe	0.477738	0.200205	0.1523128
Hg	0.010397	0.196687	0.6350644
La	-0.18221	0.195027	0.5536757
Mg	-0.64117	-0.09561	0.1695548
Mn	0.779409	-0.03444	0.1571613
Mo	0.323629	0.201907	0.2130779
Na	0.279406	0.113684	0.5578514
Ni	0.684277	-0.17383	-0.3135911
P	0.523246	-0.64266	0.145282
Pb	-0.26056	0.700949	0.441984
Sb	-0.39687	0.105178	-0.0824207
Sc	-0.00167	0.789739	0.0658181
Sr	0.087482	0.602869	-0.2782079
V	-0.07988	-0.51774	-0.1198526
Zn	-0.87569	-0.07973	0.1737638
Expl.Var	5.177734	3.387925	3.5243737
Prp.Totl	0.207109	0.135517	0.1409749

Eigenevalues

Factor	Eigenval	Variance (%)	% Eigenval	Cum. %
1	5.390402	21.56161	5.3904019	21.56
2	3.830683	15.32273	9.2210847	36.88
3	3.30907	13.23628	12.530154	50.11
4	2.662634	10.65054	15.192789	60.76

Oxides in Al Soudah

	Factor 1	Factor 2	Factor 3
AL_2O_3	-0.39341	-0.87102	-0.0665873
CaO	0.047742	-0.01439	0.8131811
Cr_2O_3	0.911086	0.242628	0.2347934
Fe_2O_3	0.972391	0.174571	0.0061776
K_2O	-0.87155	-0.15185	-0.1456297
MgO	0.894737	0.176545	0.1942506
MnO	-0.46454	0.519081	0.3029422
Na_2O	0.911075	0.242678	0.2347912
P_2O_5	0.316148	0.093256	0.7540773
SiO_2	-0.86329	0.454291	0.0254611
TiO_2	-0.39043	-0.86799	0.0348933
LOI	0.026466	-0.9244	-0.0264471
Expl.Var	5.537046	3.05381	1.4979034
Prp.Totl	0.46142	0.254484	0.1248253

Eigenvalues

Factor	Eigenval	Variance	Eigenval	Cum. %
1	6.063978	50.53315	6.063978	50.53
2	2.743713	22.86427	8.8076909	73.39
3	1.281068	10.67557	10.088759	84.06

APPENDIX IV

Factor Loadings for Q-mode Analysis : **Geochemical Data**

Oxides Data

	Factor 1	Factor 2	Factor 3	Factor 4
AR3	0.145381	0.867943	0.094885	0.15928
AR6	0.432635	0.3183	0.321106	0.65244
AR9A	0.147776	0.873628	0.112285	0.15053
AR15	0.425037	0.29355	0.309199	0.67982
AR19	0.418639	0.26122	0.300878	0.69408
AR20	0.278069	0.247541	0.733815	0.36447
AR21	0.795874	0.232001	0.195896	0.30964
AR22	0.167305	0.875313	0.115318	0.14201
AR23	0.521917	0.322023	0.557909	-0.2259
AR25	0.157441	0.876941	0.111964	0.14761
AR35	0.161849	0.876403	0.11555	0.14422
AR43	0.424984	0.318809	0.323047	0.66028
AR51	0.131862	0.873294	0.117373	0.15491
ARLC4K1	0.413552	0.285891	0.324395	0.683
ARLC4K2	0.278695	0.253285	0.73192	0.36315
ARLC4K3	0.416513	0.292177	0.326603	0.68021
ARLC3SC	0.084843	0.837446	0.081067	0.17953
HA2	0.101703	0.378174	0.729395	0.0936
HA9	0.650977	0.15123	0.615479	0.05817
HA13	0.418964	0.297624	0.323761	0.67576
HA14	0.14442	0.828003	0.092884	0.1634
HA15	0.168348	0.875121	0.115137	0.14165
HA18	0.426172	0.317143	0.32002	0.66329
HA20	0.614247	0.143553	0.490043	0.00786
HA23	0.652315	0.185477	0.60171	0.05537
HA24	0.805818	0.177136	0.177538	0.32721
HA25	0.796798	0.222623	0.195928	0.31295
HA27	0.42017	0.270114	0.304695	0.69143
HA28	0.164964	0.042926	0.777016	0.39513
HA30	0.134015	-0.00327	0.763886	0.39113
HA31	0.146645	0.015032	0.769265	0.39464
HA35	0.430026	0.332938	0.319482	0.64858
HA36	0.402861	0.249664	0.322742	0.70317
HA38	0.162593	0.876391	0.11501	0.14424
HA45	0.166337	0.875554	0.116528	0.14321
HA47	0.795013	0.241176	0.195061	0.30694
HA51	0.738931	0.165396	0.069711	0.258
HA52	0.22422	0.139785	0.766861	0.3922
HA56	0.272811	0.236123	0.739814	0.36956
HA59	0.412344	0.281655	0.324833	0.68503
HA62	0.268015	0.227016	0.74538	0.37227
HA64	0.160149	0.876491	0.115897	0.14498
HAP1	0.170742	0.874815	0.115506	0.13975
HAP7	0.154583	0.87689	0.11586	0.14711

HAP9	0.172039	0.87341	0.116982	0.13884
HAP10	0.163084	0.875445	0.117163	0.14305
HAP11	0.158116	0.876663	0.115395	0.14592
HAP13	0.173949	0.872864	0.116697	0.13799
HAP16	0.170807	0.873589	0.112579	0.13662
HAP17	0.797003	0.222366	0.194828	0.31295
HAP19	0.648409	0.136081	0.620538	0.05883
HAP21	0.280013	0.255806	0.730237	0.36185
HAP23	0.649946	0.14884	0.616876	0.05831
HAP28	0.168209	0.875392	0.11342	0.14259
HAP29	0.651685	0.168831	0.609632	0.05697
HAP31	0.378471	0.20189	0.321299	0.71579
HAP33	0.648718	0.141971	0.619193	0.05898
HAP37	0.169411	0.874498	0.116337	0.14039
HAP40	0.161814	0.876226	0.116237	0.14407
OUT5K	0.28164	0.524812	0.271289	0.41455
OUT5I1	0.743479	0.165075	0.060174	0.25877
OUT5I2	0.429087	0.307228	0.310295	0.66977
OUT6C	0.13194	-0.01011	0.766508	0.39385
OUT6I	0.41358	0.264132	0.314241	0.69989
S1	0.805251	0.181254	0.174446	0.32579
S2	0.174554	0.872674	0.117449	0.1379
S5	0.803919	0.212863	0.183395	0.31721
S8	0.165148	0.875595	0.116526	0.14245
S12	0.167147	0.875636	0.112869	0.14352
S13	0.131328	0.873194	0.109339	0.15811
S13B	0.804651	0.202604	0.182365	0.32039
S15	0.42929	0.315081	0.313014	0.66535
S20	0.805369	0.19163	0.177579	0.32318
S26	0.804327	0.20535	0.181884	0.3204
S28	0.805356	0.189743	0.1762	0.3239
S30	0.805315	0.191967	0.177905	0.32341
S39	0.805014	0.178868	0.17377	0.32615
Expl.Var	16.71477	22.70389	11.47374	11.1042
Prp.Totl	0.217075	0.294856	0.14901	0.14421

Eigenvalues

Factor	Eigenval	Variance (%)	Cum. Eigenval	Cum. %
1	41.90602	54.4234	41.90602	54.4234
2	12.45246	16.17202	54.35848	70.5954
3	4.401198	5.715841	58.75967	76.3113
4	3.236958	4.203842	61.99663	80.5151

Elemental Data

	Factor 1	Factor 2	Factor 3	
AR3	0.876144	0.055326	0.136289	
AR6	0.078342	0.711112	0.51103	
AR9A	0.87479	0.081107	0.13102	
AR15	0.877252	0.058031	0.128229	
AR19	0.877786	0.068448	0.119521	
AR20	0.839585	0.203707	0.20141	
AR21	0.073922	0.885113	0.083676	
AR22	0.694297	0.509059	0.217167	
AR23	0.743025	0.354692	0.300367	
AR25	0.717419	0.504096	0.142529	
AR35	0.696371	0.347642	0.422442	
AR43	-0.01244	0.889053	0.078961	
AR51	-0.01245	0.889888	0.066014	
ARLC4K1	0.797038	0.19987	0.332794	
ARLC4K2	0.616784	0.54835	0.298923	
ARLC4K3	0.149548	0.876039	0.079965	
ARLC3SC	0.861145	0.173775	0.130621	
HA2	0.794343	0.290612	0.266277	
HA9	0.840233	0.134119	0.25251	
HA13	0.73523	0.3801	0.319345	
HA14	0.835122	0.111926	0.278894	
HA15	-0.09438	-0.06584	0.891786	
HA18	0.74178	0.465723	0.147229	
HA20	0.561778	0.588534	0.351864	
HA23	0.818533	0.233431	0.24137	
HA24	0.878367	0.052062	0.12344	
HA25	0.145299	0.876245	0.079175	
HA27	0.877948	0.053171	0.125779	
HA28	-0.08131	0.888836	0.033022	
HA30	-0.08153	0.888683	0.034816	
HA31	-0.02207	0.891615	0.041529	
HA35	0.404197	0.772714	0.175392	
HA36	0.864617	0.073145	0.189176	
HA38	0.819016	0.05086	0.338755	
HA45	0.820613	0.063547	0.33281	
HA47	0.700682	0.05799	0.543238	
HA51	0.722542	0.493358	0.152544	
HA52	0.273263	0.096951	0.847714	
HA56	0.851413	0.075609	0.240153	
HA59	0.669197	0.117099	0.573262	
HA62	0.535671	0.488102	0.502	
HA64	0.554526	0.36848	0.586127	
HAP1	0.737327	0.246678	0.336509	
HAP7	0.110602	0.827031	0.305482	
HAP9	0.353173	0.777682	0.248474	
HAP10	0.036386	0.886066	0.102317	
HAP11	0.385883	0.023964	0.806793	

HAP13	0.608151	0.571991	0.297641	
HAP16	0.543946	0.58728	0.381119	
HAP17	0.266445	0.166118	0.832118	
HAP19	0.219489	0.49381	0.706724	
HAP21	0.297212	0.361528	0.746944	
HAP23	0.187109	0.447438	0.748128	
HAP28	0.862732	0.082361	0.193565	
HAP29	0.225509	0.287314	0.816354	
HAP31	0.841162	0.167648	0.228098	
HAP33	0.433736	0.33098	0.703186	
HAP37	0.624545	0.515643	0.358035	
HAP40	0.460037	0.67163	0.35464	
OUT5K	0.583026	0.444804	0.499555	
OUT5I1	0.878682	0.058184	0.118471	
OUT5I2	0.876079	0.087066	0.119493	
OUT6C	0.042541	0.868809	0.1826	
OUT6I	0.87416	0.058445	0.147045	
S1	0.878625	0.05036	0.122399	
S2	0.798348	0.314491	0.22561	
S5	0.878027	0.055452	0.124265	
S8	0.546483	0.267764	0.647227	
S12	0.874204	0.052592	0.148928	
S13	0.867962	0.059981	0.178532	
S13B	0.869398	0.134773	0.122735	
S15	0.874907	0.056895	0.143214	
S20	0.879217	0.050622	0.118162	
S26	0.877202	0.061977	0.126685	
S28	0.878989	0.050923	0.119632	
S30	0.878614	0.04852	0.123197	
S39	0.879922	0.049304	0.113662	
Expl.Var	34.46631	15.65564	10.58371	
Prp.Totl	0.447614	0.20332	0.137451	

Eigenvalues				
Factor	Eigeneval.	Variance (%)	Cum. Eigenval	Cum. %
1	44.04235	57.19785	44.04235	57.1979
2	11.8753	15.42246	55.91764	72.6203
3	4.788016	6.218202	60.70566	78.8385

VITAE

- ***Mr. Lameed Olabode Babalola***, earned B.Sc (Honors) in Geology from the University of Ilorin, Nigeria in 1985.
- Did one year national youth service attachment in Gulf Oil Company (now Chevron) of Nigeria as a trainee Geologist (1985/86).
- He received M.Sc in Applied Geology (with bias in micropaleontology) from the Obafemi Awolowo University, Nigeria in 1992.
- Mr. Babalola worked as consultant Palynologist/Geologist in oil service companies in Nigeria between March 1991 and early 1997.
- He joined KFUPM as a Research Assistant in the Earth Sciences Department in February 1997.
- His current research interests are in the area of clastic sedimentology.
- Mr. Babalola was a recipient of an AAPG grants-in-aid award in 1998.